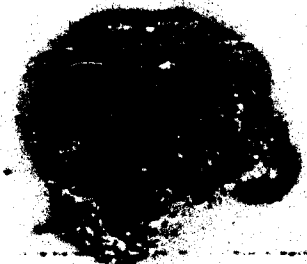WADD TECHNICAL NOTE 61-
PART I

2619433

(Unclassified Title)

TRANSIENT RADIATION EFFECTS ON ELECTRONICS
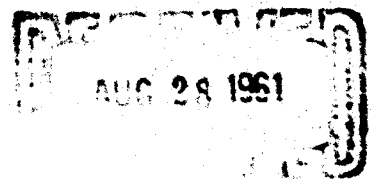# PART I.   KUKLA TRANSIENT RADIATION TESTS

BOEING AIRPLANE COMPANY

Boeing Document
D2-7899

JANUARY 1961

ASTIA

AUG 28 1961

5

Communications Laboratory

WRIGHT AIR DEVELOPMENT DIVISION
AIR RESEARCH AND DEVELOPMENT COMMAND
UNITED STATES AIR FORCE
WRIGHT-PATTERSON AIR FORCE BASE, OHIO

NOTICES

When Government drawings, specifications, or other data are used for any purpose other than in connection with a definitely related Government procurement operation, the United States Government thereby incurs no responsibility nor any obligation whatsoever; and the fact that the Government may have formulated, furnished, or in any way supplied the said drawings, specifications, or other data, is not to be regarded by implication or otherwise as in any manner licensing the holder or any other person or corporation, or conveying any rights or permission to manufacture, use, or sell any patented invention that may in any way be related thereto.

Qualified requesters may obtain copies of this report from the Armed Services Technical Information Agency, (ASTIA), Arlington Hall Station, Arlington 12, Virginia.

Copies of WADD Technical Reports and Technical Notes should not be returned to the Wright Air Development Division unless return is required by security considerations, contractual obligations, or notice on a specific document.

UNCLASSIFIED

WADD TECHNICAL NOTE 61-8
PART I

(Unclassified Title)
TRANSIENT RADIATION EFFECTS ON ELECTRONICS
PART I.   KUKLA TRANSIENT RADIATION TESTS

Applied Physics Section
Physics Technology Department
Aero-Space Division
BOEING AIRPLANE COMPANY
Seattle 24, Washington

Boeing Document
D2-7899

JANUARY 1961

Communications Laboratory

Contract Nr AF 33(616)-7531
Project Nr 0(1-5237)
Task Nr 42018

WRIGHT AIR DEVELOPMENT DIVISION
AIR RESEARCH AND DEVELOPMENT COMMAND
UNITED STATES AIR FORCE
WRIGHT-PATTERSON AIR FORCE BASE, OHIO

UNCLASSIFIED

ABSTRACT

A series of tests were performed at the Kukla pulse reactor at Livermore, California. These tests verified that the operation of the reactor for transient radiation testing was similar to the Godiva pulse reactor. New radiation effects information was obtained on transient radiation induced breakdown of spark gaps and thryatrons; transient conductivity in several types of dielectric materials, capacitors, and a Germanium semiconductor diode. A description of the reactor operation and dosimetry used during the tests is discussed. Existing information on the transient radiation pulse from a weapon detonation was compiled and discussed. The correlation of pulse reactor information with the weapon environment is considered. The implication of weapon system requirements on transient radiation effects testing is also presented.

TABLE OF CONTENTS

KUKLA TRANSIENT RADIATION TESTS

by

G. L. Keister

INTRODUCTION

This report contains the results of the radiation effects test carried out at the Kukla critical assembly, Lawrence Radiation Laboratory, Livermore, California, in June, 1960. The Kukla facility was constructed by the Lawrence Radiation Laboratory during the period from December, 1959 to May, 1960 with the aid of Boeing personnel. The Boeing work was funded under Air Force Contract AF 33(600)-35030. Since the facility is new, special tests were required to allow it to be successfully utilized. These included dosimetry measurements and tests of the interaction of radiation with cables and instrumentation. Making use of tests already planned for CCN No. 11 to Contract AF 33(600)-35050 allowed specific part information to be obtained on gaseous and solid dielectric materials, semiconductor diodes, and thyratrons.

The organization of this report was keyed toward providing the results of the program in a form which may be quickly assimilated by either the limited or specialized reader. Details and test data have been placed in appendices to free the body of the report for summary and correlation data. To achieve additional utility, the report was divided into two separately bound parts. Part I, which is Unclassified, contains all of the test data, including summary and conclusions. Part II, which is classified Secret--Restricted Data, discusses the problems encountered in attempting to correlate the test environment with the nuclear weapon environment. The material contained in Part I may stand independently from Part II.

PROGRAM PURPOSE AND OBJECTIVES

This program was keyed toward providing test data in a form which will be useful to component and systems designers who are concerned with operations in a nuclear or potential nuclear environment.

The primary purpose of this program was to:

1. Determine the effect of nuclear radiation on basic electronic piece parts, and

2. Apply this information to the synthesis and testing of basic building block circuitry which may be used in extra-atmospheric vehicle systems in a manner which could be used to make them resistant to transient radiation effects.

In addition to the test, work was to be performed on the analysis of circuit and piece part test requirements for transient radiation effects prediction. This work was specifically directed toward extra-atmospheric systems. In addition, the nuclear weapon environment associated with these systems was to be studied.

SUMMARY OF WORK ACCOMPLISHED

WEAPON SYSTEM ANALYSIS

Since the purpose of testing materials in a transient radiation environment is to produce data for use in designing future military systems, the requirements of such systems should influence the testing performed. A future weapon systems study was made in order to determine the systems requirements so that the radiation testing program could be directed toward satisfying those requirements which were discovered. The results of such a weapon systems study could not influence the testing program under this contract; therefore the study was directed toward establishing goals for a future testing program.

The results of the weapon system study indicated that transistorized circuitry of the type which may be found in a digital computer were in general the most susceptible to a transient radiation environment and at the same time most commonly used. Typical examples of these circuits, as used in design stage weapon systems, were obtained. They proved to be more complex than would be desired for a "first attempt" analysis program.

BASIC BUILDING BLOCK CONCEPT

The sample circuits obtained could either be tested in their entirety or they could be broken down into simpler component circuits. To test them in their entirety would supply a basic go-no-go answer; it would either certify or reject those particular circuits for use in a given application. It was believed that this was not wanted; but rather, that it would be desirable to develop analytical methods which would allow the prediction of the behavior of any circuit configuration. Therefore, an analysis program was indicated. The typical circuits were broken down into simpler basic building block types. The building blocks obtained were:

1. Balanced amplifiers (differential amplifier stages).

2. Multivibrators (free running, one shot and controlled).

3. D.C. coupled multivibrators (flip-flop and trigger circuits).

4. Clipper and limiter networks.

5. Blocking oscillators.

6. Phase inverter circuits.

7. Single stage amplifiers (grounded emitter, grounded collector, and grounded base).

All of the above building blocks were transistorized; simplified schematic diagrams of each of these circuit types are shown in Appendix VII. An analysis technique, which can pre-

dict the behavior of each of these circuit types under radiation, can be extended to predict the behavior of the more complex circuitry found in the typical circuits used in the actual weapon systems.

Having determined what should be analyzed and studied, the next step was to decide upon a method of attack. It was known that the circuits obtained commonly used only resistors, capacitors, diodes, and transistors. If attention was directed toward only selected representative types of these piece parts, then sufficiently detailed information could be obtained about the behavior of them to permit circuit analysis. Therefore, an intensive program, limited to specific piece parts, was planned.

The specific information on the piece parts obtained in the testing program can be used to determine the circuit behavior of each of these parts. This circuit behavior may be either represented by means of an equivalent circuit or by means of a matrix with time varying coefficients. Behavior can also be simulated on an analog computer directly. Once the piece part behavior is known, the behavior of the circuit to be analyzed may be determined by either analytical methods or by purely analog methods, whichever appears more feasible. In the first instance, the analog computer solves the equations; in the second, the computer becomes a direct analog. Both possibilities should be examined.

The requirements for piece part representation specify the measurements which must be obtained in the testing program. Therefore, work was initiated to determine the expected piece part circuit representation so that the desired measurements could be defined. In some cases (resistors and capacitors) this work has been carried to the point where not only the desired measurements have been defined, but also the method of measurement.

MATERIALS AND PIECE PART TESTS

A test series was conducted at the Kukla prompt critical assembly in Livermore, California to determine the transient radiation effects on gases, dielectrics, and semiconductors. This test was the first radiation effects test to be carried out at the Kukla facility and considerable dosimetry was performed by both the Lawrence Radiation Laboratory and Boeing personnel to determine the test radiation environment. Detailed technical reports are included on each phase of the test series as appendices to this report.

The Kukla reactor was undergoing preliminary tests to check its operation during this test series and maximum excursions were not obtained. Livermore operated nuclear weapon diagnostic equipment during the test series and made the information on fission rate as a function of time available for dosimetry purposes. This information proved valuable in reducing the effects data on gases and dielectrics. This is the first time equipment of this type was used in this manner. In addition to the photodiode diagnostic equipment, information was obtained on test environment with the following types of dosimeters:

> Fission foils
> Sulfur
> Gold-cadmium covered gold
> Sigoloff
> SEMIRAD

The fission foils were furnished by Livermore and the remainder were furnished by Boeing.

The experiments in gas ionization problems were directed toward the fairly well investigated problem of transient induced firing of thyratrons and the not so well investigated problem of transient radiation induced firing of spark gaps.

The thyratron experiments were not conclusive because of the low radiation rates. However, the information obtained was consistent with the data available from DOFL on the same type thyratron. Figure 56 shows the voltage setting and radiation rates superimposed on the DOFL curve.

The investigation of the spark gap made use of the diagnostic data to determine the radiation rate at which the gap fired. This technique allowed a considerable amount of information to be obtained from the test, although the radiation rates were not above 10^6 r/sec.

Figure 54 shows the percent reduction in the firing potential of a spark gap as a function of radiation rate for 14.7 PSI of air and 23°C. Time did not permit this information to be obtained for any other conditions.

Investigation of dielectric materials exposed to gamma radiation up to 10^3 r/sec has shown that the conductivity change can be represented by:

$$\sigma = \sigma_o \phi^\Delta$$

where ϕ is the radiation rate
Δ is between 0.5 and 1

The present investigations of Vitamin Q and mylar dielectrics have verified this relationship up to radiation rates of 10^6 r/sec. Figures 38 and 39 show the consistency of these data. These data were also generated using the diagnostic dosimetry information. Correlation of this information was also established with various types of capacitor construction to allow prediction of capacitor dielectric leakage. The variation in dielectric constant for the dielectrics considered was determined to remain constant through radiation pulses up to 10^6 r/sec.

Investigation of the 1N277 germanium gold-bonded diode indicates that changes in the forward characteristics were small enough to be neglected for pulses up to 10^6 r/sec. The reverse current pulse varied largely among diodes but it was found that the amplitude of the current pulse could be related to the dynamic resistance of the diode as measured at the applied voltage. The relationship is defined by:

$$\Delta I = (a + b\, R_{sh})\dot{R}$$

where ΔI is the current change
a and b are constant
R_{sh} = diode initial shunt resistance
$\dot{R}$ = gamma rate in r/sec

Two sets of diodes were measured having considerably different R_{sh} and R. Set one was used to predict the result of set two. The result of this prediction is shown in Figure 69.

WEAPON ENVIRONMENT

The prompt nuclear radiation from a nuclear detonation was investigated and the implications of transient radiation effects considered. Since any quantitative reference to this work would involve the discussion of Secret--Restricted Data, the reader is referred to Part II of this report for the discussion in its entirety.

CONCLUSIONS

This report provides new information in defining the radiation effects on:

1. Spark breakdown

2. Dielectrics

3. Semiconductor diodes.

It also presents a new dosimetry and instrumentation technique that can increase the data output of radiation tests many fold.

A program for transient radiation testing is outlined based on an evaluation of system needs. This program includes discussion of circuits, piece part testing, and analysis methods.

All known information on the transient radiation environment of a nuclear weapon is presented and evaluated in terms of test requirements.

RECOMMENDATIONS

Recommendations for the individual portions of the work are discussed at the end of each appendix. A detailed technical proposal for the continuation of this work is presented in Boeing Document D2-7677, "A Program for the Prediction of Transient Radiation Effects in Electronics," (Secret--Restricted Data).

APPENDIX I

THE KUKLA PROMPT CRITICAL FACILITY

by

Harold B. Almond and Brian W. Mar

TABLE OF CONTENTS

LIST OF ILLUSTRATIONS

INTRODUCTION

The Kukla prompt critical facility, Lawrence Radiation Laboratory, Livermore, California is designed to produce self-limiting neutron fission bursts similar to those of Godiva I and II. Construction of the Kukla facility, in which Lawrence Radiation Laboratory was assisted by the Boeing Airplane Company under Air Force sponsorship, began in December, 1959, and first criticality was achieved in May, 1960. The radiation effects tests covered in this report were performed at Kukla during the period June 24-30, 1960. This was the first radiation effects testing performed at the facility and served as a shakedown run to establish operation procedures, instrumentation techniques, cabling installation, personnel exposure problems, etc. At the time of the test the facility had achieved neither maximum burst capability nor burst reproducibility. The discussion of the Kukla facility in this section is limited to general operational information. A complete discussion of the present burst characteristics is covered in the section on Dosimetry.

Two other facilities were required for operation at Kukla, a van-type trailer for housing the required test and recording instrumentation, and a house trailer to serve as a general personnel area for data reduction.

KUKLA PROMPT CRITICAL ASSEMBLY

It is anticipated, when the assembly is fully operational, that the maximum burst generated will have the following characteristics:

Fission yield from burst	2×10^{16} fissions
Excess reactivity producing burst	8 cents above prompt critical
Prompt alpha	$0.09 \, \mu \, \sec^{-1}$
Burst width at half maximum	$60 \, \mu \, \sec$
Fission rate (max)	2×10^{20} fission/sec
Leakage neutron rate (max)	2.8×10^{20} neutrons/sec
Leakage neutrons	2.8×10^{16} neutrons
Estimated dose at one meter	60 rem gamma

Present operation of the facility is limited to a lower yield per burst until instrumentation has been fully checked out.

A sketch of the assembly is shown in Figure 1. Figure 2 shows the actual assembly with Boeing test equipment around it. The triangular plates which make up the support stand are thirty inches on a side with the exception of the bottom plate which is thirty-six inches on a side. The oralloy sphere is approximately 3.60 inches in radius and its center is approximately sixty-eight inches above the floor. A heavy wire cage surrounds the oralloy. This prevents placement of material closer than one-half inch from the outer surface of the oralloy. The wire cage is cylindrical with a radius of 4.2 inches and an overall height, including the conical top, of about twenty-four inches.

When fully assembled in a prompt critical configuration, Kukla contains approximately 60 Kg of enriched uranium (oralloy). A sketch of the disassembled components in the oralloy sphere is shown in Figure 3. The reactivity contributions of the control elements are:

Safety block	$25
Control rods (two)	$1.6 each
Burst rod	$2.0

Pneumatic drives are employed for safety block and burst rod movement. A mechanical cam provides an inch per minute velocity over the last 7/8 inches of movement of the safety block for fine control. The two control rods are driven by motor worm gear units at 0.024 inches/second and 0.012 inches/second. A scram is actuated by applying 150 PSI air to the top side of the safety block and burst rod air cylinders.
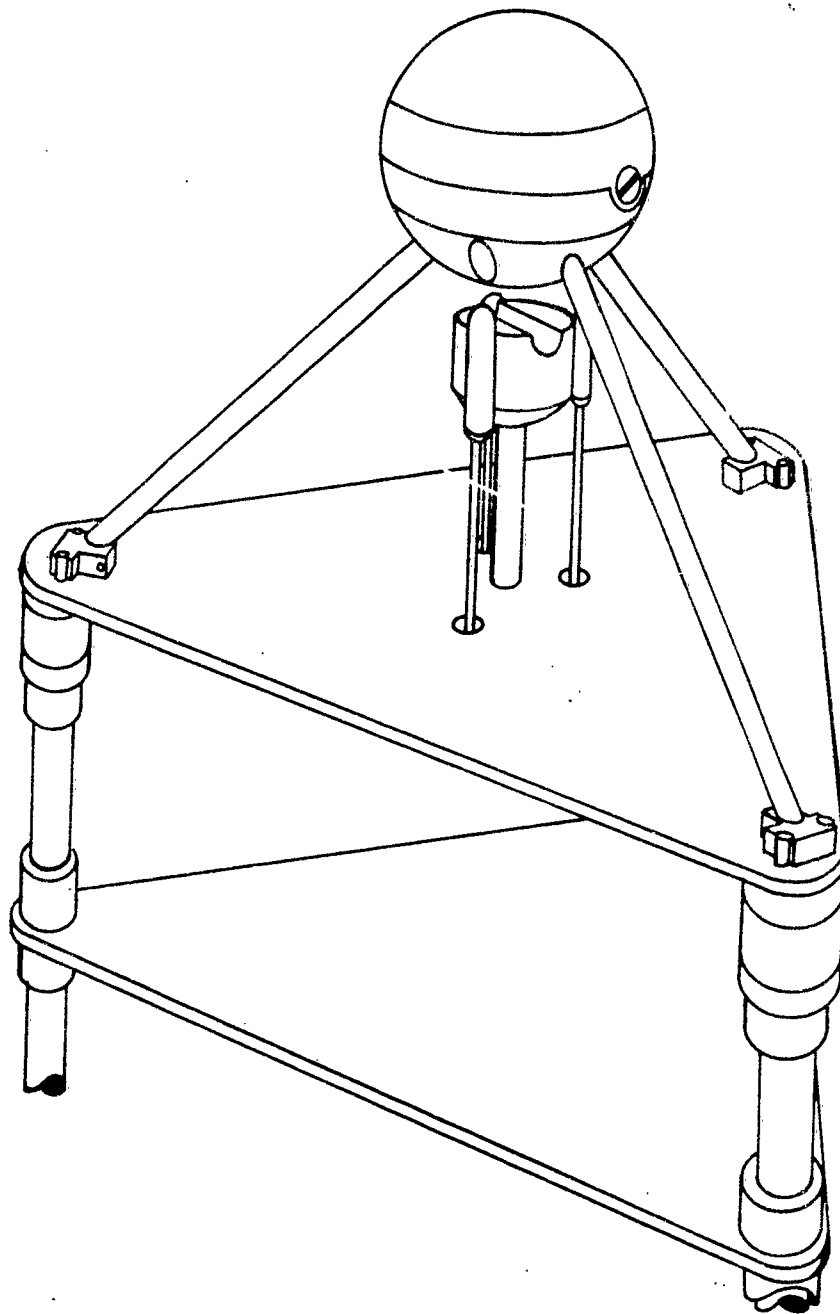
Figure 1 - Top of Kukla Assembly.
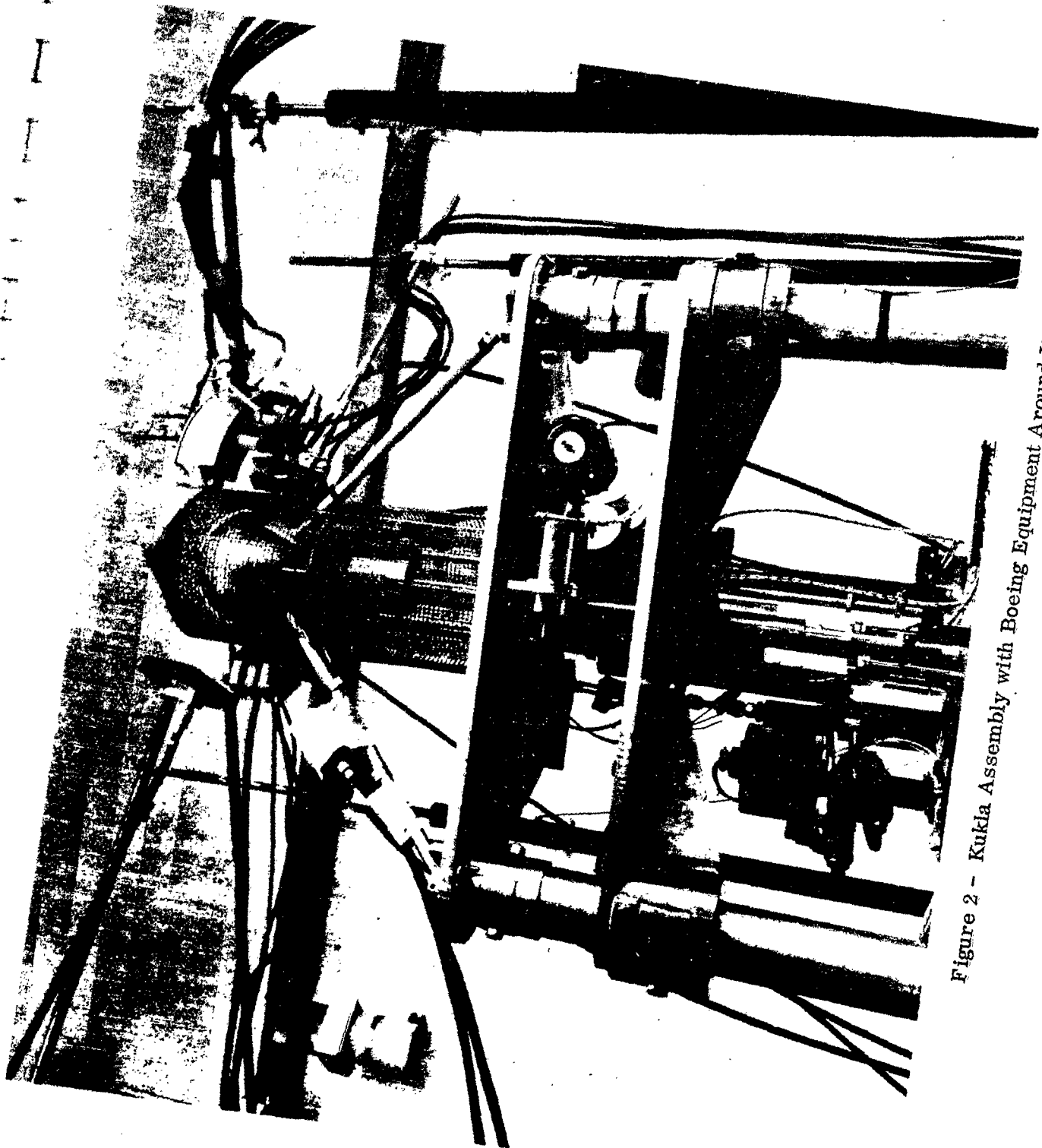
Figure 2 – Kukla Assembly with Boeing Equipment Around It

BURST ROD RELIEF PLUG
0.6 kg

TOP SPHERICAL
SECTION 14 kg

GLORY HOLE

TOP CENTRAL
SECTION 15 kg

BOTTOM CENTRAL
SECTION 8 kg

BOTTOM SPHERICAL
SECTION 11 kg

CONTROL ROD

CONTROL ROD

BURST ROD 1 kg

SAFETY BLOCK
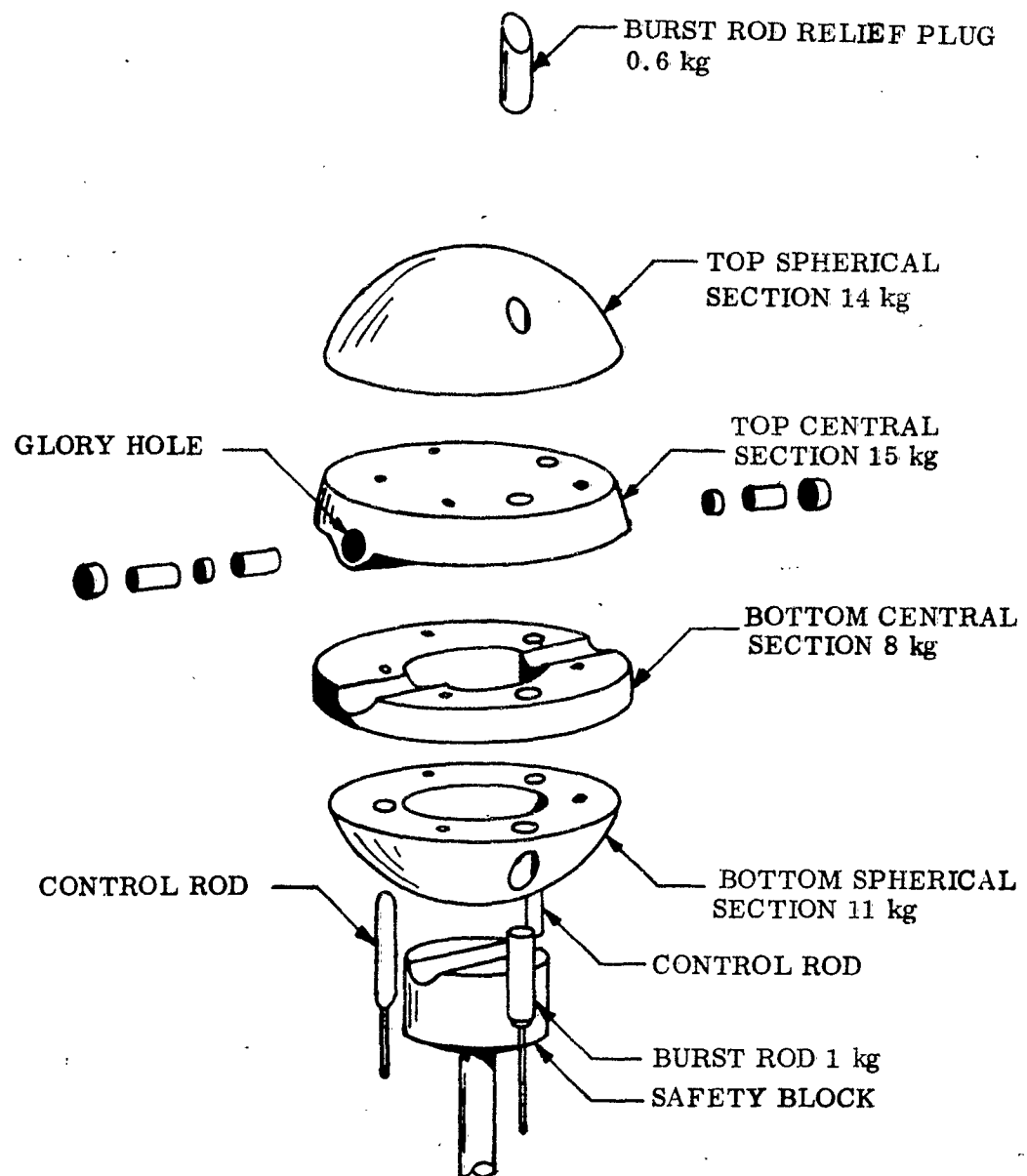
Figure 3 – Disassembled Oralloy Components.

BURST GENERATION

Kukla burst generation is similar to that of Godiva II with a fission burst generated by the rapid assembly of a super-critical configuration before the buildup of an appreciable neutron population. This achievement of a super-critical assembly requires a three step procedure:

1. The oralloy is assembled to a delayed critical configuration with the burst rod set at a predetermined position so that the reactivity difference between this position and its fully inserted position is the amount necessary to obtain the desired super-critical configuration.

2. The control rods are locked in position and the safety rod and burst rod are withdrawn. The assembly is allowed to cool.

3. One control rod may be withdrawn slightly to compensate for cooling of the assembly. The safety block, and then the burst rod, are rapidly inserted to achieve a super-critical configuration.

A neutron source in center of sphere provides the initial neutrons to start the fission chain.

The prompt fission burst is self-limited by thermal expansion, but the delayed neutrons sustain a power level which causes a temperature rise in the assembly of $100°C/seconds$. To prevent melting of the oralloy, the system is scrammed automatically after a burst by a solenoid valve triggered at a preset power level of the reactor. Due to mechanical delays, this occurs approximately 105 milliseconds after burst initiation.

KUKLA FACILITY BUILDING

The Kukla assembly is housed in the West Vault in Building 110 at the Livermore site of the Lawrence Radiation Laboratory. A floor plan of this area and the location of the Boeing trailer laboratory and house trailer alongside the building is shown in Figure 4. Access to Building 110 is restricted to those "Q" cleared (or equivalent) persons who have a need to conduct business in this building.

The West Vault is fifteen feet wide, twenty feet long and twelve feet high. The five feet thick walls and two and one-half feet thick ceiling are of reinforced concrete construction. The interior of the walls is coated with a 30 mil coat of plastic vinyl paint to provide a smooth finish and a non-porous seal. The floor is covered with linoleum tile. A water window affords visual access from the control room. Personnel access to the vault is by means of a labyrinth and sealed doors. An air conditioner is installed on the vault roof; however, during calibration and burst operation, dampers in the vault ceiling are closed to provide complete containment in case of an excursion.

All electrical connections and electrical power in the West Vault are carried through two junction boxes located on the East wall of the vault. One of the junction boxes contains cable connections to a corresponding junction box located outdoors on the North side of the building. Interconnecting the two boxes are approximately seventy feet of each of the following cables:

CABLE	QUANTITY
RG-164/U	One
RG-8/U	Five
RG-11/U	Ten
RG-22/U	Ten
Twisted pair No. 20, audio cable	Fifteen
Single shielded No. 20	Fourteen
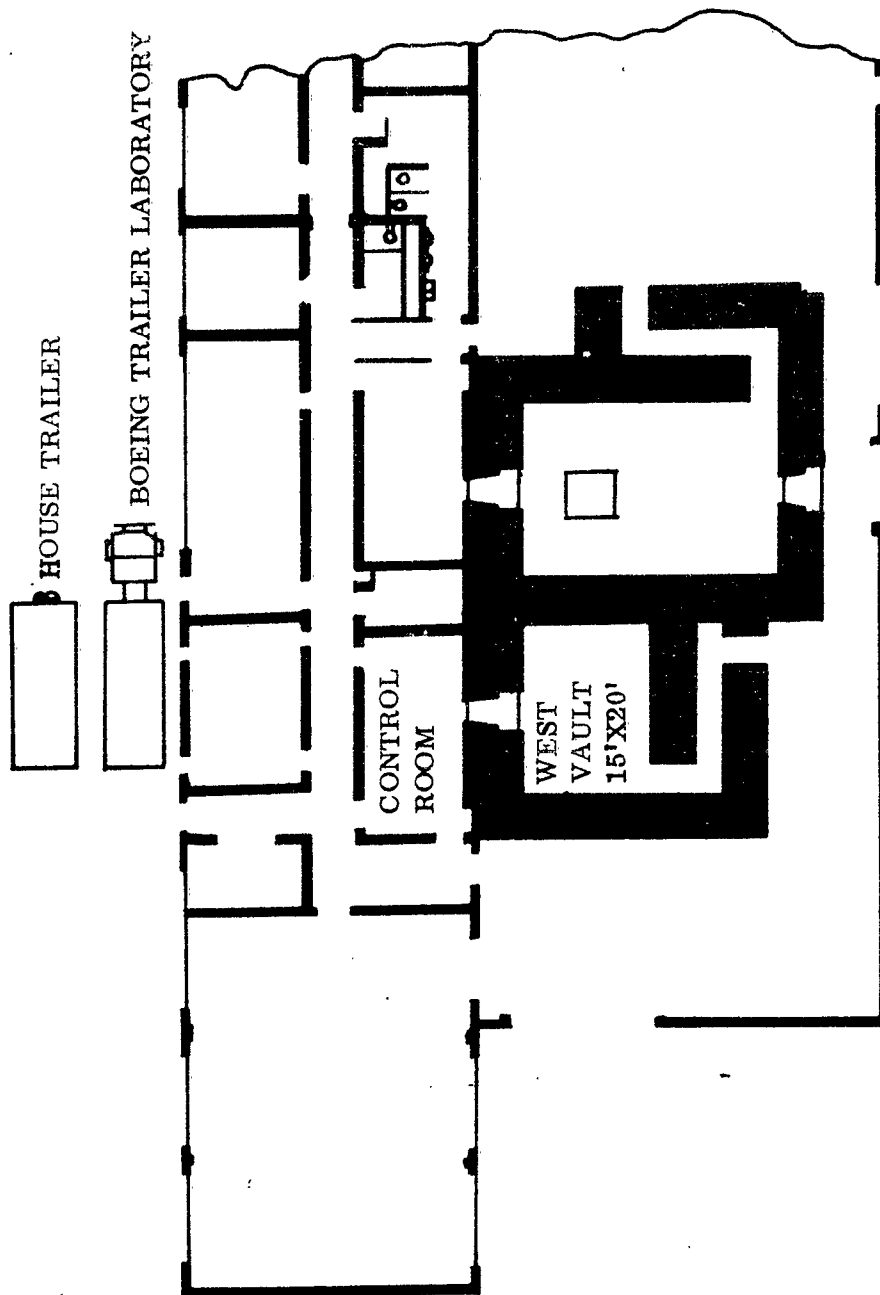
Figure 4 – Section of Building 110 Showing West Vault, Control Room and Trailer Location.

HOUSE TRAILER

BOEING TRAILER LABORATORY

CONTROL ROOM

WEST VAULT 15'X20'

OPERATING PROCEDURE AND PERSONNEL EXPOSURE

The operating cycle of Kukla during the period of testing varied between two to three hours from burst to burst. It is anticipated that in the near future the working cycle will be two hours per burst over a sixteen hour working period. The down time between burst termination and the commencement of calibration for the next burst is about one and one-half hours. This is the time required for the temperature of the oralloy sphere to drop to within a few degrees of room temperature.

The radiation level in the West Vault after a burst drops to a workable level before the oralloy temperature drops to a few degrees of room temperature. Personnel were allowed to enter the vault when the temperature of the oralloy was within about four to five degrees of the necessary recycle temperature. The amount of time required to make necessary equipment changes, adjustments, and dosimeter changes was about fifteen minutes. At the end of this time the oralloy temperature was about low enough to begin the next burst calibration. Operating time for any one individual in the vault was never over one and one-half minutes, with the exception of the first entry in the morning.

The general radiation levels noted for entry into the area were:

First entry in the morning after four bursts preceding day

$$22 \text{ mr/hr } \gamma, \ 25 \text{ mr/hr } \beta, \ \gamma \ \text{ at door (11 feet)}$$

$$110 \text{ mr/hr } \gamma, \ 140 \text{ mr/hr } \beta, \ \gamma \ \text{ at one meter}$$

Entry about one and a half hours after third burst

140 mr at door

about 1.5 r at one meter

During the period Monday, June 27 through Thursday morning, June 30, covering fifteen Kukla bursts, the maximum pocket dosimeter reading achieved by any of the personnel involved in working in the West Vault was 155 mr. All personnel who were required to enter the West Vault carried one each of the following:

Boeing self-reading pocket dosimeter

Livermore self-reading pocket dosimeter

Boeing , finger badge

Boeing , film badge

Livermore , film badge

Livermore neutron badge

BOEING TRAILER LABORATORY

A twenty by seven and one-half foot Boeing van-type trailer outfitted as a mobile laboratory was used during the test. The trailer contains general bench space, storage space, power outlets, and a cable panel. The cable panel matches the cable panel on the outside of the 110 Building and, for the purpose of the test, the two panels are connected by means of forty foot extensions attached to the back of the trailer panel. This provides a direct connection between the inside of the trailer and the inside of the West Vault. Figure 4 shows the general location of the trailer with respect to the West Vault and Figure 5 shows the trailer as it was located beside the 110 Building with connections made to the outside panel. All the transient data was recorded during the bursts, with the exception of the thyratron firing tests, by means of Tektronix 545 or 551 oscilloscopes and Polaroid cameras located in the trailer. All the oscilloscopes were triggered simultaneously from a photomultiplier-discriminator circuit. Figure 6 shows the general interior arrangement of the trailer during the test.
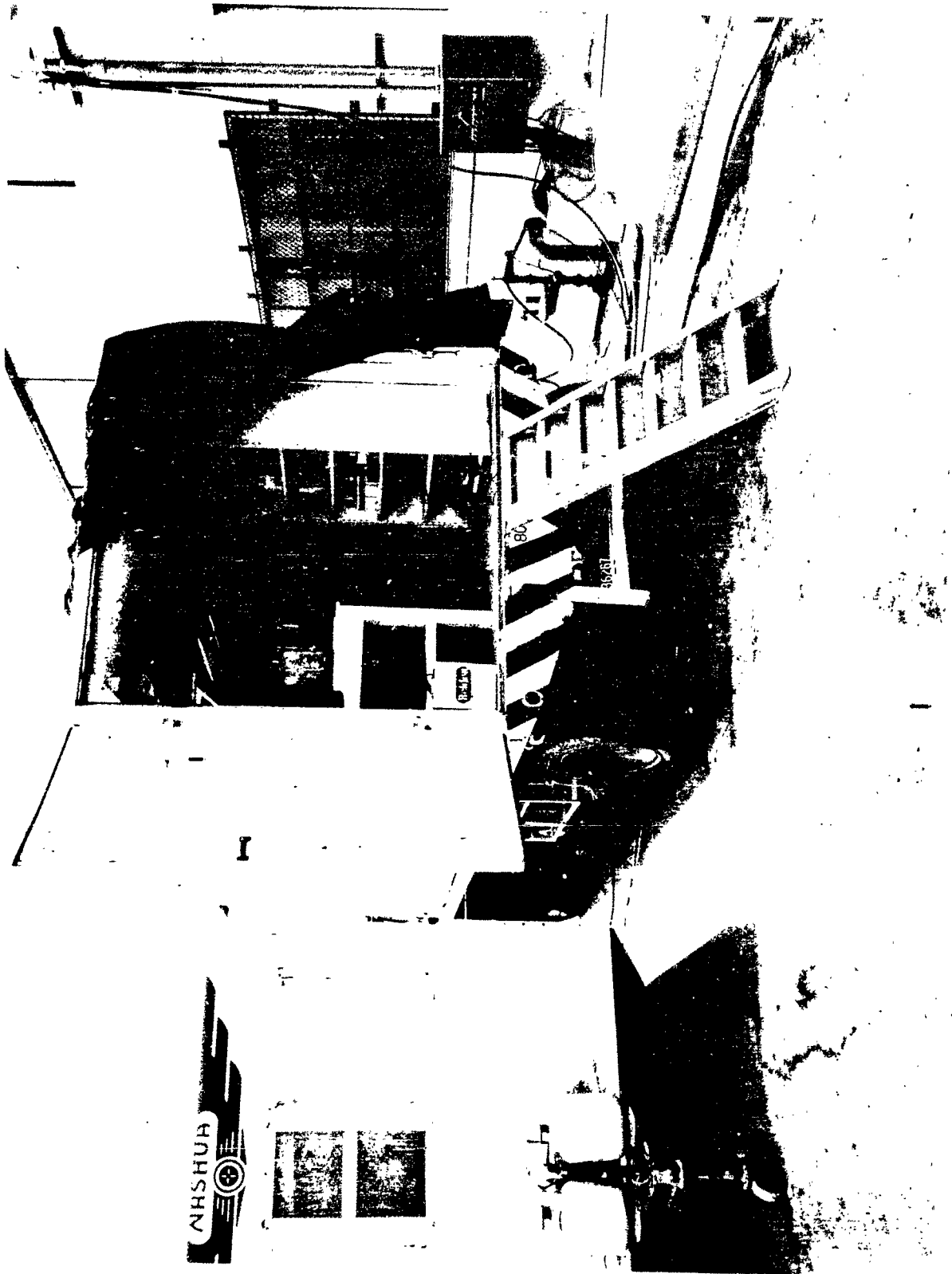
Figure 5 — Boeing Trailer and House Trailer

Figure 6 – Interior Arrangement of Boeing Trailer

HOUSE TRAILER

A forty foot house trailer was rented in Tracy, California for the period of the test and was parked alongside the Boeing trailer, Figure 5.

This trailer provided housing for the Boeing personnel during the period between bursts. This was necessary for three reasons:

1. Boeing personnel were not permitted inside the 110 Building except during test set-up period.

2. The trailer laboratory was too small to handle all the equipment and the personnel.

3. Space was required for data analysis between test runs.

APPENDIX II

KUKLA DOSIMETRY

by

Richard L. Lander, Robin K. Durkee, Donald W. Blincow

TABLE OF CONTENTS

LIST OF ILLUSTRATIONS

LIST OF TABLES

INTRODUCTION

Dosimetry is of prime importance in any radiation effects test. Parameters needed in defining and analyzing the results of radiation tests are:

1. Intensity of the radiation as a function of time.

2. Energy spectrum of the radiation.

3. Total radiation dose.

4. Particle composition of the radiation.

Pulsed critical assemblies such as Godiva I, II, and III have been used for several years in both permanent and transient radiation testing. The definition of the environment has been historically determined by the following method. (Ref. 1)

1. The neutron energy spectrum and total neutron dose have been defined by fission foil, gold and sulfur threshold detectors; and monitored by sulfur threshold detectors.

2. The gamma energy spectrum has been assumed to be composed of a fission spectrum plus gamma rays from inelastic scattering of neutrons in uranium. The total dose is established by a gamma integrating dosimeter such as a Sigoloff or glass type.

3. The particle composition is defined by the fission process and inelastic scattering of neutrons.

4. The radiation pulse shape can be defined by several radiation sensitive devices such as photodiodes, semiconductor diodes, or SEMIRADS.

The Kukla pulsed critical assembly (see Appendix I) was placed in operation in May, 1960 and used for radiation testing in June, 1960. The dosimetry described in this appendix represents the first attempt to define the Kukla environment for radiation effects testing.

Lawrence Radiation Laboratory personnel used nuclear weapon diagnostic equipment to establish the reactor characteristics for all excursions. This information was made available for evaluation of the radiation effects tests. This is the first time these techniques have been used in definition of the environment for radiation effects testing. This diagnostic information allowed an exceptional amount of new experimental information to be obtained from the individual materials and parts tests.

The analysis of the proposed transient radiation effects tests required a knowledge of both the amplitude and time history of the radiation environment. This was particularly true with the type of instrumentation used in the analysis of thyratron and spark gap breakdown described in Appendix IV. Radiation intensities were required over at least three decades during the pulse. Reactor theory also allows several experimental checks on the reactor operation, if this is known.

Information on the total gamma ray dose was required for monitoring permanent damage and the computation of the radial dependence of the gamma intensity. This was used to determine self-shielding distortions in the field which might cause deviation from the inverse square fall-off of the radiation intensity. Neutron total dose can be used to determine the total number of fissions and for correlations with the temperature rise of the reactor fuel.

Since these tests were the first operation of the reactor as a radiation test facility, it was desirable to obtain information on the spectrum and possible asymmetries due to scattering.

To obtain this information a variety of dosimeters were used. The Lawrence Radiation Laboratory supplied:

1. Photodiode diagnostic information.

2. Three sets of fission foil threshold detectors.

Boeing supplied:

1. Gold and sulfur threshold detectors.

2. Sigoloff dosimeters.

3. SEMIRADS.

PURPOSE

The purpose of the dosimetry tests was to determine the necessary information about the Kukla nuclear radiation environment to allow the radiation effects information to be analyzed. This includes information on the time history, intensity, angular and radial distribution, and total dose. It was also necessary to obtain this information in sufficient quantity and under those conditions which would allow an analysis of the operation of the reactor.

DOSIMETRY TECHNIQUES

PHOTODIODE DOSIMETRY TECHNIQUES

To obtain the time dependence of the fission rate during a Kukla burst, the Lawrence Radiation Laboratory personnel constructed and operated several monitor counters. A large plastic scintillator was viewed by two special photodiodes. Two additional scintillators mounted on photomultiplier tubes were used. The outputs of all these devices were fed to oscilloscopes where the traces were photographed on Polaroid Land film. The outputs of photodiode number one and photodiode number two (hereafter PD-1 and PD-2) were recorded for 2000 microseconds after the trigger time. On nine of the sixteen bursts the first fifty microseconds of the PD-2 trace was recorded with an additional amplification of twenty or forty in order to read the low fission rates occuring early in the burst. The outputs of photomultiplier number three (PM-3) and photomultiplier number four (PM-4) were recorded only during the first fifty microseconds after trigger time. Table 1 summarizes the monitor coverage. The output of one photomultiplier was set to trigger the scopes displaying the full traces of PD-1 and PD-2 when the fission rate reached some specified value ($\simeq 10^{15}$ fissions/second). The same trigger was used for the experimenters' oscilloscopes, so that times could be correlated. The scopes displaying the early portions of the burst were internally triggered, and time correlations were not available. The calibration factor (Ref. 2) for these monitors was measured for a Co^{60} flux and converted to the estimated average energy of the leakage gamma rays. The monitors were also calibrated for neutrons and a conversion to the average leakage neutron energy made.

Photographic reproductions of the Polaroid pictures at a magnification of about 1.6 were provided by the Lawrence Radiation Laboratory. A typical photodiode curve is shown in Figure 7. Knowing the calibration constant, one can read directly to obtain fission rate versus time. For early times during the pulse, the deflection of the trace is too small to be read. Fission rates for these times can be obtained by extrapolating the curve on the assumption that it is a single exponential. This procedure is necessary, since finite amplitude scope traces over several decades of the burst were not available.

To obtain the period, $1/\alpha$, of the exponential rise, a piece of transparent graph paper was aligned over each photograph and the center of the trace marked out. Each trace was about 2.5 mm wide on the enlarged photographs and its center could be located within ± 1/2 mm. The vertical deflection and horizontal sweep of the trace were then read from the graph paper grid lines at several points. These values were plotted on semilog paper and a visual-best-fit straight line drawn, whose slope gave the value of $1/\alpha$. The ± 1/2 mm error quoted above is probably excessive, since the points consistently fell much closer to the straight lines than ± 1/2 mm (See Figure 8). A repeat of the procedure indicated an overall error of about ± 5 percent in $1/\alpha$ from this graphical analysis.

The integrated number of fissions up to the peak of the pulse was obtained by integrating the area under the photodiode fission rate curve. The integration was performed by counting squares on the graph paper, and was reproducible to better than two percent. The total number of fissions in the whole burst could not be obtained in this way, since the tail of the burst, ex-

TABLE 1

Time Interval Recorded by Each Photodiode or Photomultiplier Monitor

Burst No.	Time Interval	
	0 – 50 μs	0 – 2000 μs
1	--	--
2	--	PD-1 PD-2
3	--	-- PD-2
4	--	PD-1 PD-2
5	--	PD-1 PD-2
6	--	PD-1 PD-2
7	PM-4	PD-1 PD-2
8	PD-2 PM-4	PD-1 PD-2
9	PD-2 PM-4	PD-1 PD-2
10	PD-2 PM-3	PD-1 PD-2
11	PD-2 PM-4	PD-1 PD-2
12	PD-2 PM-3	PD-1 PD-2
13	PD-2 PM-4	PD-1 PD-2
14	PD-2 PM-4	PD-1 PD-2
15	PD-2 PM-4	PD-1 PD-2
16	PD-2 PM-3 PM-4	PD-1 PD-2
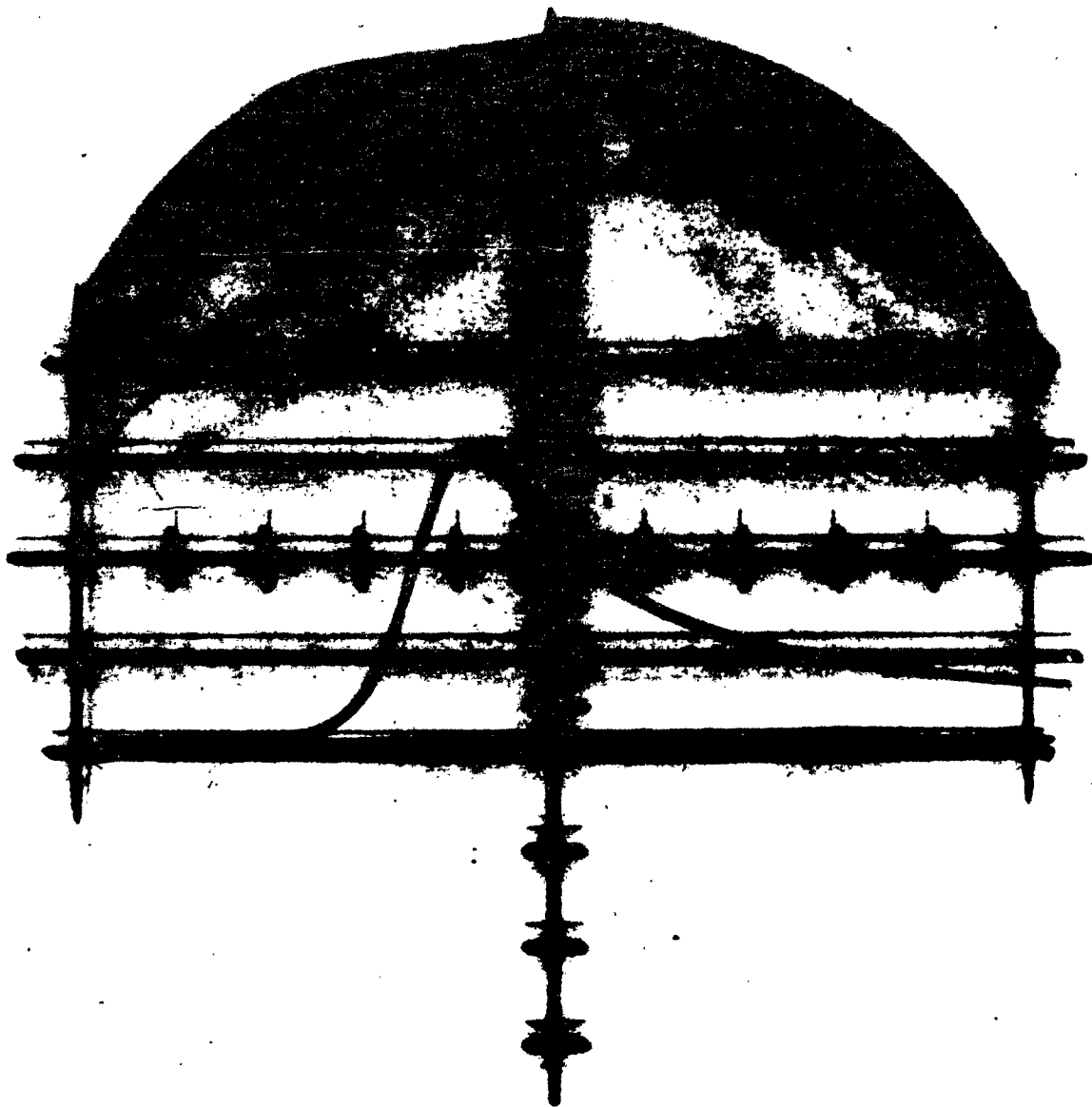
Figure 7 - Response of Photodiode No. 1 During Kukla Burst No.1
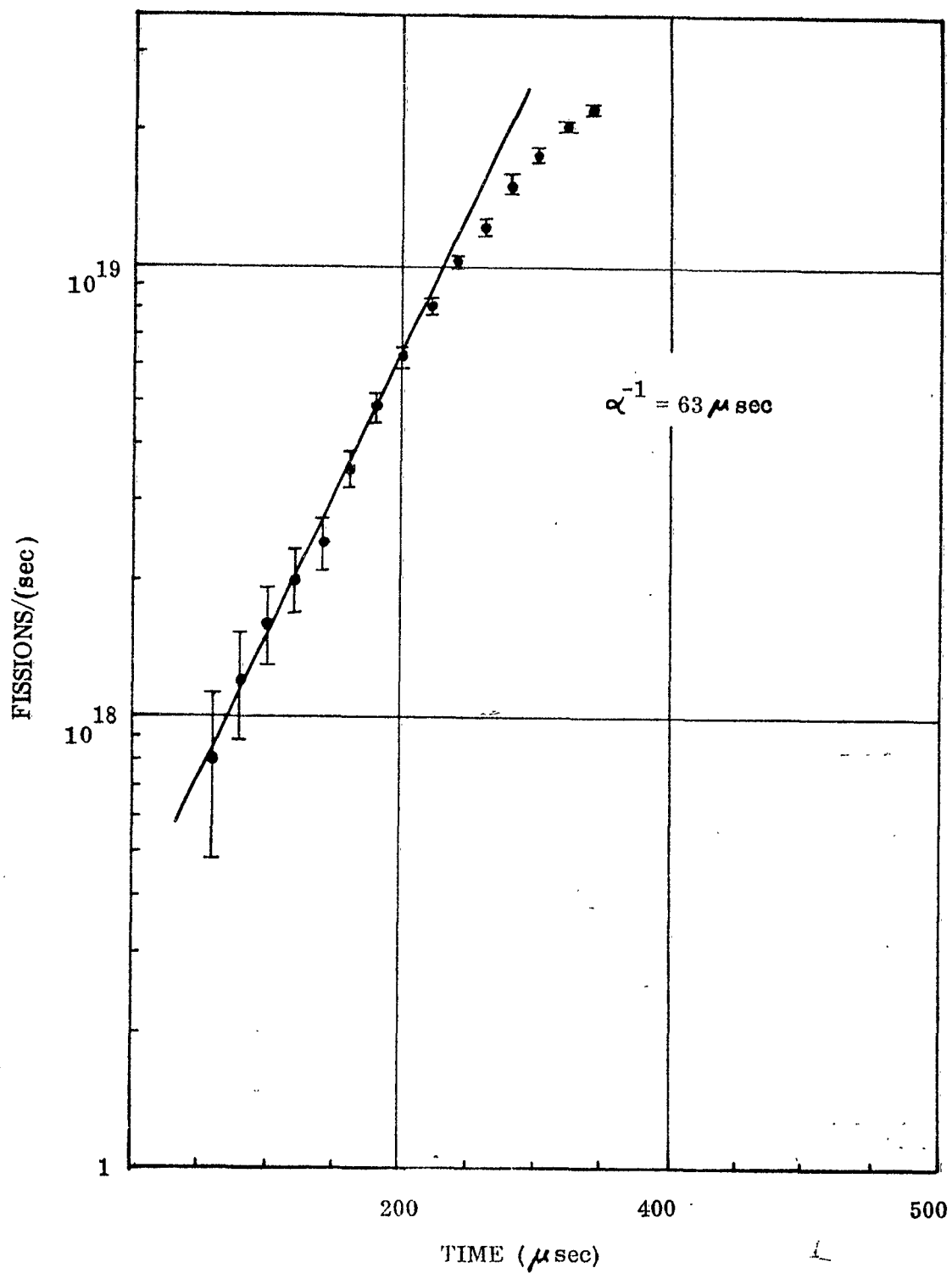
Figure 8 – Fissions Per Second Versus Time as Plotted From Figure 7.

tending off the photograph for many milliseconds, could contain an appreciable fraction of the total number of fissions.

THRESHOLD DETECTOR TECHNIQUES

To determine the approximate shape of the neutron spectrum emitted from the Kukla facility, a system of threshold detectors (Ref. 1) was used. In order to cover the full fission spectrum, a total of five detectors is necessary. The detectors with their respective threshold energies are:

Gold – Cadmium covered gold	< 0.5 ev
Plutonium (Pu 239)	> 4 Kev
Neptunium (Np 237)	> 0.75 Mev
Uranium (U 238)	> 1.5 Mev
Sulfur (S 32)	> 2.5 Mev

Gold Minus Cadmium Covered Gold

This detector uses two separate foils. The bare gold foil is receptive to all neutrons both in the thermal and epithermal range. Cadmium, which has a very high absorption for only thermal neutrons (< 0.5 ev), is used to cover a similar gold foil. The difference in activation between these two foils corresponds to the number of thermal neutrons present.

Plutonium (Pu 239)

This detector has a high fission cross section for neutrons of all energies, particularly in the thermal region. Shielding this foil by 2 cm of Boron 10 gives an effective threshold of 4 Kev. Since the fission spectrum peaks at 1-2 Mev, this detector will respond to practically all fission neutrons.

Neptunium (Np 237)

This detector has a natural fission threshold at 0.75 Mev. It is placed in the boron 10 shield with the Pu 239 for convenience and also to prevent thermal neutron activation of any Np 238 impurities.

Uranium (U-238)

This detector has a natural fission threshold at 1.5 Mev. It is placed in the boron 10 shield with the Pu 239 for convenience and also to prevent thermal neutron activation of any U-235 impurities.

Sulfur ($S^{32}(n,p) P^{32}$)

This detector has a natural (n, p) reaction threshold at 2.5 Mev. It can be placed in or out of the B-10 shield since the thermal cross section is extremely small.

Evaluation of these foils is accomplished in the following manner: the activated gold has a half life of 2.70 days, emitting a 0.96 Mev beta and a 0.411 Mev gamma. These can be detected by conventional means.

The fission foils (Pu 239, Np 237, and U 238) have a residual gamma activity from the fission products formed by the neutron fission (n, f) reaction. This is filtered by a lead absorber and counted by a scintillator detector.

The phosphorous formed in the S^{32}(np) P^{32} reaction has a half life of 14.22 days and emits a 1.71 Mev beta. This beta can also be detected by conventional means.

SULFUR DOSIMETRY TECHNIQUES

Sulfur pellets, requiring no shielding and being inexpensive and easily made, constitute a good general dosimetry tool. Provided that the neutron spectrum remains constant, a ratio of plutonium to sulfur neutrons can be made and all subsequent sulfur measurements converted to plutonium as a measure of total neutron flux.

The sulfur pellets were pressed in the form of cylinders one-fourth inch high by one-half inch in diameter. Since the flux is inversely proportional to the square of the distance, a pellet with its flat surfaces normal to the flux at five inches from the center of the reactor has a flux difference of approximately nine percent between its front and back surfaces. The exact position at which the measured flux applies depends on the depth in sulfur over which the induced radioactivity is counted. Since the pellet thickness is only slightly larger than the maximum range of the emitted betas, the effective volume of the pellet should extend through most of the depth of the pellet; however, a test count with reversed pellet orientation verified the nine percent effect above. The effective distance at which the measured flux applies is then close to the high flux surface of the pellet. This surface of the pellet was chosen as the reference position.

Several pellets were placed in the vicinity of each device being tested. Additional pellets were placed on the guard screen surrounding the sphere and three and one-half inches back from it during each of bursts nine through sixteen. A radial wire carrying three pellets at each of ten distances from the screen out to two feet was exposed during burst number one to test the applicability of the inverse square law. Eight positions at fifteen degree intervals along a concentric arc of nine-inch radius were also monitored with sulfur pellets on one burst to test for azimuthal variation.

The pellets were returned to Boeing and counted on an automatic counting wheel consisting of a 1/2 inch thick dural plate containing 1/2 inch diameter by 1/4 inch deep holes into which the pellets were placed, high flux side up. The wheel transferred each pellet in turn to a position centered 3/16 inches below a one inch diameter by 1/4 inch thick plastic scintillator optically coupled to the face of a Dumont 6292 photomultiplier tube. Calibration was effected by means of 1 1/2 inch diameter by 3/8 inch thick sulfur pellets which had been exposed to a known neutron flux (Ref 3). These pellets were powdered and new pellets pressed conforming to the size used in this report. An additional calibration was effected by preparing sample pel-

lets doped with a known activity of phosphorus-32. Agreement between these two methods was better than six percent and the value used was the average. Continuous calibration monitoring was then effected by normalizing the count rate from a long lived thallium 204 source to the calibration sulfur pellet count rate.

A total of 10^4 counts was obtained for each pellet normally, so counting statistical errors are small compared to other errors. The activities of the pellets from the radial wire test were followed for four weeks to verify the 14.22 day half-life and insure no large contamination. This value was then used to extrapolate count rates back to burst time.

SIGOLOFF DOSIMETRY TECHNIQUES

The gamma rays emerging from the Kukla reactor are derived from two primary sources within the U 235 sphere: (1) fissions and (2) inelastic neutron collisions with uranium nuclei.

The energy spectrum of gamma rays from uranium fissions will be modified by absorption and scattering of the gamma rays before they leave the sphere. The energy spectrum of the gamma rays produced by inelastic neutron collisions depends on the energy spectrum of the neutrons within the sphere and will be modified by absorption and scattering of the gamma rays as they traverse the sphere. The resultant gamma ray spectrum outside Kukla (or similar devices) has not been measured. Considerable work on fission foil gamma spectra has been done (Ref. 4). Calculations of the energy spectrum of the escaping gammas are difficult; however, estimates of the integrated gamma ray energy leaving the sphere have been made (Ref. 2), and indicate about 0.8 Mev/fission.

Chemical dosimeters having a flat response curve for gamma rays of energy from 0.1 to 10 Mev (Ref. 5) and linear response to dose from 2 to 10^6 roentgens were obtained from Edgerton, Germeshausen, and Grier, Inc. (E.G.&G).

These dosimeters consisted of three glass vials each about 5 mm in diameter and 3 cm long enclosed in a~1 mm lead shield, so that the outside dimensions were about 1 cm in diameter by 5 cm in length. Each vial contained chemicals responsive to a different dose range in order that a wide range could be obtained. This procedure meant that only one measurement per dosimeter was obtained. These dosimeters were placed alongside the sulfur pellets with their axes vertical and centered on a horizontal plane through the center of the critical assembly sphere. Their positions were measured with respect to the center of the cylinder. Since the locations of the internal vials were not known when the dosimeters were positioned, and since only one of the three vials yielded the measurement, there exists a random position uncertainty of~±3 mm.

The dosimeters were returned to E.G. and G. after exposure for analysis. Their quoted accuracy is ±10 percent for doses under 1000 rad and ±15 percent for those dosimeters which received more than the 1000 rad limit on their intended dose range.

SEMIRAD DOSIMETRY TECHNIQUES

Preliminary studies of the response of SEMIRAD (secondary-electron mixed-radiation dosimeter) to high-intensity, fast pulse radiation fields have been reported (Refs. 6, 7, 8). The device

is essentially a pair of electrodes enclosed in an evacuated envelope, i.e., a vacuum diode. When placed in an intense gamma field, the Compton electrons, photoelectrons, and possibly pair production electrons originating in the walls and electrodes of the device cause ionization during their passage through the electrodes. These secondary electrons have energies of a few electron volts in contrast to the kilovolt energy range of the primaries.

The secondaries formed near the surface of the electrodes are easily swept up by a collecting voltage applied between them. The SEMIRAD device thus acts as a current generator, with current proportional to the radiation rate, and a voltage pulse will be developed across a load resistor connected in series with the electrodes and collecting battery.

Experiments indicate that if the pressure in the SEMIRAD is maintained at less than 10^{-4} mm Hg, the current generated in a gamma field is of the order of 10^{-12} amperes/rad/sec for each square cm of surface of the positive electrode. Thus in a radiation field of 10^6 rad/sec a peak current of one μamp/sq. cm is expected.

While acceptable devices can be built in the laboratory if good vacuum equipment is available, uniformity of construction is difficult to maintain. Therefore several conventional vacuum diode tubes were tried out as SEMIRAD devices. The tubes selected for trial were:

Vacuum Diodes	6 x 4
	2 x 2A
	5675 (Triode with grid tied to center electrode)
Vacuum Photo Diodes	919
Vacuum Capacitors	VC50-5

These tubes were tested under moderate intensity, constant flux radiation environments (a 150 Kev X-ray machine and a 300 curie Cobalt[60] source) to find optimum operating voltages and to test dose-rate dependency. Figure 9 gives the SEMIRAD current, as read on a Kiethley electrometer, versus applied voltage.

These curves are useful, not only for selecting an operating voltage for the SEMIRAD, but also for estimating the amount of ionization current; as secondary electron current is proportional to the area of the emitter electrode, while the ionization current is not.

Figure 10 is a plot of SEMIRAD current as a function of radiation intensity for several tubes. Due to the very limited range of radiation intensities used here, these curves give only an indication of the dose rate independency desired in higher intensity fields. However, several experimental tubes that were known to have pressures of 10^{-3} mm Hg or more were found to be non-linear even in this range.
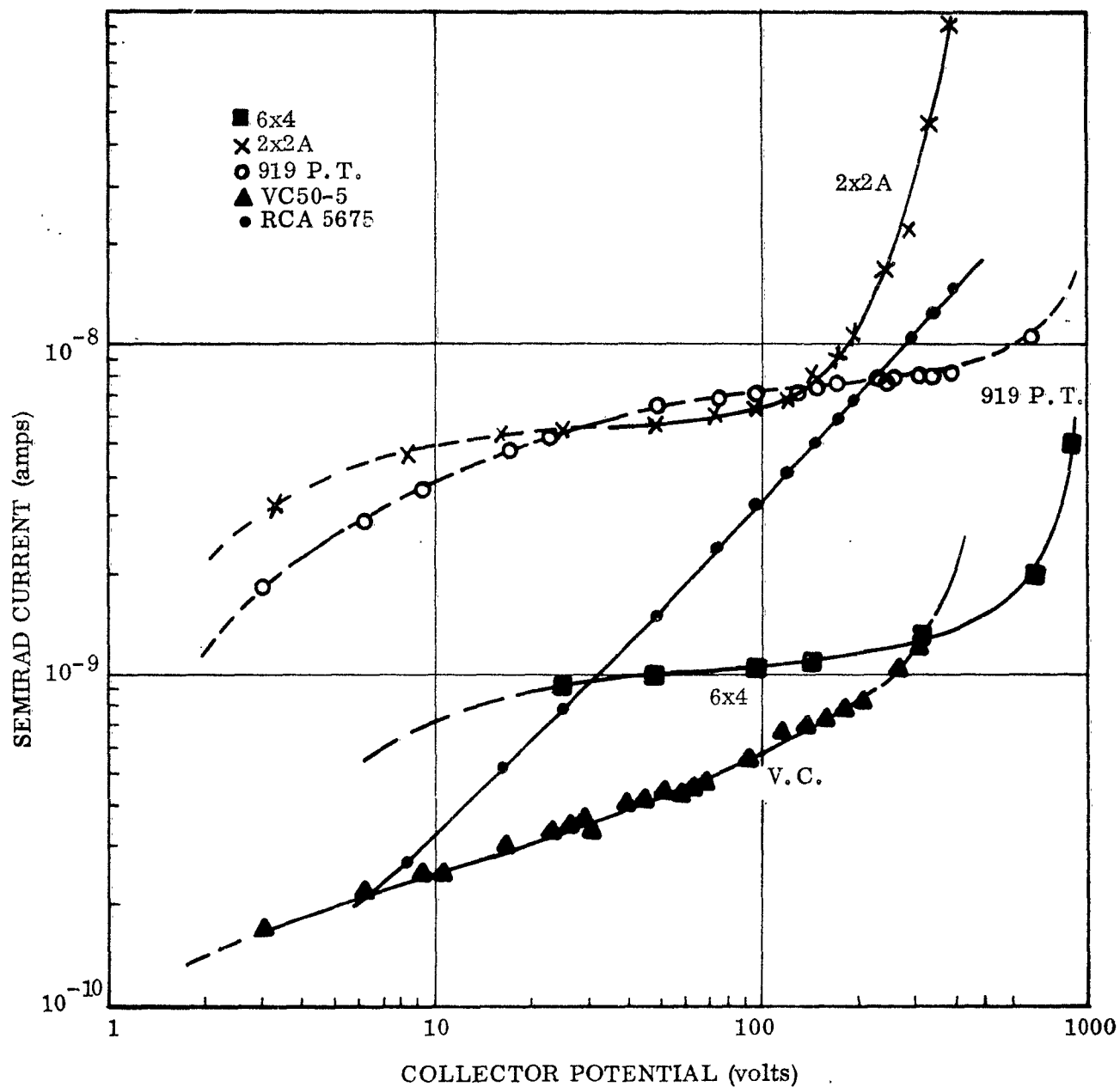
Figure 9 - Voltage Plateau of Devices Tested as Semirads.
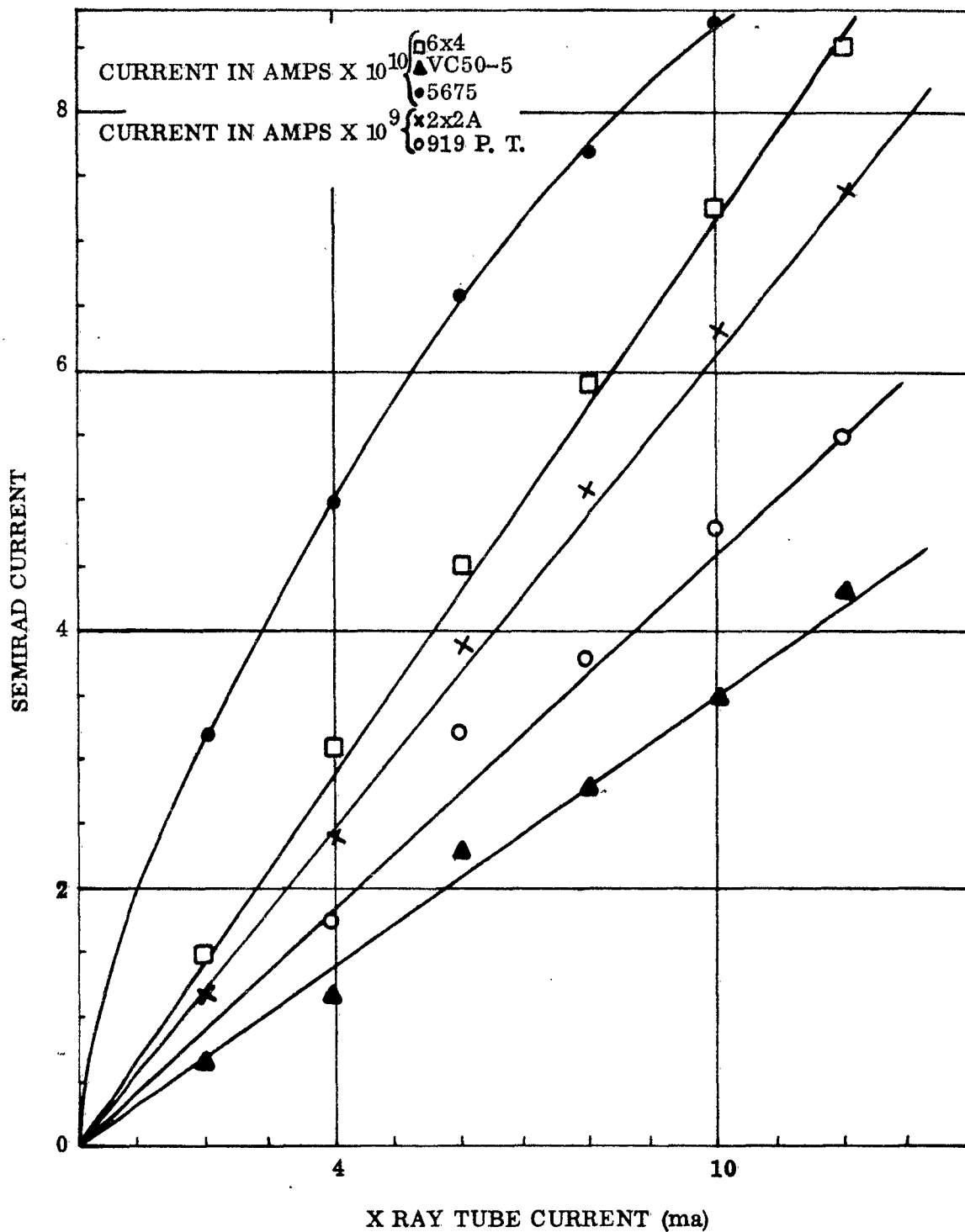
Figure 10 - Linearity of Devices Tested as Semirads.

The 6 x 4 vacuum diode was selected for experimental use at Kukla, due to its excellent voltage plateau and linear response. The plate and cathode were connected to the twin conductors of 20 feet of RG/22 coaxial cable and the connection potted with epoxy resin. The other end of the cable was connected to a 10 K load resistor and a 180 volt battery.

The signal developed across the 10K resistor was amplified and matched to cable impedance with $>10^6$ cps, two-stage amplifier and fed to an oscilloscope through another 125 feet of RG/22 terminated in a 100 ohm resistor.

DOSIMETRY RESULTS

PHOTODIODE DOSIMETRY RESULTS

The $1/\alpha$ values for all photodiodes and photomultipliers were measured and the results are tabulated in Table 2. The agreement in $1/\alpha$ values for PD-1 and PD-2 is good. The values from the 50 μs traces (PD-2, PM-3, PM-4) erable scatter. The fission rate at any time, t, during the early part of the burst was obtained from the relation:

$$\dot{F}(t) = \dot{F}(t')e^{\alpha(t-t')}$$

where $\dot{F}(t')$ is the fission rate read from the scope trace at time t'. The error associated with this calculated fission rate is given by:

$$\Delta\dot{F}(t) = \dot{F}(t)\sqrt{\left[\frac{\Delta\dot{F}(t')}{\dot{F}(t')}\right]^2 + \left[\frac{(t-t')}{(1/\alpha)}\frac{\Delta(1/\alpha)}{(1/\alpha)}\right]^2}$$

where $\Delta\dot{F}(t') = \pm .03 \times 10^{19}$ fissions/ sec from scaling the photographs only and $\frac{\Delta\alpha}{\alpha} = 7$ percent. $\dot{F}(t')$ is subject to possible systematic errors, such as calibration uncertainties, while the measurement of α depends only on linerity of response, not absolute calibration. Burst parameters are shown in Table 3.

The rate $\dot{F}(t_0)$ at the beginning of the sweep has been calculated for each burst from PD-1 and PD-2 traces and is shown in Table 4. The values obtained for $\dot{F}(t_0)$ are of the order of 10^{15} - 10^{16} fissions/second.

The rates $\dot{F}(t_0)$ can be obtained from the calibrated PM-3 and PM-4 traces and the amplified early portion of PD-2 by direct reading. They are of the order of 10^{14} fissions per second for PM-3, 10^{15} for PM-4 and 10^{17} - 10^{-18} for PD-2. The values from PM-3 and PM-4 are in rough agreement with the extrapolated values from PD-1 and PD-2 full traces so these trigger times were about the same.

TABLE 2

Values of $1/\alpha$ Obtained from Semilog Plots of Monitor Readings

Burst No.	PD-1[a]	PD-2[a]	PD-2[b]	PM-3[b]	PM-4[b]
1	--	--	--	--	--
2	68	64	--	--	--
3	--	39	--	--	--
4	39	39	--	--	--
5	36	38	--	--	--
6	99	105	--	--	--
7	76	75	--	--	69
8	63	60	( )	--	38
9	75	82	34	--	56
10	79	75	63	89	--
11	116	123	92	--	48
12	79	93	60	49	--
13	120	121	80	--	86
14	100	112	79	--	97
15	75	71	65	--	78
16	105	100	( )	( )	( )

a. Last two decades of exponential part of burst.

b. Fifty microsecond interval after trigger time.

TABLE 3

Photodiode Data
PD-1

Burst No.	Δt_- (μsec)	Δt_+ (μsec)	t_m (μsec)	$\dot{F}(t_m)$ (fissions/sec)	t' (μsec)	$F(t')$ (fissions/sec)
1	–	–	–	–	–	–
2	126 ± 10	336 ± 10	764 ± 10	$(2.70 \pm .03) \times 10^{19}$	536	$(.45 \pm .03) \times 10^{19}$
3	–	–	–	–	–	–
4	58	148	422	5.51	294	.90
5	54	126	376	6.35	282	1.80
6	176	410	1078	1.71	808	.45
7	140	312	872	2.67	692	.90
8	92	206	532	4.23	380	.90
9	126	294	760	2.49	600	.90
10	140	328	678	2.23	452	.45
11	228	515	980	1.29	684	.45
12	122	276	722	2.70	560	.90
13	212	495	938	1.25	670	.45
14	190	435	976	1.63	716	.45
15	138	304	782	2.47	554	.45
16	240	578	1422	1.27	1088	.32

Δt_- Time from 1/2 maximum to peak

Δt_+ Time from peak to 1/2 maximum on trailing edge of pulse

tm   Time to peak

TABLE 3 (cont'd)

Photodiode Data
PD-2

Burst No.	Δt_- (μsec)	Δt_+ (μsec)	t_m (μsec)	$F(t_m)$ (fissions/sec)	t' (μsec)	$F(t')$ (fissions/sec)
1	–	–	–	–	–	–
2	123 ± 10	228 ± 10	(*)	$(1.76 \pm .03) \times 10^{19}$	571	$(.48 \pm .03) 10^{19}$
3	84	136	374 ± 10	3.02	268	.96
4	66	101	409	4.28	300	.96
5	166	79	368	5.10	254	.96
6	182	284	1066	1.02	860	.48
7	125	194	853	1.72	674	.48
8	86	126	(*)	2.98	258	.48
9	118	198	738	1.65	560	.48
10	134	214	656	1.39	480	.48
11	190	306	934	0.61	720	.29
12	140	214	738	1.37	564	.48
13	194	300	890	0.66	646	.24
14	174	296	926	1.00	708	.384
15	122	204	754	1.60	556	.384
16	200	340	1387	0.66	1086	.165

*   Start of trace was outside field of view of scope camera

Δt_- Time from 1/2 maximum to peak

Δt_+ Time from peak to 1/2 maximum on trailing edge of pulse

t_m Time to peak

TABLE 4

Fission Rate at Start of Trace

Burst No.	PD-1	PD-2
1	--	--
2	1.6×10^{15}	$.65 \times 10^{15}$
3	--	9.9
4	4.7	4.4
5	7.2	12.0
6	1.3	1.3
7	1.0	0.5
8	21.7	8.6
9	3.0	5.1
10	14.6	8.0
11	12.4	8.3
12	7.5	11.0
13	16.9	12.0
14	3.5	7.1
15	2.8	1.5
16	0.1	0.03

PD-1 and PD-2 were not linear with respect to one another. A plot of PD-1 versus PD-2 showed gentle negative curvature from the rising portion of the burst and even greater curvature from the falling portion. A similar plot of PD-1 and PD-2 with respect to the pulse shape obtained from one of the experimental setups showed linearity for PD-2 on the rising portion only, and non-linearity for PD-1 over the whole burst (See Figures 11 and 12). PD-2 has been taken to be correct, and the experiments reported here have been analyzed in terms of PD-2 rates. The reason for these non-linearities is not yet known.

SULFUR DOSIMETRY RESULTS

Table 5 shows the integrated sulfur neutron and gamma ray fluxes for each burst. ΔT is the temperature rise of the reactor sphere, Z is the distance from the center of the sphere to the dosimeter, ϕ_s is the number of neutrons/cm^2 of energy > 2.5 Mev and must be multiplied by 5.4 to obtain the total neutron flux of all energies, and ϕ_γ is the total gamma ray dose in rads.

The neutron fluxes obtained from the radially positioned sulfur pellets, Table 6, have been multiplied by the squares of their respective distances and plotted in Figure 13. The data are consistent with a straight line of slope = - 0.4 percent per inch. Thus the inverse square law seems to hold from 4.2 inches out to 27 inches, with an apparent additional attenuation of 0.4 percent per inch.

The sulfur neutron doses obtained from the azimuthally arranged pellets are also shown in Table 6 and are plotted in Figure 14. The data show that neutron flux is independent of azimuth to within about ± 3 percent.

THRESHOLD DETECTOR MEASUREMENTS RESULTS

An array of three threshold detector systems was placed about Kukla. These were furnished and evaluated by Livermore Radiation Laboratory personnel. On this preliminary measurement a plutonium to sulfur ratio of about seven or eight was obtained. This value appears high in comparison with the Godiva II spectrum (Ref. 9). Due to the preliminary nature of these measurements, the Livermore Radiation Laboratory personnel advised that further calibration checks be made before using this data.

For the purpose of this report, Godiva II data were used to establish a plutonium to sulfur neutron ratio (Ref. 9 and 10). The results of past measurements are presented in Figure 15. A value of 5.4 has been chosen for a typical ratio at close range (less than 10 cm from the edge of the assembly). It is believed that, due to the similarity of the design, there should be little variation between the spectrum of Godiva II and Kukla.

Bare gold foils and cadmium-covered gold foils were placed at several distances from the center of the reactor to measure the thermal neutron flux in the room. The results are shown in Figure 16. The fact that the thermal neutron flux does not decrease with distance from the reactor implies that much of the flux results from scattering by the concrete walls of the room. Higher energy neutrons may be thermalized by such scattering, and thermal neutrons may make multiple traversals of the gold foils. The observed flux gives a measure of the total thermal neutron flux to which equipment in the room is exposed.

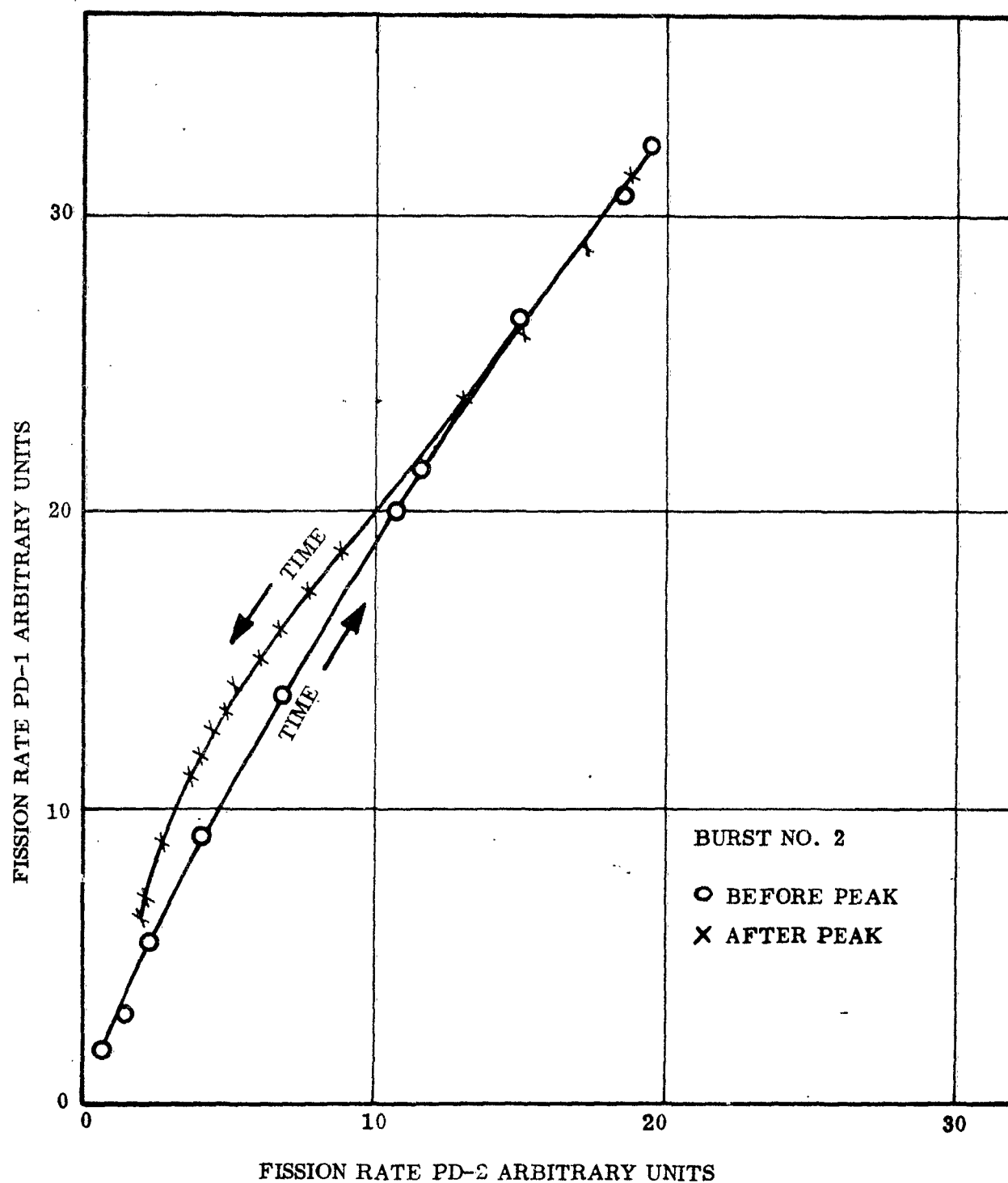Figure 11 - Comparison of the Response of Photodiode No. 1 and No. 2.

KUKLA BURST NO. 14

× PHOTODIODE NO. 1
O PHOTODIODE NO. 2

ARROWS INDICATE DIRECTION OF INCREASING TIME.
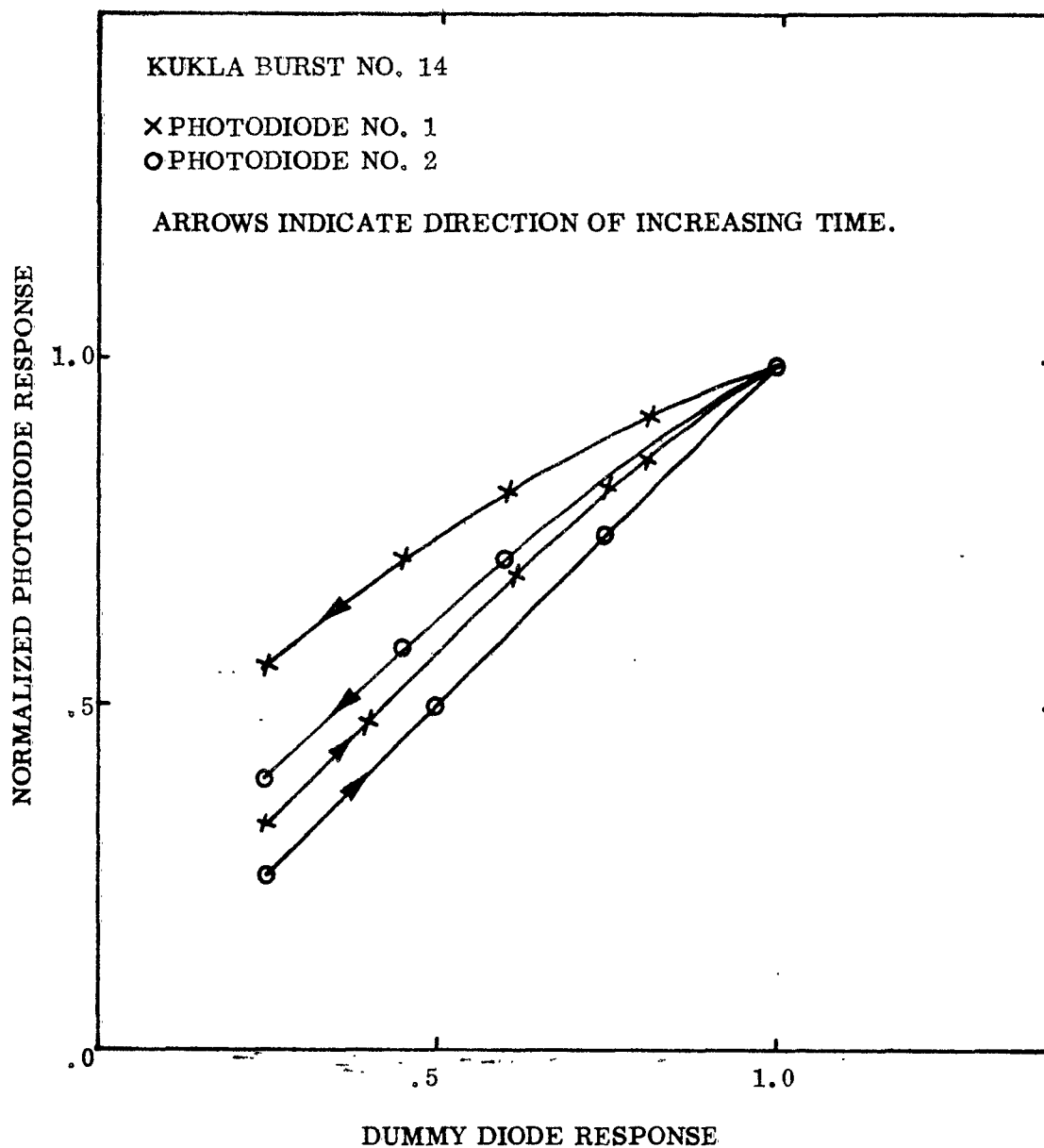
Figure 12 – Comparison of the Normalized Response of Photodiodes With
Dummy Diode.

TABLE 5

Sulfur Neutron Fluxes and Gamma Ray Doses

Burst No.	ΔT °C	Diode Z (inches)	Diode $\phi_s \times 10^{-11}$ (neutrons/cm²)	Diode ϕ_γ^α (rads)	Capacitor Z (inches)	Capacitor $\phi_s \times 10^{-11}$ (neutrons/cm²)	Capacitor ϕ_γ (rads)	Spark Z_s (inches)	Spark $\phi_s \times 10^{-11}$ (neutrons/cm²)	Gap Z_γ (inches)	Gap ϕ_γ (rads)
1	60	5.7±.25	—	—	9.6	3.87	590	—	—	—	—
2	59	"	4.14	—	8.5	( )	760	—	—	—	—
3	56	"	9.57	—	8.0	4.52	1000	32.8	.484	—	—
4	59	"	8.72	—	8.0	5.05	710	28.7	.547	—	—
5	62	"	8.58	1550	7.1	4.51	1000	"	.544	9.5	630
6	46	"	7.37	1100	6.8	9.97	860	26.0	.360	8.5	690
7	51	"	9.05	1440	7.1	}	~740	"	.410	"	630
8	56	"	7.93	1450	"	6.48	~1160	24.5	.453	7.5	990
9	45	"	7.82	1250	6.0	5.79	1250	25.5	.344	"	770
10	46	"	6.75	1500	5.6	3.98	1000	"	.341	"	770
11	43	"	6.24	1100	6.0	5.36	1350	"	.425	"	840
12	48	"	7.74	1300	5.6	7.78	1550	"	.366	"	1050
13	42	"	6.81	990	4.6	4.68	2100	"	.273	"	890
14	45	"	7.21	1700	6.0	3.71	780	"	.311	"	930
15	49	"	7.65	1450	7.1	5.70	920	24.75	.323	7.0	850
16	36	"	5.73	1100	5.2	—	1250	"	.247	"	880

α ± 10 percent for values ≤ 1000 rad, ± 15 percent for values > 1000 rad.

TABLE 6

Radial and Azimuthal Distribution of Neutron Flux

(a)

Z (inches)	$\phi_S \times 10^{-11}$ (neutrons/cm^2)	$Z^2\phi_S$ (arbitrary)
4 3/8	13.8	2.65
5 1/4	9.36	2.95
6 3/8	7.25	2.96
8 1/8	3.76	2.49
10 1/4	2.38	2.51
12 1/8	1.69	2.49
16 5/8	.928	2.57
20 1/8	.613	2.49
23 7/8	.409	2.34
27 5/8	.305	2.33

(b)

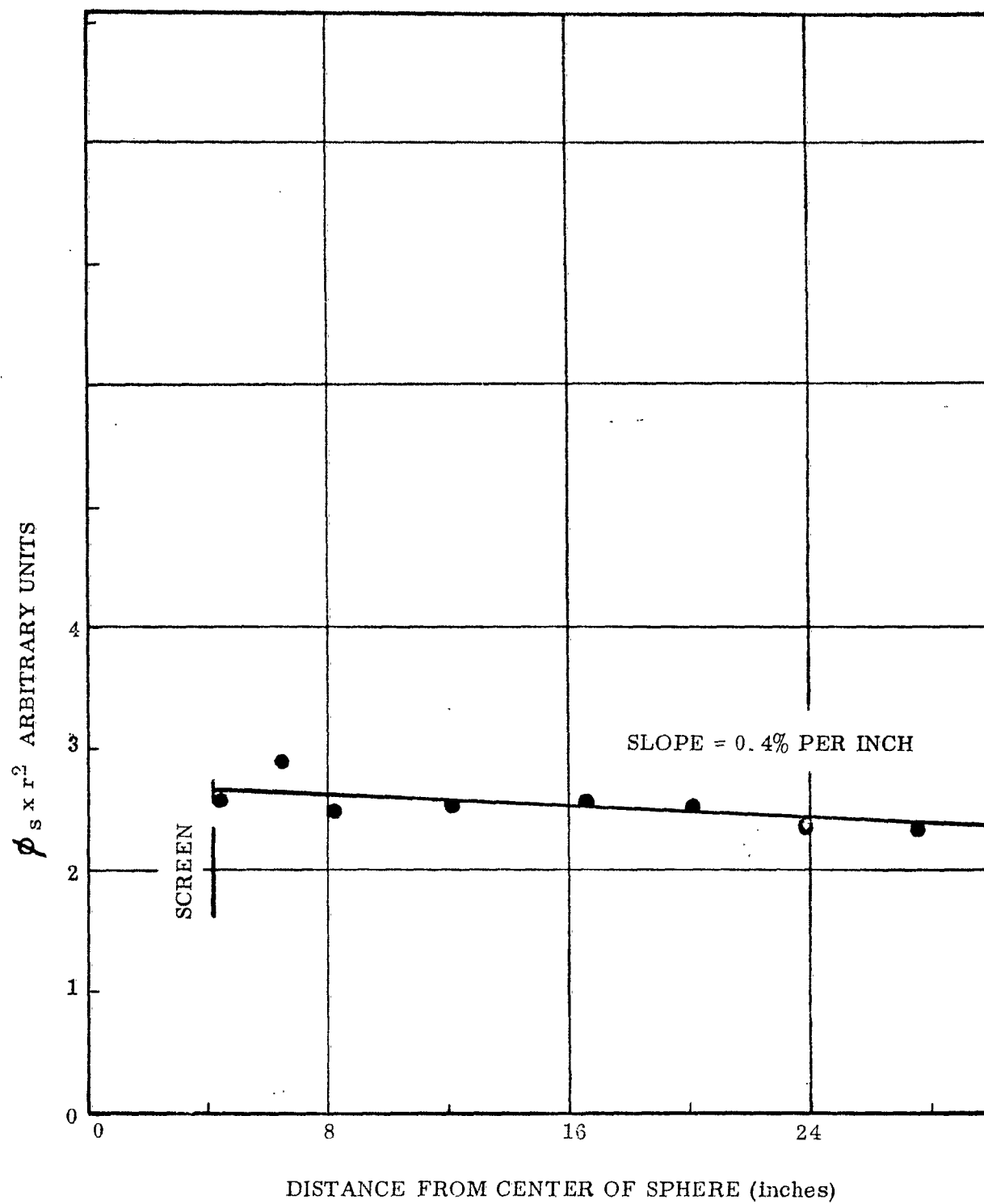| (deg)	$\phi_S \times 10^{-11}$ (neutrons/cm^2)
0	3.31
5	3.39
10	3.39
15	3.31
20	3.42
25	3.48
30	3.55
35	3.38

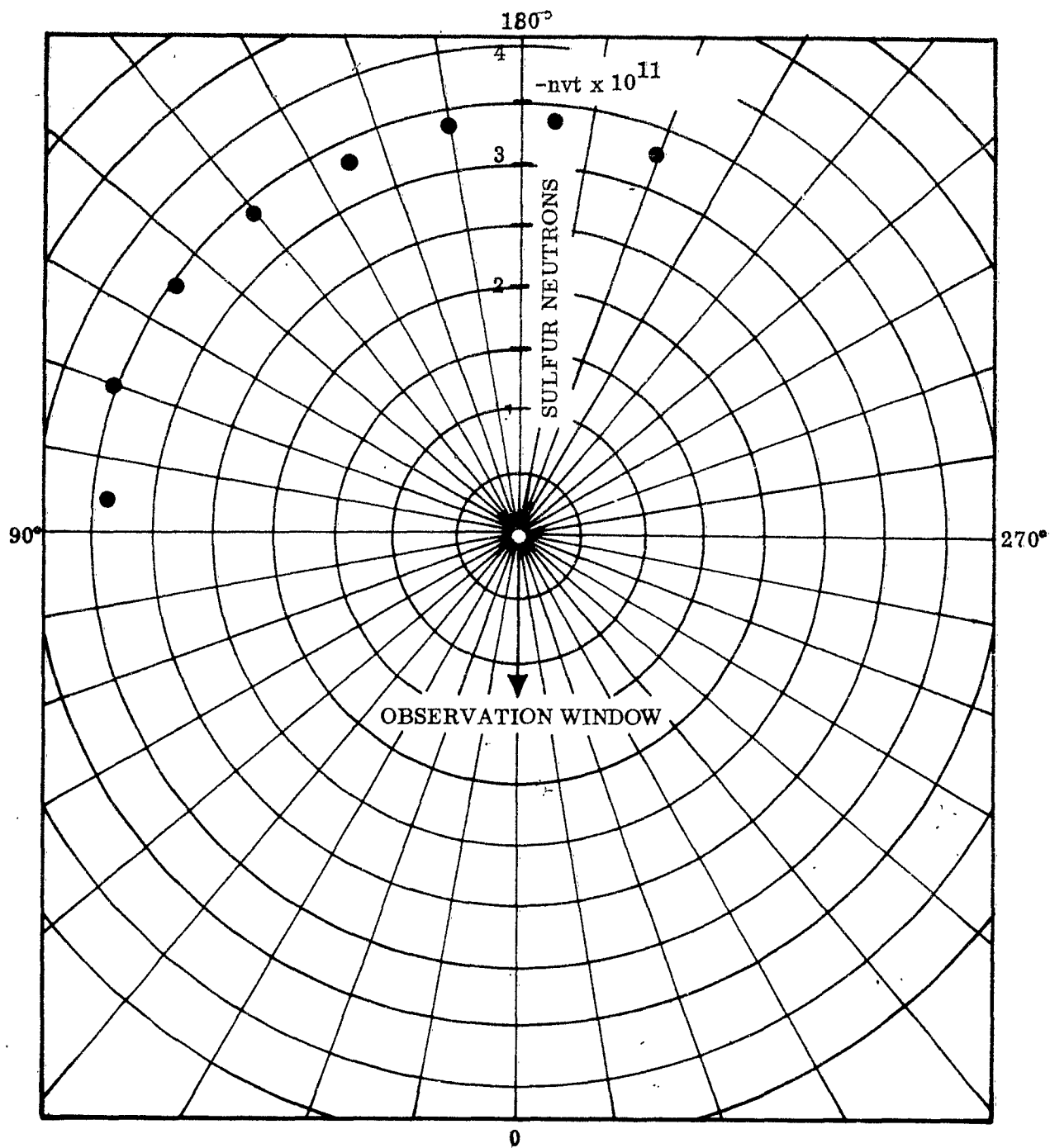Figure 13 – Radial Sulfur Neutron Distribution

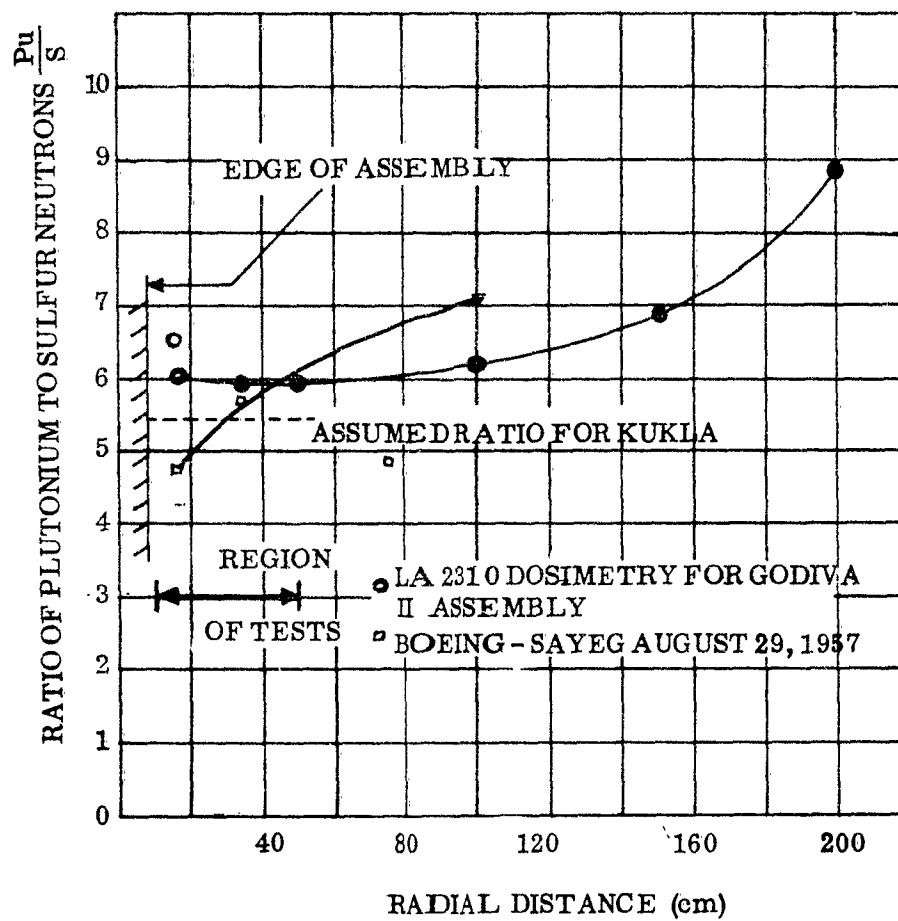Figure 14 – Azimuthal Sulfur Neutron Distribution at 9 Inches From Center of Shpere.

Figure 15 - Ratio of Plutonium to Sulfur Neutrons Versus Distance For
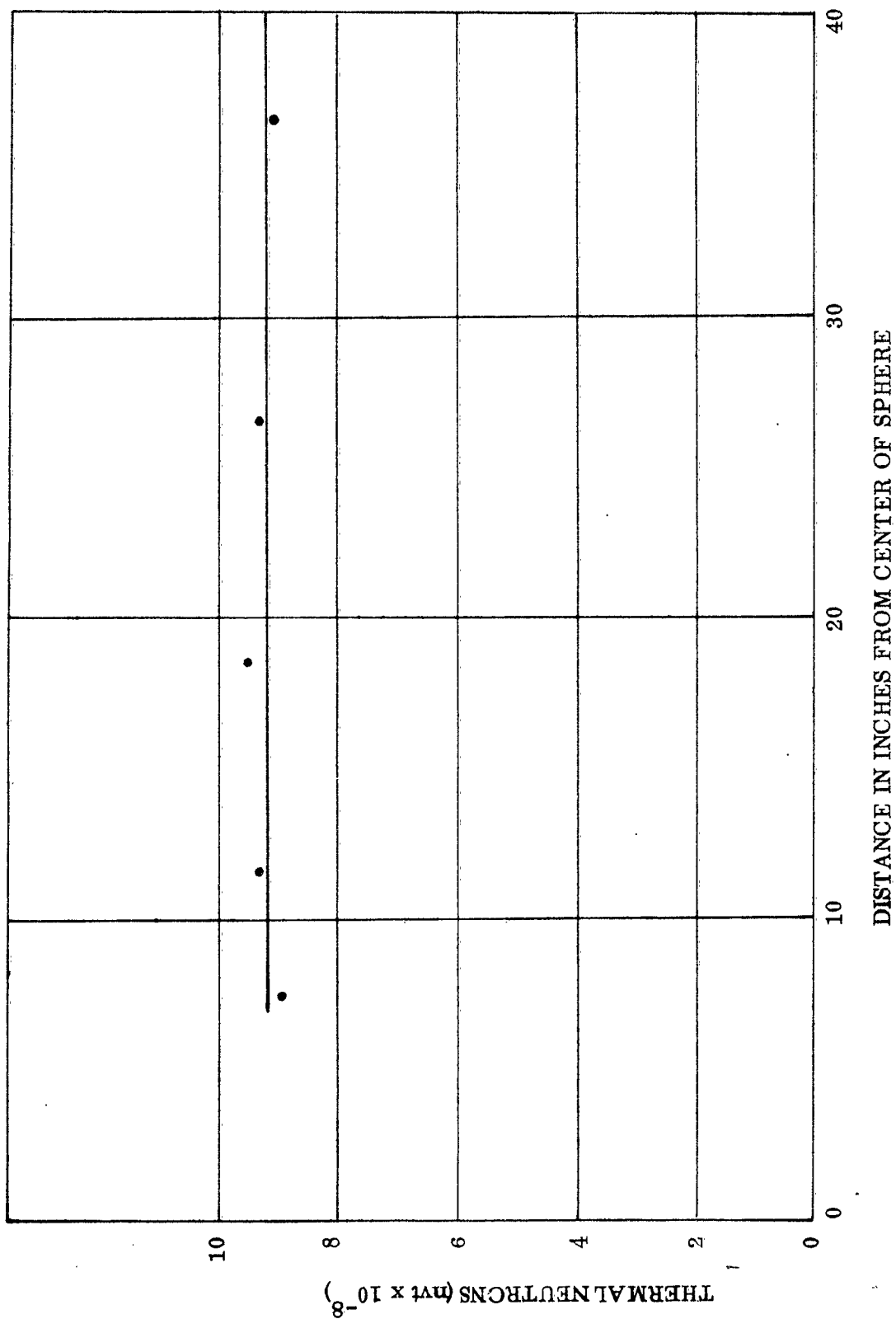Godiva II and Assumed Ratio for Kukla.

Figure 16 – Thermal Neutron Level in Reactor Room.

SIGOLOFF DOSIMETRY RESULTS

In order to obtain the gamma ray flux dependence on radial distance from the center of the sphere, the doses measured by the chemical dosimeters were normalized by dividing by the temperature rise of the burst and then these normalized values were plotted as a function of distance in Figure 17. Typical 10 percent and 15 percent errors are shown. The distribution is quite consistent with an inverse square dependence from 4.6 inches to 9 1/2 inches from the center of the sphere. The visual best-fit yields a slope of $(2.12 \pm {}^{.10}_{.31})$.

Having established the radial behavior of the gamma ray flux, we may obtain the dose rate at any distance using photodiode fission rates if the total gamma ray leakage energy per fission is known. The Sigoloff dosimeters provide a measurement of this total energy release. A comparison of the ratio of gamma to neutron fluxes from Kukla and Godiva is also made.

A plot of gamma dose versus temperature rise is shown in Figure 18, where the doses have been normalized to 5.7 inches by the inverse square law. A trend to lower doses at lower temperature rises is evident. A straight line fit through the origin would have a slope of about $(28.6 \pm {}^{9.0}_{6.0})$ rads/$^{\circ}$C. The sulfur pellet data gave $(1.47 \pm .65) \times 10^{10}$ sulfur nvt per $^{\circ}$C at 5.7 inches. Using 5.4 total neutrons per sulfur neutron we have 7.95×10^{10} neutrons/cm^2 per degree temperature rise. Then $(7.95 \times 10^{10})/(28.6) = (2.78 \pm {}^{.9}_{.6}) \times 10^9$ neutrons/cm^2 per rad. This number compares with 1.63×10^9 neutrons/cm^2 per rad for Godiva II (Ref. 11).

A measure of the gamma ray energy leaving the sphere may be obtained by converting the chemical dosimeter readings in roentgens to energy flux in Mev/cm^2 (Ref. 12). The conversion factor will depend on the gamma ray energy spectrum, but is nearly constant between 0.1 and 1.0 Mev and increases by~50 percent at 6.0 Mev. From the plot of gamma dose versus temperature rise we obtain a value 28.6 rad/$^{\circ}$C at 14.5 cm, or $28.6/.9 \cong 32$ roentgen/$^{\circ}$C. The number of fissions per degree temperature rise is 2×10^{14} (see Discussion of Kukla Flux Characteristics). Thus the number of roentgens/fission at 14.5 cm is 1.6×10^{-13}.

For one Mev gamma rays the conversion factor (Ref. 12) is 5.3 r per 1.06×10^{10} Mev/cm^2. The total gamma energy leakage would then be:

$$4 \pi (14.5)^2 \ \frac{1.06 \times 10^{10}}{5.3} \ 1.6 \times 10^{-13} = 0.84 \text{ Mev/fission.}$$

For various other effective gamma ray energies, the leakage energy per fission is shown in Figure 19. Although high accuracy is not obtained (2.0×10^{14} fission/$^{\circ}$C ~ ± 10 percent, 32 r/$^{\circ}$C ~ ± 25 percent, 0.9 rad/roentgen~± 10 percent, so~± 30 percent in Mev/fission) we have an absolute determination of the leakage gamma ray energy per fission. This agrees with the photodiode calibration factor, 0.8 Mev/fission, used by the Lawrence Radiation Laboratory.

SEMIRAD DOSIMETRY RESULTS

SEMIRAD pulses were obtained from a 6 x 4 vacuum tube mounted at $5.70 \pm .25$ inches from the Kukla center for ten of the sixteen bursts. The pulses were generally narrower, i.e., shorter widths at half maximum, than were those from the photodiodes, although they were wider

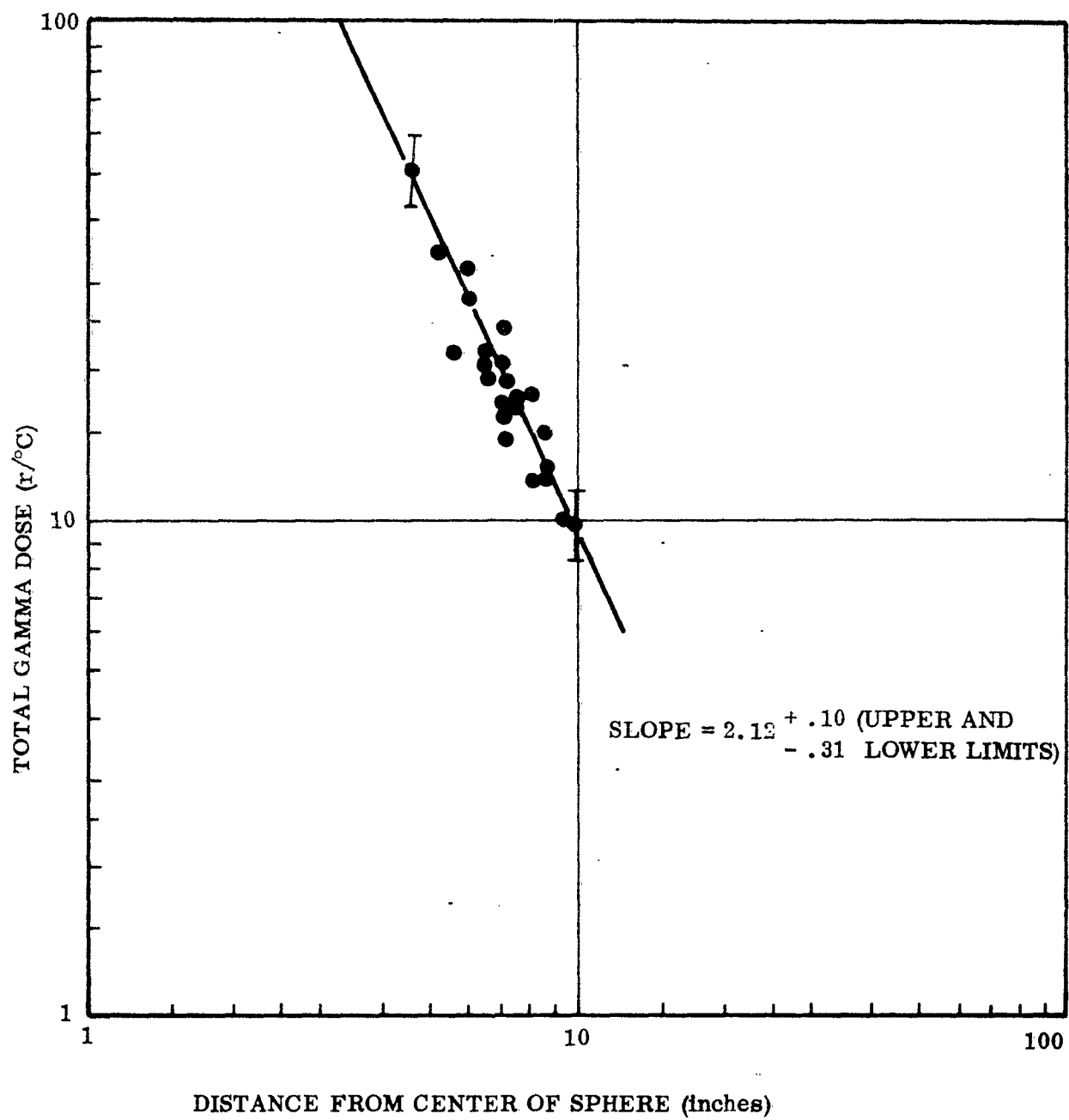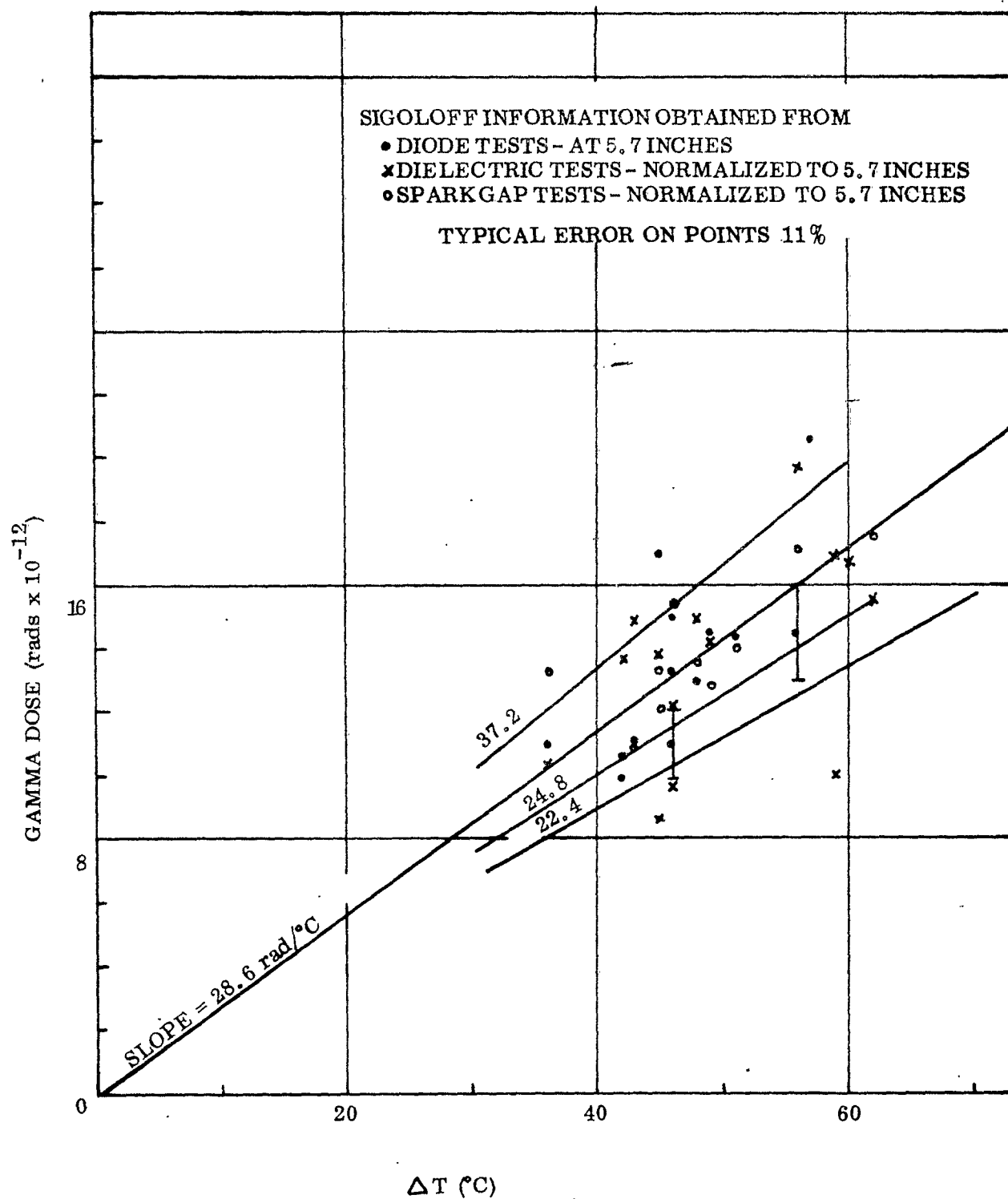Figure 17 – Total Gamma Dose/°C Versus Distance.

Figure 18 - Total Gamma Dose at 5.7 Inches Versus Temperature Rise
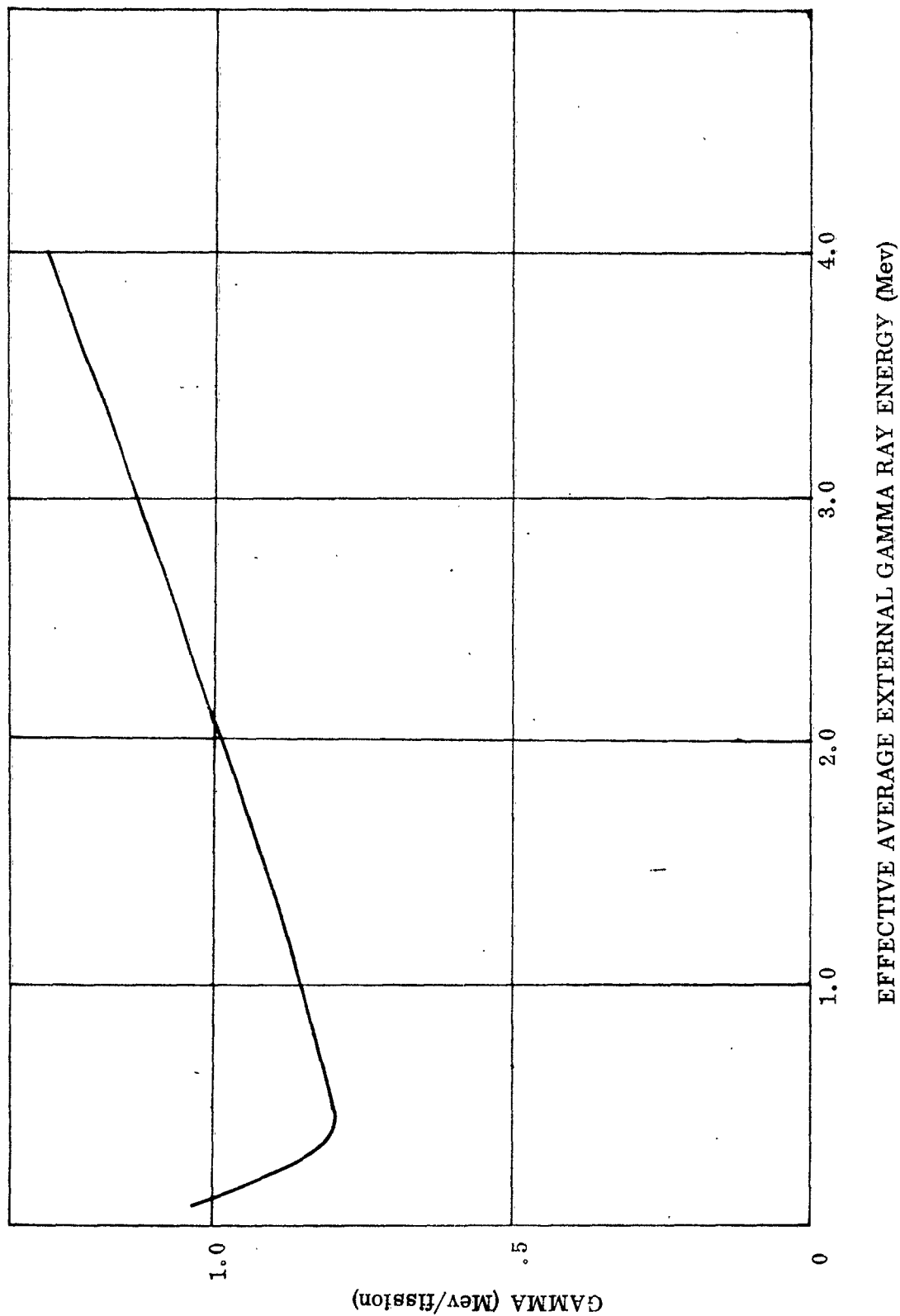of Critical Assembly.

Figure 19 – Mev of Gamma Ray Energy Per Fission Versus Effective Average Energy of Gamma Rays Leaving Sphere.

near the base line. For five of these ten bursts there was fair agreement between the SEMIRAD and photodiode pulses, especially in the first half of the pulse. To illustrate this, comparison plots of the SEMIRAD and photodiode pulses for burst numbers four and five are shown in Figure 20. The pulses are normalized to the same peak height and plotted against time before and after the peak using the same center line.

Burst five is an example of the several bursts for which the SEMIRAD and photodiode pulses are in fairly good agreement. The differences in the pulses ahead of the peak are no more than the reading errors involved. There are definite differences in the pulses for the other five bursts, however, as illustrated in the comparison plot for burst number four.

Since α as computed for the early rising portion of the pulses, the peak rates, and the first half widths, is much more consistent for the photodiode than for the SEMIRAD, it is believed that the SEMIRAD techniques developed by Boeing do not yet provide a good diagnostic tool. The inconsistencies in the SEMIRAD pulses, however, are thought to be due more to the electronics of the system than to the 6 x 4 itself.

The use of a detector with larger emitter area and greater interelectrode spacing, such as the 2 x 2A or 919 phototube, along with an improved amplifier should provide more consistent results.
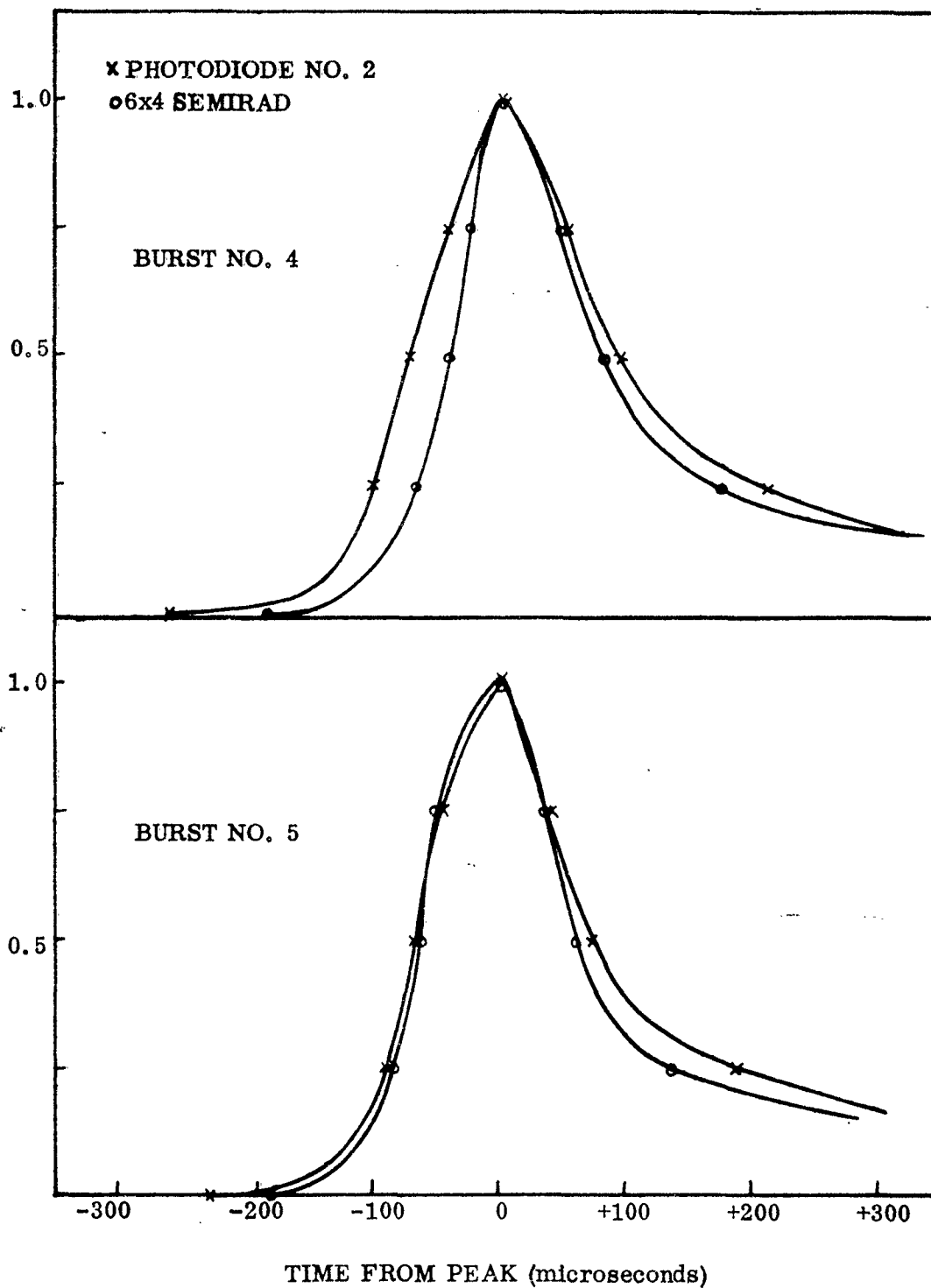
Figure 20 – Comparison of Semirad and Photodiode Pulse Shapes.

DISCUSSION AND CONCLUSIONS

TEST DOSIMETRY

The diagnostic photodiode provided by the Lawrence Radiation Laboratory (LRL) turned out to be the primary tool for the test dosimetry. The inconsistency in the two photodiode traces was not resolved, but since photodiode number two provided the most consistent check with the theoretical operation of the reactor, it was used for all measurements. The calibration of the photodiode as quoted by LRL was checked independently by the Boeing total integrating dosimeters.

The first check was on the assumed energy release in gamma ray energy. As was shown in the section on results, the value of 28.6 rad/$^\circ$C as measured with the Sigoloff gamma ray dosimeters gives an energy release of 0.84 Mev/fission $\pm$ 30 percent, which agrees with the value of 0.8 Mev/fission that was assumed in the Lawrence Radiation Laboratory calibration procedures.

The second check was on the fission rate calibration. The integral was taken under the prompt portion of the burst as defined by the photodiode and as described in detail in the section on Kukla theory and operation. This total number of fissions was related to the sulfur neutron numbers by assuming 5.4 total (plutonium) neutrons per sulfur neutron. The number of sulfur prompt neutrons was corrected for the fissions occurring in the delayed tail by subtracting out a constant value as defined in the section on Kukla theory and operation. The resultant neutron flux and total fission numbers yield a value of 1.2 leakage neutrons per fission. This number agrees roughly with the value 1.4 used in the Lawrence Radiation Laboratory calibration.

The first half of the photodiode curve is independent of the tail of the burst, so that relative dose rates from burst-to-burst should be accurate. For this reason, and since the photodiode calibration has been independently checked, the neutron dose rate $\dot{\phi}_n(t)$ at each experimental setup covered in this report was taken to be:

$$\dot{\phi}_n(t) = \frac{\dot{F}(t)\ (1.4)}{4\pi\ r^2} \quad \text{where}$$

$\dot{F}(t)$ = fissions/second as read from calibrated trace of PD-2.

1.4 = prompt neutrons/fission leaving the sphere.

r = distance from center of sphere to experimental position.

The gamma ray flux was obtained from $\dot{F}(t)$ and the curve of Figure 21. This curve assumes 0.8 Mev gamma ray leakage per fission and inverse square radial dependence. This procedure will not compensate for variations in flux at each experimental setup caused by scattering from nearby material.
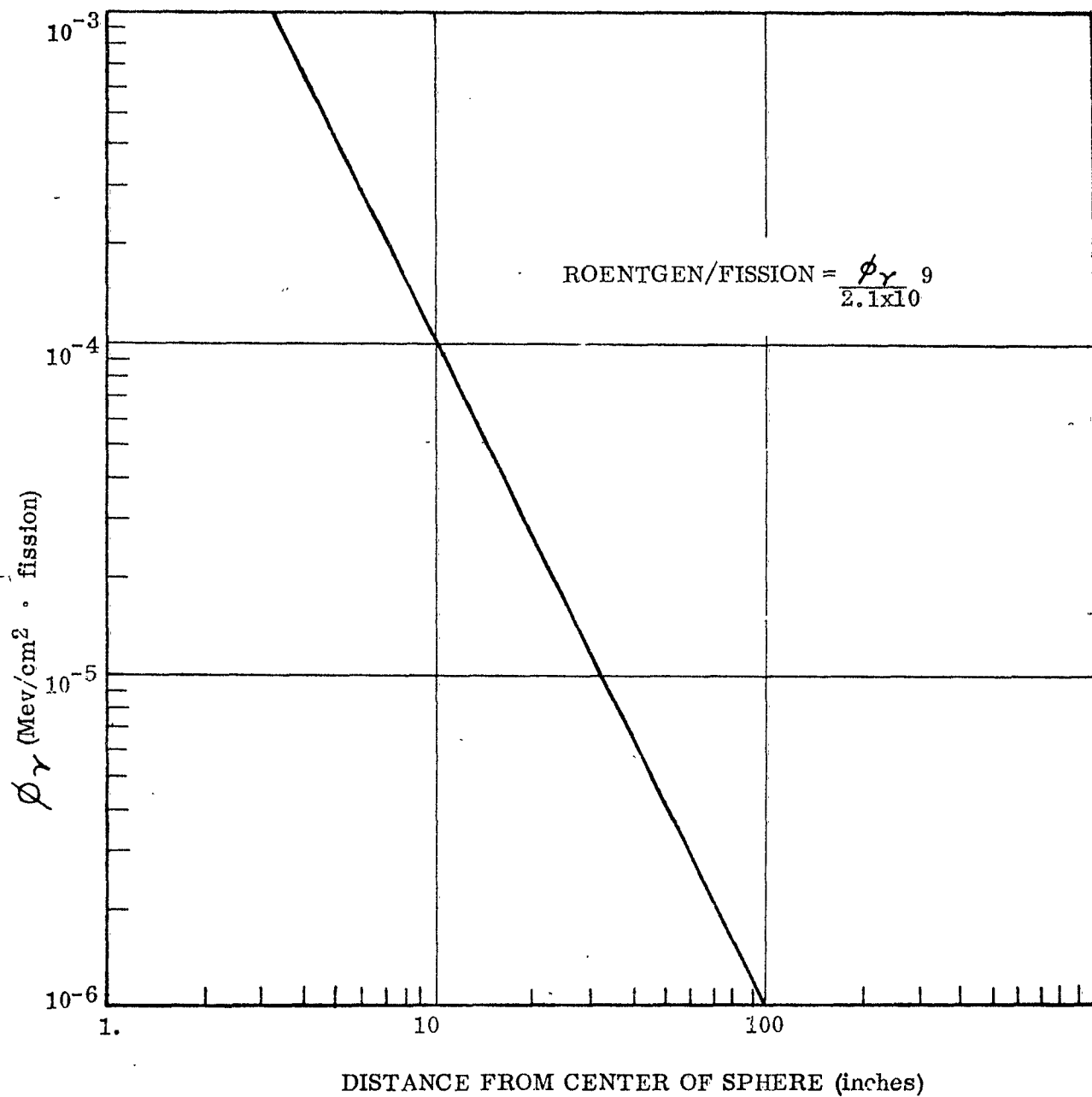
Figure 21 – Gamma Dose Per Fission Versus Distance Based on 0.8 Mev Leakage Per Fission and Inverse Square Law.

For times so early that the deflection of the scope trace from PD-2 could not be read, the fission rate $\dot{F}(t')$, measured at time t' on the rising exponential portion of the curve, was extrapolated back using the measured alpha and the relation:

$$\dot{F}(t) = \dot{F}(t')e^{\alpha(t-t')}$$

The values used are shown in Table 7.

The error in α^{-1} is estimated to be $\pm$ seven percent and that in $\dot{F}(t')$ to be $\pm .03 \times 10^{19}$ fissions/sec. The percentage error in the extrapolated values of $\dot{F}(t)$ will increase with increasing time intervals of extrapolation, and will be larger for smaller values of $\dot{F}(t')$. For large time intervals the error in $(\Delta\alpha^{-1})/(\alpha^{-1})$ will dominate because of the multiplier $(t-t')/(\alpha^{-1})$. See discussion in section on Dosimetry Results. An extrapolation to the start of the photodiode two trace of burst two may result in an error on $\dot{F}(t_o)$ of ± 60 percent, for example.

KUKLA FLUX CHARACTERISTICS

Analytic expressions for the time dependent behavior of a critical assembly such as Kukla have been derived (Ref. 11). Assuming that the delayed neutron contribution can be neglected during the prompt burst, the following relationships hold:

$$\dot{F}(t) = \frac{4\dot{F}(t_m) e^{\alpha(t-t_m)}}{\left[1 + e^{(t-t_m)}\right]^2} \tag{1}$$

$$w = \frac{1}{\alpha} \ln \left[\frac{3 + 2\sqrt{2}}{3 - 2\sqrt{2}}\right] = 3.52 \frac{1}{\alpha} \tag{2}$$

$$\dot{F}(t_m) = \frac{\alpha \int_{-\infty}^{\infty} \dot{F}(t) \, dt}{4} \tag{3}$$

where
$\dot{F}(t)$ = fission rate as function of time, t,
α = constant
w = full width at half maximum
t_m = time at maximum fission rate

It has also been found (from Ref. 11) for Godiva II that: $\alpha = 500\Delta T$, where ΔT is the temperature rise of the critical assembly in degrees centigrade, and alpha is in reciprocal seconds. With these relationships, one need know, in principle, only the temperature rise, the radial fall-off in intensity, and the leakage constant for neutrons and gamma rays in order to calculate the flux rate at any time at any position with respect to the critical assembly. However, the temperature rise is a measure of the total number of fissions, while the equations above apply to the fissions during the prompt part of the burst, so that a correction for the tail of the burst is required.

TABLE 7

CHARACTERISTICS OF KUKLA BURSTS

Burst No.	ΔT °C	$1/\alpha$ usec	$2\int_{-\infty}^{tm} F(t)dt$ fissions [a]	$2W_{1/2}$ usec [b]	$\dot{F}(t)_{max}$ fission/sec
1	60	--	--	--	
2	59	$64\pm7\%$ [c]	$4.55\times10^{15}\pm3\%$ [d]	246 ± 10 [d]	$1.76\times10^{19}\pm.03\times10^{19}$ [d]
3	56	39	5.37	168	3.02 "
4	59	39	7.22	132	4.28 "
5	62	38	7.80	132	5.10 "
6	46	105	4.18	364	1.02
7	51	75	4.80	249	1.72
8	56	60	5.41	178	2.98
9	45	82	4.65	234	1.65
10	46	75	4.20	268	1.39
11	43	123	2.48	412	.61
12	48	93	4.09	280	1.37
13	42	121	3.23	388	.66
14	45	112	5.15	348	1.00
15	49	71	4.69	244	1.60
16	36	100	2.38	400	.66

a. $2\int_{-\infty}^{tm} F(t)dt$ = twice the integral of the fission rate up to the peak of the burst.

b. $2W_{1/2}$ = twice the time between the first 1/2 maximum and the peak of the burst.

c. Errors in measuring photos plus error in visual st. line fit.

d. Errors in measuring photos only.

The contribution from this tail is reported (Ref. 11) to be a constant for nominal bursts of Godiva II; hence could be subtracted out. The resultant neutron dose is then proportional to the total fissions during the prompt part of the burst, and so the above relationships still hold with $\dot{\varphi}(t)$, the prompt neutron dose rate, substituted for $\dot{F}(t)$. IBM has taken this approach.

In order to test the reactor theory and the empirical relationships stated above, the dosimetry data from the Kukla tests have been analyzed in a variety of ways. The agreement is generally good, and only the empirically determined dependence of $1/\alpha$ on ΔT for Godiva II seems to be inconsistent with Kukla data.

The relation $w = (1/\alpha)\, 3.52$, defined in (Ref. 11), has been tested by taking w to be twice the time interval, Δt-, from the first 1/2 maximum point to the peak of the PD-2 curve. Figure 22 shows the agreement.

The relation $F(t_m) = \frac{\alpha}{4} \int_{-\infty}^{\infty} F(t)\, dt$ has been tested by taking $\int_{-\infty}^{\infty} F(t)\, dt$ to be twice the area under the curve up to the peak. Figure 23 shows the agreement. Thus equation (1) above adequately describes the symmetric curve obtained by reflecting the rising portion of the fission rate curve about the peak value. Figure 24 is a plot of $1/\alpha$ versus ΔT, the temperature rise. The form $\alpha = $ (constant) x ΔT, as reported by IBM, is not well verified. The data would seem to be roughly represented by $\Delta T = (65 - \frac{0.18}{\alpha})$ for these low yield bursts, where $\Delta T = $ degrees centigrade and $1/\alpha = $ microseconds. More data will be required, preferably with larger temperature rises, to determine if a clear relationship exists. The relatively low temperature rises of the sixteen bursts of this series are associated with the fact that the facility had only recently become operational. Maximum burst levels were not then being attempted. This series comprised the 25th through the 40th bursts of the device.

Figure 25 shows a plot of twice the integrated number of fissions up to the peak of the burst versus the neutron flux measured at the screen by means of sulfur pellets. Only bursts eight through sixteen were monitored at the screen, so the first seven shots are not displayed.

A tentative straight line is drawn through the points, having an intercept on the abscissa at 5.6×10^{11} sulfur nvt. This line has the form:

$$\text{Total prompt fissions} = \text{constant x (Sulfur nvt} - 5.6 \times 10^{11})$$

The constant obtained from the slope of the line is 6.2×10^3 fissions/sulfur nvt. The number of leakage neutrons per fission is then $\frac{4\pi r^2}{(6.2 \times 10^3)} \times 5.4 = 1.2$, where 5.4 is the ratio of the flux measured by plutonium foils to the flux measured by sulfur pellets. The value 1.2 compares with the value 1.4 used in the Livermore Radiation Laboratory photodiode calibration. This provides a rough independent check of the PD-2 calibration.

Figure 26 is a plot of twice the integrated number of fissions up to the peak of the burst versus temperature rise of the sphere. The slope of the visual-best-fit straight line is $(1.94^{+.7}_{-.3})$ x 10^{14} fissions per degree centigrade. From the known mass (59.2kg) and specific heat (0.028 cal/gm°C) of the uranium sphere, and making the approximation that all of the 200 Mev per fission energy release remains in the sphere, the value 2.15×10^{14} is obtained.
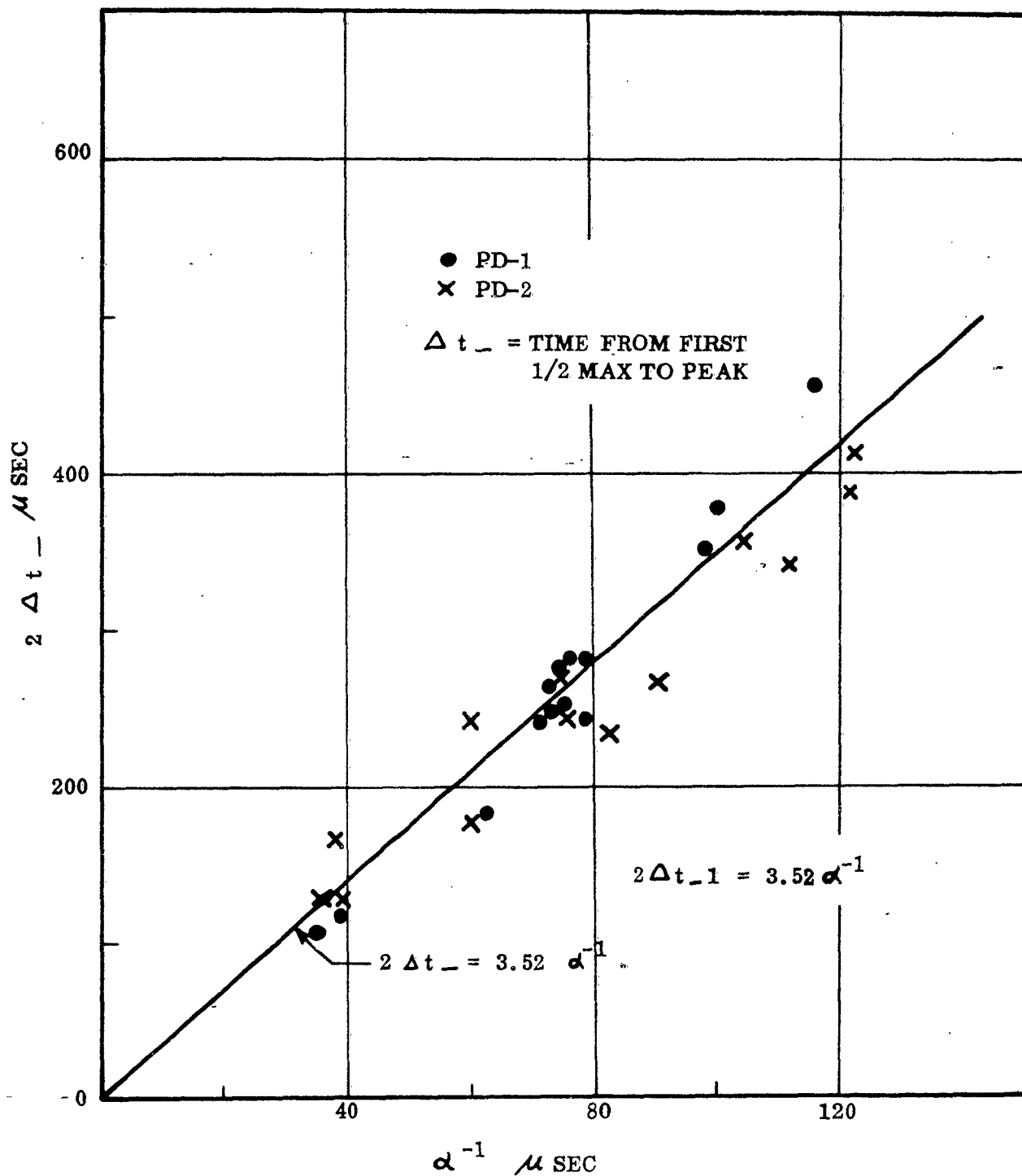
Figure 22 - Comparison of Kukla Burst Data With Analytical Expression for Pulse Width.
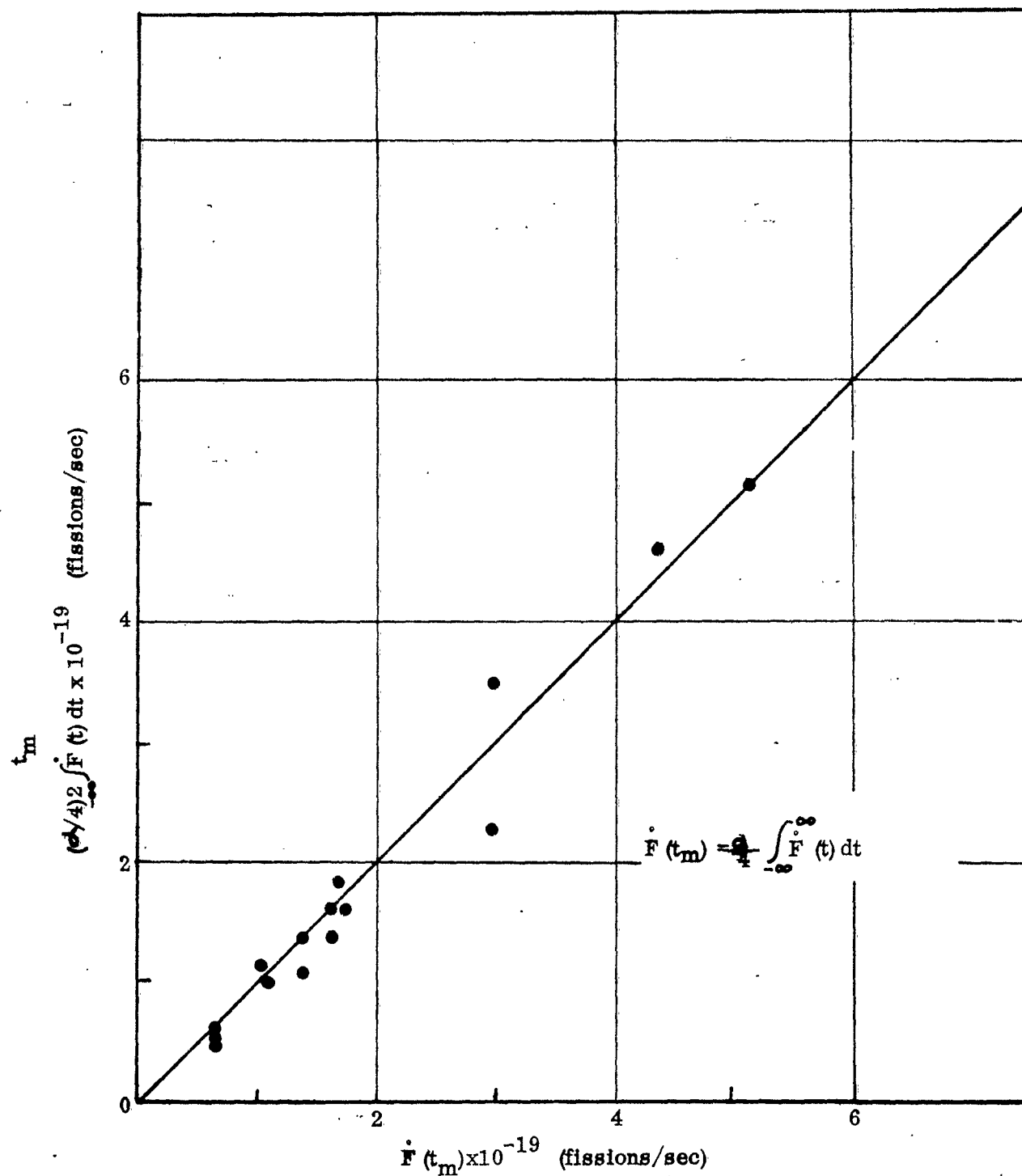
Figure 23 - Comparison of Kukla Burst Data With Analytical Expression
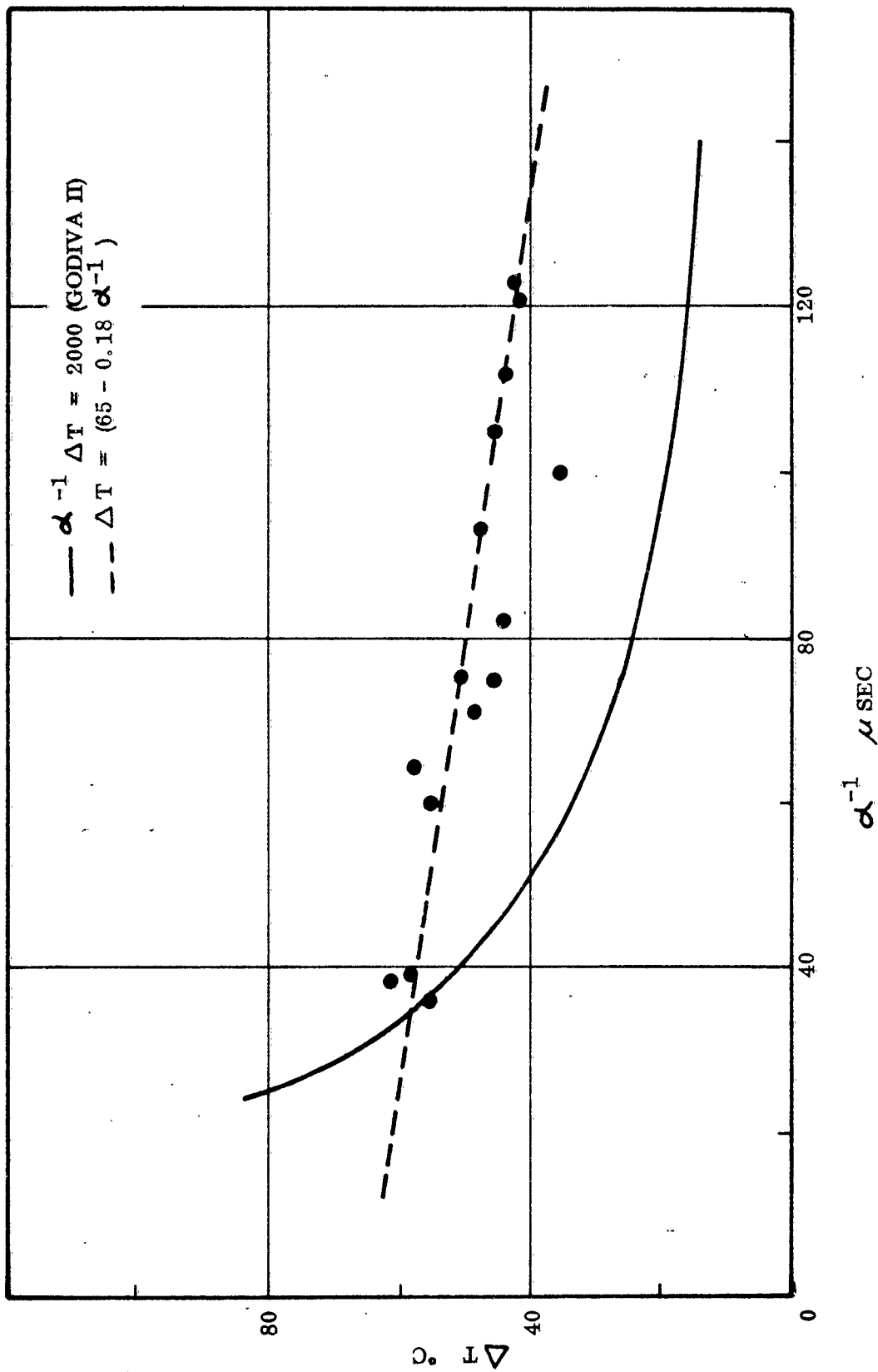for Fission Rate.

Figure 24 – Plot of α^{-1} Versus Temperature Rise ΔT. Solid Line Is Empirical Relationship Measured for Godiva II.
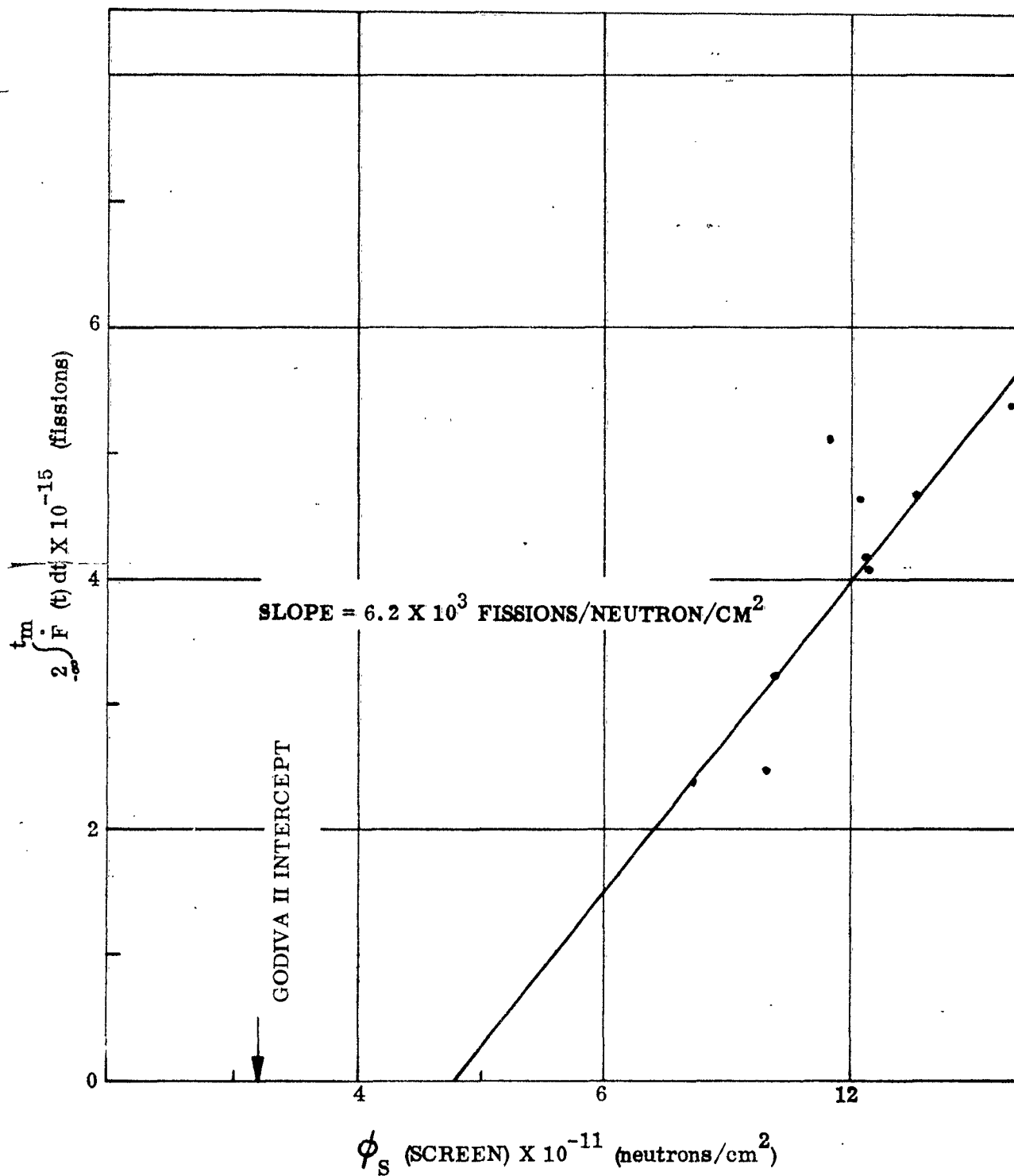
Figure 25 – Sulfur Neutron Dose Measured at the Screen Versus Total
Fissions Under Prompt Peak.
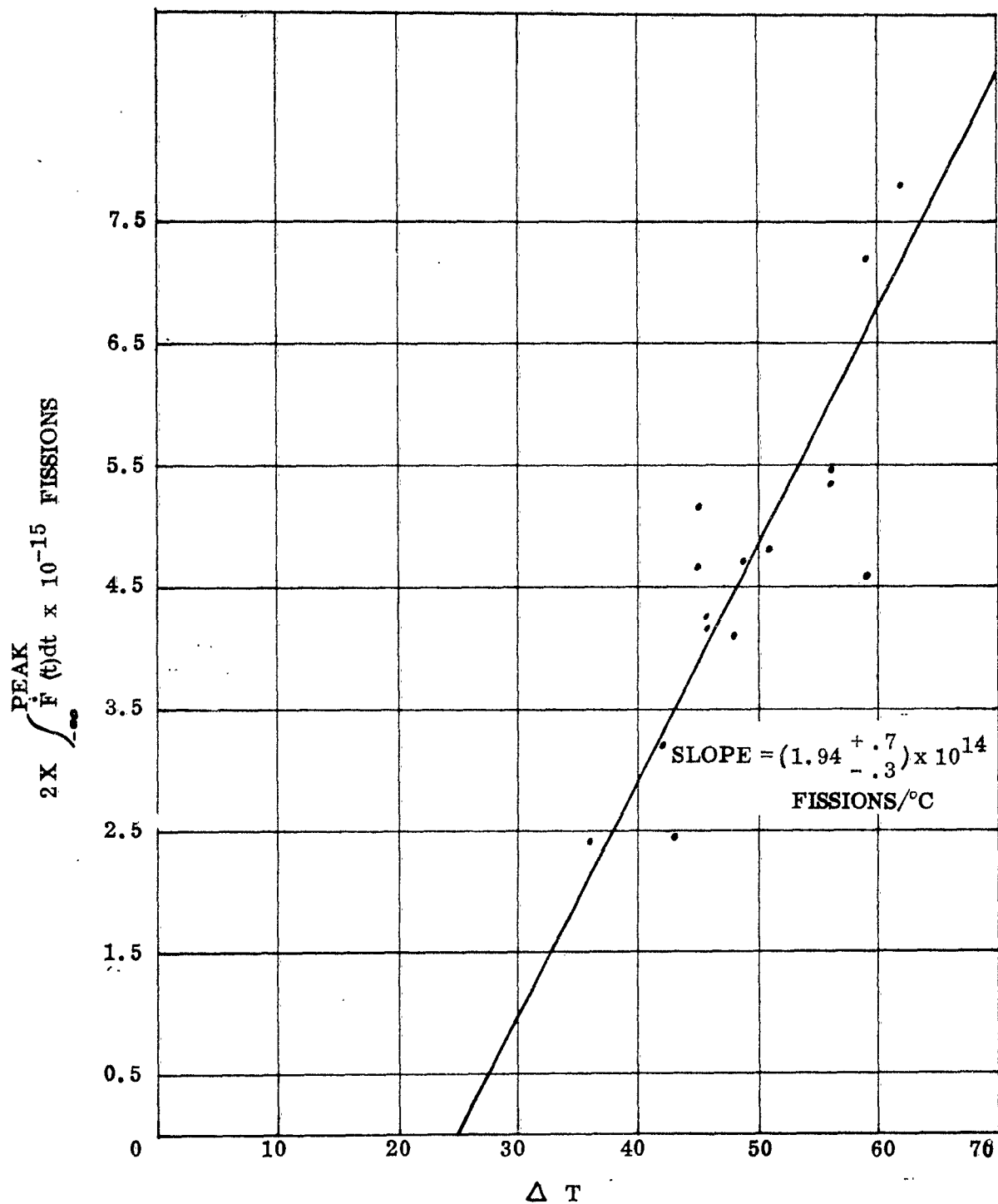
Figure 26 – Total Prompt Fission Versus Temperature Rise of Critical Assembly.

The y-axis is labeled $2X \int_{-\infty}^{PEAK} \dot{F}(t)dt \times 10^{-15}$ FISSIONS with values 0.5, 1.5, 2.5, 3.5, 4.5, 5.5, 6.5, 7.5.

The x-axis is labeled Δ T with values 0, 10, 20, 30, 40, 50, 60, 70.

$$\text{SLOPE} = \left(1.94 \begin{array}{c} + .7 \\ - .3 \end{array}\right) \times 10^{14}$$
$$\text{FISSIONS/}^\circ C$$

RECOMMENDATIONS

Several improvements in the dosimetry techniques immediately suggest themselves. One of the easiest and potentially most useful is an extension of the time interval observed on the photodiode traces to include all of the burst. If ~99 percent of the energy release could be monitored, then the area under the photodiode trace could be plotted as a function of temperature rise, total neutron dose (sulfur or other monitors), and total gamma dose. Linearity in such a graph would imply linearity of the photodiode response and at the same time would provide an independent calibration of the photodiode to the extent that the total dose monitor calibrations were known. In line with this procedure, a duplicate set of traces, as was attempted with PD-1 and PD-2, would of course be highly valuable.

The temperature rise by itself would appear to have possibilities as a total fission monitor. The energy liberated per fission is relatively well known, and the nuclear radiation energy escaping from the reactor is small and known approximately. Thus a knowledge of the specific heat of the reactor material and the temperature rise will allow a calculation of the total number of fissions, provided the temperature measured is effectively the uniform temperature of the reactor and the heat loss is small and/or known. Photodiode fission data in this report (Figure 26) agree within the experimental uncertainties (~30 percent) with the total fissions calculated from the temperature rise as presently measured, so the method looks promising.

Considerable work remains to be done with threshold detectors. The neutron energy spectrum outside Kukla has not been measured to any extent, although there is no reason to believe it is different from that of other prompt reactors such as Godiva. In particular the conversion factor to obtain total neutron flux from sulfur pellet data has considerable uncertainty. More intensive application of present techniques is required.

The effect of nearby material on neutron and gamma fluxes is not well known although it has been suggested that the effect is large (Ref. 13). Controlled experiments with and without nearby equipment would help to resolve this question. Particular attention to commonly used experimental material might be helpful, e.g., dosimeters potted in Silastic, enclosed in metallic cans, etc.

Calculations of the radial dependence of the gamma flux indicate that the radial fall-off near the reactor surface should be less steep than an inverse square dependence. Although only approximate, the calculations make one uncomfortable about using the inverse square law within a few inches of the reactor surface, where most of the radiation damage tests are performed. A more accurate measurement of both the gamma ray and neutron flux fall-off with distance is desirable. Measurements all the way to the surface of the reactor should be made in an effort to obtain some indication of deviation from an inverse square dependence. Gamma dosimeters smaller than the Sigoloff type (e.g., glass Ref. 5) would be useful.

After an extended period of non-operation of the reactor, when the residual activity is small, the reactor could be operated in a continuous manner at a low power level, and standard counter techniques employed to measure the gamma ray and neutron energy spectra. This program would require a sizeable effort, but the information sought is highly desired.

REFERENCES

1. Techniques of Measuring Neutron Spectra with Threshold Detectors-Tissue Dose Determination, Hurst et al., Rev. Sci. Instr. 27, 153 (1956).

2. Equivalent Gamma Flux Outside of.Kukla, W. F. Lindsay, Lawrence Radiation Laboratory internal report, UOPB 60-17.

3. Exposure performed by Dr. J. Sayeg, Los Alamos Scientific Laboratory.

4. First International Conference on Peaceful Uses of Atomic Energy, Vol. 2, p. 198, and Second International Conference, Vol. 15, p. 366.

5. Radiation Accidents: Dosimetric Aspects of Neutron and Gamma Ray Exposures, ORNL-2748 Part A.

6. Evaluation of SEMIRAD for Dose-Rate-Independent Measurement of Fast-Neutron and Gamma Radiations, S. Kronenberg and H. M. Murphy, Jr., USASRDL, Oct. 10, 1958.

7. Godiva II Irradiation of SEMIRAD, S. Kronenberg and H. M. Murphy, Jr., USASRDL, Dec. 17, 1958.

8. Irradiation of SEMIRAD of the General Atomic Linear Accelerator (LINAC), S. Kronenberg and H. M. Murphy, Jr., May 5, 1959.

9. Dosimetry for the Godiva II Critical Assembly, Neutron Flux and Tissue Dose Measurements, J. A. Sayeg, E. R. Ballinger, and P. S. Harris, Los Alamos Scientific Laboratory internal report, LA 2310.

10. Boeing measurements in conjunction with Dr. J. Sayeg during tests at Godiva II, and LA 2310.

11. Derivation and Integration of the Pile Kinetic Equations, H. Hurwitz, Jr., Nucleonics 5, 61, July 1949; and Applications of Godiva II Neutron Pulses, T. F. Wimett and J. D. Orndoff. (See also IBM report "Godiva Test Series Dosimetry Techniques" for a resume.)

12. "Radiation Dosimetry," Hine and Brownell, Academic Press, 1956.

13. Los Alamos report, LA 2335.

APPENDIX III

TRANSIENT EFFECTS IN DIELECTRICS AND CAPACITORS

by

Howard W. Wicklein, Willard E. Spencer and Cecil W. Sandifer

TABLE OF CONTENTS

LIST OF ILLUSTRATIONS

LIST OF TABLES

INTRODUCTION

Dielectrics are recognized as one of the classes of materials which are most affected by nuclear radiation. The behavior of a large number of electronic piece parts when exposed to nuclear radiation depends upon the behavior of the dielectric materials which are a major part of their structure. Such electronic piece parts include capacitors, wiring and cables, switches, transformers, and many others. A thorough understanding of the changes which may occur in dielectric materials when subjected to nuclear radiation is necessary in order to predict and analyze the behavior of the piece parts when irradiated.

Many studies have been performed to determine permanent radiation effects in dielectric materials and capacitors when exposed to nuclear radiation from reactors and Co^{60} gamma sources. These effects are reasonably well known (Ref. 14 through 22).

A smaller quantity of data has been obtained for changes in the electrical properties of capacitors and dielectric materials when exposed to constant gamma irradiation levels produced by Co^{60}, reactors, and other sources (Ref. 18 through 25). The rate-dependent behavior of conductivity has been determined for a large number of dielectric materials at gamma irradiation rates up to 10^3 r/sec. These measurements indicate that conductivity varies proportional to $\emptyset \Delta$ where $\emptyset$ is the gamma radiation rate and $\Delta = 0.5$ to 1.0, depending on the dielectric material. Scattered measurements of the effects of gamma radiation at rates up to 10^3 r/sec on such electrical properties as electric strength, dielectric constant, and dissipation factor have been performed on several dielectric materials (i.e. Ref. 22). The transient effects on these electrical properties are small compared with the conductivity changes and vary considerably, depending on the type of material and the test condition.

Before the present program little data had been determined on transient effects caused by short, high level pulses of neutron and gamma radiation. The quantity and quality of these data were limited by the shortage of appropriate radiation facilities and the experimental difficulties peculiar to such tests. Some transient radiation effects data for capacitors and dielectric materials, when subjected to pulsed neutron, gamma and/or electron radiation, had been obtained with the Godiva II critical assembly, linear accelerators, and other sources (Ref. 26 through 31). Transient conductivity changes had been noted in the form of electrical leakage in capacitors and dielectric materials; minimum resistances as low as 15 KΩ had been measured during the radiation pulse. Detailed data presenting conductivity as a function of rate at levels of 10^6 to 10^7 r/sec had not been determined. Conductivity and emf's induced in electrical cables had been studied, but results were far from conclusive. Inconclusive changes in capacitance (up to 10 percent or 15 percent) had been noted during the radiation pulse, but the data are sparse and of limited validity. Useful data concerning electric strength during a pulse of radiation were non-existent. Few basic studies concerning pulsed radiation effects in dielectric materials had been conducted.

The experiments described in this section were designed to obtain additional information in the critical area of transient radiation effects in dielectric materials, and specifically to investigate dielectric breakdown, dielectric constant, and conductivity changes.

PURPOSE

The purpose of these tests is to study the electrical characteristics of capacitors and dielectric materials during a short, intense pulse of neutron and gamma radiation. Specific characteristics of interest are conductivity and electrical leakage, dielectric constant and capacitance, and electric strength. The object of the tests is the collection of basic parametric data concerning these characteristics. The analysis of capacitor test data should yield basic data concerning the dielectric materials, and the dielectric material data should be useful in analyzing or predicting pulsed radiation effects in capacitors and other electronic piece parts.

DESCRIPTION OF TEST SPECIMENS

TEST ITEMS

Several dielectric materials and capacitor types were selected for testing. An effort was made to choose a variety of high quality materials and capacitors which are widely used in electronic systems. The materials and capacitors selected were:

1. Mylar (polyethylene terephthalate) - 0.75×10^{-3} cm thickness
   conductivity $\leqslant 3.8 \times 10^{-17}$ (ohm-cm)$^{-1}$
   electric strength = $1.64 \pm .39 \times 10^{6}$ volts/cm for
   double layer (1.5×10^{-3} cm)

2. Sprague Vitamin Q impregnated paper - 1.5×10^{-3} cm thickness
   conductivity $\leqslant 7.5 \times 10^{-16}$ (ohm-cm)$^{-1}$
   electric strength = $8.86 \pm 1.97 \times 10^{5}$ volts/cm for
   double layer (3.0×10^{-3} cm)

3. Good-All mylar capacitors, 1μf, 600 VDC

4. Sprague Vitamin Q impregnated paper capacitor, 0.47μf, 400 VDC

5. Six-ohm carbon composition resistor

6. Dykanol G (chlorinated diphenyl) oil capacitor, 6μf, 600 VDC, GE TJU 6060J

7. Cornell-Dublier "PUP" wax-impregnated paper capacitors, 1.0μf, 600 VDC

8. Cornell-Dublier "CUB" oil-impregnated paper capacitor, 0.1μf, 600 VDC
   (CP28A1EF104K)

9. El Menco silver-mica capacitors, 0.01μf, 500 VDC

10. Disk type ceramic capacitors, 0.01μf, 600 VDC.

The mylar and Vitamin Q paper were tested in multiple layers to avoid difficulties caused by "pin-holes" in the thin single layers. Mylar capacitor specimens consisted of two or three of the 1.0μf type in series. The mylar and Vitamin Q capacitors were mounted on terminal boards which were then equipped with cable connectors and mounting brackets. These specimens were not potted; however, the tests were such that there would be no air ionization problem. The 6 ohm resistor was prepared similarly as a dummy load. These specimens are shown in Figure 27.

The remaining capacitors were mounted similar to those above, but they were potted with Epoxy Kish compound to prevent air ionization effects at high impedances and voltages. The 6μf oil and 0.1μf "CUB" capacitors were mounted singly. Test specimens for the mica and

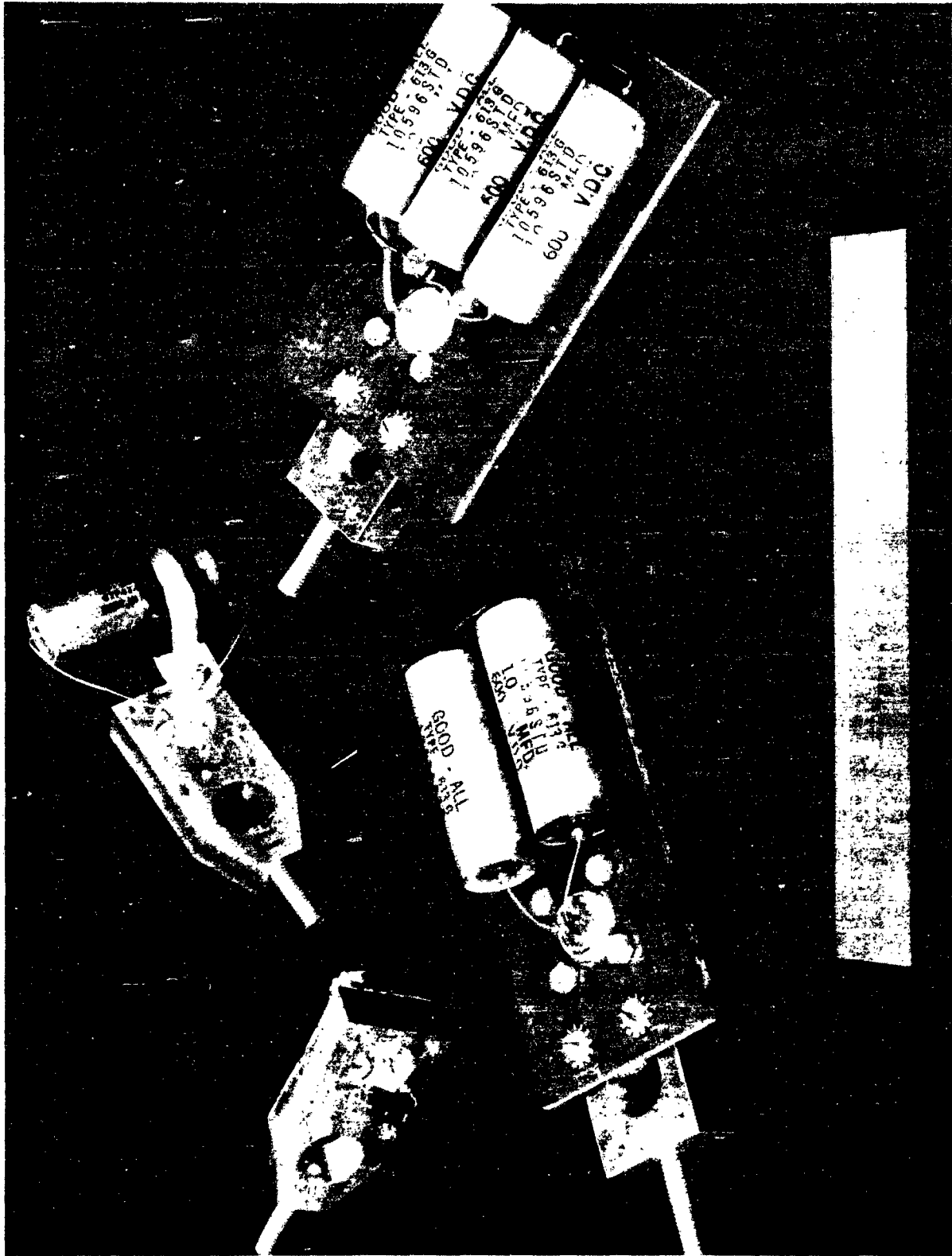Figure 27 – Constant–Voltage A.C. Test Specimens

ceramic each consisted of ten 0.01μf capacitors in parallel. Six 1μf "PUP" capacitors were used in parallel.

TEST EQUIPMENT AND TECHNIQUES

Four types of tests were performed:

    A.   D.C. Conductivity and Electric Strength

    B.   D.C. Capacitor Leakage

    C.   Constant-Voltage A.C. Capacitor Tests

    D.   Constant-Current A.C. Capacitor Tests

A description of the test equipment and techniques for each type of test follows.

A.   <u>D.C. Conductivity and Electric Strength</u>

This test was used to determine the effects of pulsed radiation on the mylar and Vitamin Q impregnated paper. Conductivity and voltage breakdown during the radiation pulse were measured simultaneously for multiple layers of the dielectric materials.

A special test fixture, Figure 28, was designed for use with the circuit for Test A, Figure 29. The test fixture consists of two parallel plate carbonsteel electrodes mounted within polystyrene insulators on a steel frame. The upper and lower electrodes are 1.0 and 1.5 inches in diameter, respectively, and are flat within 0.0001 inch. The upper plate rides on a centering point attached to a micrometer shaft; the plate is detachable for ease in placing the dielectric layers smoothly between the plates. The micrometer allows measurement of, and adjustment for, specimen thickness within ± 0.0001 inch. The electrode thicknesses (0.25 inch), diameters and rounded edges are appropriate for electric strength measurements. A 0.25 inch thick nylon ring surrounds the upper electrode, extending to the edges of the lower electrode. This ring was designed to reduce the possibility of air ionization effects and surface breakdown. The upper electrode and ring sit snugly upon the dielectric sample and lower electrode so that the major path for air ionization conduction is from above the nylon ring on the high voltage (upper) electrode, around the edges of the dielectric material which extends at least 0.25 inch past the lower electrode on all sides, and then to the measuring (lower) electrode. Ionization currents from the upper electrode to the frame are not included in the measurements. The dielectric test fixture was designed to withstand >4000 VDC across the electrodes. Electrical connections are made directly from coaxial cables to the electrode shafts and adequate grounding of frame and cable shield is provided in order to reduce noise pickup. Mounting brackets are provided for vertical or horizontal mounting of the test fixture (Figure 28).

Conductivity for the materials was measured before and after the radiation pulse, with a Keithley Model 200B Electrometer and Model 2008 Decade Shunt indicating the current produced
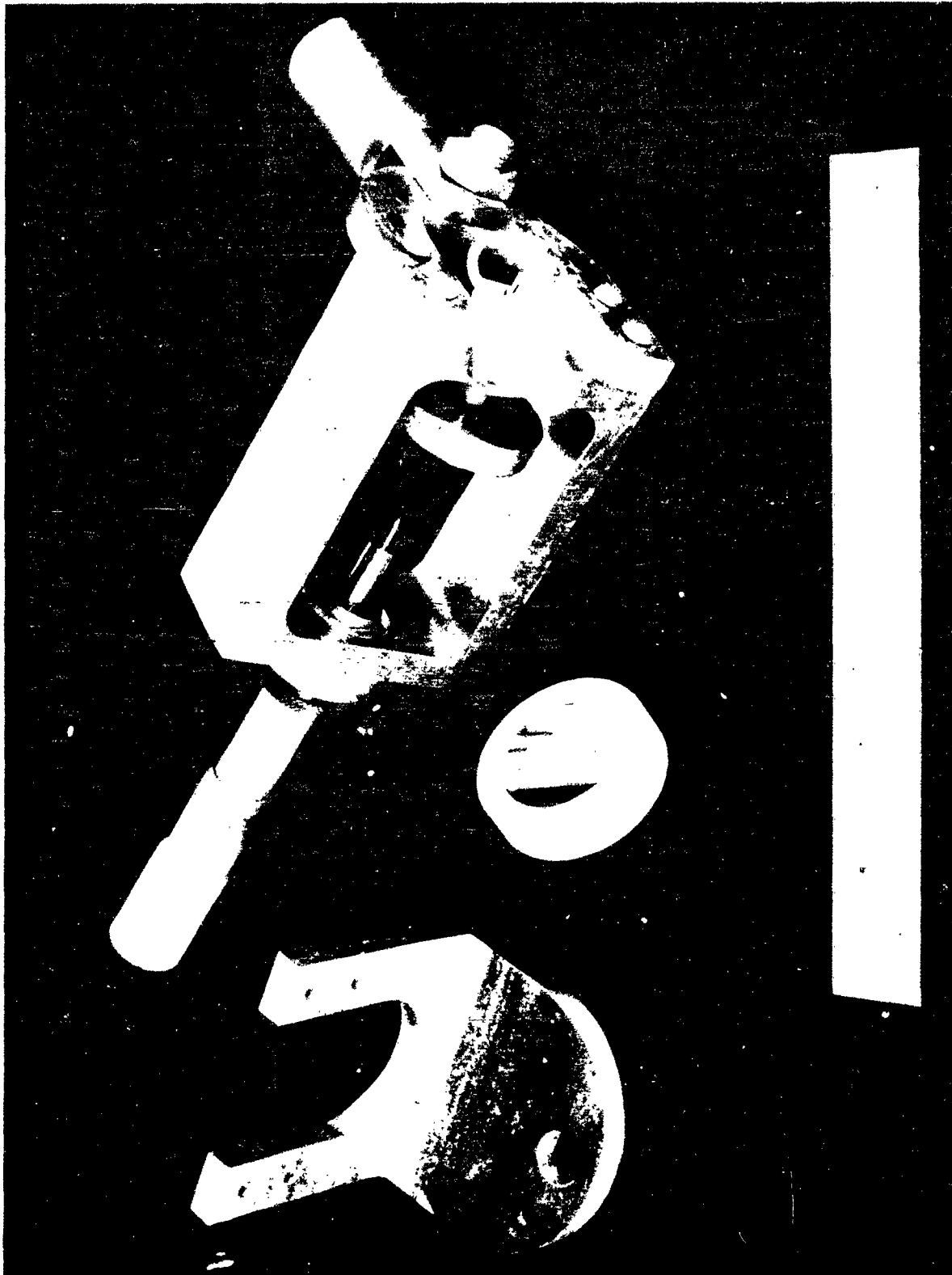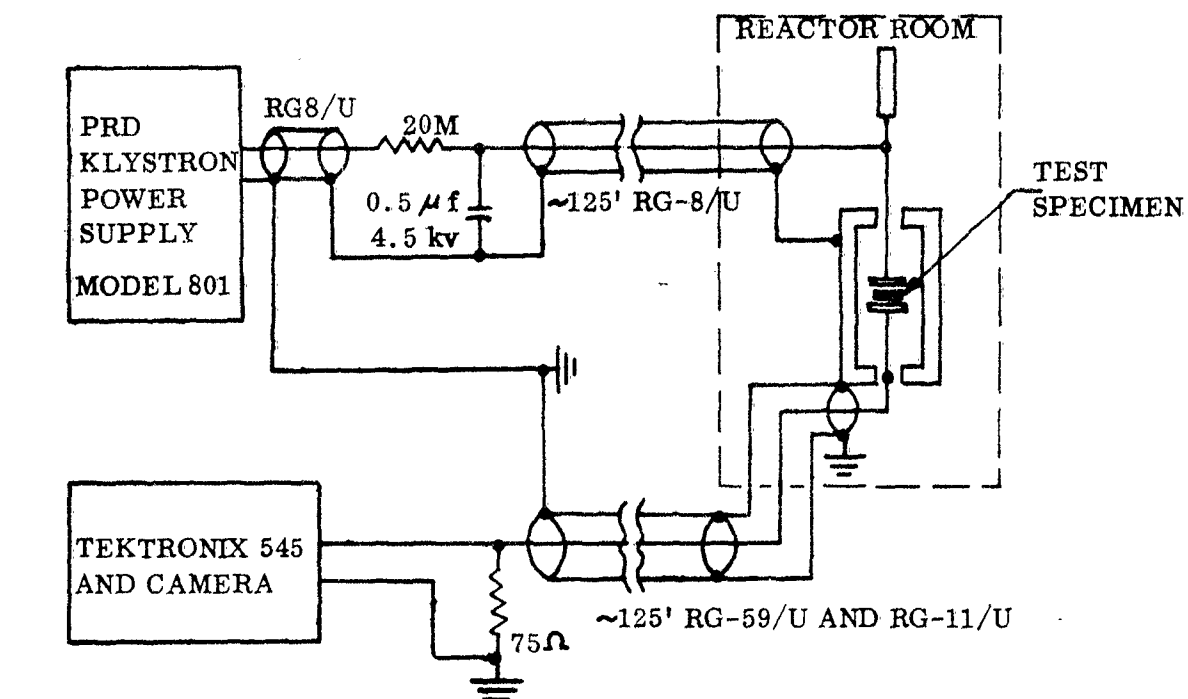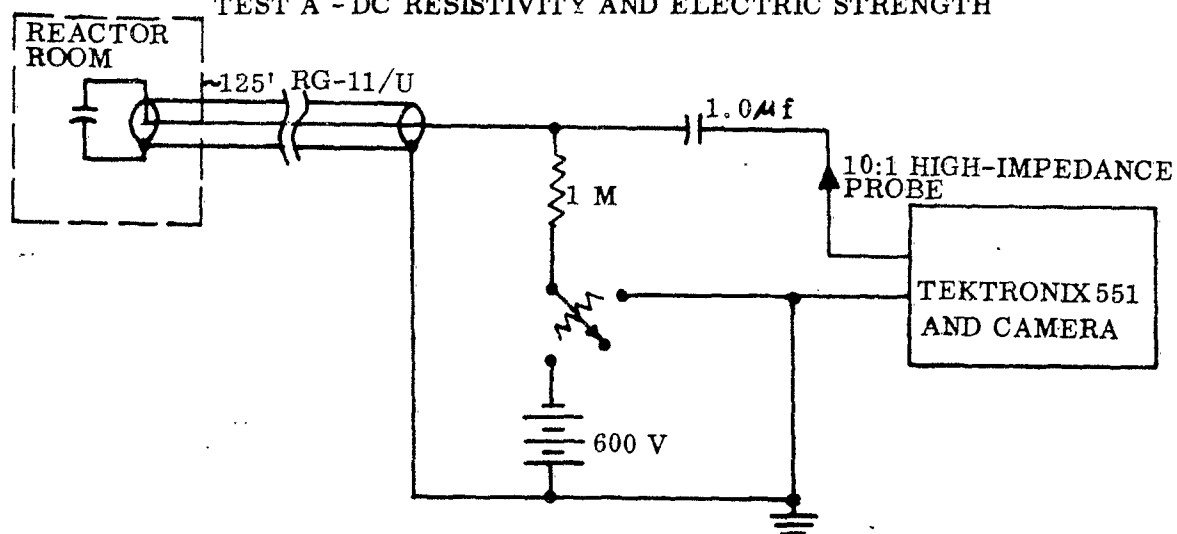
Figure 28 – Dielectric Test Fixture and Mounting Brackets

TEST A - DC RESISTIVITY AND ELECTRIC STRENGTH

TEST B - DC CAPACITOR LEAKAGE

Figure 29 - DC Test Equipment and Circuitry.

in the material by application of high voltage. The high voltage supply used in these tests is shown in Figure 30, along with the limiter-decoupling R-C network to protect the supply in case of voltage breakdown or extremely high specimen conductivity during the pulse of radiation. Conductivity during the pulse was measured by observing the voltage developed across the 75 ohm cable-terminating resistor and calculating conductivity values from the known test fixture geometry and applied voltage (See Analysis Section). Voltage breakdown during the pulse would be indicated by a sharp increase in monitored voltage. The test voltage during radiation was chosen to be~75 percent of the average measured breakdown voltage without radiation. One test was performed with the plates shorted to check for cable effects.

B. D.C. Capacitor Leakage

This test was used to determine the electrical leakage induced in the oil, "CUB," "PUP," mica and ceramic capacitors during the radiation pulse. The capacitors were charged to 600 VDC immediately before the radiation pulse. The voltage across the capacitors was monitored during and after the pulse with the circuit shown in Figure 29 for Test B.

The oil and "CUB" capacitors were dismantled after testing, and the area and thickness of the "parallel plate" geometry were measured so that leakage data could be converted to conductivity changes (See Analysis Section). The initial leakage resistance of a $0.1 \mu f$ "CUB" capacitor was also measured for reference.

C. Constant-Voltage A.C. Capacitor Tests

This test was used to determine capacity or dielectric constant changes in the mylar and Vitamin Q capacitors (and materials) during the radiation pulse. The A.C. current through the capacitor at 50 kc/s was monitored during the pulse with the circuit shown in Figure 31 for Test C. The voltage across the capacitor remains nearly constant, so that the voltage across the 0.5 ohm resistor (and 95Ω terminating resistor) is nearly proportional to the capacitance of the specimen. The A.C. signals were small, being limited by the constant-voltage circuit used with the oscillator. The entire peak-to-peak A.C. signal was observed in all tests; this procedure limits the sensitivity attainable with the circuit. One test was performed using the 6Ω resistor as a load in order to check cable effects.

D. Constant-Current A.C. Capacitor Tests

This test was used to determine capacity or dielectric constant changes in the $0.1 \mu f$ test specimens ("CUB," mica, ceramic) during the radiation pulse. The A.C. voltage across the capacitor at 50 kc/s was monitored during the pulse with the circuit shown in Figure 31 for Test D. Initial voltage was 20 volts p-p in all cases. The current through the capacitor is nearly constant; the voltage across the capacitor (and 75Ω terminating resistor) is nearly proportional to the capacitive reactance of the specimen (voltage percent change $\cong$ 0.9 capacitive reactance percent change). The entire peak-to-peak A.C. signal was observed at first, with consequent reduction in sensitivity. A greatly magnified view of the lower portion of the signal was observed in later tests; in this case, the sensitivity is increased to detect $< \pm 1$ percent change, but any
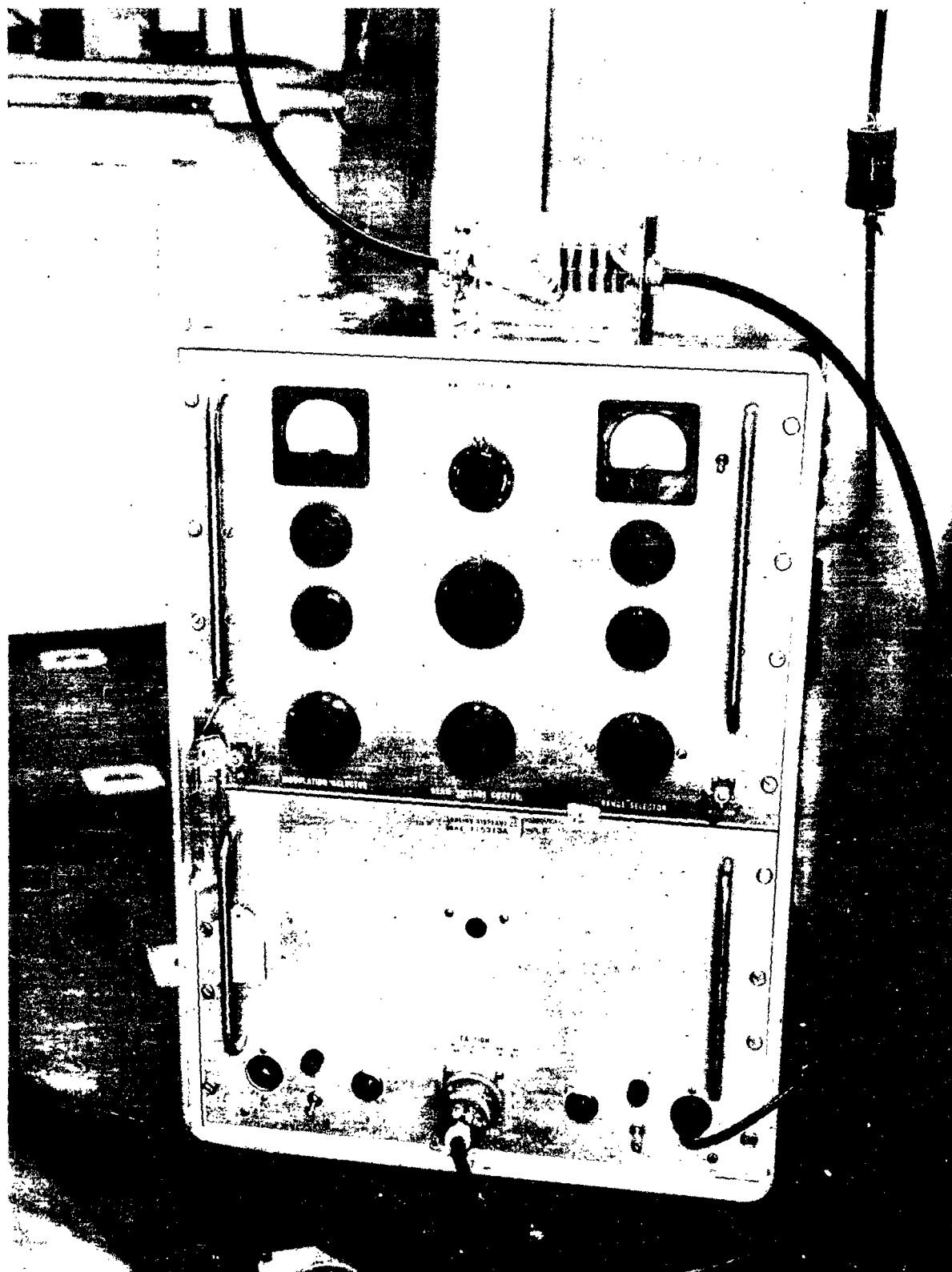
Figure 30 - High-Voltage Power Supply and Decoupling-Limiting Circuit
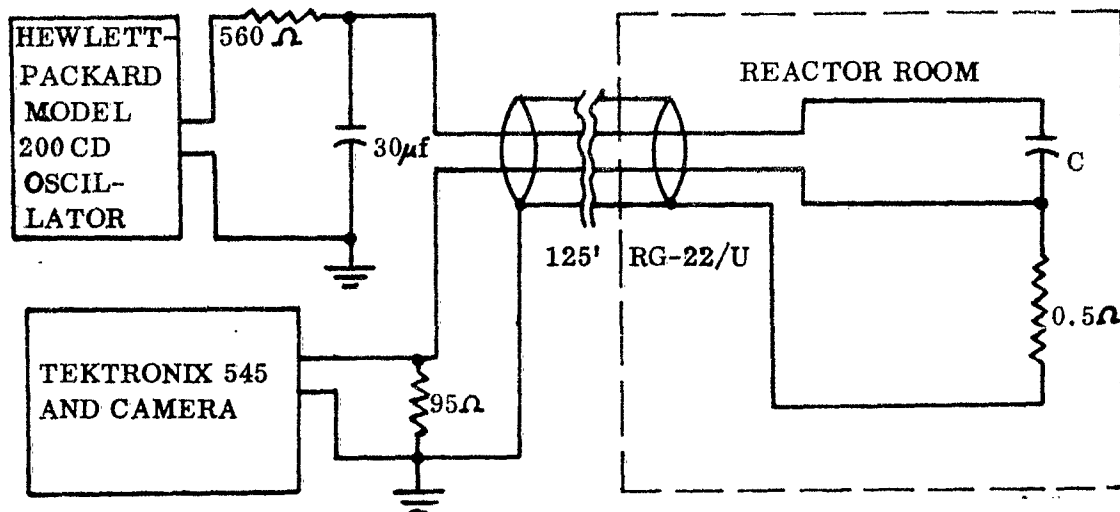
TEST C - CONSTANT-VOLTAGE AC CAPACITOR TEST
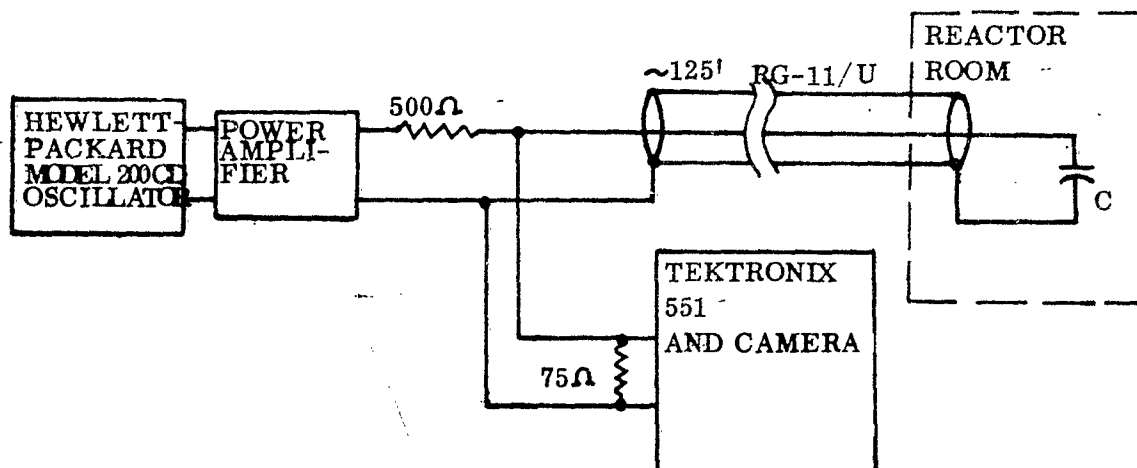
TEST D - CONSTANT-CURRENT AC CAPACITOR TEST

Figure 31 - AC Test Equipment and Circuitry.

observed change could be due to either the modulation of the A.C. signal or a shift in the D.C. level of the signal on the oscilloscope. The inability to observe the entire A.C. signal in the latter case introduces an uncertainty in the nature of any observed changes.

In both Test C and Test D, the capacitive reactance of the specimens was sufficiently low that resistance decrease in the capacitor during radiation would not influence the measurement. The capacitance values used for specimens were much larger than the cable capacitance; hence, one would not expect changes in cable capacitance during radiation to affect the results.

Table 8 contains a list of test specimens, types, and conditions for the sixteen shots performed at the Kukla critical assembly in this test series. Tests which did not yield usable data due to experimental difficulties or poor equipment settings are not included in Table 8. One or two sulfur pellets and a Sigoloff gamma dosimeter were used on the test specimen during each shot.

Figure 32 shows the oil capacitor and the dielectric test fixture mounted on the test stands and positioned next to a mockup of the Kukla facility. A similar photograph for the $0.5\mu f$ mylar capacitor specimen is shown in Figure 33. Figure 2 shows a typical arrangement of test specimens around the Kukla facility.

TABLE 8

SUMMARY OF DIELECTRIC AND CAPACITOR TESTS

Shot No.	Test Specimen	Test Type	Test Conditions	Peak Gamma Rate (Roentgen/sec. x 10^6)	Plutonium Neutron Flux (Neutrons/cm^2 x 10^{12})	Accumulated Dose Prior to Test (Neutrons/cm^2 x 10^{12})
2	6μf Oil Capac.	B	600 VDC	0.73	4.03	2.96
3	6μf Oil Capac.	B	600 VDC	1.22	3.18	6.99
4	6μf Oil Capac.	B	600 VDC	1.73	3.26	10.17
5	Mylar – 4 layers	A	1600 VDC	4.7	2.72	0.00
6	6μf Oil Capac.	B	600 VDC	2.06	4.35	13.43
	6μf "PUP" Capac. (6 – 1μf in parallel)	B	600 VDC	1.21	1.50	0.00
7	Vitamin Q paper – 2 layers	A	2000 VDC	1.58	2.73	0.00
	6μf "PUP" Capac.	B	600 VDC	0.69	1.62	1.50
8	Vitamin Q paper – 2 layers	A	2000 VDC	2.79	2.67	2.73
	0.1μf "CUB" Capac.	D	20V, p-p, 50kc/s	4.30	4.75	0.00
9	None – Fixture shorted	A	4000 VDC (0.2x10^{-3} Amp.)	2.18	3.60	0.00
	0.1μf Mica (10–0.01μf in parallel)	B	600 VDC	2.93	2.39	0.00
10	0.1μf "CUB" Capac.	D	20V, p-p, 50 kc/s	2.93	4.13	4.75
	0.1μf Mica	B	600 VDC	2.42	4.85	2.39
	0.47μf Vitamin Q Capac.	C	8 mv, p-p, 50kc/s	2.06	3.13	0.00
	0.1μf "CUB" Capac.	D	20V, p-p, 50kc/s	2.42	4.04	8.88

TABLE 8 CONT'D.

| Shot No.	Test Specimen	Test Type	Test Conditions	Peak Gamma Rate (Roentgen/sec. x 10^6)	Plutonium Neutron Flux (Neutrons/cm^2 x 10^{12})	Accumulated Dose Prior to Test (Neutrons/cm^2 x 10^{12})
11	0.5μf Mylar Capac. (2-1.0μf in series)	C	8 mv, p-p, 50kc/s	0.83	2.15	0.00
	0.1μf Mica	D	20V, p-p, 50kc/s	1.12	4.09	7.24
12	0.1μf "CUB" Capac.	B	600 VDC	2.42	5.22	15.66
	0.33μf Mylar Capac. (3-1.0μf in series)	C	4.5 mv, p-p, 50kc/s	2.06	2.90	0.00
	0.1μf Mica	D	20V, p-p, 50kc/s	2.42	5.72	11.33
13	0.1μf "CUB" Capac.	B	600 VDC	1.21	3.84	20.88
	6Ω Resistor	C	2 mv, p-p, 50kc/s	1.54	4.20	0.00
	0.1μf Ceramic Capac. (10-0.1μf in parallel)	D	20V, p-p, 50kc/s	1.21	4.75	0.00
14	Vitamin Q paper - 4 layers	A	2000 VDC	1.28	2.52	0.00
	0.1μf "CUB" Capac.	B	600 VDC	1.73	4.83	24.72
	0.1μf Ceramic Capac.	D	20V, p-p, 50kc/s	1.73	4.69	4.75
15	Mylar - 4 layers	A	1600 VDC	1.49	2.00	0.00
	0.1μf Ceramic Capac.	B	600 VDC	2.75	5.05	9.44
	0.1μf "CUB" Capac.	D	20V, p-p, 50kc/s	2.75	5.45	29.55
16	6μf Oil Capac.	B	600 VDC	1.13	4.98	17.78
	0.1μf "CUB" Capac.	D	20V, p-p, 50kc/s	1.13	4.66	35.00
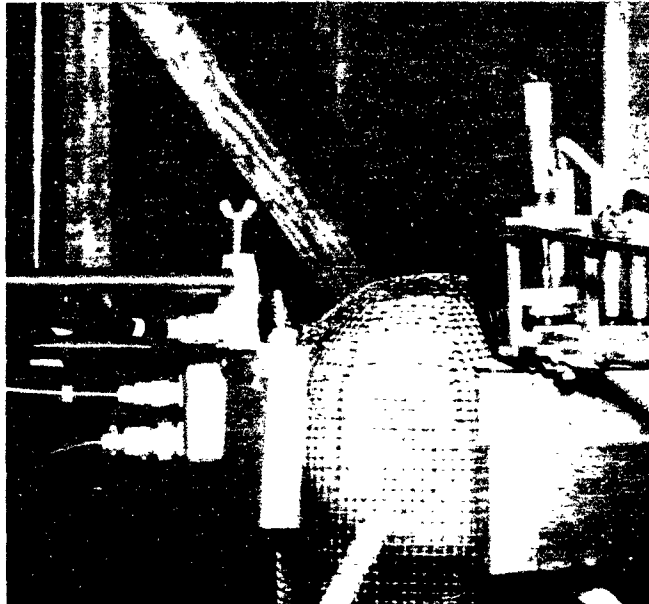
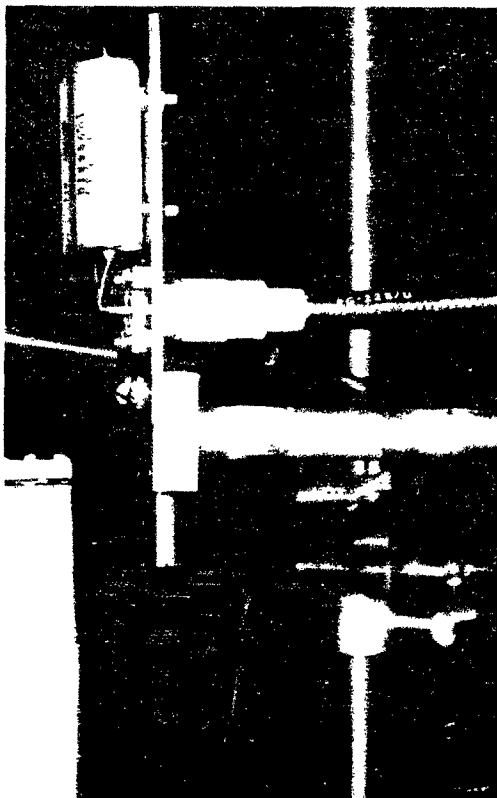Figure 32 - Dielectric Test Fixture and Oil Capacitor in Test Position

Figure 33 - Mylar Capacitor Specimen in Test Position

TEST RESULTS AND DISCUSSION

TEST RESULTS

In the presentation and analysis of results which follow, the dosimetry defines all transient effects in terms of the gamma radiation portion of the critical assembly output. The contribution to ionization from the neutron portion of the critical assembly output has not been established for low atomic weight materials such as the dielectrics, and one might expect an appreciable transient effect from neutron flux in these materials. However, the data and analyses presented here are consistent with the assumption that the gamma radiation alone causes the effects. Essentially no permanent damage effects were noted in these experiments.

Electric Strength

No effect on the electric strength of Vitamin Q paper due to the pulsed radiation was noted within 25 percent of normal breakdown voltage (Shots 7 and 8). The maximum rate was 1.5×10^6 r/sec for the first test and 2.64×10^6 r/sec for the second test. The specimen for the second test had received 2.73×10^{12} neutrons/cm^2 prior irradiation and still did not show transient electric strength changes. Difficulties were experienced with fatigue and premature breakdown in the mylar before testing, so the mylar was tested with applied fields that were only 35 to 40 percent of the normal electric strength. Typical results for electric strength tests are shown in Figure 34a.

It should be noted that the mica, ceramic, oil, "CUB", and "PUP" capacitors were all tested for D.C. leakage at rated voltage and showed no breakdown during radiation at the rates listed in Table 8. Apparently the ionization and increased conduction in the dielectric materials due to gamma radiation cause no large decreases in electric strength for the materials and radiation rates used in these tests.

Capacitance

Typical results for the constant-voltage A.C. tests are shown in Figure 34b (in this case for the 0.5μf mylar capacitor). Results for the constant-current A.C. tests are shown in Figures 35a,b, 36a,b,c and 37a for the 0.1μf ceramic, 0.1μf mica and 0.1μf "CUB" capacitors. The results of the A.C. capacitance tests are summarized in Table 9. The only apparent change in capacitance within the sensitivity of the tests was the 3.5 percent reduction in capacitance listed for the 0.1μf "CUB" capacitor in Shot 15 (Figure 35a). However, an identical test on the same capacitor in Shot 16 (Figure 35b) did not show the change indicated in Shot 15 when extrapolated linearly to the radiation rate of Shot 16. Three prior tests (i.e. Figure 37a) on the same capacitor also showed no measurable change. The change in Shot 15 can probably be attributed to a change in the overall D.C. level rather than A.C. modulation. Shot 13, with the 6 ohm resistor as a dummy load, did not indicate any measurable changes due to cable effects during radiation (the 6Ω resistor should remain stable at the radiation rates of these tests). The mica and ceramic capacitors, as well as the 0.1μf "CUB" capacitor were retested after one or more prior radiation pulses; the amount of prior irradiation is listed in Table 8 for each test.
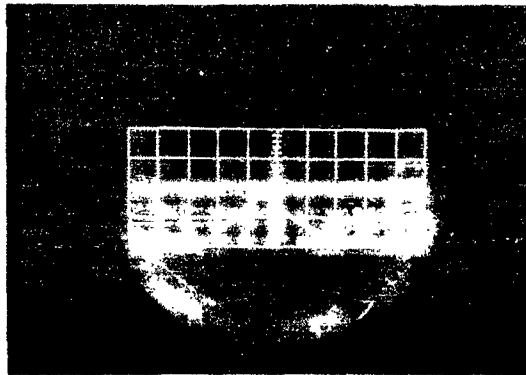
Shot No. 14

D.C. Conductivity and
    Breakdown Test
6.1×10^{-3} cm Vitamin Q Paper
5 mv/cm Vertical
200 μs/cm Horizontal

(a)
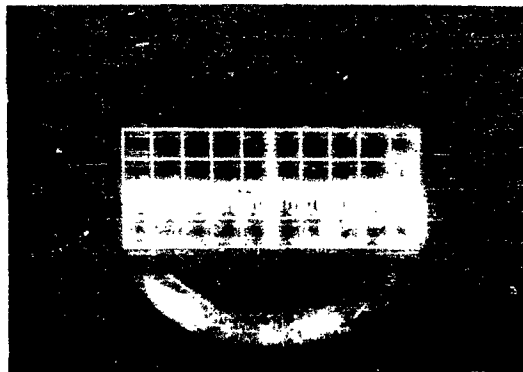
Shot No. 11

A.C. Capacitor Test
0.5μf Mylar Capacitor
10 mv/cm Vertical
100 μs/cm Horizontal

(b)

Figure 34 - Sample Data--D. C. Conductivity and Constant-Voltage
A. C. Capacitor Tests
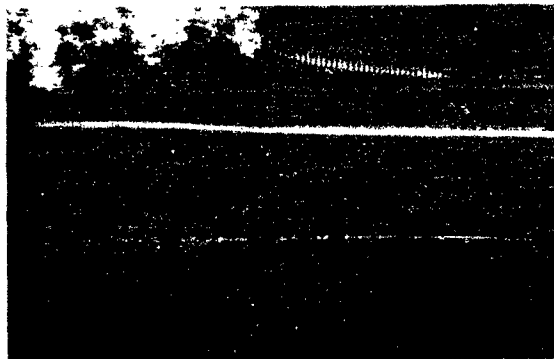
Shot No. 15

Upper Trace:

    A.C. Capacitor Test
    0.1 μf "CUB" Capacitor
    1 V/cm Vertical
    50 Kc/s A.C.

Lower Trace:

    D.C. Leakage Test
    0.1 μf Ceramic Capacitor
    20 V/cm Vertical
    200 μs/cm Horizontal

(a)
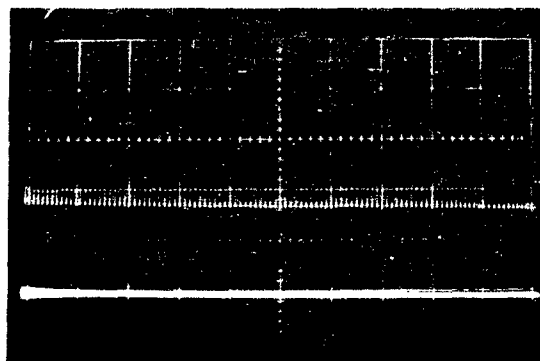
Shot No. 16

Upper Trace:

    A.C. Capacitor Test
    0.1 μf "CUB" Capacitor
    1 V/cm Vertical
    200 μs/cm Horizontal

Lower Trace:

    Thyratron Test

(b)

Figure 35 – D.C. Leakage Test Data and 0.1 μf "CUB" Capacitor
Constant-Current A.C. Test

Upper Trace:

A. C. Capacitor Test
0.1 μf Mica Capacitor
1 V/cm Vertical
50 Kc/s

Lower Trace:

D. C. Leakage Test
0.1 μf "CUB" Capacitor
2 V/cm Vertical
200 μs/cm Horizontal
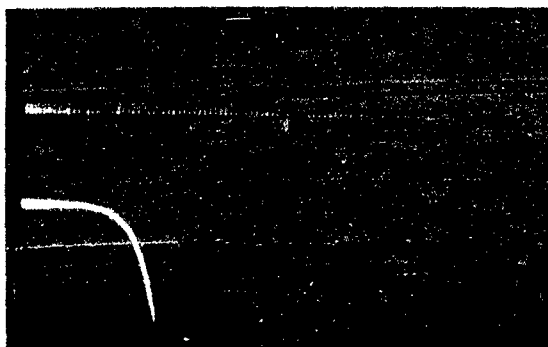
Shot No. 12

Upper Trace:

A. C. Capacitor Test
0.1 μf Ceramic Capacitor
1 V/cm Vertical
50 Kc/s

Lower Trace:

D. C. Leakage Test
0.1 μf "CUB" Capacitor
20 V/cm Vertical
200 μs/cm Horizontal
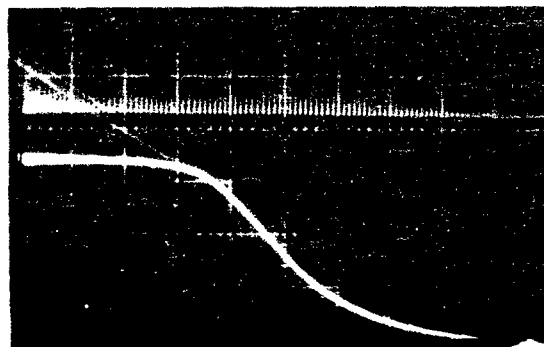
Shot No. 13

Upper Trace:

A. C. Capacitor Test
0.1 μf Ceramic Capacitor
1 V/cm Vertical
200 μs/cm Horizontal

Lower Trace:

D. C. Leakage Test
0.1 μf "CUB" Capacitor
20 V/cm Vertical
200 μs/cm Horizontal
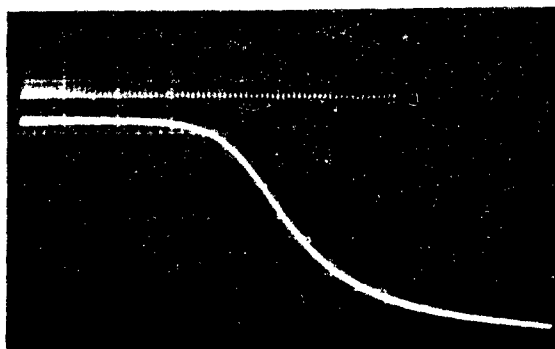
Shot.No. 14

Figure 36 – Constant-Current A.C. Capacitor Test and 0.1 μf "CUB"
Capacitor D.C. Leakage Data
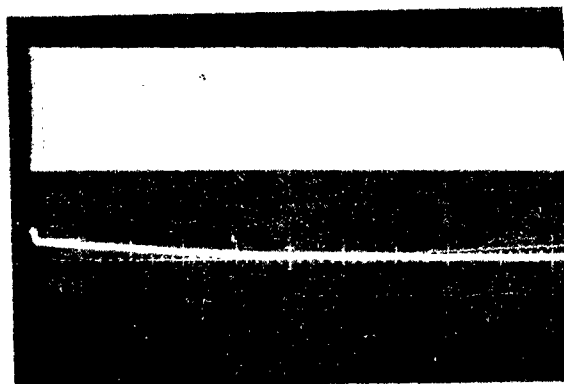
Shot No. 10

Upper Trace:
   A.C. Capacitor Test
   0.1 μf "CUB" Capacitor
   20 Vp-p A.C. Signal
   50 Kc/s

Lower Trace:
   D.C. Leakage Test
   0.1 μf Mica Capacitor
   10 V/cm Vertical
   20 ms/cm Horizontal

(a)
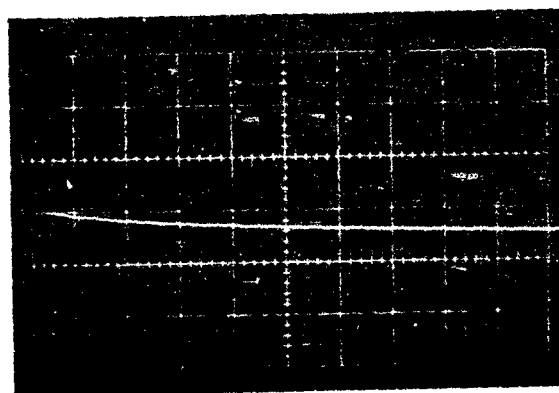
Shot No. 6

D.C. Leakage Test
6 μf "PUP" Capacitor
20 V/cm Vertical
20 ms/cm Horizontal

(b)

Figure 37 – D.C. Capacitor Leakage and Constant-Current
A.C. Capacitor Test Data

TABLE 9

CAPACITANCE EFFECTS DUE TO PULSED RADIATION

Capacitor Type	Shot No.	Percent Change in Capacitance at Peak Rate	Peak Gamma Rate ($r/sec \times 10^6$)
1.0 μf mylar	11	0 ± 15	0.83
	12	0 ± 15	2.06
0.47 μf Vitamin Q	10	0 ± 12	2.06
Dummy (6 Ω resistor)	13	0 ± 11	1.54
0.1 μf "CUB"	8	0 ± 3	4.30
	9	0 ± 5	2.93
	10	0 ± 2	2.42
	15	-3.5	2.75
	16	0 ± 1	1.13
0.01 μf silver-mica	11	0 ± 5	1.12
	12	0 ± 0.5	2.42
	13	0 ± 0.5	1.21
	14	0 ± 0.5	1.73

These tests indicate no measurable change in the dielectric constant of the capacitor materials tested; such changes could conceivably occur due to polarization or other effects caused by the presence of the ionizing radiation.

Conductivity

Since dielectric constant changes were not indicated by the A.C tests, it is assumed that the conduction changes in the dielectric materials during the radiation pulses were entirely due to conductivity changes. Figure 34a shows typical results for conductivity tests of type A (in this case for the Vitamin Q paper). Figure 38 shows the computed conductivity values as a function of gamma rate for the Vitamin Q paper, and Figure 39 shows the results for mylar. The analysis methods are presented in the Analysis Section of this appendix. The rates quoted represent extrapolations from known dosimeter positions to the center position of the test item and do not include attenuation of the gamma radiation by the test fixture or secondary electron production in the electrodes. The absorption of gamma radiation in the electrodes would more than compensate for any increases in rate caused by production of secondary electrons in the electrode material. There is some non-uniformity in the rates across the test specimen due to the variation with distance from the critical assembly. The conductivity of the mylar and Vitamin Q paper returned to its pre-irradiation value several minutes after the radiation pulse.

A study of Figure 38 shows that the conductivity versus rate dependence was not changed by prior irradiation, electric field strength changes, or speciman thickness within the ranges tested for the Vitamin Q paper. All mylar specimens were tested under identical conditions without prior irradiation.

The fact that the four-layer thickness of Vitamin Q paper showed the same conductivity versus rate as the two-layer thickness indicates no appreciable contribution to the conductivity due to induced conductivity in the surrounding air during the radiation pulse. The air conduction path and applied electric field in the air were essentially the same in all cases (Shots 7, 8 and 14). The absence of air ionization effects is also indicated by the different conductivity versus rate curves obtained for mylar and Vitamin Q paper with equivalent air conduction paths. An absence of appreciable cable effects in Test A was indicated by Shot 9 with the electrodes shorted and 0.2×10^{-3} amp (15 mv) applied through the 20MΩ limiting resistor during the radiation pulse. No signal was noted within ± 0.5 mv.

Figure 40 shows conductivity versus rate for the oil-impregnated paper used in the "CUB" capacitor. This data was obtained from an analysis (Analysis Section) of the leakage curves presented in Figure 36a, b, c. Considering the experimental and analysis errors possible, the data from the three tests show reasonable agreement, indicating no measurable effect due to prior irradiation.

Conductivity versus time for the Dykanol G oil of the 6μf oil capacitor (Figure 41) was obtained (See Analysis Section) from the leakage curves of Figure 42a,b. Again no appreciable effect due to prior irradiation is noted. This material is actually a heavily impregnated paper; however, one would expect a much stronger dependence of conductivity on the properties of the oil than with the other oil-impregnated papers which were tested.

$\sigma \sim \phi^{\Delta}$
$\Delta = 0.7 \pm .1$
$\sigma_0 \lessdot 7.5 \times 10^{-6}$ $(OHM-CM)^{-1}$

○ SHOT NO. 14: THICKNESS = 6.1×10^{-3} CM
        APPLIED FIELD = 3.28×10^5 VOLT/CM
⊡ SHOT NO. 7: THICKNESS = 3.05×10^{-3} CM
        APPLIED FIELD = 6.56×10^5 VOLT/CM
◇ SHOT NO. 8: THICKNESS = 3.05×10^{-3} CM
        APPLIED FIELD = 5.56×10^5 VOLT/CM
        2.73×10^{12} PU NT/CM PRIOR.
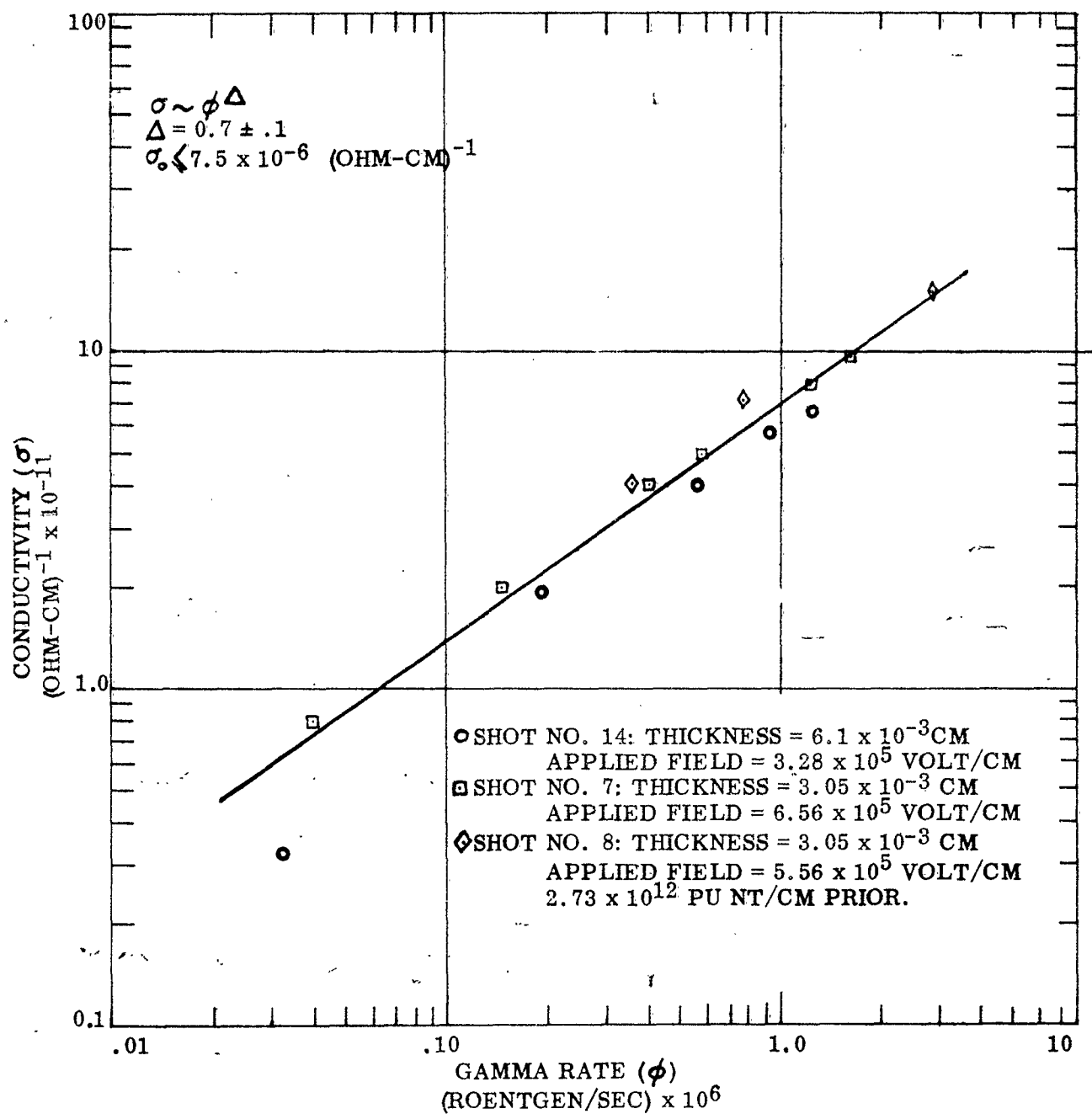
Figure 38 - Conductivity Versus Radiation Rate -- Sprague Vitamin Q
Impregnated Paper.
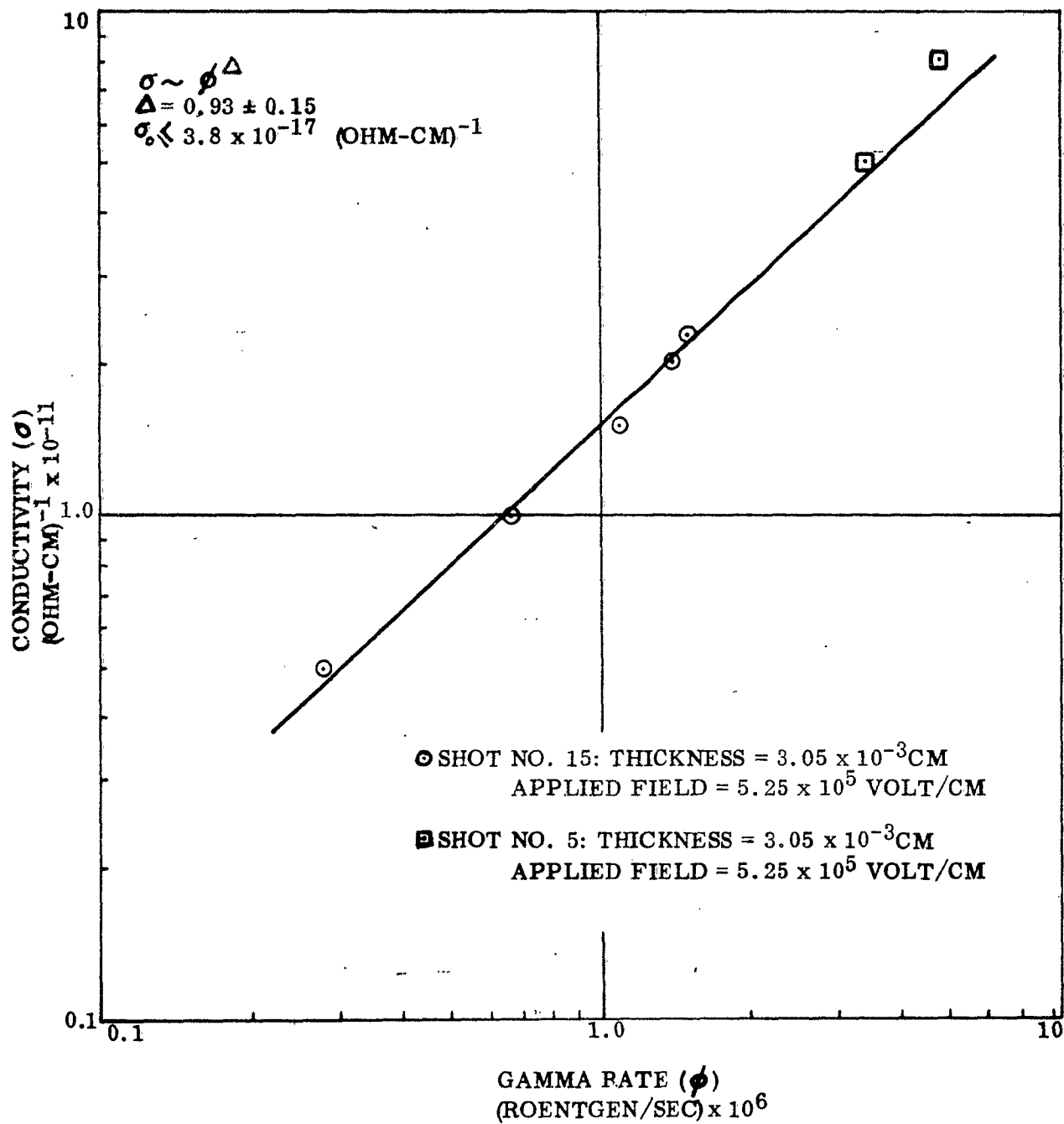
Figure 39 - Conductivity Versus Radiation Rate -- Mylar.
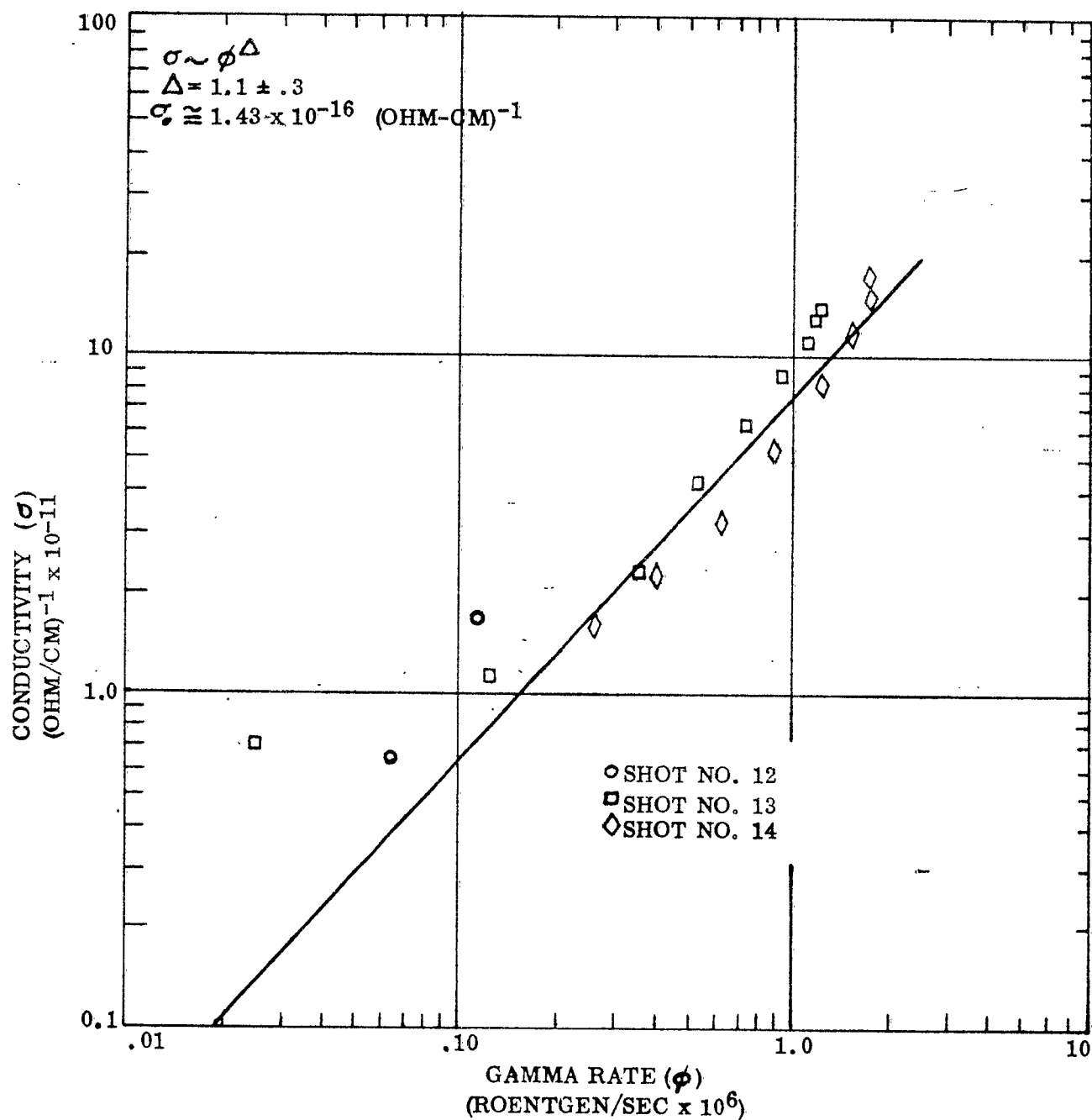
Figure 40 – Conductivity Versus Radiation Rate -- Oil-Impregnated Paper
(0.1μf Cornell-Dublier "Cub" capacitor).

$$\sigma \sim e^{-t/T}$$

O SHOT NO. 16, T=45 MS
□ SHOT NO. 5, T=40 MS

10

1

CONDUCTIVITY (σ) (OHM-CM)$^{-1}$ x 10^{-13}

0   50   110

TIME (ms)
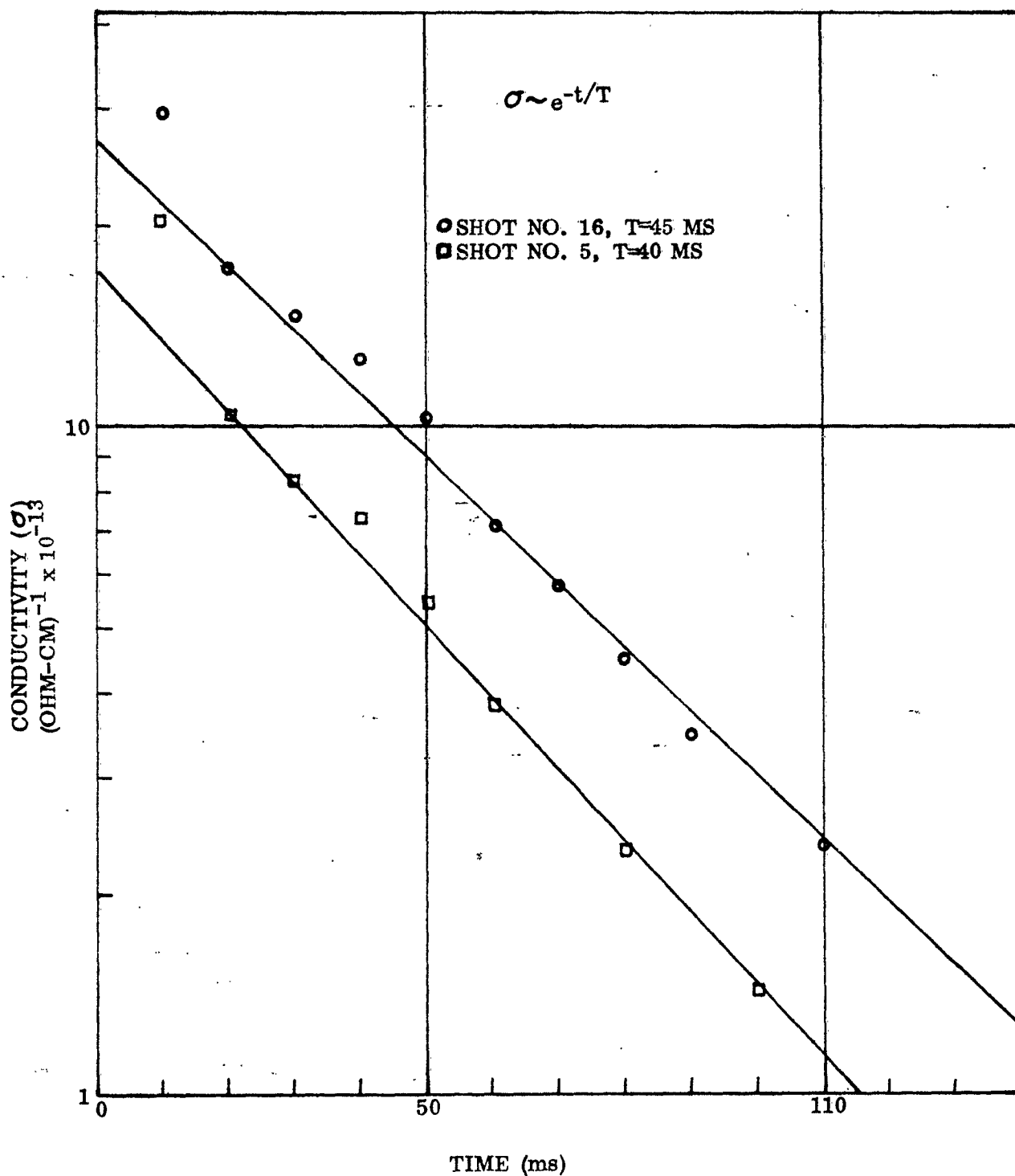
Figure 41 - Conductivity Versus Time After Radiation Pulse -- 6.0 μf Oil-
Capacitor (Dykanol G Oil-Impregnated Paper).
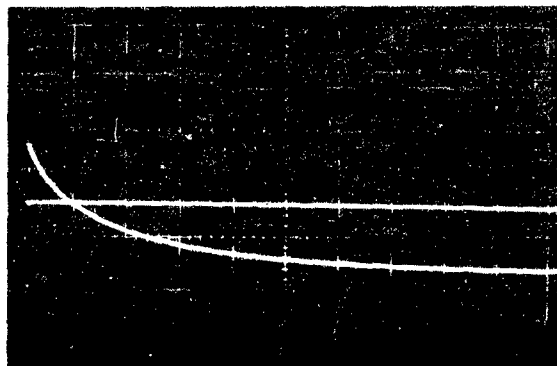
Shot No. 5

Upper Trace: Lower Trace:

                                    SEMIRAD Dosimeter

    D.C. Leakage Test
    6 μf Oil Capacitor
    20 V/cm Vertical
    20 ms/cm Horizontal

(a)
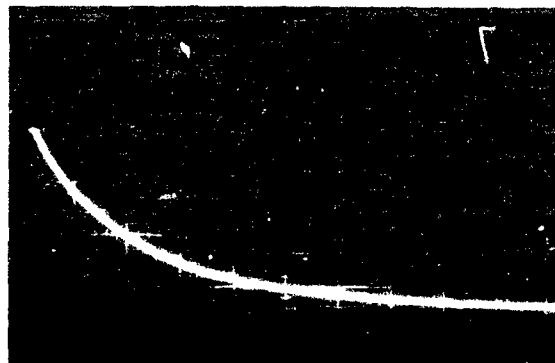
Shot No. 16

    D.C. Leakage Test
    6 μf Oil Capacitor
    20 V/cm Vertical
    20 ms/cm Horizontal

(b)

Figure 42 - D.C. Leakage Test Data--6 μf Oil Capacitor

DISCUSSION OF RESULTS

Table 10 shows a tabulation of D.C. leakage in mica, ceramic, "PUP," and "CUB" capacitors during the radiation pulse. The data is taken from curves such as shown in Figures 35a, 36b, c and 37a, b. The capacitors show an initial leakage at the time of the main radiation pulse with gradual leakage as the critical assembly "cools". An appreciable gamma rate exists for some time after the main pulse, although the rate has not been accurately determined. The times over which the leakage changes in Table 10 were taken were somewhat arbitrarily chosen, however they indicate that the solid dielectrics show similar response to the dielectric pulse. These results and the calculated conductivity vs. rate curves show that the conductivity follows the radiation pulse. The carrier lifetimes for the radiation-generated carriers are much shorter than the radiation pulse so that recombination occurs instantly, relatively speaking. This agrees with the discussions by Fowler (Ref. 25) who states that carrier lifetimes in most dielectric materials are $\sim 10^{-8}$ sec.

The conductivity of the Vitamin Q paper, mylar, and "CUB" oil-impregnated paper is found to obey the relation:

$$\sigma \sim \phi^{\Delta}$$

where: $\quad \sigma$ = conductivity

ϕ = gamma radiation rate

It is found that Δ = 0.7 ± .1 for the Vitamin Q paper, 0.93 ± 0.15 for the mylar and 1.1 ± .3 for the "CUB" oil-impregnated paper. The more inaccurate points, at the lower and upper ends of the curves in Figures 38, 39 and 40, are due to difficulty in reading the data at low rates and dosimetry error at high rates. The conductivity induced by steady gamma irradiation rates up to 10^3 r/sec has been found to follow a similar relationship with Δ = 0.5 to 1.0 for most dielectric materials (Ref. 21, 22, 23 and 25). Fowler (Ref. 25) quotes a value of Δ = 0.83 for equilibrium conductivity in mylar when irradiated at steady X-ray rates. Extrapolation of Fowler's X-irradiation data for polyethylene yields conductivity values in the range 10^{-11} to 10^{-10} (ohm-cm)$^{-1}$ for rates in the range 10^6 to 10^7 r/sec with Δ = 0.75. Extrapolation of the conductivity curves presented here to very low rates yields conductivity values approaching those without radiation. Hence, there is at least semi-quantitative agreement of these results with conductivity data taken at much lower gamma and X-ray steady radiation rates.

Fowler (Ref. 25) proposes mechanisms and theories for radiation-induced conductivity and trapping in dielectric materials. His theory agrees well with results obtained with X-radiation. He states that the induced-conductivity arises mainly from the secondary (not primary) electrons produced by the radiation in the dielectric materials. These electrons drift in the presence of an electric field, thereby increasing the material conductivity. There is no reason to believe that material conductivities would not obey Fowler's theory at higher radiation rates until saturation effects, such as space charge or other effects, occur. Hence one would expect the results at low rates to extrapolate to the high rates used here. Experiments at low, steady radiation rates (Ref. 19, 23, 24 and 25) have shown a slow asymptotic rise in conductivity after an initial large change when the radiation level is maintained for minutes or hours. This change would not be noted for the short irradiation times noted here, so that slightly lower conductivities would

TABLE 10

D. C. LEAKAGE EFFECTS IN SOLID DIELECTRIC CAPACITORS

Capacitor Type	Shot No.	Initial Voltage Change (% of original)	Total Change After 100 ms (% of original)	Peak Gamma Rate (r/sec x 10^6)
1.0 μf "PUP"	6	-0.7	-1.8	1.21
	7	-0.5	-1.6	0.69
0.1 μf "CUB"	12	<- .9	<- .9	2.42
	13	-11	<-11	1.21
	14	-12	<-13	1.73
0.01 μf silver mica	9	-0.6	<-0.6	2.93
	10	-0.4	-0.9	2.42
0.01 μf ceramic	15	-0.4	<-0.6	2.75

be expected than those extrapolated from low, constant rates where saturation was reached. This "build-up" does not have time to occur with the short radiation pulses. At very short irradiation times, one would expect decreases in the conductivity levels attained at given rates and decay of conductivity after the radiation pulse associated with the carrier lifetime in the dielectric material.

The time response of the Dykanol G oil conductivity (Figure 41) shows a large rise at the time of the radiation pulse, decaying exponentially with a time constant of 40 to 45 ms after initial "cooling" of the critical assembly. The conductivity does not follow the radiation pulse as with the "solid" dielectric materials. The conduction properties of this heavily-oil-impregnated paper apparently depend largely on the properties of the oil. This exponential behavior could arise from one of the following causes:

1. A trapping mechanism for induced carriers in the dielectric material with a time constant of 40 to 45 ms.

2. A small increase in capacitance (or dielectric constant) causing a long time constant. Since the leakage resistance across the oil capacitor did not appear to reach a very low value during the burst, a long time would be required for readjustment of charge after the capacitance change. The A.C. capacitance test was not performed for the $6\mu f$ oil capacitor.

The latter case seems more probable; a capacitance change might occur due to polarization effects in the oil. The 40 to 45 ms time constant is rather long for trapping phenomena which could cause the effects noted here.

Table 11 shows minimum leakage resistance values in the "CUB," "PUP," mica and ceramic capacitors. The values for the "PUP," mica and ceramic are approximations based on values for the "CUB" capacitor and utilizing the boltage change and peak rate data of Table 10 as adjustment factors. It is difficult to compare these capacitors, since the minimum leakage resistance depends on capacitor geometry and original leakage resistance as well as the behavior of the dielectric conductivity during radiation.

Values of minimum resistance in a $0.01\mu f$, 400 VDC Sprague Vitamin Q capacitor have been calculated from the capacitor geometry and extrapolated data from Figure 38 (see Analysis Section). These values are compared with leakage values obtained for $0.01\mu f$ Sprague Vitamin Q capacitors by International Business Machines Corp. at the Godiva II facility (Ref. 27 and 28) as follows:

Gamma Rate (Roentgen/sec x 10^6)	Calculated (KΩ)	Measured (IBM) (KΩ)
10	266	65.2
7.4	327	399
4.0	506	261

The difference between calculated and measured values can be explained largely by capacitor manufacturing variations and dosimetry uncertainties.

TABLE 11

MINIMUM D.C. LEAKAGE RESISTANCE IN SOLID DIELECTRIC CAPACITORS

Capacitor Type	Shot No.	Minimum Resistance (KΩ)	Maximum Gamma Rate (r/sec) x 10^6
0.1 μf "CUB"	13	47	1.21
	14	36	1.73
0.01 μf ceramic	15	6200*	2.75
1.0 μf "PUP"	6	770*	1.21
	7	2000	0.69
0.01 μf silver mica	9	2900*	2.93
	10	7100*	2.42

* Approximate values

ANALYSIS

The ideal parallel-plate geometry has been utilized in all analyses concerning capacitor leakage resistance and conductivity in the dielectric materials. Fringing effects are considered negligible for the small dielectric thicknesses involved. The following equation was utilized:

$$\sigma = \frac{d}{RA} \tag{4}$$

where: σ = conductivity = $(ohm-cm)^{-1}$

   d = thickness = cm

   A = area = cm^2

   R = resistance = ohms

ANALYSIS OF TEST A

Values for the test parameters and data were used in equation (4) with:

$$R = \frac{ER_o}{v}$$

where: E = applied high voltage (volts)

   v = measured voltage across R_o (volts)

   R_o = 75 Ω terminating resistance

   A = area of upper electrode = 5.06 cm^2

ANALYSIS OF TEST B

The capacitor leakage curves (Figure 36 and Figure 42) were re-plotted. Resistance values were determined from the equation:

$$R = \frac{E}{I} = \frac{E}{dQ/dt} = \frac{E}{C\frac{dE}{dt}}$$

where: I = current at voltage E

   E = measured voltage from data

   $\frac{dQ}{dt}$ = time rate of change of capacitor charge = I

   $\frac{dE}{dt}$ = time rate of change of voltage at the voltage E. (Slope at E)

C = capacitance of test specimen

These resistance values were then used in equation (4) to determine conductivity.

COMPUTATION OF LEAKAGE RESISTANCE FOR COMPARISON WITH IBM DATA

Equation (4) was solved for R. Values of σ were taken from an extrapolation of Figure 38 at the appropriate radiation rates.

MEASURED VALUES OF CAPACITOR GEOMETRY

The following values of capacitor plate area and dielectric material thickness were measured for use in the analyses given above:

Capacitor	A (cm^2)	d (cm)
6 μf Oil	1.67 x 10^4	3.3 x 10^{-3}
0.1 μf "CUB"	363	2.29 x 10^{-3}
0.01 μf Vitamin Q	24.4	2.29 x 10^{-3}

CONCLUSIONS

The following conclusions are noted from the results of these experiments:

1. The electric strength of Vitamin Q impregnated paper is unaffected within -25 percent for pulsed gamma rates up to 2.8×10^6 r/sec.

2. "CUB," "PUP," ceramic disk, silver-mica, and Dykanol G oil cap tors exhibit no electric breakdown at rated voltage during gamma radiation rates up to 3×10^6 r/sec.

3. Mylar, Vitamin Q impregnated paper, "CUB" oil-impregnated paper, "PUP" wax-impregnated paper, mica, ceramic, and Dykanol G oil exhibit no dielectric constant changes (capacitance effects) within the sensitivity of these experiments at gamma rates up to 4.3×10^6 r/sec.

4. The conductivity of mylar, Vitamin Q impregnated paper, and "CUB" oil-impregnated paper is proportional to ϕ^Δ (ϕ = gamma rate) for $\phi = 3 \times 10^4$ to 5×10^6 r/sec where $\Delta = 0.7 \pm .1$ for Vitamin Q paper, $0.93 \pm .15$ for mylar, and $1.1 \pm .3$ for "CUB" paper. Conductivity variation with pulsed gamma rate is consistent with data taken at steady gamma rates up to 10^3 r/sec.

5. The radiation-induced conductivity of Vitamin Q impregnated paper does not vary appreciably with specimen thickness or applied electric field within the ranges tested.

6. The conductivity of "PUP" wax-impregnated paper, mica, and ceramic follows the radiation pulse as for the materials listed in (4) above. Carrier lifetimes much shorter than the pulse duration are indicated.

7. Capacitor leakage test data can be used effectively to determine radiation effects on dielectric material conductivity, and conductivity data for materials can be used to predict capacitor leakage during a radiation pulse.

8. Prior irradiation appears to have no effect on the transient radiation behavior of dielectric materials for prior irradiation up to 3.5×10^{13} nvt.

RECOMMENDATIONS

The following recommendations are made for future effort:

1. More sensitive measurements of capacitance or dielectric constant during radiation should be performed for a variety of solid and liquid materials. Bridge or frequency measurement techniques are recommended. Theory should be developed for any observed changes.

2. Dielectric materials and capacitors should be checked for generation of emf during radiation. Theory should be developed for any observed changes.

3. A detailed study should be performed on several classes of dielectric materials to determine the effect of radiation on electric strength. Sufficient data should be obtained for good measurement statistics. Any observed effects should be developed theoretically.

4. Conductivity vs. gamma rate should be determined for a wider range of materials; recovery after radiation pulse should be noted, with appropriate extension of the dosimetry. Liquid dielectrics should be included.

5. Quantitative correlation should be developed between conductivity values taken at high, pulsed rates and low, constant rates. The theory and mechanisms developed for low rates should be extended to high levels.

6. Short radiation pulses ($\lesssim 1 \mu$s) of varying width should be used in order to determine conductivity build-up and carrier lifetime limitations in dielectric materials.

7. The applied field and thickness dependence of radiation effects on conductivity in dielectric materials should be checked over a wider range of variation.

REFERENCES

14. Mayer, R. et al., The Effect of Nuclear Radiation on Silicone Elastomeric and Plastic Materials, Battelle Memorial Institute, REIC Report No. 9, Oct. 15, 1959.

15. Broadway, N. J. and Palinchak, S., The Effect of Nuclear Radiation on Elastomeric and Plastic Materials, (First Addendum), Battelle Memorial Institute, REIC Report No. 3 (First Addendum), May 31, 1959.

16. Broadway, N. J. et al., The Effect of Nuclear Radiation on Elastomeric and Plastic Materials (Second Addendum), Battelle Memorial Institute, REIC Report No. 3 (Second Addendum), Apr. 30, 1960.

17. Moody, J. W., The Effect of Nuclear Radiation on Electrical Insulating Materials, Battelle Memorial Institute, REIC Memorandum 14, Mar. 31, 1959.

18. Cary, H. et al., The Effect of Nuclear Radiation on Electronic Components, Battelle Memorial Institute, REIC Report No. 8, Jul. 31, 1959.

19. Loy, W. E., Jr., The Effects of Gamma Radiation on Some Electrical Properties of Teflon, The Martin Company, Paper No. 193, Third Pacific Area Nat'l. Meeting of ASTM, 11-16 Oct., 1959.

20. Conference on Effects of Radiation on Dielectric Materials, ONR Symposium Report ACR-2, Naval Research Laboratory, Dec. 14-15, 1954.

21. Alexander, D., Radiation Effects on Wire Insulation, Philco Government and Industrial Division, Report WDL-TR1222, Mar. 15, 1960.

22. Currin, C. G., Effects of Gamma Radiation at 25C on Silicone Dielectrics, Communications and Electronics, No. 44, pp 297-308, Sept., 1959.

23. Huth, G. C., Conductivity Induced in Solid Insulating Materials During Gamma Irradiation, General Electric Co., ANPD, 58-331, 1958.

24. Lamale, G. E. and Schall, P., Electrical Leakage in Insulators Exposed to a Nuclear Environment, Battelle Memorial Institute, REIC Memorandum 2, Jan 15, 1958.

25. Fowler, J. F., X-Ray Induced Conductivity in Insulating Materials, Proc. Royal Soc., Vol. 236, p. 464, Sept. 11, 1956.

26. Some Effects of Pulsed Neutron Radiation on Electrical Components, International Business Machines Corp., Owego, N. Y., Oct. 9, 1958.

27. Some Effects of Pulsed Radiation on Electronic Components – II, International Business Machines Corp., Owego, N. Y., August, 1958.

28. Some Effects of Pulsed Radiation on Electronic Components - III, International Business Machines Corp., Owego, N. Y., Jan., 1959.

29. Denney, J. M., Pulsed Neutron Irradiation of Electronic Components, Hughes Aircraft Co., T. M. No. 522, Jul. 16, 1958.

30. Perkins, C. W. et al., Third Experiment on Pulsed Neutron Radiation Effects, Hughes Aircraft Co., T. M. No. 623, Oct., 1959.

31. Zipprich, L. J., Godiva II Radiation Effects Tests Report Summaries, Sandia Corporation, Div. 1626, Nov., 1959.

APPENDIX IV

TRANSIENT RADIATION INDUCED
SPARK GAP BREAKDOWN IN AIR

by

Richard H. Dickhaut

TABLE OF CONTENTS

LIST OF TABLES

INTRODUCTION

Relatively little information has been obtained on the problem of high voltage breakdown in gaseous dielectrics in an extreme radiation environment. Unpublished data from an exploratory test by the Sandia Corporation (Ref. 32), conducted at Godiva with conventional spark gaps, indicated that a decrease in breakdown voltage on the order of 50 to 60 percent could be expected for a 0.109 inch gap in nitrogen between pressures of 15 and 55 cm Hg in a radiation environment of 10^7 r/sec. General Electric (Ref. 33) conducted a study at 10^3 r/sec in air with nickel spark plug electrodes. They reported the results as a function of voltage, temperature, and pressure for a 1/16 inch gap. At 100°C and 130°C the decrease in breakdown voltage varied from 10 to 20 percent as the pressure was increased from 2.5 mm Hg to 760 mm Hg. At 160°C, over the same range in pressure, there appeared to be a constant decrease in voltage of about 16 percent as the pressure was increased.

Other investigations have been carried out using radium and ultraviolet illumination for radiation sources. The most recent of these, an investigation performed by Allen and Phillips (Ref. 34), used 0.1 mgm of radium in a nickel pellet situated behind the cathode in one case, and 30 cm away from the gap in a second case. Results were reported for weak irradiation (radium 30 cm away) in a comparison between the performance of spheres and plane electrodes in nitrogen at 760 mm Hg pressure. The unirradiated breakdown voltage of a uniform field gap on one cm was about two percent less than for the same spacing between five cm spheres. The separation of the shperes was then reduced to 0.975 cm so that both gaps broke down at the same voltage. The gaps were then connected in parallel and placed so that the radium was 30 cm from both. The result was that the apparent reduction of the breakdown voltage was only about 0.1 percent for the uniform field, but it was about one percent for the spheres. Rogowski and Wallraff (Ref. 35) found that a current density of 5×10^{-12} amps/cm^2 in a spark gap, produced by radiation, would reduce the minimum breakdown voltage of about 0.5 percent for a gap of 1.5 cm between spheres at atmospheric pressure.

Further investigations (Ref. 36, 37, 38 and 39) have been made using ultraviolet illumination and results have indicated lowering of the breakdown potential by as much as 20 percent, depending on intensity. Comparison of all the available data failed to give either an adequate or comprehensive picture of high voltage breakdown as a function of electrode separation, electrode geometry, or radiation rate in an extreme radiation environment.

PURPOSE

The purpose of this first investigation was to determine the effect of nuclear radiation on the minimum breakdown potential for spark gaps in air as a function of electrode separation and radiation rate for spherical geometry and a standard pressure. Within the ranges studied, this would provide the capability of predicting breakdown as functions of the above-named parameters.

The work was started June 23 and completed June 30. It was done at the Kukla facility of the University of California Radiation Laboratory at Livermore, California.

DESCRIPTION OF TEST

TEST SPECIMEN

The geometry of the electrodes to be tested consisted of spheres opposing spheres. Precision ball bearings of one-half inch diameter were used as the electrodes. The bearings were modified so as to be interchangeable with other types of electrodes on a supporting shaft and were thoroughly cleaned and polished. The ground electrode of each spark gap was mounted on the shaft of a micrometer, which allowed setting of the gap to within 0.0001 inch. The high voltage electrode was mounted on a ceramic high voltage feed-through insulator. Four pairs of electrodes were mounted equally spaced within a 3/16 inch wall aluminum box with light shielding between each pair of electrodes. The box was curved to conform with the radius of the screen on Kukla and was designed to take up one-third of the circumference. Figure 43 shows the completed assembly. Figure 44 shows the box with the top cover and electrodes removed. A "T" type pressure fitting was connected to one side of the box; one side of the fitting was used for pressure control; the other side served as an entry for one end of a copper-constantan thermocouple.

TEST SET-UP

Figure 45 shows the general arrangement of the spark gap assembly mounted for testing at Kukla.

Air pressure within the assembly was controlled by means of a pressure regulator, gauge, and compressed air bottle, located in the West Vault. The pressure was regulated to within 0.1 pound.

The temperature of the assembly was monitored with the copper-constantan thermocouple. A small thermos containing water and ice was located in the West Vault and used as the cold junction reference. The thermocouple leads were connected through the cable panel to a Wheelco potentiometer located in the trailer.

A signal isolation and high voltage distribution panel for the spark gap assembly was located behind lead bricks about seven feet from the Kukla assembly. RG-17/U coaxial cable was used to carry the high voltage from the trailer to the panel and RG-11/U coaxial cables carried the signal information from the panel back to the trailer. The remainder of the electronics required was located in the trailer.

TEST CIRCUITRY

Figure 46 is an overall block diagram of the electronic circuitry. Each spark gap was charged through 4.4×10^7 ohms resistance (Figure 47). This size resistance was chosen to make the charging time long compared to the Kukla pulse and prevented repetitive firing of a gap during the pulse. Each spark gap circuit contained a 0.0005 μf, 20 KV high voltage isolation capacitor and a 100 ohm load resistor. The signals developed across each 100 ohm resistor during gap discharge were fed through shaping networks (Figure 48).
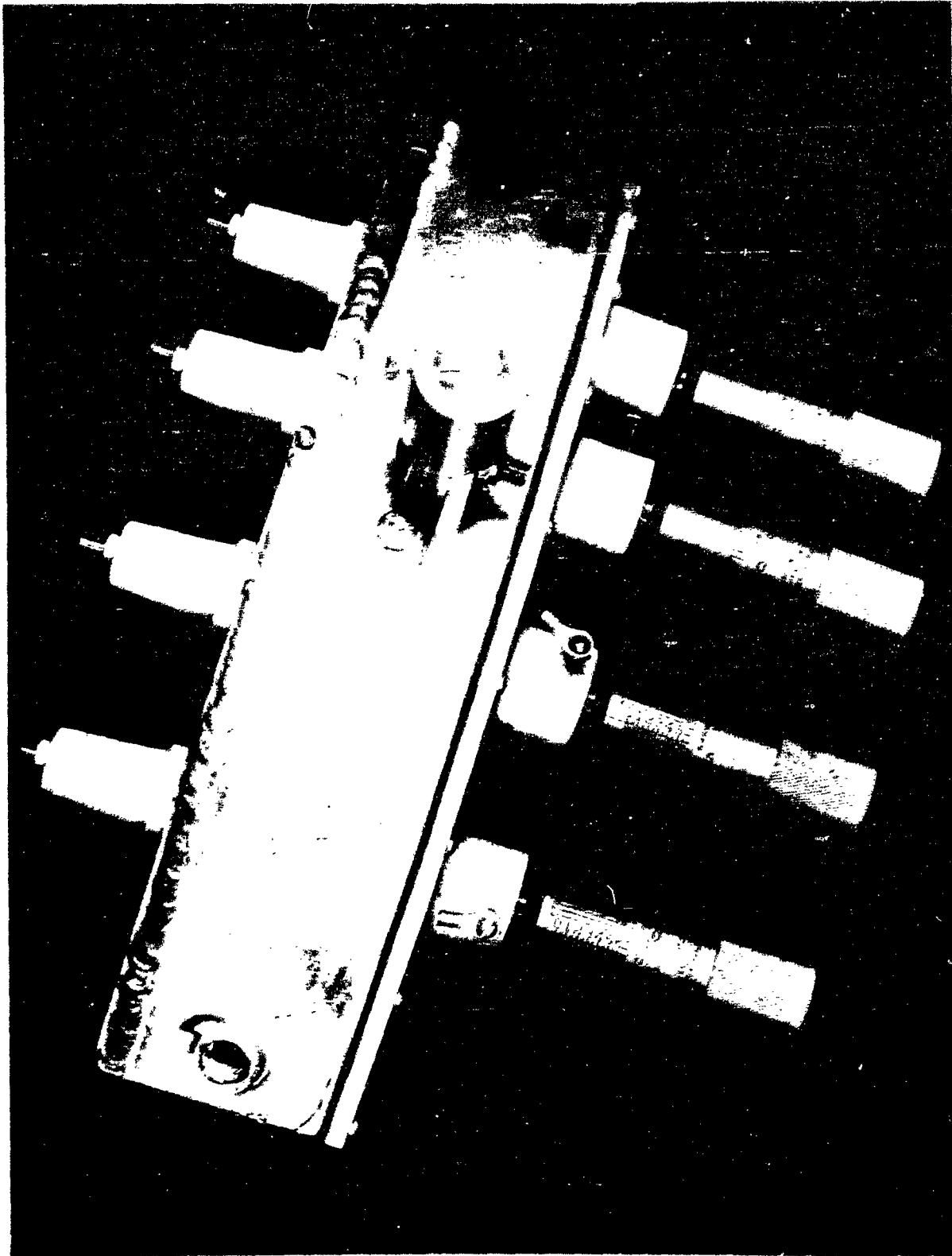
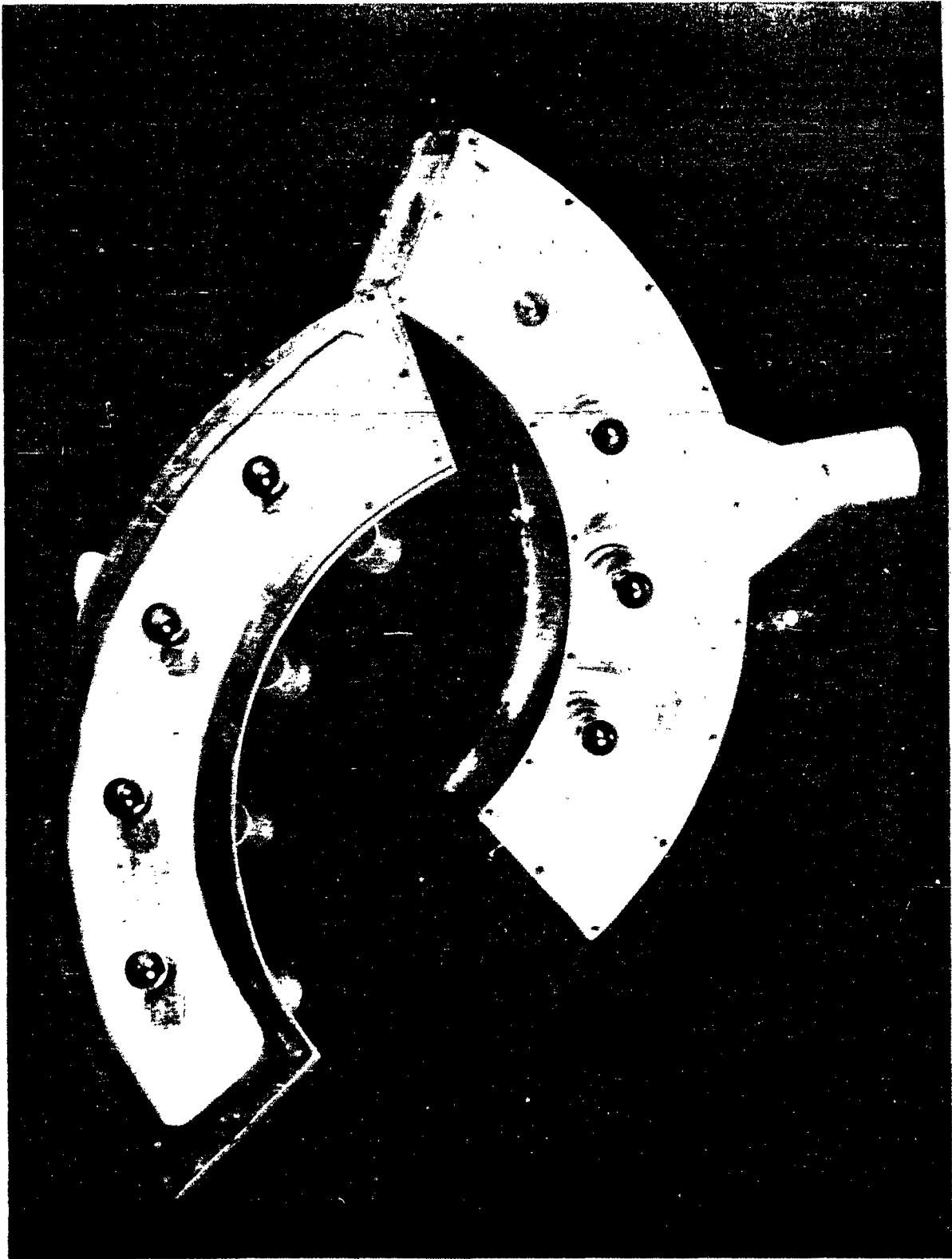Figure 43 - External View of Sparkgap Assembly

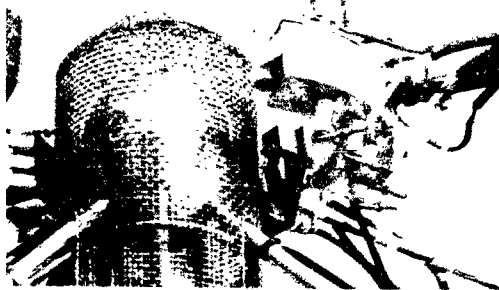Figure 44 – Internal View of Sparkgap Assembly

Figure 45 – The Sparkgap Assembly as
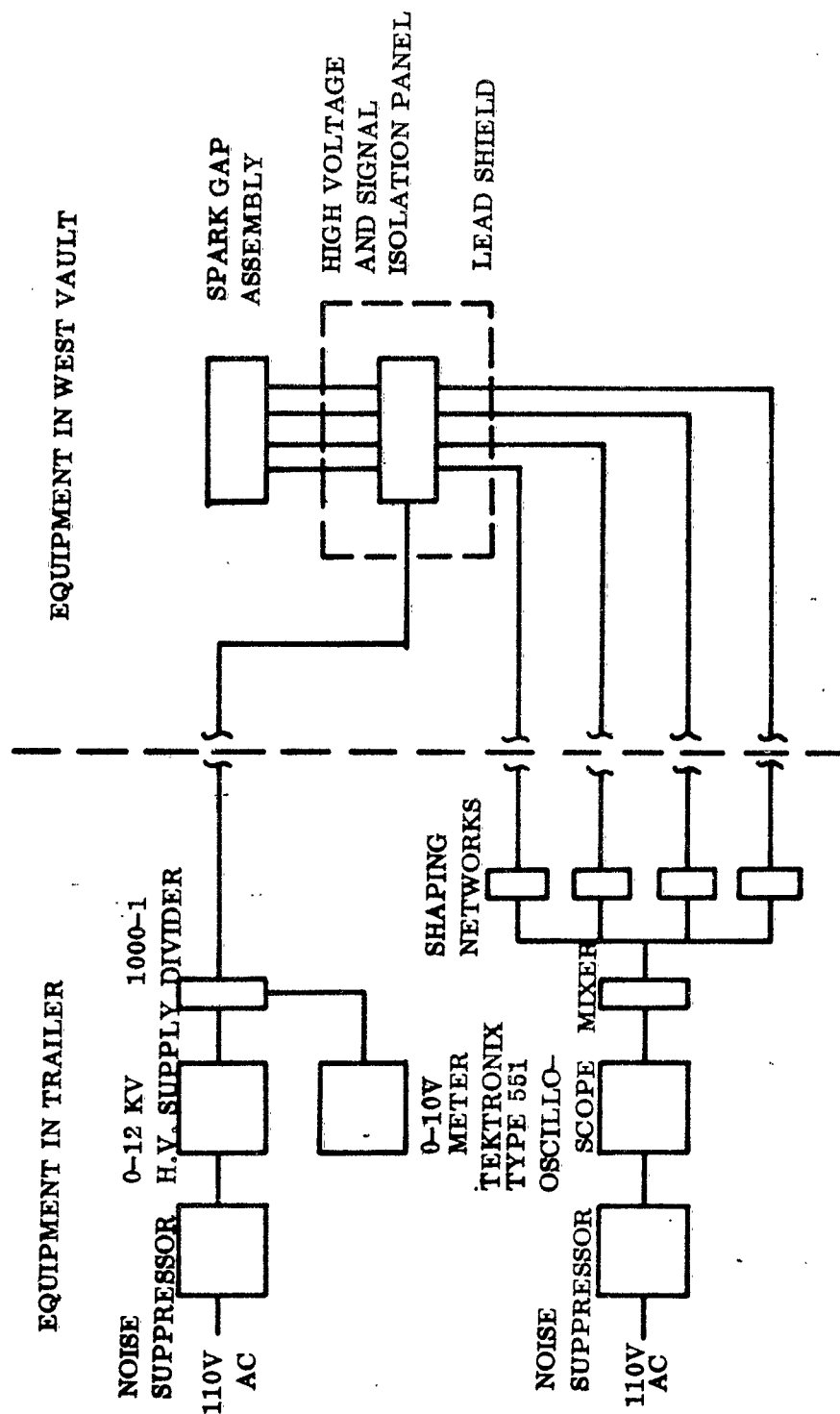Positioned Near the Kukla Reactor

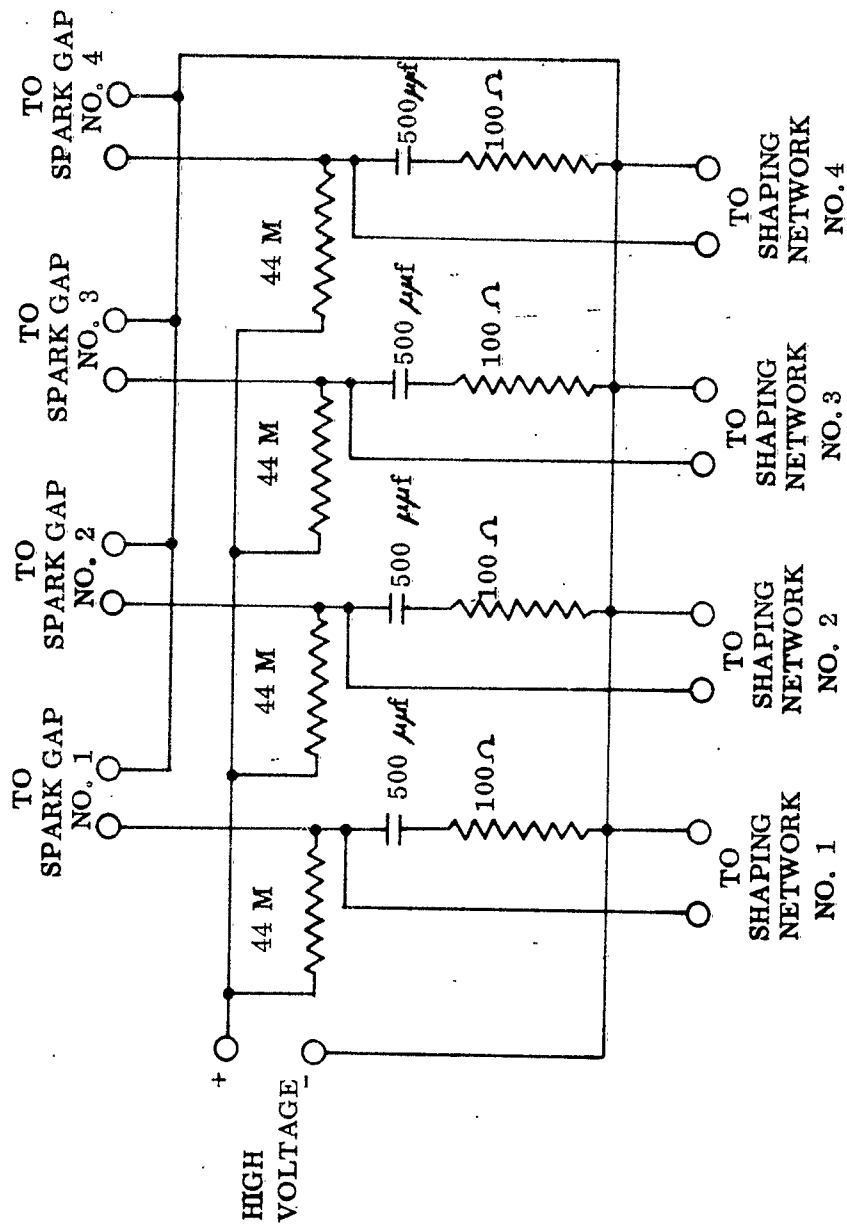Figure 46 – Block Diagram of Electronic Circuitry.

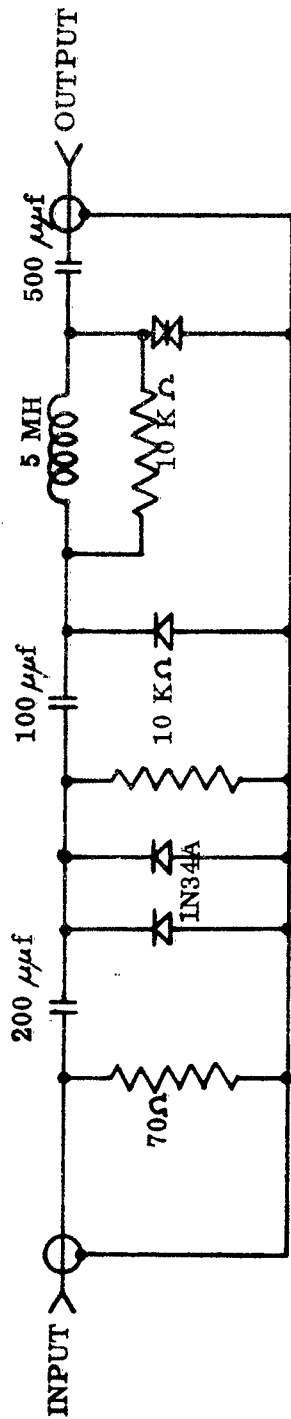Figure 47 – Charging and Signal Isolation Panel.

Figure 48 – Circuit Diagram of Shaping Network.

Each shaping network differed slightly in the amplitude and decay of its output pulse. The outputs of the shaping network fed through an isolation and mixing circuit (Figure 49) to one channel of a Tektronix type 551 dual beam oscilloscope. The Tektronix was set for external triggering by a pulse available from the Kukla assembly on the rise of the radiation pulse. Figure 50a, 50b, 51a, and 51b are typical of the data obtained, where the spark gap data appears on the upper trace. The time at which a gap fired and its identity can be determined from the trace. A comparison of firing time and dosimetry data allowed correlation of firing voltage, gap width, and radiation rate.

TEST PROCEDURE

The voltage was monitored before, during, and just after each burst. The voltage and micrometer readings were prescribed for each burst as indicated in Table 12, Tabulation of Data. The temperature was monitored before and just after each burst.

When the vault was opened between bursts, the stand was pulled back to a convenient working location where the micrometers were set to the newly prescribed values, the sulfur pellets were changed on the stand, and the Sigoloff detector was changed on the end of the spark gap assembly. The stand was then pushed back into place near the assembly and a measurement was taken of the distance from the screen to the specimen. In those instances where the micrometer settings were the same from one burst to another, the stand was not moved, and the sulfur pellets and the Sigoloff detector were changed at the location of the stand.
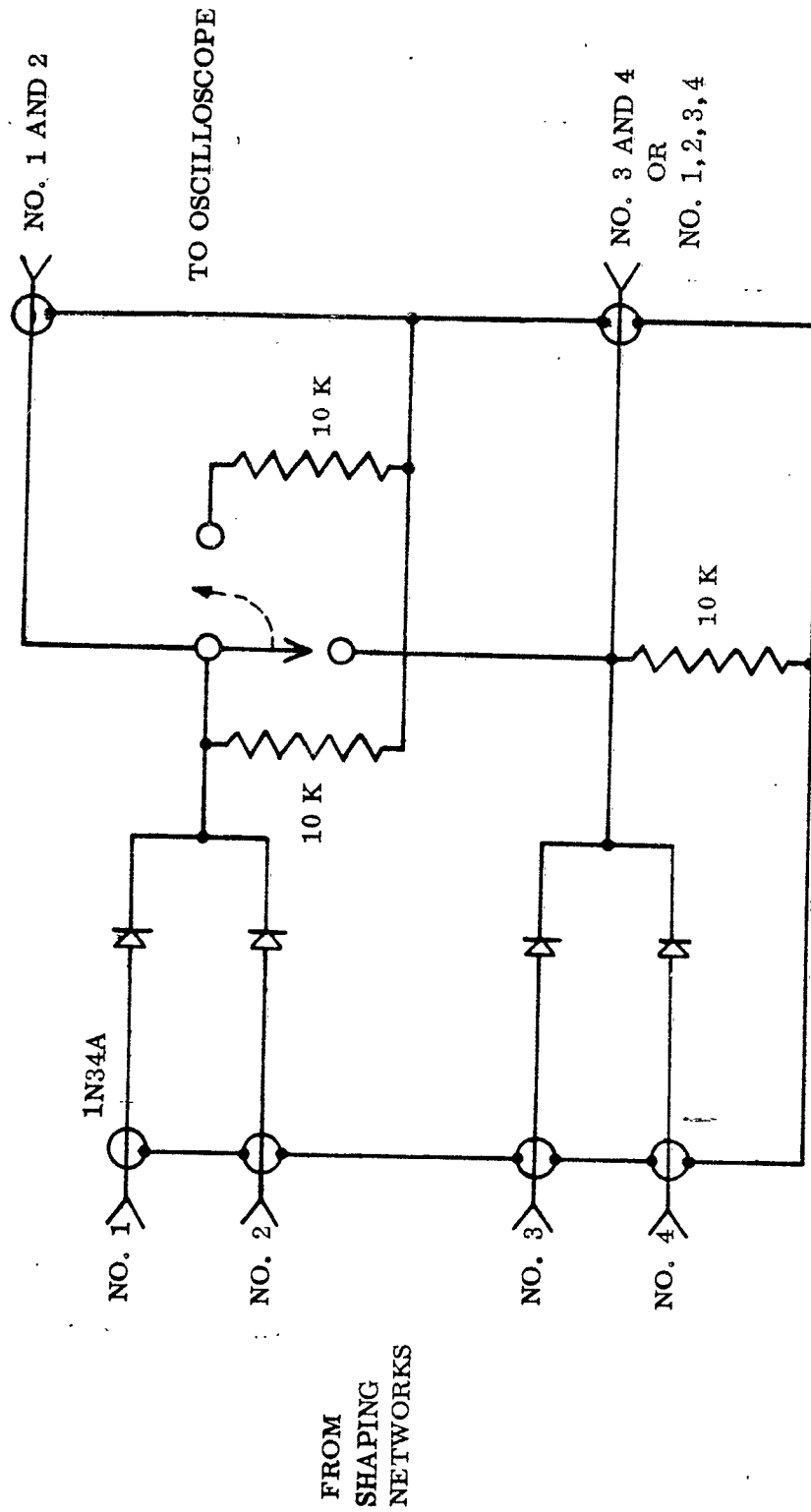
Figure 49 – Circuit Diagram of Mixing and Isolation Network.

Times When
Sparkgaps
Fired
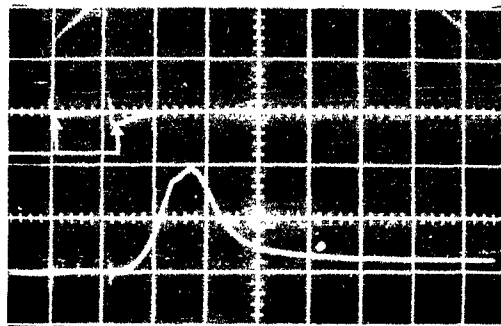
Kukla Burst No. 4

Upper Trace:	Spark Gap
Lower Trace:	Semirad
Sweep Speed:	0.1 msec/cm
Voltage on Gaps:	4580V
Gap Settings:	0.042"
	0.045"
	0.048"
	0.051"

Times When
Sparksgaps
Fired
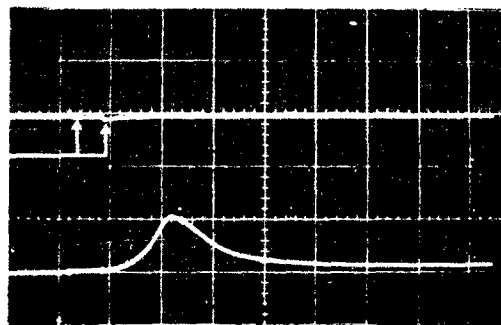
Kukla Burst No. 7

Upper Trace:	Spark Gap
Lower Trace:	Semirad
Sweep Speed:	150 usec/cm
Voltage on Gaps:	7650V
Gap Settings:	0.0735"
	0.079"
	0.084"
	0.089"

Figure 50 – Sample Oscilloscope Traces Showing Times
When Sparkgaps Fired (Burst 4 and 7)

Times When
Sparkgaps Fired
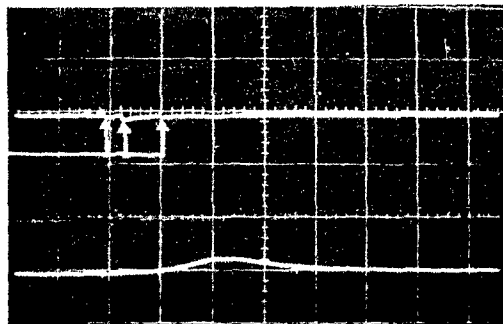
Kukla Burst No. 9

Upper Trace:	Spark Gap
Lower Trace:	Semirad
Sweep Speed:	150 usec/cm
Voltage on Gaps:	10,200
Gap Settings:	0.104"
	0.108"
	0.112"
	0.116"

Times When
Sparkgaps Fired
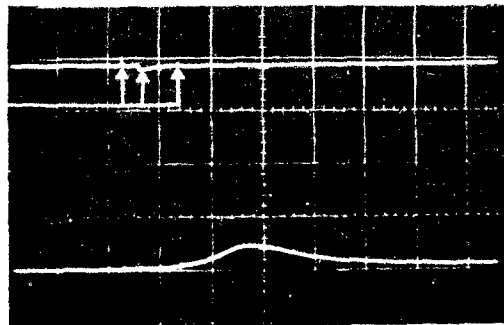
Kukla Burst No. 8

Upper Trace:	Spark Gap
Lower Trace:	Semirad
Sweep Speed:	150 usec/cm
Voltage on Gaps:	10,200
Gap Settings:	0.104"
	0.108"
	0.112"
	0.116"

Figure 51 – Sample Oscilloscope Traces Showing Times
When Sparkgaps Fired.(Burst 8 and 9)

TABLE 12

TABULATION OF DATA

Electrode geometry - spherical

Air pressure - 14.7 psi

Voltage normalized to 23°C

Burst No.	Spark Gap No.	Gap Setting (in inches)	Voltage on all gaps	Firing Rate in r/sec x 10^{-4}	Peak Rate in r/sec at first gap not fired - x 10^{-6}
1 - 3	no data - equipment trouble				
4	1	0.042	4580	0.297	
	2	0.045	↑	7.9	
	3	0.048	↓	--	1.89
	4	0.051	4580	--	
5	1	0.0735	7665	--	
	2	0.079	↑	--	
	3	0.084	↓	--	
	4	0.089	7665	--	
6	1	0.0735	7665	2.29	
	2	0.079	↑	--	0.770
	3	0.084	↓	--	
	4	0.089	7665	--	
7	1	0.0735	7650	1.155	
	2	0.079	↑	5.45	
	3	0.084	↓	--	1.77
	4	0.089	7650	--	
8	1	0.104	10200	1.855	
	2	0.108	↑	3.02	
	3	0.112	↓	13.08	
	4	0.116	10200	--	1.07
9	1	0.104	10200	1.96	
	2	0.108	↑	3.13	
	3	0.112	↓	13.35	
	4	0.116	10200	--	0.900

Table 12 Continued

Burst No.	Spark Gap No.	Gap Setting (in inches)	Voltage on all gaps	Firing Rate in r/sec x 10^{-4}	Peak Rate in r/sec at first gap not fired - x 10^{-6}
10	1	0.088	8880	0.391	
	2	0.092	↑	1.245	
	3	0.095	↓	5.15	
	4	0.099	8880	--	0.500
11	1	0.088	8880	0.299	
	2	0.092	↑	0.43	
	3	0.095	↓	4.01	
	4	0.099	8880	--	1.12
12	1	0.052	5610	0.487	
	2	0.054	↑	4.3	
	3	0.055	↓	--	0.504
	4	0.056	5610	--	
13	1	0.052	5610	0.0842	
	2	0.054	↑	0.503	
	3	0.055	↓	3.86	
	4	0.056	5610	--	0.819
14	1	0.0208	2500	--	
	2	0.0214	↑	--	
	3	0.022	↓	--	
	4	0.0226	2500	--	
15	1	0.042	4590	18.4	
	2	0.043	↑	--	0.456
	3	0.044	↓	--	
	4	0.045	4590	--	

TEST RESULTS AND DISCUSSION

TEST RESULTS

The technical data collected in the test are shown in Table 12. All data points were taken at 14.7 PSIA and normalized to a temperature of $23^\circ C$. The gamma radiation rate, indicated in the table, at which each spark gap broke down was calculated from photodiode information. (See Appendix II on Dosimetry)

The data were first plotted in terms of r/sec versus gap separation for various gap voltages (Figure 52). The curves obtained were extrapolated beyond the last gap which broke down, to give an indication of what might happen at higher rates. In order to aid in the extrapolation, the peak rate data for the next largest gap separation which did not break down was plotted. Since a higher peak rate than was available at the gap would be necessary to cause the gap to break down, the extrapolation would have to pass to the left of the point in question.

The results of the above graphs were cross-plotted at constant radiation rate to obtain curves of breakdown voltage versus gap separation. This information is shown in Figure 53. Curve I of Figure 53 represents the breakdown potential as a function of electrode separation in the absence of radiation. This curve is corrected from STP conditions to $23^\circ C$. Curve II indicates a decrease in breakdown potential, over the range of voltage considered, of about 5.68 percent for any given gap separation at a rate of 2×10^4 r/sec. Curve III indicates decrease in breakdown potential of 8.9 percent at 10^5 r/sec. Curves IV and V represent the results of extrapolating to higher rates and indicate decreases in breakdown potential of 11.75 percent for 8×10^5 r/sec and 14.2 percent for 2×10^7 r/sec respectively. The portions of Curves II through V below 4 KV were extrapolated from the data in the higher voltage region. One experiment in the region below 4 KV yielded negative results and because of the limited number of bursts available no further exploration of this region was possible.

Figure 54 illustrates most clearly what can be expected in the way of percentage change as the radiation rate increases. The trend of the curve indicates a decreasing percentage change for each higher decade of radiation rate. Thus for a 15 percent reduction in breakdown potential, a rate of $\sim 10^8$ r/sec is indicated.

DISCUSSION OF RESULTS

An attempt can be made to explain the observed results on the basis of positive space charge buildup, time lag, and geometric considerations. Measurements reported in the literature (Ref. 40) show that time lags in air for a given electrode separation and pressure increase continuously and smoothly as the percent overvoltage decreases from two percent to very low values (i.e. as the field strength becomes less supercritical). The existence of long time lags (on the order of microseconds) at low percent overvoltages indicates that the motion of positive ions plays an important role in the breakdown process and the steady increase in time lags indicates that the role of the positive ions increases in importance as the field strength is decreased. Indeed, the role of the positive ions in producing breakdown is assur-

ed in that the positive ions aid the breakdown process by producing a distorted field in the gap due to space charge buildup (Ref. 41 and 42).

The present experiment had gaps with subcritical field strengths approaching ten percent in some cases. It is suggested that the phenomenon observed in a radiation field is precipitated by a greatly enhanced case of space charge buildup resulting primarily from Compton scattering in the gas. The distortion of the field in the gap, due to the increasing space charge buildup, then ultimately leads to a critical field at which time the gap breaks down.

Further, it is expected that the formative time lag is at least as long as, if not longer than, in the case of low overvoltage in the absence of radiation. As the positive ions move toward the cathode, the field strength in the cathode region increases more and more rapidly with time. In the absence of a critical field when the first avalanche crosses the gap, it is possible that this and subsequent avalanches may supply a sufficient number of ions to produce a critical charge density; hence a critical field strength, in which the avalanche is born which will initiate breakdown. This type of mechanism could involve times corresponding to many positive-ion transit times before the gap breaks down.

Finally, a non-linear field strength between spherical electrodes yields larger regions in the gap which have sufficiently high field strengths to support ionization growth (Ref. 34). It is therefore expected that homogeneous field electrodes would yield a smaller percentage change in voltage for a given radiation rate than would spherical electrodes. Conversely, geometries which would give greater non-linearities in field strength than would spheres, might be expected to give greater voltage differences for a given rate. These ideas must be borne in mind when comparing the results of the present experiment to those in Ref. 32 and 33. In each of those cases conventional spark gaps having sharp edges were used, which, by the account above, would indicate that a larger voltage change could be expected than in the case of spherical electrodes. In addition, the study referred to in Ref. 32 utilized nitrogen gas, which involves an additional consideration in making an analysis.
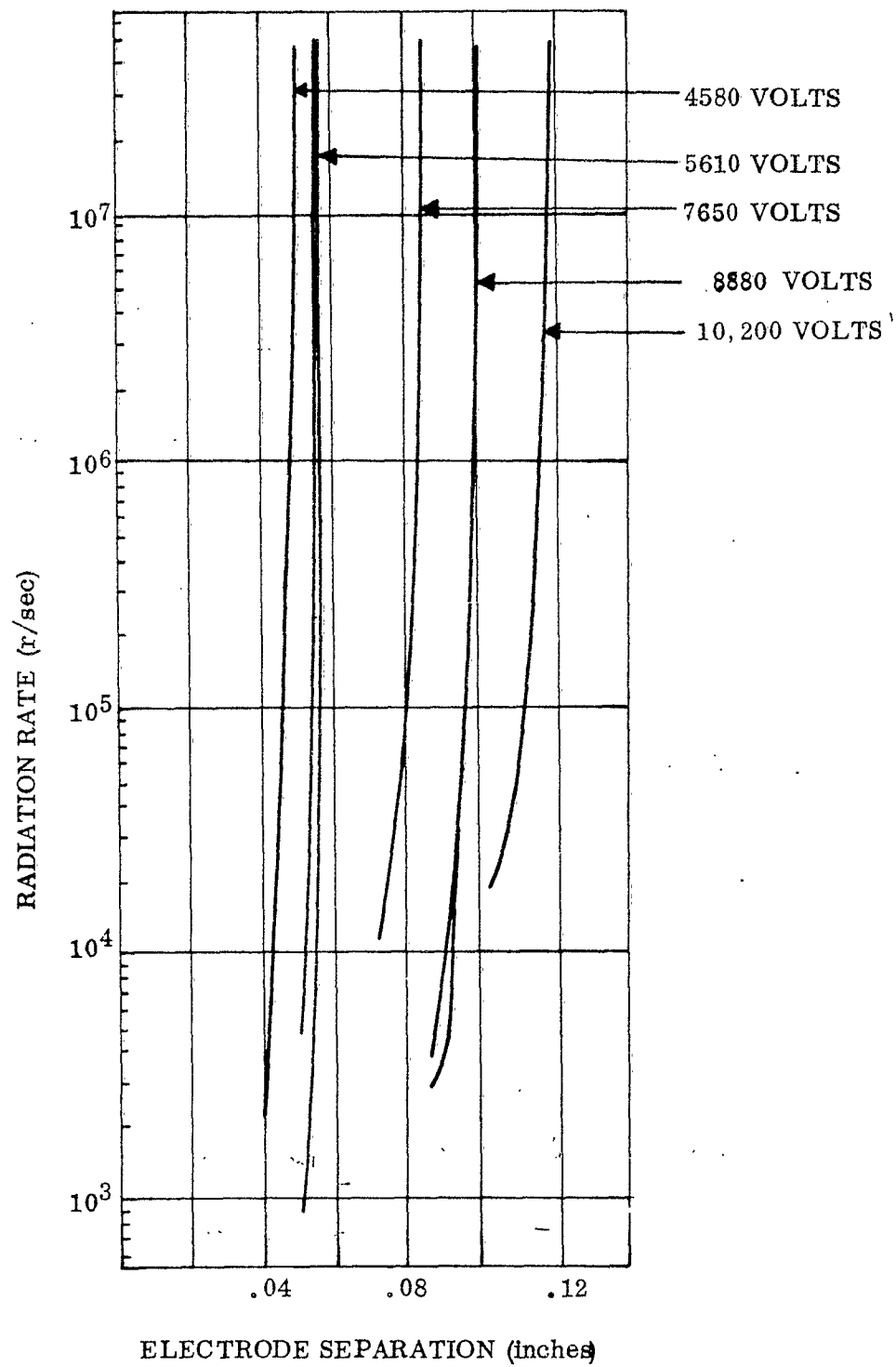
Figure 52 – Plot of Actual Data Points Obtained From Table 12.

I – Breakdown potential in the absence of radiation.
II – Breakdown potential at a rate of 2×10^4 r/sec.
III – Breakdown potential at a rate of 1×10^5 r/sec.
IV – Breakdown potential at a rate of 8×10^5 r/sec.
V – Breakdown potential at a rate of 2×10^7 r/sec.

(curves represent a data for air at 14.7 psia and 23°C)

KILOVOLTS

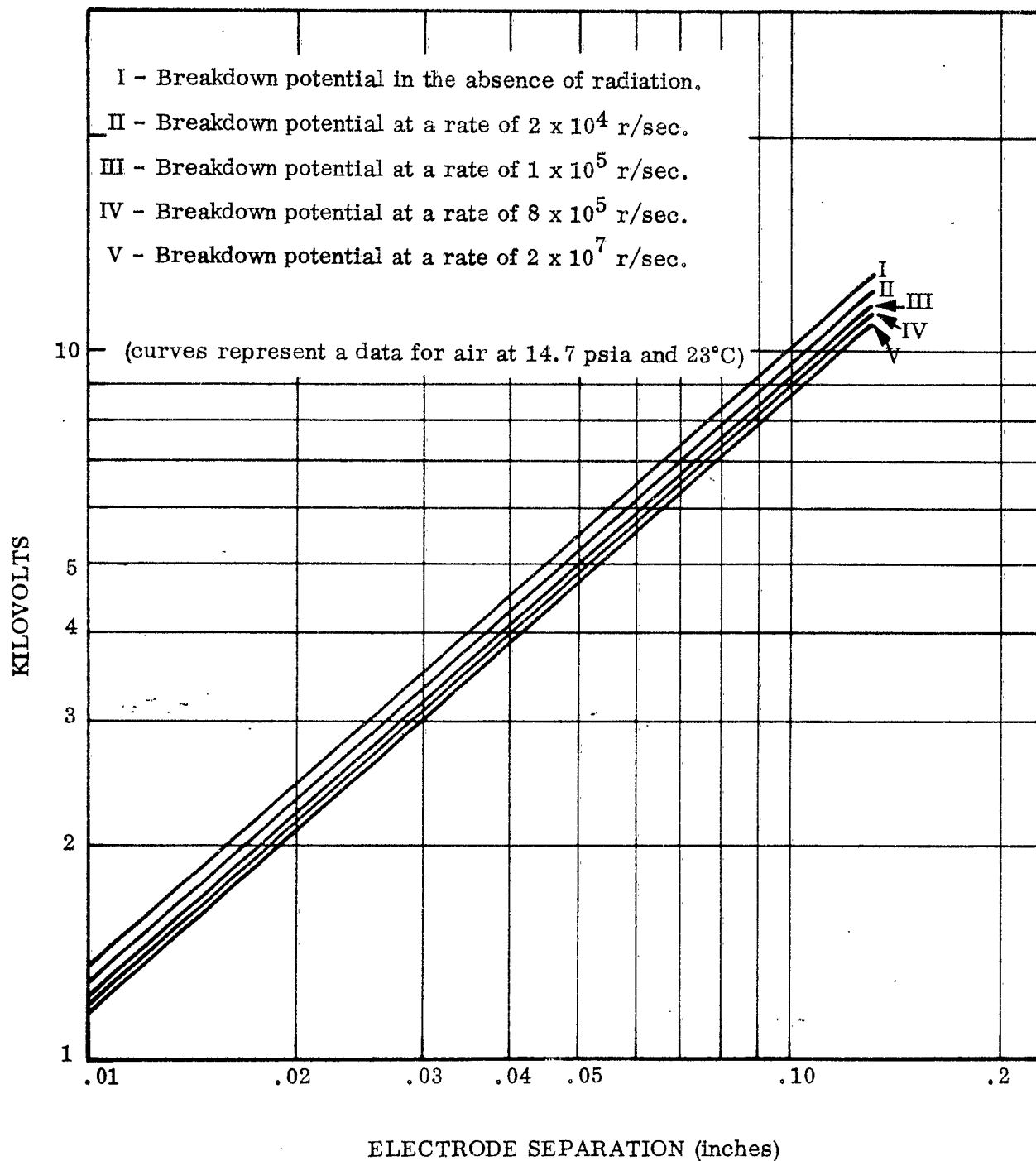ELECTRODE SEPARATION (inches)

Figure 53 – The Breakdown Potential of Spherical Electrodes for Several Radiation Rates.
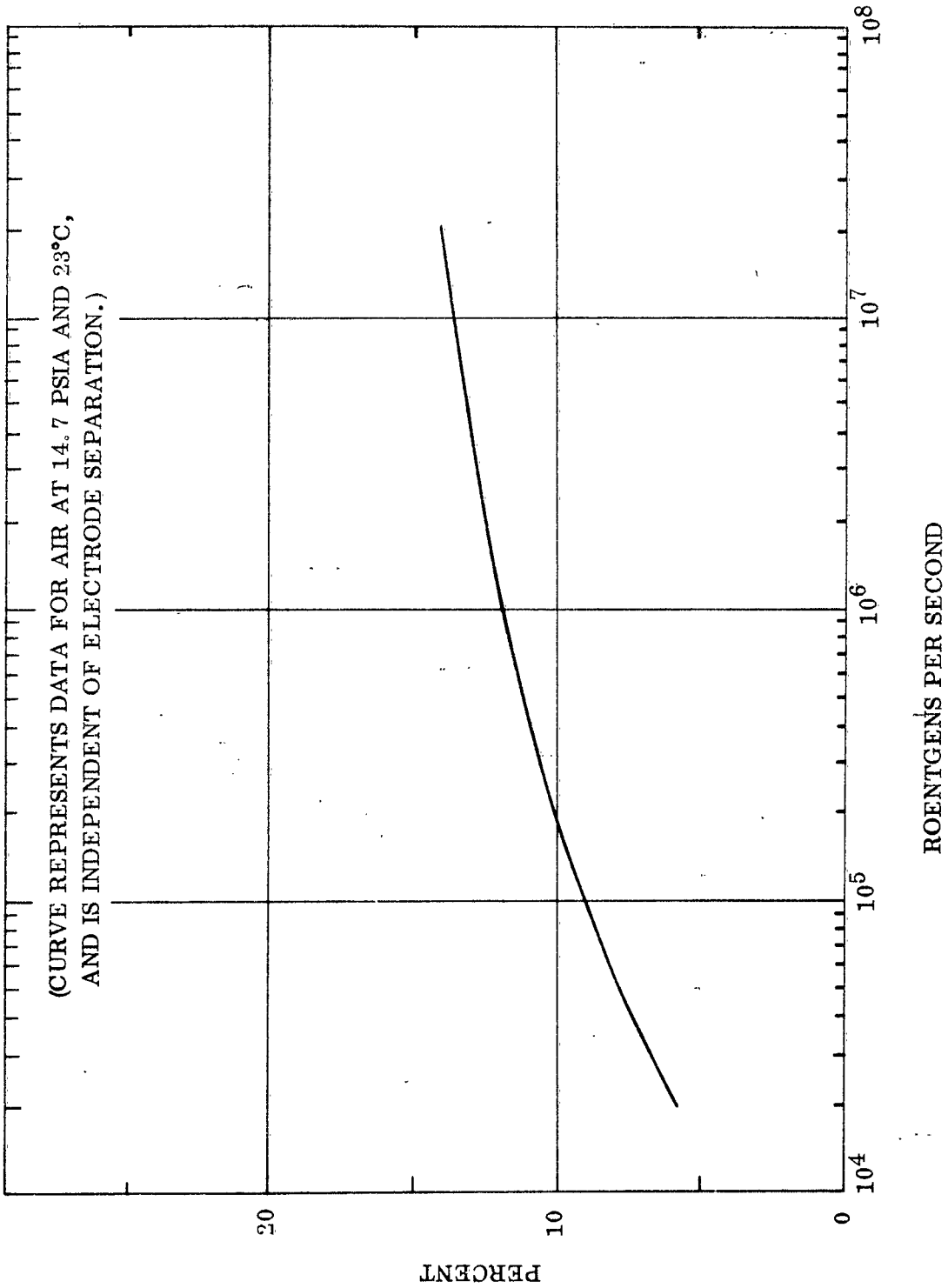
Figure 54 – Percent Reduction of Breakdown Potential Versus Radiation Rate.

(CURVE REPRESENTS DATA FOR AIR AT 14.7 PSIA AND 23°C, AND IS INDEPENDENT OF ELECTRODE SEPARATION.)

ROENTGENS PER SECOND

PERCENT

CONCLUSIONS

The experiment has provided the capability of predicting high voltage breakdown in air as a function of electrode spacing and radiation rate for spherical geometry and a standard pressure. Further, indications have been given of what can be expected for higher rates than were obtained in the present experiment. One of the most noticeable indications is that a decreasing percentage change is expected for each increasing decade in radiation rate, so that a reduction in breakdown potential of 15 percent would require a rate similar to 10^8 r/sec. Finally, a qualitative analysis of the phenomenon has been given in terms of space charge buildup, formative time lags, and geometrical considerations.

RECOMMENDATIONS

Further experimentation is needed before a comprehensive picture of high voltage breakdown in intense radiation fields can be given. Specifically needed are experiments performed at higher rates; and experiments performed as functions of other electrode geometries, of pressure, and of different gases. Experimentation should also be included which would assess the contribution of preferential Compton scattering and of photoelectric emission from the cathode. In a somewhat different vein, experiments should be performed to determine quantitatively the magnitude of the time lags as functions of the above named parameters. In connection with this, it should be possible, with the aid of a digital computer, to calculate the space charge buildup as a function of time. This information, together with that of the time lags, would provide the capability of quantitatively comparing theory and experiment.

REFERENCES

32   Urquhart, K. L., Sandia Corp. (personal communication) - unpublished data.

33   Duncan, G. J., et al., "The Effects of Nuclear Radiation on Spark Gaps," Third Semi-Annual Radiation Effects Symposium, Vol. 2.

34   Allen, K. R. and Phillips, K., Nature (London), Vol. 183, 233-5, Jan. 24 (1959).

35   Rogowski, W., and Wallraff, A., Z. Phys. 97, 758 (1935).

36   Meek, J. M., Proc. Phys. Soc., 52, 547, 822 (1940).

37   White, H. J., Phys. Rev. 48, 113 (1935).

38   Fuchs, W. and Seitz, W., Z. Phys. 103, 1 (1936).

39   Brinkman, C., Z. Phys. 111, 737 (1939).

40   Fisher, L. H., and Bederson, B., Phys. Rev. 81, 109 (1951).

41   Ward, A. L., Phys. Rev. 112, 1852 (1958).

42   Crowe, Bragg, and Thomas, Phys. Rev. 96, 10 (1954).

APPENDIX V

TRANSIENT RADIATION INDUCED FIRING OF 5643 THYRATRON

by

Richard H. Dickhaut and Willard E. Spencer

TABLE OF CONTENTS

LIST OF ILLUSTRATIONS

INTRODUCTION

The greatest amount of experimentation on thyratron breakdown which is readily available has been performed by the Diamond Ordnance Fuze Laboratory (DOFL) (Ref. 43). They have tested a 5643 thyratron in various radiation environments and the results of their experiments are shown in Figure 55. As there was no experimental information available on the mechanisms involved which could explain such results, it was suggested in dicussions with DOFL personnel that the grid current of the thyratron should be measured to determine possible mechanisms for both gas and hard tube transient effects. If a current flow during the radiation pulse was sufficient to change the grid bias and fire the thyratron, the mechanism for the observed transient effect could be influenced by external circuitry configurations. In accordance with this suggestion, an experiment was planned which would simultaneously measure the grid current of one thyratron and display the successive firing of four other thyratrons as a function of radiation rate in the same burst.

PURPOSE

The purpose of this investigation was to attempt to determine possible mechanisms for the observed transient effect on a subminiature type 5643 thyratron by analysis and comparison of results from grid conduction and breakdown tests.
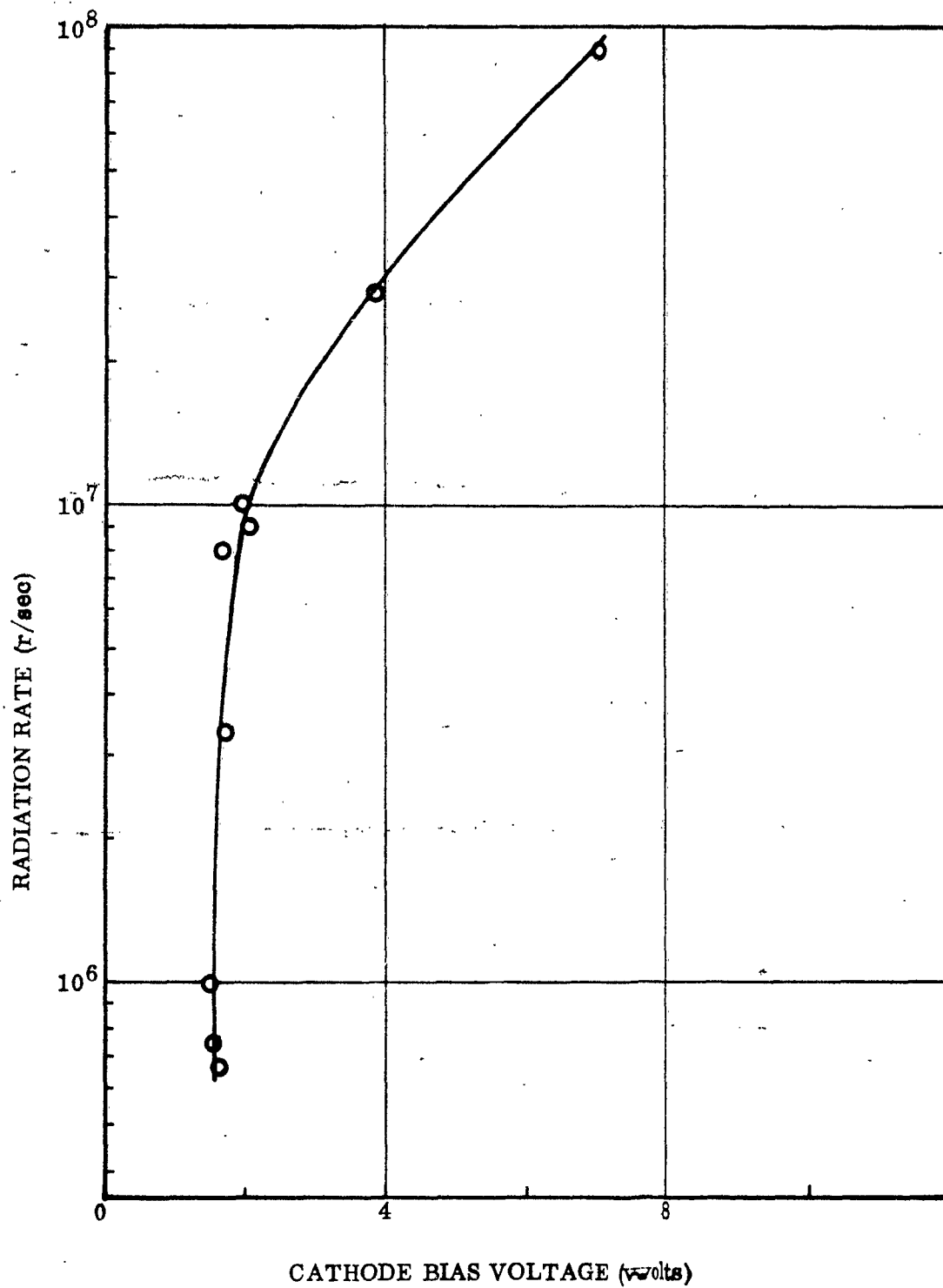
Figure 55 – DOFL Radiation Rate Firing Point Data For Type 5643 Thyratron.

TEST DESCRIPTION

For the grid conduction test, the bias was set at a value at which the tube would not be apt to fire during the radiation burst. A resistor of one megohm was placed in series with the grid of the thyratron. A pair of cathode followers, one at each end of the resistor, was designed to indicate by their differential output the amount of current drawn by the grid. This voltage drop, which is proportional to the current drawn, was presented on one of the traces of a dual beam oscilloscope. The test equipment was entirely contained within the reactor room with the exception of the RG-22/U coaxial cables through which were carried the signals to the oscilloscope in the trailer. Figure 57 is a circuit diagram of the test instrumentation for the grid conduction tests. The minimum detectable current for this circuit was 10^{-8} amps.

For the breakdown tests, four separately shielded thyratrons were used and the circuit was designed so that the successive firing of the thyratrons in the order of their increasing bias voltages would be displayed on an oscilloscope. The thyratrons were operated by a control box and power supplies positioned about twelve feet from the reactor behind some lead bricks. The circuitry was arranged so that the bias voltages could be precisely adjusted by potentiometers. The biases on the control grids were set at various values during the series of bursts and a pictorial representation of their settings is given in Figure 56. The plate voltage used on the thyratrons was 450 volts in all cases. In addition to the display on the oscilloscope, small fuzes were shorted out when the thyratrons fired. The shorting out caused a neon bulb to light, thereby giving an indication of the action the thyratron had taken. The complete circuit for the breakdown tests is shown in Figure 58.
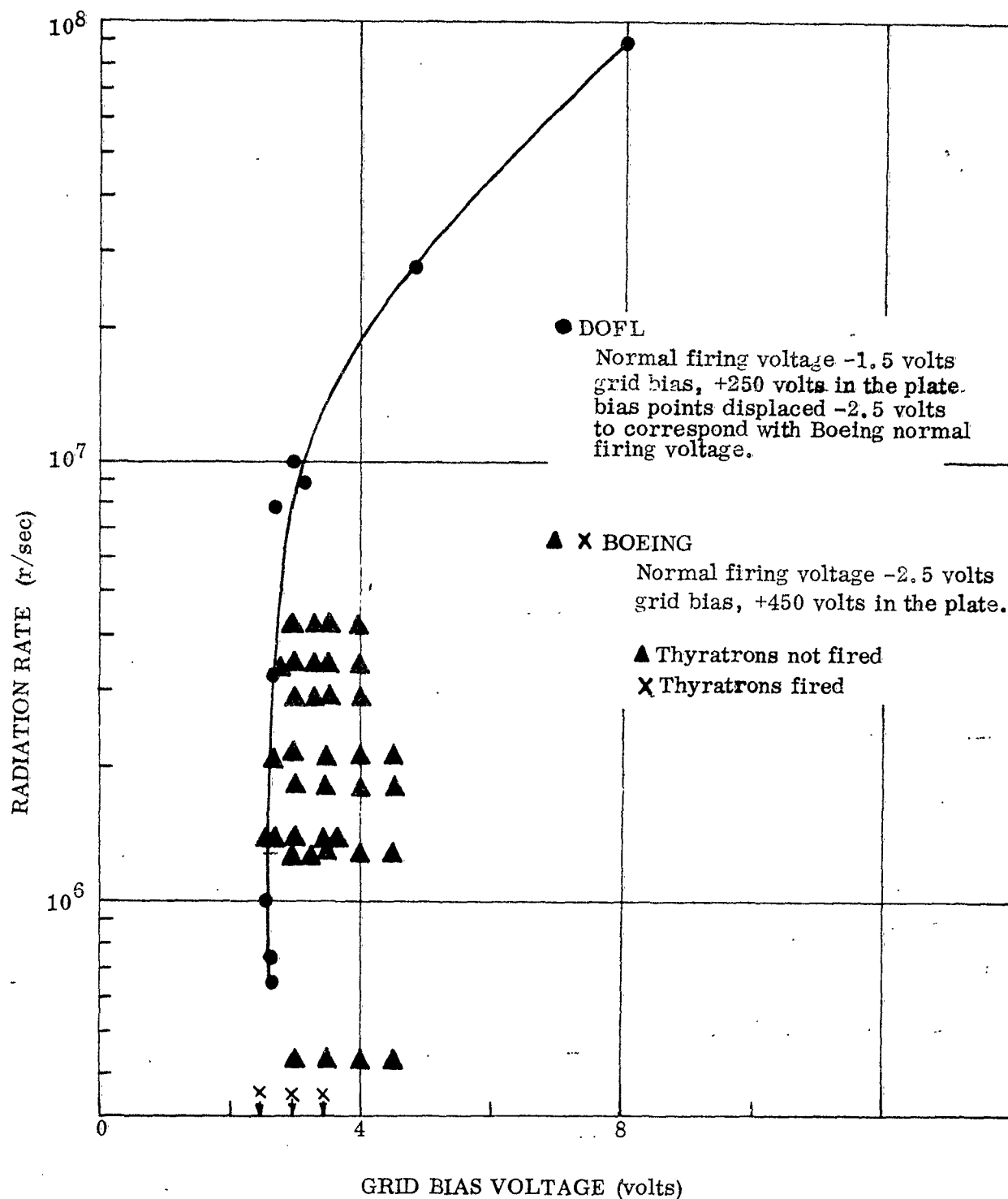
Figure 56 – DOFL Radiation Rate Firing Data for Type 5643 Thyratron With BAC Grid Bias Voltage.
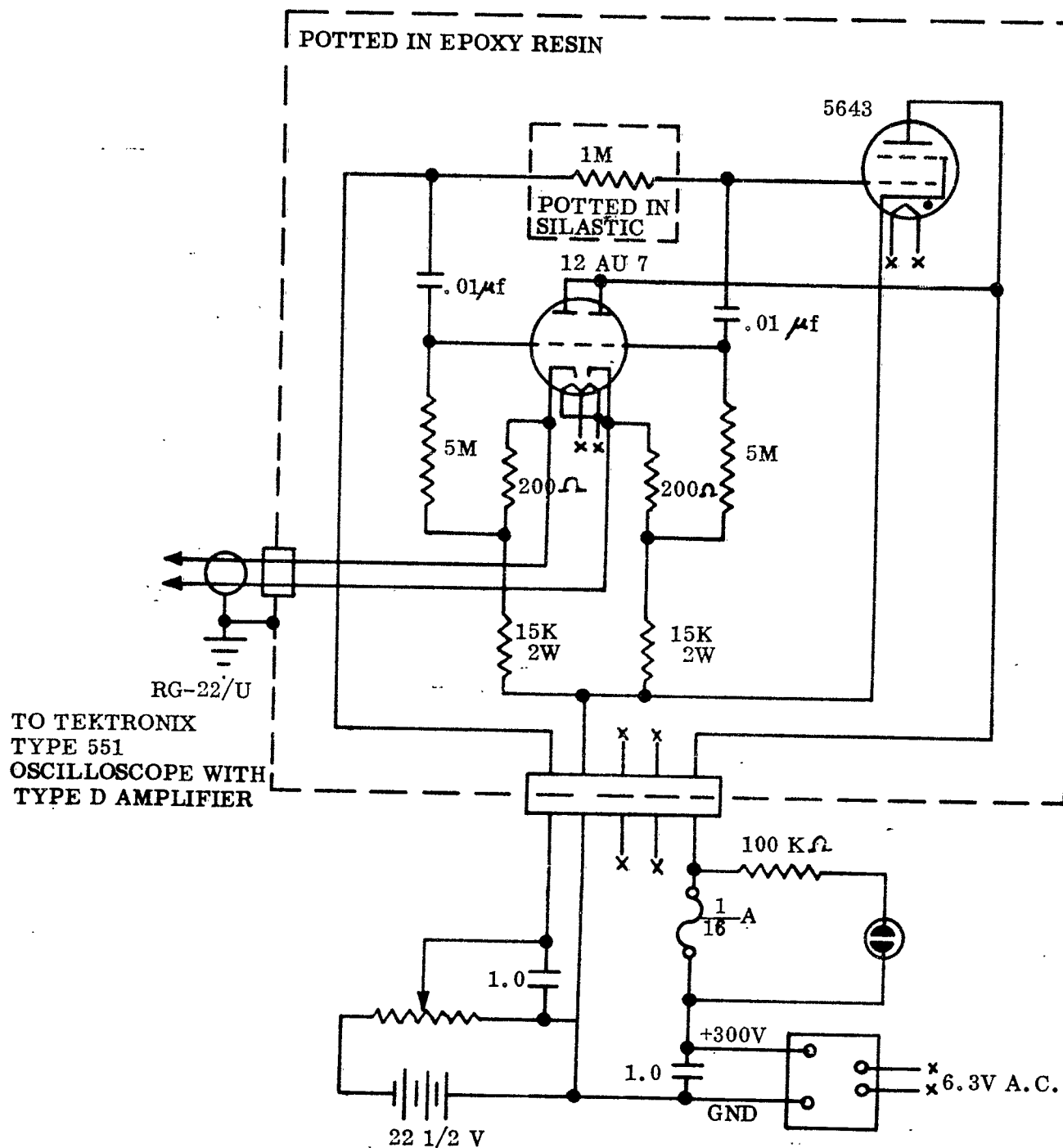
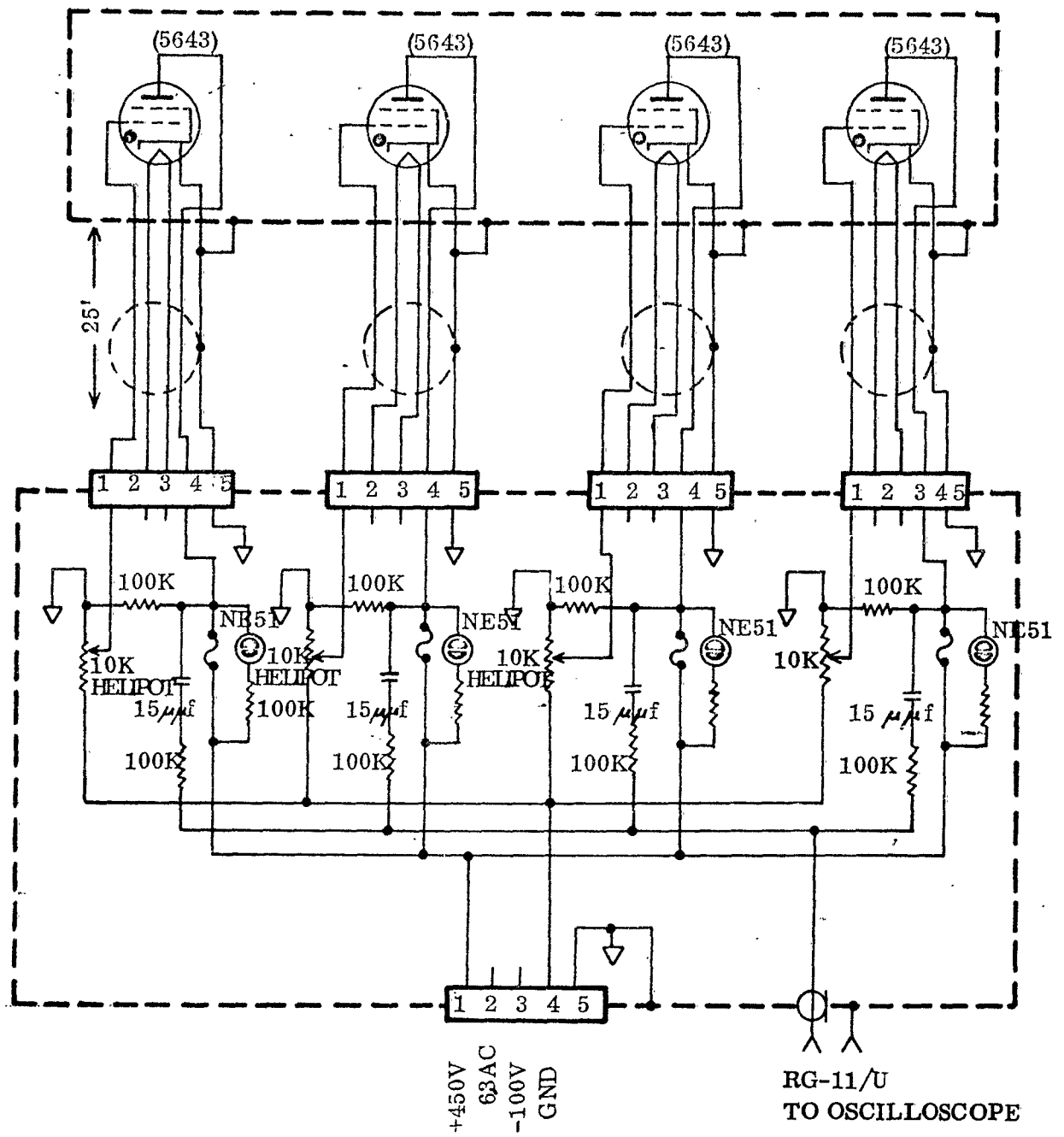Figure 57 – Thyratron Grid Conduction Circuit.

Figure 58 – Thyratron Firing Circuit.

TEST RESULTS AND DISCUSSION

No observable signal was obtained in the grid conduction tests, and none of the thyratrons fired in the breakdown tests, with the exception of two cases in which circuit difficulties accidently caused the thyratrons to fire. Although the results of the tests were completely negative, due to a combination of low radiation rates and high bias settings, an attempt was made to determine if the results were consistent with existing information.

Comparison of the biases and the peak radiation rates in the breakdown tests with the thyratron data given in Ref. 43, shows that all the points lie to the right of the curve in Figure 56. This indicates that with these bias values and radiation rates, none of the thyratrons could have been expected to fire. Thus the data obtained is consistent with the DOFL curve Figure 55.

The lack of a signal in the grid current measurement suggests that the mechanism which causes the thyratron to fire is not affected by the external circuitry. This statement has more strength when one considers that the DOFL circuit had a grid resistance of 5000 ohms, and fired at rates in the region of 10^7 r/sec. This would have required a signal of 0.5 volts or a current of 100μa.

CONCLUSIONS

The thyratron breakdown tests proved to be consistent with the data of Ref. 43. In this preliminary experiment, no signal was observed in the grid conduction tests. This indicates that grid voltage changes caused by radiation induced grid current is not a mechanism to explain thyratron firing.

Note: From results obtained from DOFL after this test was run (Ref. 44), it appears that photoelectric emission can account for the transient behavior observed in response to light pulses, and the strong similarity of this behavior to that observed in response to higher energy radiation suggested that photoelectric emission may be a significant part of the nuclear radiation effect observed in vacuum tubes and thyratrons.

RECOMMENDATIONS

A thorough investigation should be performed with nuclear radiation at higher rates to illuminate the mechanisms or combination of mechanisms which are responsible for the observed transient effects on thyratrons. These experiments should be performed in such a way as to separate effects of photoelectric emission due to fluorescence accompanying pulsed nuclear environments from those due to volume ionization of the gas or other processes.

REFERENCES

43   Bishop, M., Diamond Ordnance Fuze Lab. (Personal communication) unpublished data.

44   Caldwell, P. A., and Allen, J. K., TM-230-60-2, 14 February 1960.

APPENDIX VI

TRANSIENT EFFECTS IN SEMICONDUCTOR DIODES

by

August G. Berger, Jr.

TABLE OF CONTENTS

LIST OF ILLUSTRATIONS

LIST OF TABLES

INTRODUCTION

Radiation effects in semiconductors are of considerable interest, with regard to the physical mechanisms involved, and also device behavior for circuit applications. In general, passage of nuclear radiation through a material may introduce a wide variety of defects, varying with the particular crystal involved, initial impurities, and character and time-dependence of the radiation. The lifetimes of these defects may depend upon the temperature as well as the factors mentioned. In semiconductors, fast neutron irradiation causes atomic displacements and heavy ionizing secondaries. Gammas cause ionization and ionizing secondary electrons. Thus permanent changes in minority carrier lifetime, resistivity, and mobility, as well as increases in carrier concentration may be expected upon irradiation with a neutron-plus-gamma field. For pulsed neutron and gamma irradiation these effects may produce both transient and permanent changes in electrical properties of semiconductor materials.

Several tests have been performed on the transient current pulses obtained from reverse biased diodes and transistor junctions. (See for instance Ref. 46, 47, 48, 49, 51 and 55.) This work is beginning to yield a fairly consistent picture of the mechanisms of the current pulse generation. However, little or no information is available on the changes in forward characteristics of diodes, or the variation of the reverse current pulse with applied voltage.

The work described in this appendix was directed toward establishing sufficient information to allow a preliminary circuit representation of the diode in a transient radiation environment to be developed.

PURPOSE

The tests herein described were carried out in order to investigate the methods appropriate to measuring changes in properties of semiconductor devices exposed to the neutron-plus-gamma radiation from the Kukla prompt-critical reactor. The testing procedure was designed to yield circuit design type parameters. Preliminary information on the behavior of a specific diode was to be obtained.

DESCRIPTION OF TEST

TEST ITEMS

The 1N277, a gold-bonded germanium diode, was selected for test because of its use in a particular circuit application for another program, and because its response is fast enough to follow the pulses from a reactor of this type. Also it is known that germanium is less susceptible than silicon to permanent neutron damage, generally an undesirable effect in transient effect investigations (Ref. 45). The choice was subject to the primary difficulties associated with most device tests: a lack of knowledge of the detailed construction and material properties, and the variance in properties from diode to diode. In view of these facts and time limitations, a simple equivalent circuit approach was used in deciding which parameters to measure.

TEST SETUP AND INSTRUMENTATION

The equivalent circuit approach is based on the fact that one may describe a smooth curve over a narrow region by giving the slope of the curve and the intercept of the tangent at that point on one of the axes. For the diode this is equivalent to assumption of a dynamic resistance and a current or voltage source to describe the behavior near a given operating point on the I-V characteristic. Measurement of the radiation-induced voltage change when constant current is applied, and of the radiation-induced current change when a constant voltage is applied to the diode should give the information necessary to calculate the radiation-induced change in the I-V characteristic.

The alternative method of measuring the entire I-V characteristic during the irradiation was infeasible because the available high-gain amplifiers did not have sufficient bandpass to operate at the repetition rate required. Measurement at many points on the I-V characteristic was infeasible because of the limited number of recording channels and Kukla bursts available, unless one restricted the test to a very few diode specimens. Also, in the latter case, if an individual burst produced appreciable permanent damage, then measurement of the changes at a different point on the I-V characteristic would pertain to a "different" diode. Direct measurement of the changes in slope and operating point by imposing a small alternating voltage (or current) on the constant current (or voltage) supply would have been highly desirable, but bandpass limitations also arise in this case.

In view of these facts it was decided to measure current change at constant voltage, and voltage change at constant current, using simple resistor networks and batteries to set operating points for 1N277 diodes. The nominal operating points chosen were (+0.3V, + 1ma) and (-12V, -2μa). In the setup for each measurement four diodes were mounted in a 2-1/2 x 2-1/2 inch terminal board in an aluminum box. The open face of this header was placed near the reactor on a rod stand-mounted on a dolly. RG-58/U coaxial cables (8 feet long) for applying operating voltages and currents and for signal leads were brought into the header without connectors and attached directly to the terminal boards. The terminal boards were coated approximately 1/4 inch thick with Silastic RTV 882 (Dow-Corning) in order to reduce current conduction around the diodes and cable ends due to air ionization during a radiation burst. The cables

were brought back to a small junction box where the resistor networks were potted in Hysol 6020 (Houghton Laboratories). This junction box and a battery box were located on the dolly approximately six feet from the reactor. BNC connectors with the locking studs filed off were mounted on the junction box for quick disconnect from the RG-58/U cables (40 feet long) leading to a distribution panel in the reactor vault. RG-22/U cables (110 feet long) then led to the trailer outside the building, where they terminated at two dual-channel Tektronix Model 551 oscilloscopes, equipped with Model D preamplifiers and Beattie-Coleman/Polaroid cameras. (The twin leads of the RG-22/U were paralleled to approximately match the RG-58/U cable.) For each of the four basic setups a duplicate diode header was provided to permit gain-setting runs or repeat runs. In addition, four headers were designed with resistors in the junction boxes to simulate the diodes in operation. These were used to measure any leakage effects included in the signals from the diode headers. To get some idea of the sources of the various leakages, each of these headers included the following four circuits:

1. A cable loop in the header--to check for cable leakage.

2. Nothing in the header--to check for leakage in the junction box.

3. A burned-out diode in the header--to check for leakage inside and outside the diode case.

4. Two diode leads with the case and diode junction removed--to find out whether any leakage in (3.) was primarily external or internal to the case.

Headers one and two were designed to obtain supplementary information on resistors of the type used in constructing the networks (Welwyn-Canada, type C, 1 percent, 1/2 watt and 1 watt; and Sage, 5 ohm, 3 percent, 1 watt.) Also a 20 microfarad, 50 volt, tantalum capacitor was checked in these junction boxes in order to find out if capacitor coupling could be used in future experiments without introducing spurious signals. Header one was to be without potting material, in order to verify that the potting was necessary but this test was not performed. Additional details are given in the individual drawings of the experimental setups, Figures 59 through 67.

TEST PROCEDURE AND DOSIMETRY

By use of quick-disconnects on the cable set and header mounting, and a movable dolly mounting, working time in the reactor vault was kept to a minimum so that total exposure was limited less than 0.3 roentgen for each of the two operators. It was necessary to segregate the battery boxes as a possible beta-radiation hazard for a few hours after each burst.

Total neutron fluxes and peak gamma rates at the terminal-board position for this experiment were obtained from beta-counting on sulfur pellets and photodiode signals respectively, as discussed in Appendix II on Dosimetry. The average distance from the reactor center to the diodes in the header boxes was 14.5 ± 0.6 cm. This determines the main contribution to the probable error of ± 10 percent in the stated peak gamma rates, considering only the distance variations involved in repositioning the dolly prior to each burst. The probable error in the neutron data likewise is ± 10 percent. Systematic errors are discussed in Appendix II.
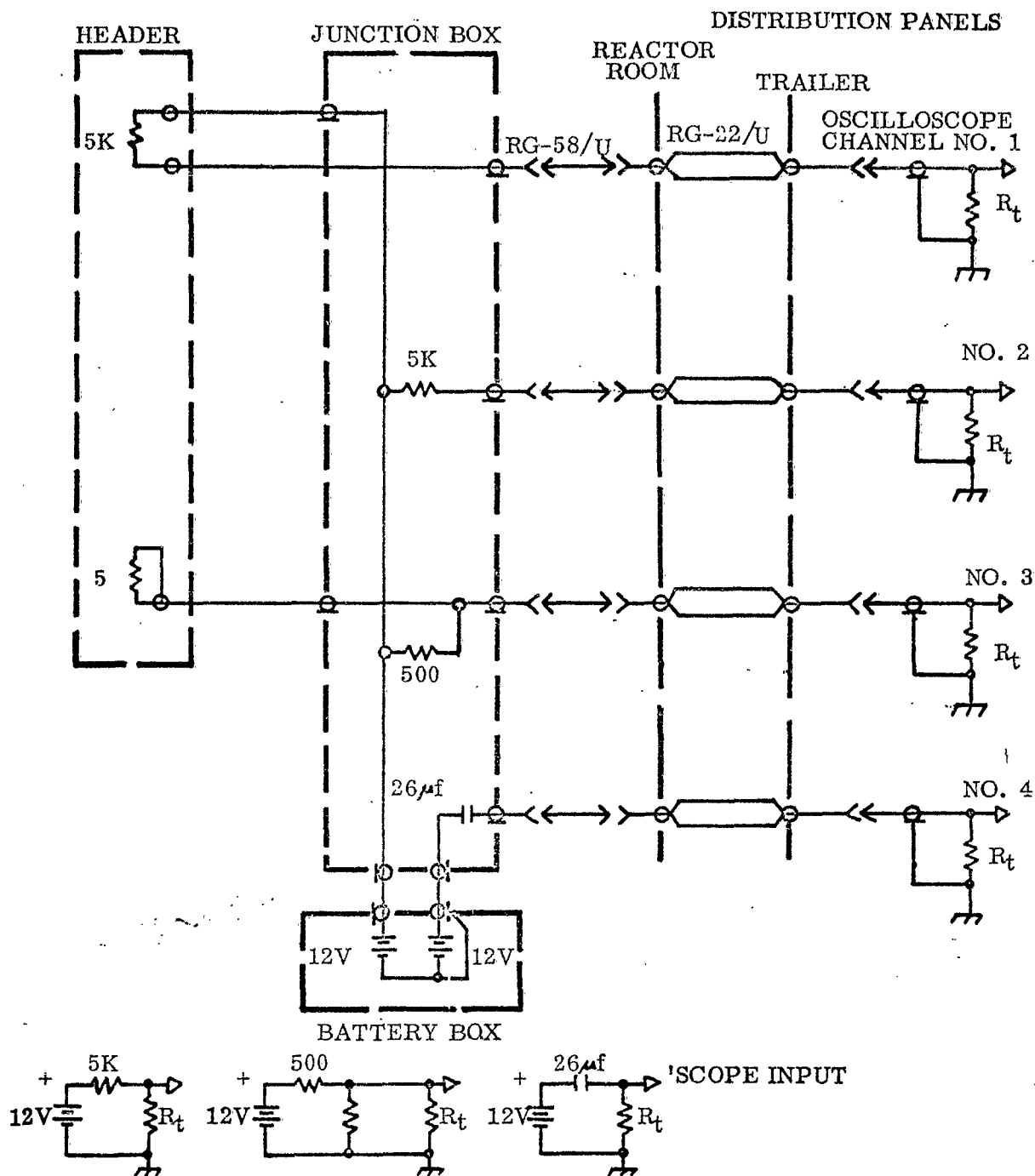
Figure 59 – Kukla Test Number 1. Diode Experiment Setups 1 and 2, Measure R and C Leakages.
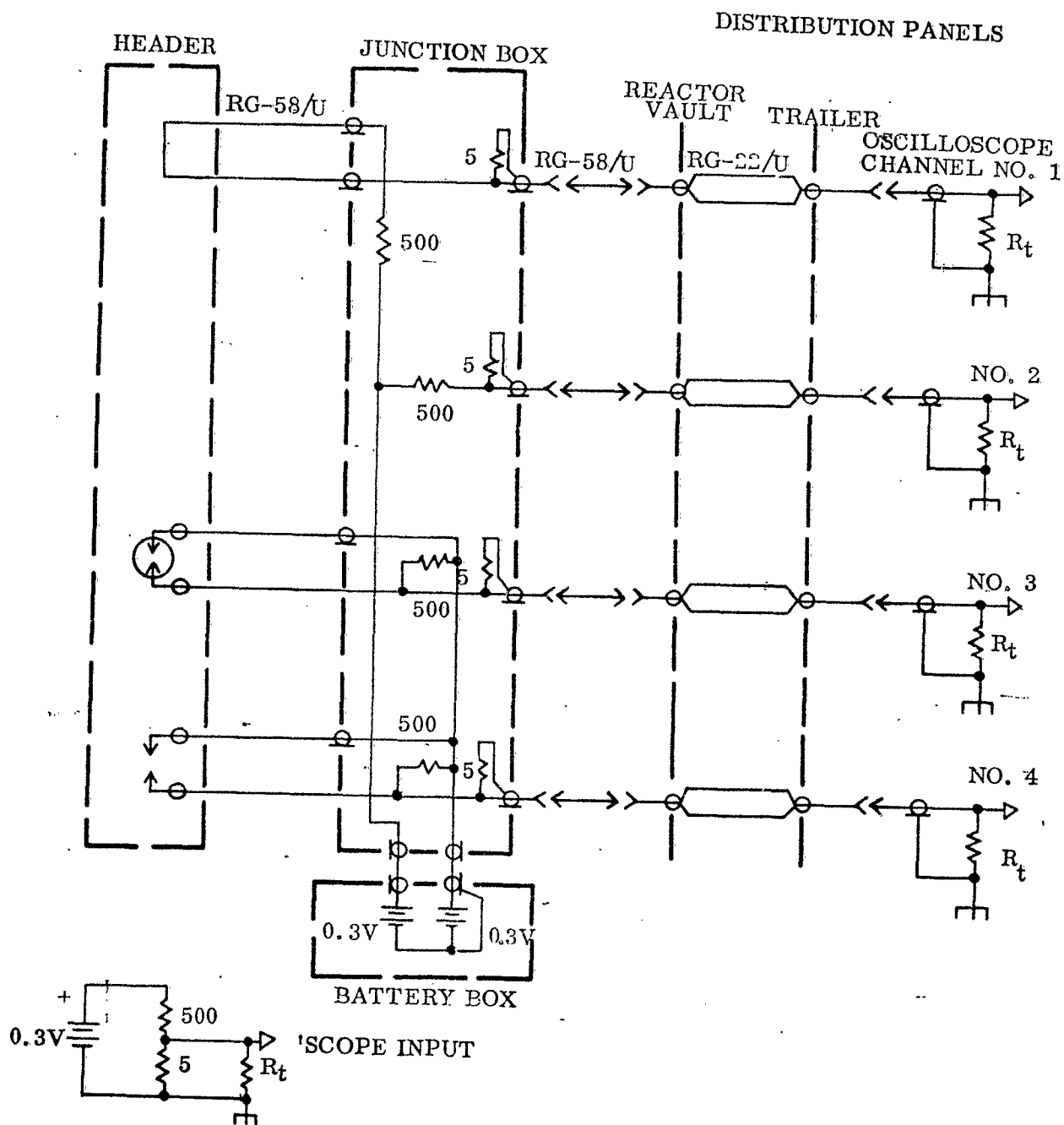
Figure 60 – Kukla Test Number 1. Diode Exponent Setup 3, Measure Leakages
for Setups 4 and 5.

Figure 61 - Kulla Test Number 1. Diode Experiment Setups 4 and 5, Measure Forward Current Changes At Constant Voltage.

Figure 62 – Kukla Test Number 1. Diode Experiment Setup 6, Measure Leakages for Setups 7 and 8.
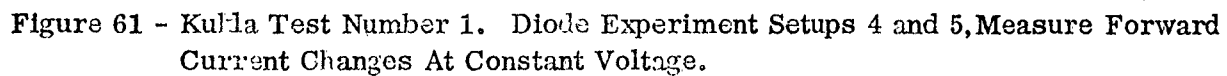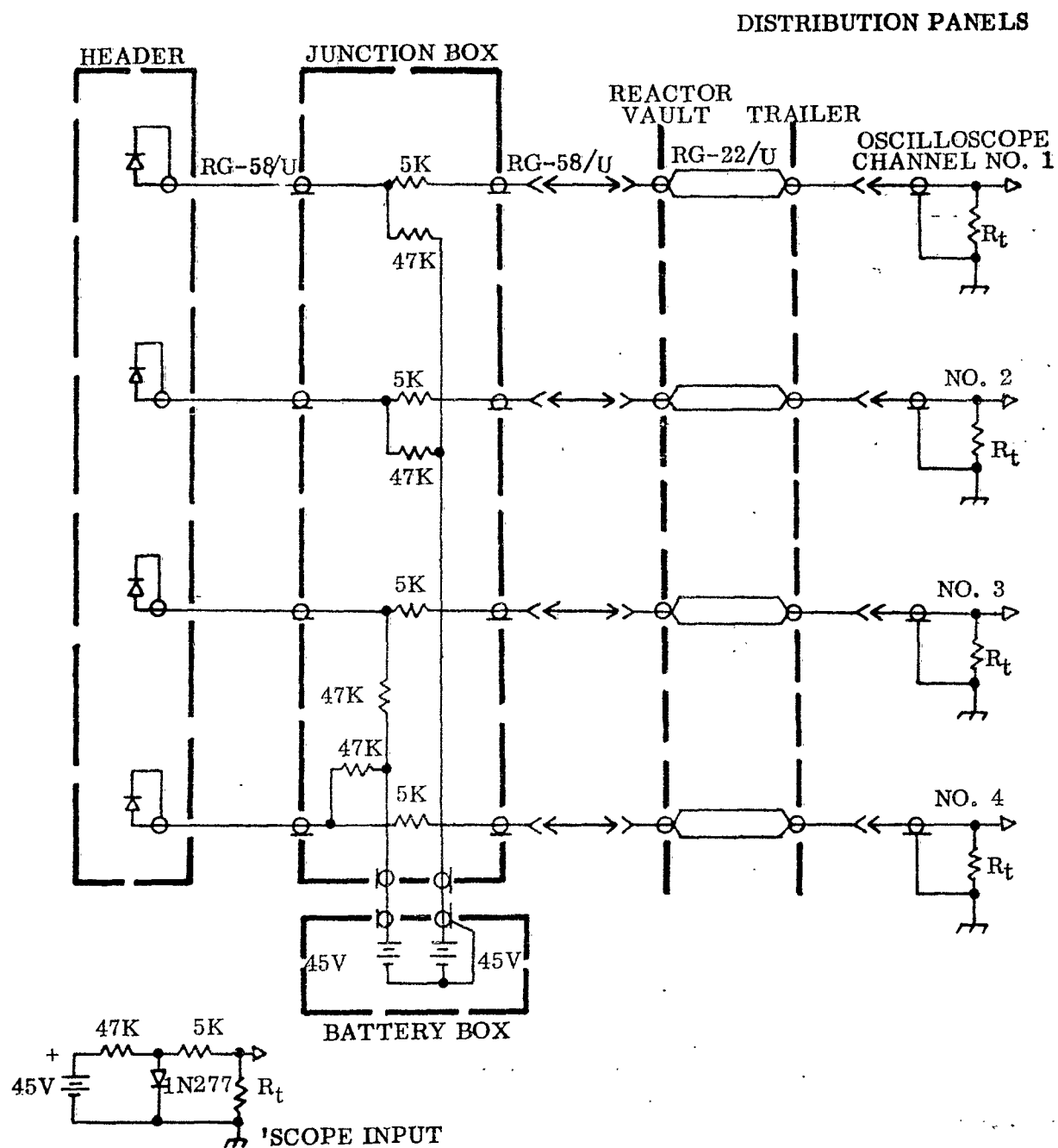
Figure 63 – Kukla Test Number 1. Diode Experiment Setups 7 and 8, Measure Forward Voltage Changes at Constant Current.
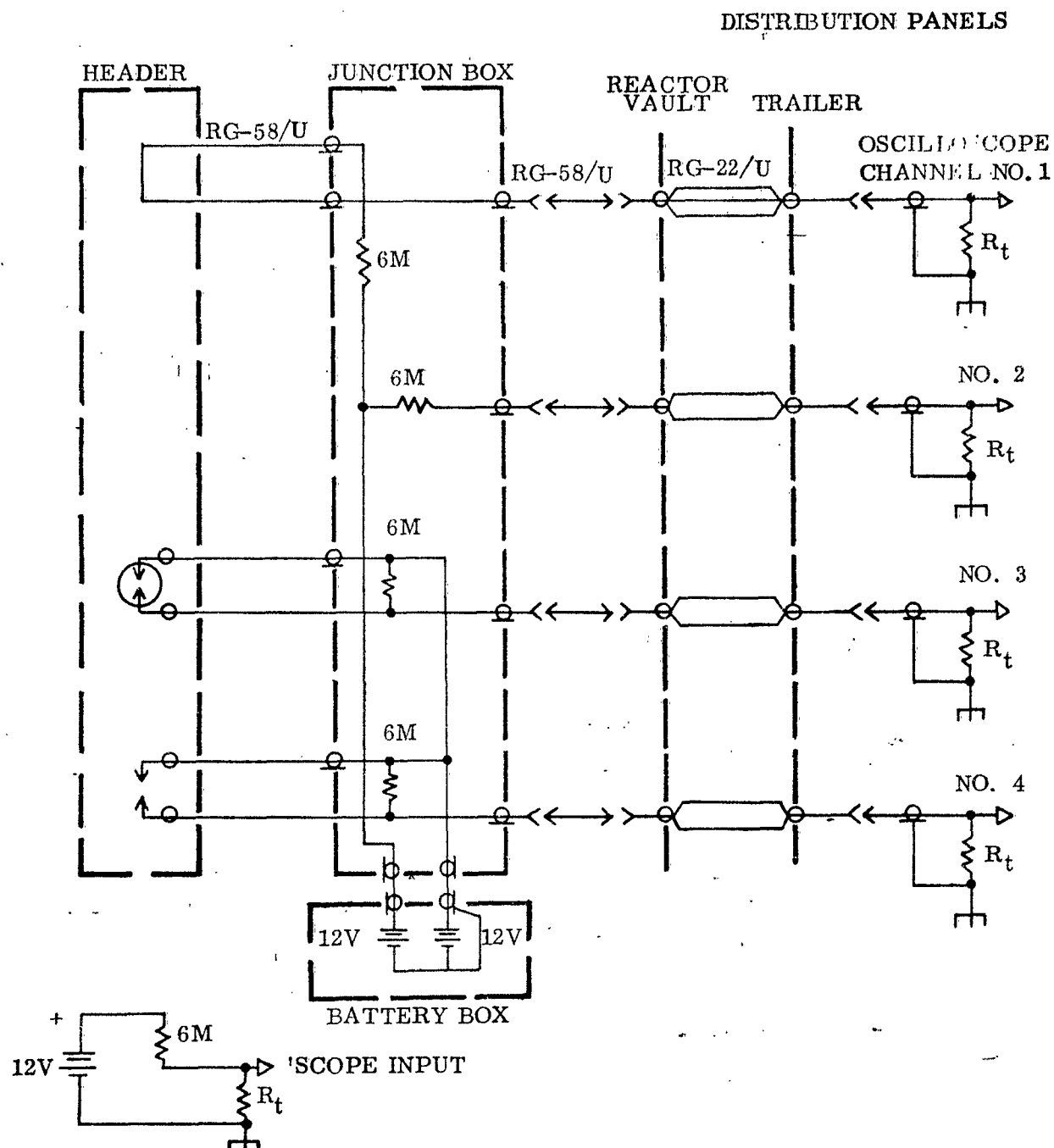
Figure 64 – Kukla Test Number 1.   Diode Experiment Setup 9, Measure Leakages
for Setups 10 and 11.
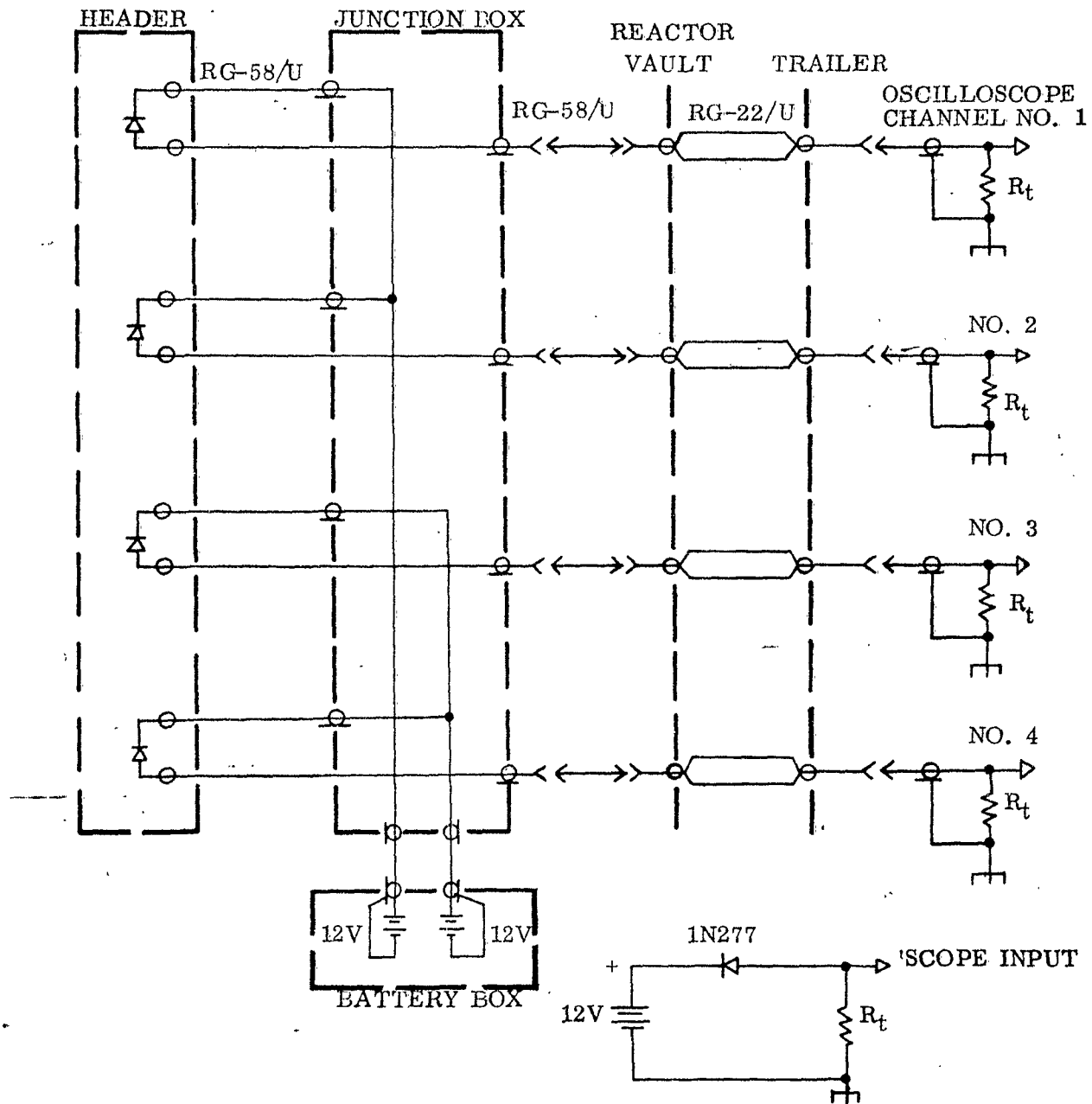
Figure 65 – Kukla Test Number 1.   Diode Experiment Setups 10 and 11,
Measure Reverse Current Changes at Constant Voltage.
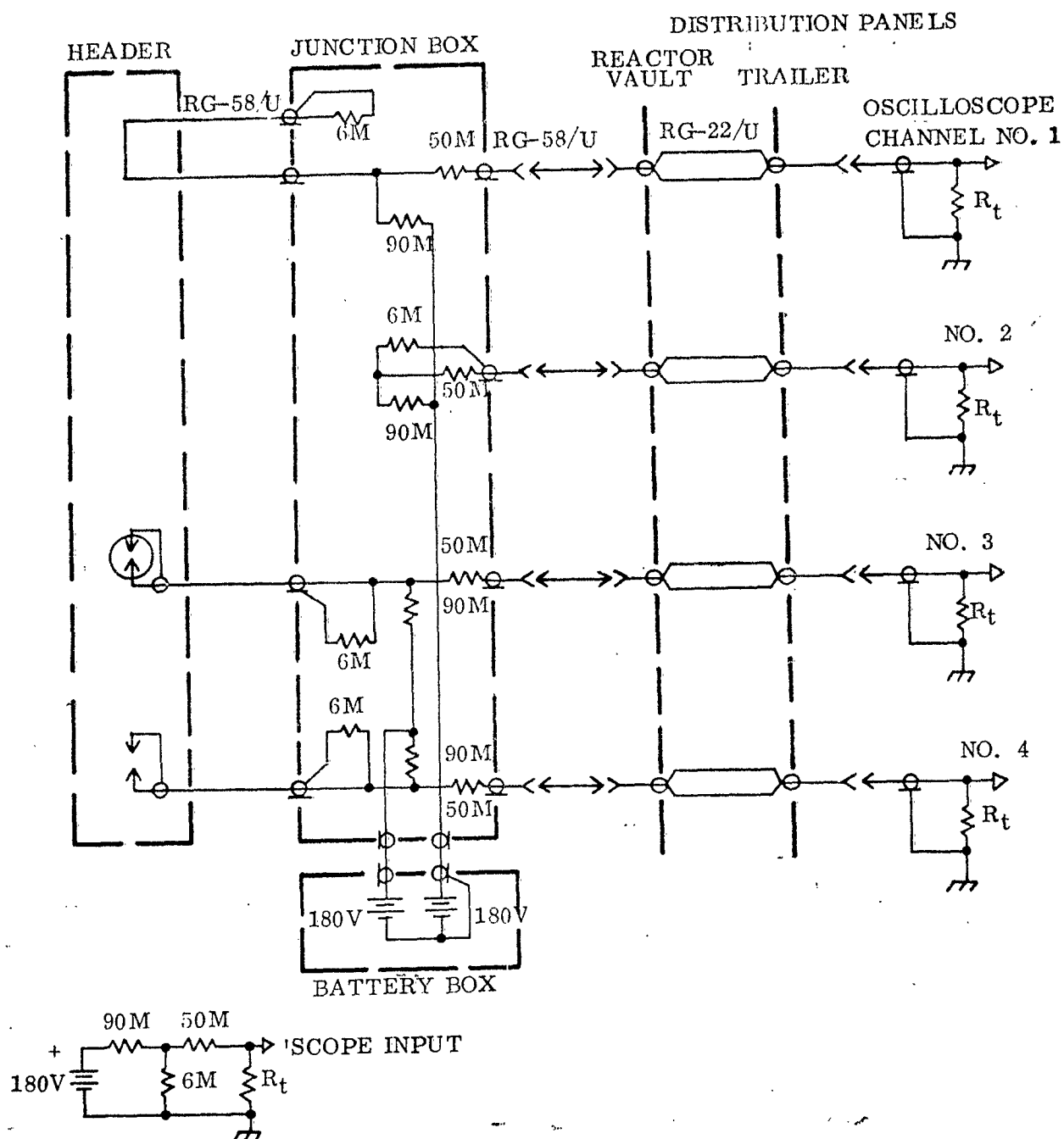
Figure 66 – Kukla Test Number 1. Diode Experiment Setup 12, Measure
Leakages for Setups 13 and 14.
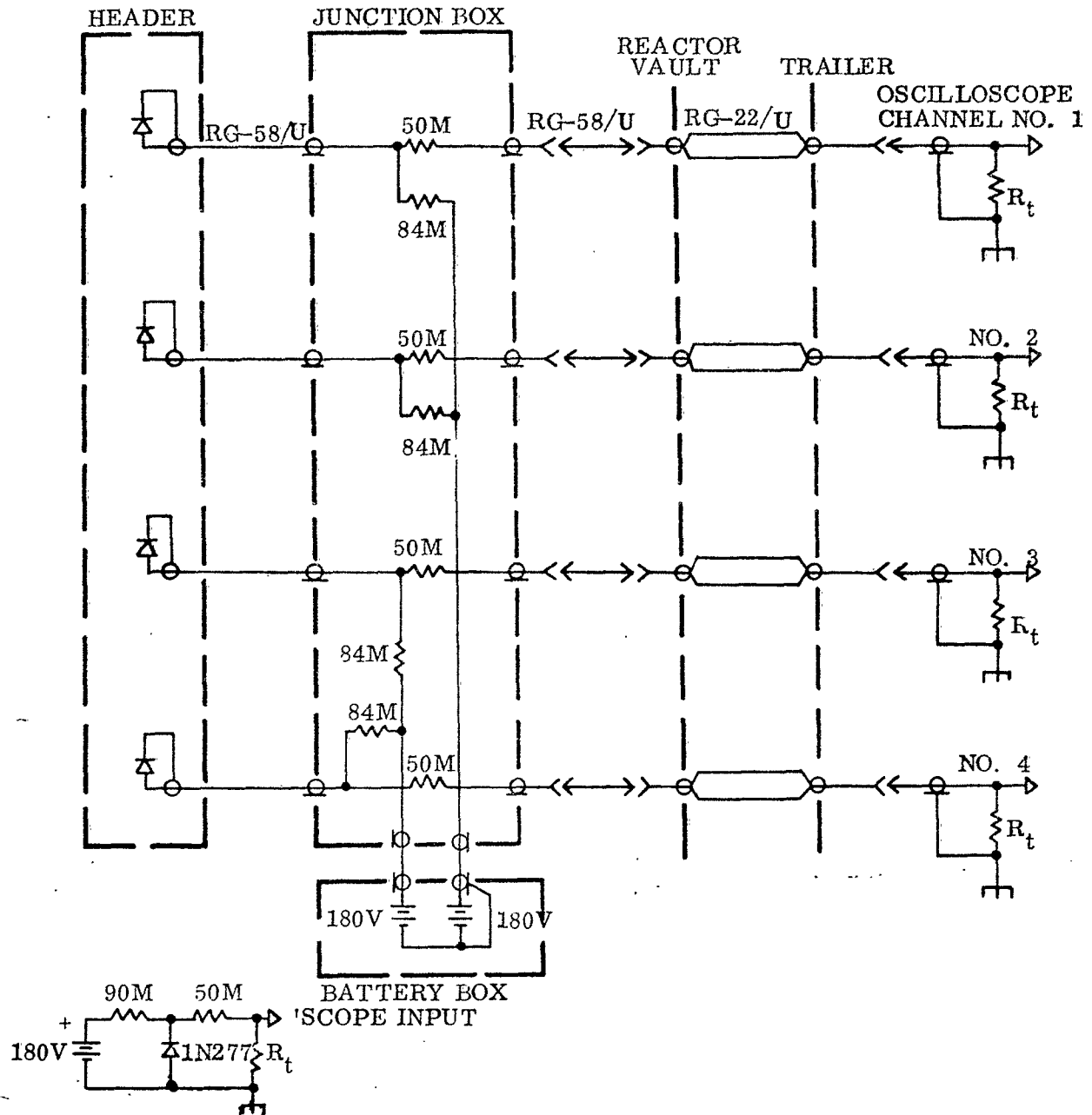
Figure 67 – Kukla Test Number 1. Diode Experiment Setups 13 and 14, Measure Reverse Voltage Changes at Constant Current.

In quoting results it is assumed that the transient effects are proportional to gamma rates in r/sec for which reasonably accurate numbers have been derived from fission rates and reactor data. Nevertheless, it is recognized that some of the ionization in the semiconductor materials may be due to fast neutrons. If this were the case here, all observed signals would be larger than could be accounted for by gammas alone, but still proportional to the gamma rate, since the neutron/gamma ratio is not expected to depend on fission rate. Not enough is known about the diodes irradiated in this test to use the observed signals to separate the neutron and gamma transient effect.

TEST RESULTS

The reactor burst data used in analyzing this test is given in Table 13. No diode information was taken on the first burst. The data on half-value times before and after peak rate, asymmetry, and time to peak rate were used to verify that the signals from a particular setup had followed the time-dependence of the fission rate. The ratio of peak rate for a given burst to that for burst 11 was used to reduce all observed signals to a single rate, so that all cases in which a signal was observed to be less than some value could be compared for consistency with cases in which measurable signals were observed on repeat runs of an individual setup. Thus we assume that all responses were proportional to peak rate, as was apparently the case for all except burst 13. The broadening of the peak for times both before and after the peak, and the delay in reaching peak response seem to indicate saturation effects in this case, but this difficulty did not appear with any other setup, even though in several other cases a high cable termination was used to obtain larger signals on the oscilloscopes than could be obtained with the proper 50 ohm termination. The time constant of the cable in the case of a 5000 ohm termination should have been about 30 microseconds. This difficulty has not been resolved, but would seem to be a result of improper cable termination, since a similar circuit with proper termination gave no delay or before-peak broadening on burst 12.

The voltage and current increases observed at the terminating resistors for each setup are given in Table 14, with the defintions of the symbols at the column heads given at the end of the table. The values of current increases normalized to the smallest burst are also given for comparison with the cases in which no measurable signal appeared on the photographs.

In order to check for permanent neutron damage the base resistance (turn-on), reverse recovery time, and relaxation time (to V_0/e) were measured for each diode with a Tektronix S-Unit before and after irradiation. No correlation between neutron exposure and measured change in parameters was assignable, although a more careful analysis of the data may reveal some effects. Comparison of the I-V characteristic before and after irradiation revealed a constant offset in values, which appeared also in a control set of diodes not removed from the laboratory. This offset was larger than could be accounted for by temperature dependence, but one may conclude that the permanent change in slope of the I-V characteristic due to irradiation was certainly less than 10 percent and the change in current at a given voltage probably less than 10 percent.

TABLE 13

KUKLA TEST NO. 1 – DIODE EXPERIMENT – BURST DATA
(See end of table for definitions of symbols)

Burst No.	S	$\hat{F}$	$\Delta t(-1/2)$	$\Delta t(+1/2)$	Δt	a	t_p	A_{11}	$\hat{R}$	Setup No.
2	4.14	1.76	123	228	351	29	trace cut off	2.89	2.51	3
3	9.57	3.02	84	136	220	24	374	4.95	4.31	4
4	8.72	4.28	66	101	167	21	409	7.01	6.11	9
5	8.58	5.10	66	79	145	9	368	8.36	7.28	10
6	7.37	1.02	182	284	466	22	1066	1.67	1.46	13
7	9.05	1.72	125	194	319	22	853	2.82	2.46	13
8	7.93	2.98	86	126	212	19	trace cut off	4.88	4.25	12
9	7.82	1.65	118	198	316	25	738	2.71	2.35	11
10	6.75	1.39	134	214	348	23	656	2.28	1.98	5
11	6.24	0.61	190	306	496	23	934	1.000	0.87	5
12	7.74	1.37	140	214	354	21	738	2.25	1.96	7
13	6.81	0.66	194	300	494	21	890	1.08	0.94	8
14	7.21	1.00	174	296	470	26	926	1.64	1.43	6
15	7.65	1.60	122	204	326	25	754	2.62	2.28	1
16	5.73	0.66	200	340	540	26	1387	1.08	0.94	5

$S = 10^{-11}$ x neutrons/cm^2 (from sulfur pellet data)
$\hat{F} = 10^{-19}$ x peak fissions/sec (± 0.03)
$\Delta t(-1/2) = $ half-width before peak (μsec)
$\Delta t(+1/2) = $ half-width after peak (μsec)
$\Delta t = $ width at half-maxima (μsec)

$a = \left[\dfrac{\Delta t(+1/2) - t(-1/2)}{\Delta t} \right] = $ asymmetry (%)
$t_p = $ time to peak (μsec)
$A_{11} = F(No.)/F(No. 11) = $ peak rate relative to smallest burst (No. 11)
$\hat{R} = 10^{-6}$ x peak gamma-Mev rate (r/sec) at 14.5 ± 0.6 cm from center of Kukla
Setup No. = diode experiment setup number

TABLE 14

KUKLA TEST NO. 1 – DIODE EXPERIMENT – DATA

Case	R_t	V_t	$\Delta\hat{v}_t$	$\Delta\hat{I}_t$	$\hat{R}$	$\Delta\hat{I}_t(B11)$	Setup Description
1-1-15	50	125	0.266±.007	5.32±0.14	2.28	2.03	5K-ohms at 12V in header
1-2-15	50	125	<.02	<.4	2.28		5K-ohms at 12V in j-box
1-3-15	50	110	<.02	<.4	2.28		5-ohms at 1V in header
1-4-15	50	<.1(5K)	1.983±.006	39.7±0.12	2.28	15.15	26-μf at 12V in j-box
3-1-2	50	3.8	<.04	<.8	2.51		Cable in header
3-2-2	50	3.8	<.04	<.8	2.51		500-ohms at 0.3V in j-box
3-3-2	50	3.8	<.04	<.8	2.51		Diode dummy in header
3-4-2	50	3.8	No trace		2.51		Wires in header
4-1-3	50	8.8	0.42*±.01	8.4*±0.2	4.31	1.69*	Diode H36 at 0.3V(F) in header
4-2-3	50	8.8	0.4*		4.31		Diode H38 at 0.3V(F) in header
4-3-3	50	7.5	No trace		4.31		Diode H39 at 0.3V(F) in header
4-4-3	50	7.0	No trace		4.31		Diode H40 at 0.3V(F) in header
5-1-10	50	8	<.02	<.4	1.98		Diode H43 at 0.3V(F) in header
5-2-10	50	7	<.02	<.4	1.98		Diode T11 at 0.3V(F) in header
5-3-10	50	10	<.02	<.4	1.98		Diode H32 at 0.3V(F) in header
5-4-10	∞	0.32V	<.02	<.4	1.98		0.3V battery (H47 in header)
5-1-11	50	5	<.02	<.4	0.87		Diode H43 at 0.3V(F) in header
5-2-11	50	4.5	<.02	<.4	0.87		Diode T11 at 0.3V(F) in header
5-3-11	50	4	<.04	<.4	0.87		Diode H32 at 0.3V(F) in header
5-4-11	50	6	<.10	<.4	0.87		Diode H47 at 0.3V(F) in header

* In cases 4-1-3 and 4-2-3 the scope amplifier was set on "A.C.," and the signal was partially differentiated. The peak-to-peak values are given for comparison only.

TABLE 14 (page 2)

Case	R_t	V_t	$\widehat{\Delta V_t}$	$\widehat{\Delta I_t}$	$\widehat{R}$	$\widehat{\Delta I_t}(B11)$	Setup Description
5-1-16	50	7	No trace		0.94		Diode H43 at 0.3V(F) in header
5-2-16	50	1	No trace		0.94		Diode T11 at 0.3V(F) in header
5-3-16	50	7	<.07	<1.4	0.94		Diode H32 at 0.3V(F) in header
5-4-16	50	6.5	<.07	<1.4	0.94		Diode H47 at 0.3V(F) in header
6-1-14	5K	230	1.323±.007	0.2650±.0014	1.43	0.167	Wires in header
6-2-14	5K	240	1.190±.007	0.2380±.0014	1.43	0.145	Diode dummy in header
6-3-14	5K	220	1.067±.006	0.2132±.0012	1.43	0.130	Cable in header
6-4-14	5K	260	0.587±.007	0.1174±.0014	1.43	0.0716	500-ohms at 1 ma in header
7-1-12	50	3	0.085±.007	1.70±.14	1.96	0.756	Diode H24 at 1 ma in header
7-2-12	50	3	<.10	<2.0	1.96		Diode H25 at 1 ma in header
7-3-12	50	3	<.4	<8.0	1.96		Diode H29 at 1 ma in header
7-4-12	50	3	<2.0	<40.0	1.96		Diode H30 at 1 ma in header
8-1-13	510	27	0.129±.007	0.253±.014	0.94	0.234	Diode T5 at 1 ma in header
8-2-13	5K	145	0.662±.014	0.132±.003	0.94	0.122	Diode T9 at 1 ma in header
8-3-13	510	26	0.227±.007	0.445±.014	0.94	0.411	Diode H22 at 1 ma in header
8-4-13	5K	140	0.641±.035	0.1283±.007	0.94	0.1186	Diode H23 at 1 ma in header
9-1-4	50	0.1	0.413±.009	8.26±.18	6.11	1.180	Cable in header
9-2-4	50	0.1	0.325±.009	6.50±.18	6.11	0.927	6M-ohms at 12V in header
9-3-4	50	0.1	0.745±.009	14.90±.18	6.11	2.135	Diode dummy in header
9-4-4	50	0.1	0.760±.009	15.20±.18	6.11	2.170	Wires in header
10-1-5	50	0.1	5±0.5	100.±10.0	7.28	12.0	Diode H12 at 12V(R) in header
10-2-5	50	0.1	5.70±.05	114.±1.0	7.28	13.6	Diode H14 at 12V(R) in header
10-3-5	50	0.1	defective		7.28		Diode H18 at 12V(R) in header
10-4-5	50	0.1	6.6±0.4	132.±8.0	7.28	15.8	Diode H19 at 12V(R) in header

TABLE 14 (page 3)

Case	R_t	V_t	$\widehat{\Delta V_t}$	$\widehat{\Delta I_t}$	$\widehat{R}$	$\widehat{\Delta I_t}(B11)$	Setup Description
11-1-9	50	0.1	1.070±.013	21.4±.3	2.35	7.89	Diode T6 at 12V(R) in header
11-2-9	50	0.1	1.316±.013	26.3±.3	2.35	9.70	Diode H9 at 12V(R) in header
11-3-9	50	0.1	1.498±.013	30.0±.3	2.35	11.04	Diode T7 at 12V(R) in header
11-4-9	∞	12V	<0.28		2.35		12V battery (H10 in header)
12-1-8	3K	4.4	defective		4.25		(Cable in header)
12-2-8	3K	0.6	defective		4.25		(6M-ohm at 2μ a in j-box)
12-3-8	3K	0.0	defective		4.25		(Diode dummy in header)
12-4-8	3K	0.7	5.3±0.5	1.77±.17	4.25	0.36	Wires in header
13-1-6	50	<.05	<.02	<.4	1.46		Diode H6 at 2μ a(R) in header
13-2-6	50	<.05	<.10	<2.0	1.46		Diode H7 at 2μ a(R) in header
13-3-6	50	<.05	<.4	<8.0	1.46		Diode H8 at 2μ a(R) in header
13-4-6	50	<.05	<2.0	<40.0	1.46		Diode H11 at 2μ a(R) in header
13-1-7	50	<.05	<.02	<.4	2.46		Diode H6 at 2μ a(R) in header
13-2-7	Channel loaned for dosimetry				2.46		Diode H7 at 2μ a(R) in header
13-3-7	5K	1.0	3.2±.3	0.64±.06	2.46	0.23	Diode H8 at 2μ a(R) in header
13-4-7	510	0.1	0.317±.007	0.622±.014	2.46	0.221	Diode H11 at 2μ a(R) in header

TABLE 14 (page 4)

Definitions of symbols used as column headings

Case: Setup No. – Channel No. – Burst No.

R_t = Terminating resistor at oscilloscope input, in ohms.

V_t = Constant voltage appearing across terminating resistor before and after a burst, in millivolts.

$\widehat{\Delta V_t}$ = Peak voltage increase appearing across terminating resistor during a burst, in millivolts.

$\widehat{\Delta I_t}$ = Current increase corresponding to $\widehat{\Delta V_t}$, in microamperes ($\widehat{\Delta I_t} = \widehat{\Delta V_t}/R_t$).

$\widehat{R}$ = Peak gamma rate during a burst, in 10^6 r/sec.

$\widehat{\Delta I_t}$(B11) = Current increases normalized to burst No. 11, the smallest one, in microamperes.

Setup Description: Corresponds to the Setup No. and Channel No. The diode numbers are arbitrary identification numbers, with T indicating Transitron, and H indicating Hughes 1N277 diodes. (F) indicates forward and (R) indicates reverse conduction through a diode.

Note: The indicated errors in $\widehat{\Delta V_t}$ and $\widehat{\Delta I_t}$ are due to reading the photographs. It is to be remembered that there may be errors of several percent due to errors in the resistor values and the oscilloscope calibrations. The probable error in $\widehat{R}$ and $\widehat{\Delta I_t}$(B11) is about ± 10 percent due to uncertainties in the position of the diodes with respect to the reactor. There are additional systematic errors without doubt.

DISCUSSION OF RESULTS AND CONCLUSIONS

Inspection of the data presented in Table 14 reveals that the diode parameter changes during irradiation produced signals of the same order of magnitude as the signals from the setups used to check for unwanted additional signals, except in the case of diode reverse conduction at constant voltage. Even in this case the corrections required were appreciable. Thus one can really only set upper limits on the diode effects, except in the latter case. It is possible, however, to analyze some of the results from the setups used to measure "leakage" in order to get some idea of the sources of the unwanted signals. One expects such signals due to:

1. Conductivity induced in the potting compound--leading to a shunting effect on the diodes and resistors during irradiation.

2. Changes in the materials of which the resistors are constructed.

3. Changes in battery voltage during irradiation.

4. Leakages in cable dielectric.

5. Photocurrents in the cables.

6. Leakage or photocurrents in the connectors exposed to radiation in the reactor room.

The principle effects seem to have been due to photocurrents from the cables and connectors, but it is possible to set some approximate limits on the contributions from the other factors.

LEAKAGE CORRECTIONS

Potting Compound Leakage

Assume that the resistors do not change in value and that there is no other leakage. In the simple series circuit of channel one in setup one, the voltage at the terminating resistor increased about 0.2 percent on burst 15 (2.3×10^6 r/sec peak gamma rate). This effect could have been produced by a 2.5 megohm shunt around the 5000 ohm resistor. Assuming the conductivity varies linearly with rate, and estimating the gamma rate six feet back from the reactor, at the junction box position, one would expect less than $10^{-3} \mu$ a increase in current in the terminating resistors in case 6-4-14 and 0.1 μa in case 9-2-4. These were cases in which there were only resistance networks in the junction boxes, with no connections to the headers mounted near the reactor. The observed currents were 0.12 μa and 6.5 μa respectively, so one believes that the leakage currents in the potting compound in the junction boxes were not major contributions to the currents observed.

Resistor Changes

A fractional decrease in resistance values could also give increased currents at the

terminating resistors, but in case 12-3-8 no steady voltage was developed at the termination, due to a shorted dummy diode in the header. Nevertheless a current of 2.4μa flowed during the burst. Changes in resistor values could not have had any effect, so one is forced to assume another source of current, at least in this case.

It is quite true that the effects found in case 1-1-15, and discussed above, could have been due to either resistance changes or potting compound leakage in the header.

Battery Voltage Changes

In case 5-4-10 a 0.3 volt series combination of dry cells and mercury cells gave less than 0.006 percent change in voltage. In case 11-4-9 a 12 volt dry battery gave less than 0.002 percent change in voltage. In these circuits one would expect that photocurrents would have been shunted to ground through the low battery impedance, and so would not have had any effect. The gamma rate at the battery box in these cases was about 10^4 r/sec. The batteries thus are eliminated from consideration for the production of unwanted signals in this experiment.

Cable Leakage and Photo Effects

Considering the magnitudes of the excess currents, and the fact that they tended to increase the current in the terminating resistors in all cases, we believe that photovoltages and/or currents were generated during the reactor pulse. The sense was as if excess electrons were being generated at the cable sheath, which may be viewed either as due to a photovoltage at some interface in the cable, or as a photocurrent due to collection of electrons generated in the dielectric. In either case cable leakage would be a competing process, and cable loading and applied voltage would probably have an effect on the net current reaching the terminating resistor. These phenomena are not new, although the observations have not yet been put into usable form. (For instance see Ref. 47 and 54). D. L. Dye of Boeing Airplane Co. also noticed photocurrents generated in coaxial cables exposed to X-radiation, with no voltage applied. Researchers at Hughes Aircraft Co. have recognized the difficulty and are investigating the competing effects and their voltage dependence, (Ref. 46). It is interesting to note that extrapolation of the results in Ref. 54 to the relatively high gamma rates of our experiment, taking into account the variation of rate along the section of cable near Kukla, one would predict photocurrents considerably less than those observed. The currents measure in Ref. 54 obeyed the law $I \propto (R)^\delta$ where $0.5 < \delta < 1$.

Connector Leakage and Photo Effects

Comparing the excess currents from those leakage testing channels for which there were cables to the header with those for which there were only networks in the junction boxes, one sees that there were probably photo effects in the latter case also. In a simple experiment recently performed by D.W. Blincow at the Kukla facility a 0.3μa current was apparently generated in a BNC connector six feet from the reactor, at about 10^6 r/sec, although less than 0.1 μa current was generated in an identical setup without the connector. The geometry was similar to that of the diode test setups. Blincow's test was performed with no voltages applied, but leakage is undoubtedly an additional factor when there is a nonzero operating voltage.

Comparison of the signals from the different circuits in leakage testing setups thus seems to point to the following facts:

1. The unshielded BNC connectors leaked and injected photocurrents.

2. The cables leaked and injected photocurrents.

3. The relative magnitudes of the signals from the dummy diodes and the wires without the diode case indicate that there was little leakage within the case.

4. The photocurrents flowed in a direction corresponding to production of excess electrons at the sheath of the cable.

5. A quantitative understanding of these effects is lacking.

In view of the above observations it was decided to simply normalize the currents from the dummy diode channels appropriate to the diode setup for which information was desired, and to subtract them from the observed currents. In all cases except setup six the terminating resistor was small compared with the impedance of the network at the other end of the cable, hence could reasonably be expected to collect all the injected current.

TRANSIENT RADIATION EFFECTS DURING DIODE FORWARD CONDUCTION

The relative signal amplitudes from setups 3 and 4 (bursts 2 and 3) indicated that it would be possible to measure the diode forward current change at 0.3 volt. However no measurable signals were seen on bursts 11 and 16 with setup 5 (similar to 4). The failure on burst 10 is not explained, since it had about one-half the peak rate of burst 3. Bursts 11 and 16 unexpectedly had about one-fifth the intensity of 3, and so could not have produced measurable signals if the signal from setup 4 was typical. Thus one can only say that the diode current increase at 0.3 volt was probably less than five percent for about 4×10^6 r/sec.

The signals from setups 6 and 8 indicate a diode voltage decrease of less than 0.1 percent at 1 ma, for 0.9×10^6 r/sec, if the normalization procedure is valid. The signals from setups 6 and 7 indicate a voltage increase across the diode of 2.3 percent at 1 ma for 2×10^6 r/sec for a single diode channel. These results are inconsistent, but then the signals from setup 8 were considerably distorted, as mentioned earlier.

All that one can say about the changes in forward conduction properties of the diode is that they are probably less than five percent at the (0.3V, 1 ma) point for peak gamma rates of the order of 10^6 r/sec.

TRANSIENT RADIATION EFFECTS DURING DIODE REVERSE CONDUCTION

Consider first the constant current case, for which there are only three pieces of information: signals from "wires in the header" and from two diodes (cases 12-4-8, 13-3-7, and

13-4-7). Assuming the diode dummy, which was defective in this case, would have given 90 percent of the signal from the plotted wires, as in setup 6, one finds that the current in the terminating resistor was reduced by $0.28\mu a$ and $0.30\mu a$ for cases 13-3-7 and 13-4-7 respectively, presumably due to diode changes during the burst. This would correspond to voltage decreases at the diodes of 14 ± 3 volts. The I-V characteristics for the two diodes used, at the ambient temperature in the reactor vault, indicate that they were operating at 12 ± 3 volts. Thus, during the burst the voltage across the diodes decreased to zero within the accuracy of measurement. One should note that in this case the excess photocurrents were of the same order of magnitude as the currents due to the diode changes, hence the large errors in the measured voltage changes. The initial operating voltages are uncertain because of the strong temperature dependence of the diode voltage drop at constant current and the $\pm 0.5°C$ uncertainty in the measurement of reactor vault temperature.

The changes in reverse current at constant voltage were considerably larger than the cable leakages and provide quantitative information about the 1N277 diode, even though the desired slope and intercept changes for the I-V characteristic cannot be calculated without good constant-current data in addition. In Table 15 the changes in diode reverse current at 12 volts for bursts 5 and 9 are tabulated together with the cable leakage information from burst 4. The diode currents are also given after correction for diode dummy leakage normalized to the peak gamma rates for bursts 5 and 9.

The rather large differences between the currents of the individual diodes irradiated on the same burst, and the failure to scale from one burst to the other were taken to be caused by differences in some diode parameter which controls the current. Upon inspection of the I-V characteristics shown in Figure 68 it will be seen that diodes H12, 14, and 19 all have similar slopes, as have the group H9, T6, and T7. In fact, the observed currents are ordered in magnitude with $\Delta V/\Delta I$, which, on a simple picture of the diode equivalent circuit, is a resistance shunting the ideal diode.

A plot of the peak diode currents ΔI_d versus the shunt resistance R_{sh} at 12 volts shows that the behavior of diodes H9, T6, and T7 is strictly linear with R_{sh}, and the following simple theory is proposed as a possible explanation. Assume that gamma irradiation generates excess electron-hole pairs with recombination times short compared with the length of the pulse of radiation in all regions of the semiconductor material. Those carriers not recombining will be swept out under the influence of the reverse field applied, and contribute a current which will be proportional to the gamma rate. On a very simple picture of the process, collection will occur from regions within a diffusion length of the junction and also from the junction region itself. If an electrode is less than a diffusion length from the junction then collection is necessarily from the region of this length rather than the full diffusion length, (Ref. 48 and 49). Thus we can write:

$$\Delta I = eg\, A\, (Ln + Lp + W) \longrightarrow egA\, (Xn + Xp + W) \text{ for } Xn, p < Ln,p.$$

Where: ΔI = the additional current due to irradiation in amperes.

        e = electron charge in coulombs

TABLE 15

SUMMARY OF 1N277 RADIATION-INDUCED CURRENT CHANGES AT 12 VOLTS REVERSE

Case	$\hat{\dot{R}}$	$\widehat{\Delta I_t}$	$\widehat{\Delta I_{dd}}$	$\widehat{\Delta I_d}$	R_{sh}	Diode
9-3-4	6.11	14.9 ± 0.3	14.9 ± 0.3	--		Dummy
10-1-5	7.28	100 ± 10	17.8 ± 0.4	82 ± 10	49 ± 2	H12
10-2-5	7.28	114.0 ± 1.0	17.8 ± 0.4	96.2 ± 1.1	57 ± 2	H14
10-4-5	7.28	132 ± 8	17.8 ± 0.4	114 ± 8	60 ± 2	H19
11-1-9	2.35	21.4 ± 0.3	5.8 ± 0.1	15.6 ± 0.3	13.5 ± 0.3	T6
11-2-9	2.35	26.3 ± 0.3	5.8 ± 0.1	20.5 ± 0.3	22.4 ± 0.5	H9
11-3-9	2.35	30.0 ± 0.3	5.8 ± 0.1	24.2 ± 0.3	27.0 ± 0.5	T7

Case = Setup No. - Channel No. - Burst No.

$\hat{\dot{R}}$ = 10^{-6} x peak gamma rate during a burst, in r/sec (±10%).

$\widehat{\Delta I_t}$ = peak increase in current through the terminating resistor, in microamperes.

$\widehat{\Delta I_{dd}}$ = the contribution to $\widehat{\Delta I_t}$ from leakage, as measured with the diode dummy.

$\widehat{\Delta I_d}$ = $\widehat{\Delta I_t} - \widehat{\Delta I_{dd}}$

R_{sh} = equivalent shunt resistance of the diode, in megohms (at reactor vault temperature).

Diode = diode identifying number.
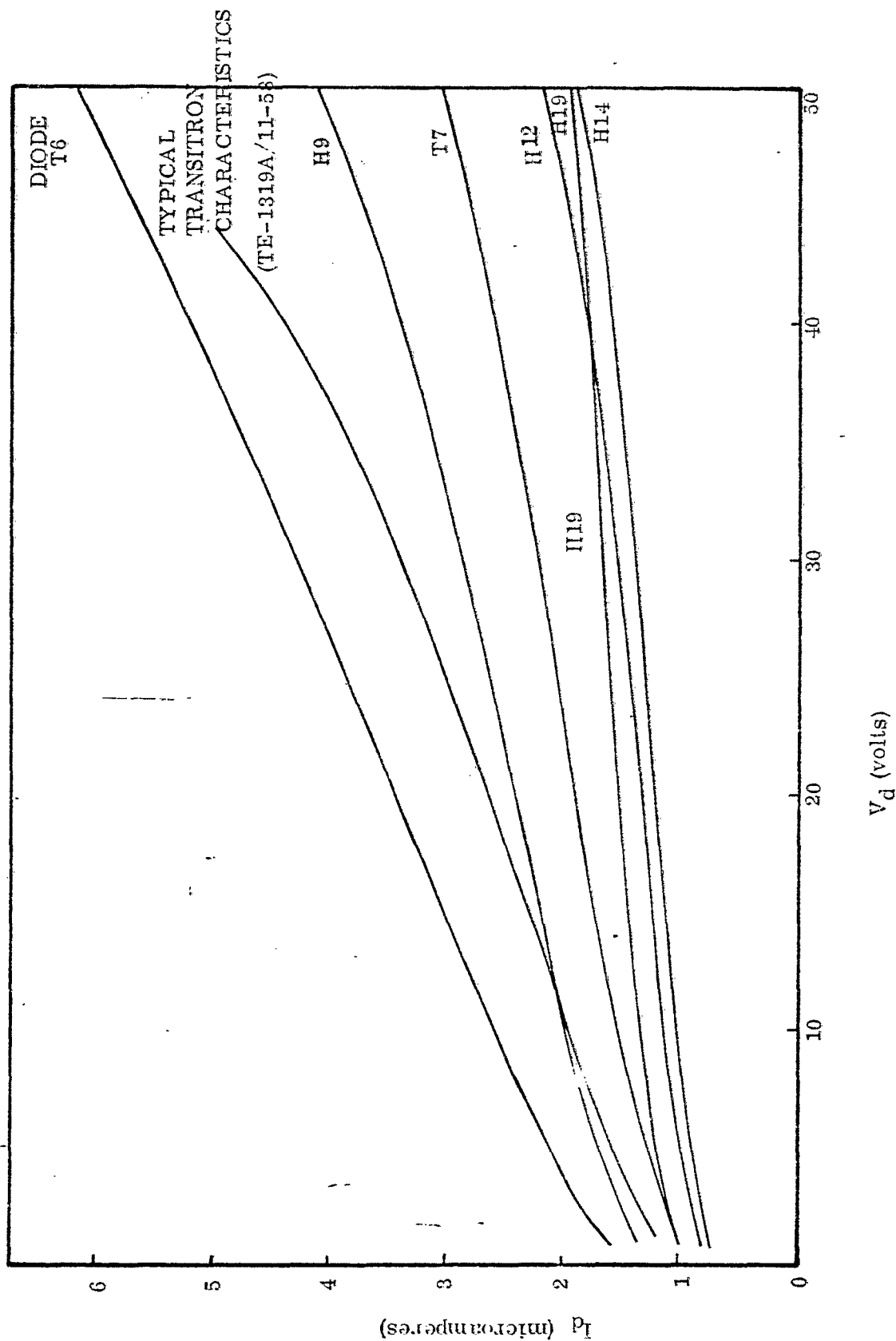
Figure 68 – Kukla Test Number 1. Diode Experiment 1N277 Diode I–V Reverse Characteristics.

g = the net number of current carriers generated per cc per second

A = effective junction area in cm^2

Ln = minority carrier diffusion length in the p-type material in cm

Lp = minority carrier diffusion length in the n-type material in cm

W = Junction width in cm

Xn, Xp = distances from the junction to the appropriate electrode in cm

Now let us assume that $g \propto \dot{R}$, the gamma rate; and also $AW \propto R_{sh}$, where R is the gamma rate and R_{sh} is the diode reverse shunt resistance. The latter assumption is the one used to interpret the results of this experiment, and it is not unreasonable, if R_{sh} is viewed as due to a current leakage across the transition region (Ref. 50). One then can write an expression for the diode reverse current increase and use the experimental data to evaluate the constants:

$$\Delta I = (a + b\, R_{sh})\, \dot{R}$$

Where: $\dot{R}a = \Delta I_d$ $(R_{sh} = 0)$ (an intercept)

$\dot{R}b = d(\Delta I_d)/d(R_{sh})$ (a slope)

For diodes H9, T6, T7, one has:

$a = (7 \pm 1) \times 10^{-6} / (2.35 \times 10^6) = 2\,(3.0 \pm 0.4) \times 10^{-12}$

$b = (0.27 \pm 0.02) \times 10^{-18}$ (an average value)

So that:

$$\widehat{\Delta I}_d = \left[(3.0 \pm 0.4) + (0.27 \pm 0.02)\, R_{sh} \right] \widehat{\dot{R}}$$

Where:

$\widehat{\Delta I}_d$ = peak reverse current in microamperes.

$\widehat{R}_{sh}$ = diode initial shunt resistance in megohms at 12 volts reverse.

$\widehat{\dot{R}} = 10^{-6} \times$ peak gamma rate in r/sec

To test the above expression for I_d it was applied to predicting the values of peak current from the diodes in setup 10, and the results are shown in Figure 69. Although the predicted values are too large, the general agreement is rather surprising in view of the large differences in rates and initial shunt resistances in the two cases. In fact, it is not worthwhile to attempt further corrections, in view of the fact that there is actually ±10 percent probable
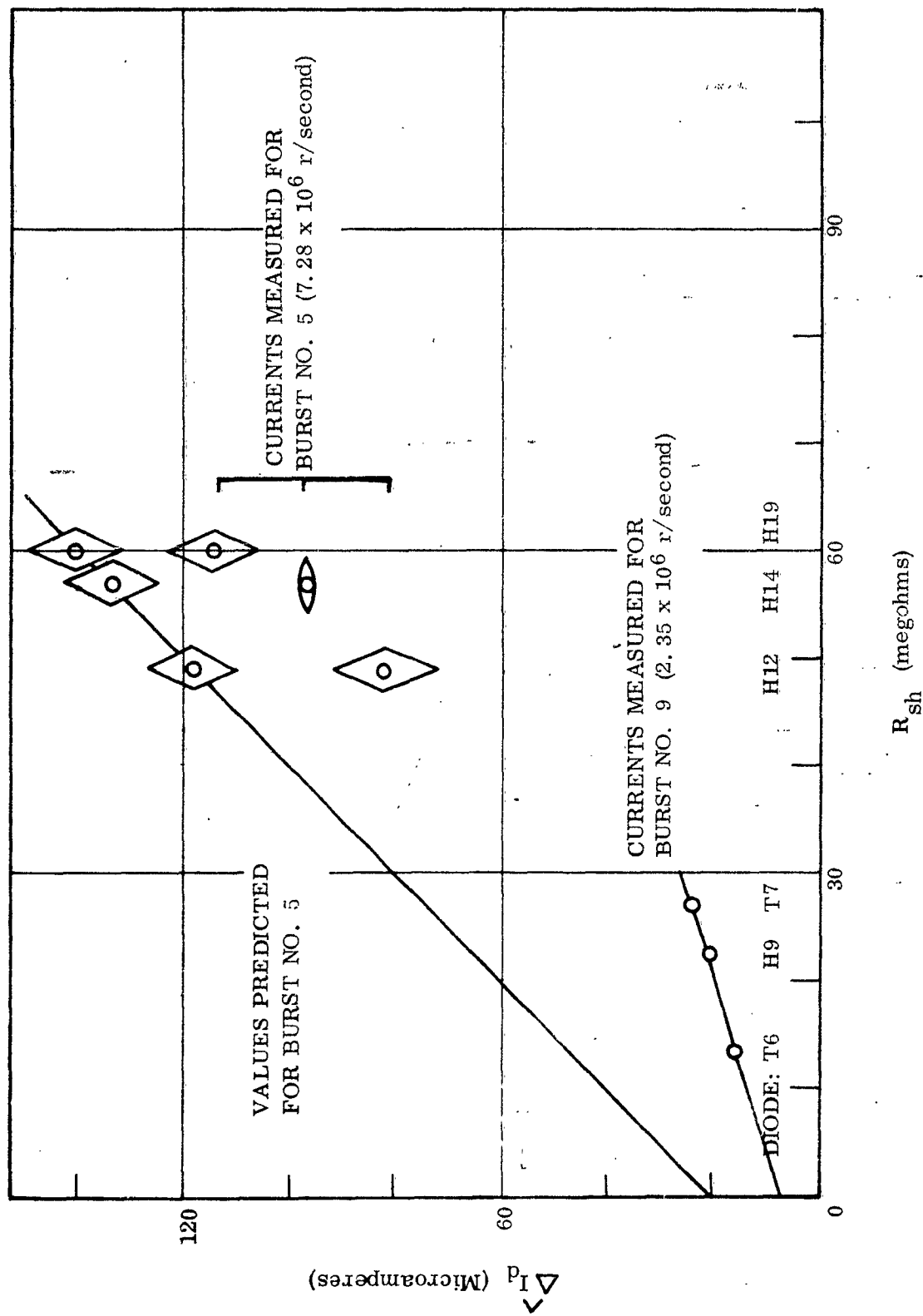
Figure 69 – Kukla Test Number 1. Diode Experiment 1N277 Diode Peak Reverse Current Versus Initial Shunt Resistance.

error in the quoted peak gamma rates due to errors in positioning the header, and also discrepancies between the peak rates indicated by the different photodiodes used to measure fission rates. That is to say, the use of rates from PD 1 gives a much closer fit. It is unlikely that the effects are very nonlinear with gamma rate in view of the good agreement in times to one-half value and to peak of these signals with the photodiode signals. Note that the agreement is not improved by assuming a different cable correction as long as that correction is taken to be proportional to gamma rate. Gamma ray joule heating (Ref. 51) could also reasonably be invoked to explain the observation of smaller currents than predicted, due to the negative temperature coefficient of R_{sh}.

The conclusion to be drawn is that the effects described above are probably real, but indicate that further investigation of the diode construction and its behavior during irradiation are required. Specifically, the shape of the I-V characteristic is dependent on diode contact geometry and also on surface phenomena. Thus the physical meaning of the observed relationship between R_{sh} and the current during irradiation is not clear at this time. See Ref. 56 and 57 for some considerations which apply to these problems.

RECOMMENDATIONS

LEAKAGE EFFECTS

In order to gather really precise data in an investigation of this type, the radiation-induced leakages and photocurrents must either be eliminated or understood quantitatively. It is possible that cable effects can be reduced in magnitude by the use of balanced lines although this is not always convenient. The potting compound leakages and resistance changes probably are small, although in this case also, quantitative information is needed. The apparent effects due to cable connectors used in the vicinity of the reactor could perhaps be reduced considerably by proper shielding, or one could eliminate the use of connectors in the radiation field. It is suggested that the investigation of these effects should be undertaken with cognizance of the work being done on this problem by Hughes Aircraft Co. personnel (Ref. 46) and by other interested parties.

EFFECTS OF IRRADIATION ON DIODE CHARACTERISTICS

The small changes in diode forward conduction probably cannot be accurately measured until the leakage problem is solved. In any event, the interpretation in terms of diode properties is probably considerably more complex than for reverse conduction (Ref. 50) and this problem may profitably be put aside as of lesser current interest than the case of reverse conduction, in which large effects are observed. One should note that in the latter case it would be wise to investigate the diode responses to low as well as high gamma rates in order to definitely establish the dependence on peak rate, and also to use data obtained from reactor irradiations (Ref. 52). Establishment of the changes in the entire I-V characteristic, either by the slope and intercept method or by an A.C. method, is vital to the circuit designer who must consider possible radiation effects.

One would like to understand in detail the radiation effects in all semiconductor devices. In this experiment and in experiments by other researchers some useful but still rather incomplete information has been obtained. It would be desirable to pursue the investigation of transient radiation-induced effects in diodes, since they are relatively simple (but really complex) devices, to as complete an understanding as could be reasonably expected. The insight thus gained would certainly help in understanding the behavior of other semiconductor devices.

This particular investigation may help to make possible a correlation and prediction of effects in diodes of the same type, although it seems unlikely that the necessary initial device parameters can be known accurately enough to establish the necessary theory unless the diodes to be investigated are fabricated in a known way, of materials whose semiconducting properties and purity are accurately known. Thus one would expect to be able to predict effects for commercially available diodes only after the precise experiments have revealed what parameters of the device are controlling factors in the response to radiation. Perhaps it may help to set up detailed models of the diode processes as suggested for instance by J. G. Linvill (Ref. 53) and then to deal with the effects of radiation by machine computation, for radiation pulses of different shapes and amplitudes. The immediate problems, however, are common to the difficulties of good experimental technique in any field.

REFERENCES

45   See for instance:

G. L. Keister and H. V. Stewart, The Effect of Nuclear Radiation on Selected Semiconductor Devices, Proc. IRE, 45, 931 (July 1957).

D. A. Hicks, D. V. Keller, J. B. Robison, R. K. Durkee, J. R. Orr and B. M. Clarke, Radiation Damage to Transistors, Boeing Airplane Co., Doc. D5-2880 (Dec. 1958).

46   T. Hanscome (Ed.), Transient Radiation Effects on Electronics III, Hughes Aircraft Co., Doc. SDN 0-58397/40 (Apr. 1960) (S-RD).

47   Godiva II Radiation Effects Tests Report Summaries, Sandia Corp., Division 1626 (Nov. 1959).

48   W. A. Bohan, J. D. Maxey and R. P. Pecoraro, Some Effects of Pulse Irradiation on Semiconductor Devices, International Business Machines Corp., Military Products Division, Owego, N. Y. (Mar. 1959).

49   J. W. Easley and R. R. Blair, Transient Phenomena in Semiconductor Devices, Nuclear Electronic Effects Program, Third Triannual Tech. Note, Appendix E, Bell Laboratories, Inc. (Mar. 1960).

50   J. L. Moll, The Evolution of the Theory for the Voltage-Current Characteristics of P-N Junctions, Proc. IRE, 46, 1076 (June 1958). See page 1080.

51   W. L. Brown and J. W. Easley, Joule Heating in Semiconducting Devices Exposed to High-Intensity Transient Radiation, Nuclear Electronic Effects Program, Second Triannual Tech. Note, Appendix D, Bell Laboratories, Inc. (Nov. 1959).

52   H. L. Wiser, Report on First Experiment on Radiation Effects on Semiconductor Diodes, Hughes Aircraft Co., Nuclear Electronics Dept. (Feb. 1957).

H. L. Wiser and M. D. Petroff, Second Experiment on Radiation Effects on Semiconductor Diodes, Hughes Aircraft Co., Nuclear Electronics Department (April 1957).

H. L. Wiser and M. D. Petroff, Third Experiment on Radiation Effects on Semiconductor Diodes, Hughes Aircraft Co., Nuclear Electronics Department (May 1957).

53   J. G. Linvill, Lumped Models of Transistors and Diodes, Proc. IRE, 46 1141 (June 1958).

54   K. Yahagi and A. Danno, Gamma-Ray Induced Conductivity in Polyethylene Coaxial Cable, J. Appl. Phys. 31, 734 (April 1960).

55   S. L. Marshall and O. Fisch, Proceedings of the Second Conference on Nuclear Radiation Effects on Semiconductor Devices, Materials and Circuits, (Cowan Pub. Co., 1960).

56   B. R. Gossick, Dipole Mode of Minority Carrier Diffusion with Reference to Point Contact Rectification, J. Appl. Phys. 31, 29 (Jan. 1960).

57   F. J. Biondi, Transistor Technology, Vol. II, (D. Van Nostrand Co., Inc., 1958). See especially Chapter 11.

APPENDIX VII

ANALYSIS OF CIRCUIT AND PIECE PART TEST REQUIREMENTS
FOR TRANSIENT RADIATION EFFECTS TESTING

by

William E. Nesbitt, Terence J. Mohan and Kurt K. Graupe

TABLE OF CONTENTS

TABLE OF CONTENTS (cont'd)

LIST OF ILLUSTRATIONS

LIST OF TABLES

PURPOSE AND SCOPE

WEAPON SYSTEM REQUIREMENT STUDY

General

The ultimate purpose of testing any basic piece parts in a transient radiation environment is to provide susceptibility data from which future military systems may be intelligently designed. Therefore, such testing should be oriented toward the furnishing of the proper susceptibility data to satisfy this purpose. In order to provide this orientation, the direction for the testing program should be obtained by considering the requirements of those future military systems which will use the data generated. For this reason, a future weapon systems requirements study was carried out. It was anticipated that the results of this weapon systems requirements study could not be applied to the testing program under this contract. This was true because the study could not be completed in time to affect the planned experiments. Thus a future radiation damage program definition is the goal toward which the study was directed.

Study Limitation

The requirements study was intentionally limited in its scope. One purpose of these limitations was to concentrate the study effort on those areas where transient nuclear radiation data is most sorely needed. The effective range of transient effects is much greater for extra-atmospheric systems than for those in the atmosphere because of atmospheric attenuation of the radiation. Because of this relatively greater importance of nuclear radiation kill effects above the atmosphere, it was decided that only those system portions which go beyond the atmosphere should be studied.

Weapon Systems Studied

Five typical future extra-atmospheric weapon system vehicles were selected for study. These vehicles are:

1. An IR reconnaissance satellite, used for surveillance of boosting ICBM's.

2. An equivalent radar reconnaissance satellite.

3. A communications relay satellite.

4. An anti-ICBM satellite, designed to intercept ICBM's during their boosting phase.

5. An anti-satellite vehicle.

None of these vehicles is in a complete design stage and therefore no complete design was available for study. However, preliminary designs were available for all of these vehicles. These preliminary designs were used in evaluating the equipment requirements.

Because these preliminary designs were not completed in sufficient detail to indicate exact functional and circuit configurations, two additional systems were chosen which did not have this drawback. These are Minuteman and the unmanned version of Dyna Soar.

Functional Sub-Systems Studied

Only those electronic sub-systems were considered which previous experience indicated were most susceptible. The size limitation of the program precluded a complete survey. The electronic sub-systems could be broken down into four categories as follows:

1. Sensors and mechanical-to-electrical transducers.

2. Logic sub-systems, including data processing, transmission, and display.

3. Motor transducers, such as solenoid valves, electric motors, etc.

4. Electrical power supplies.

Those items which fall into categories (1) and (3) are, as a group, relatively insensitive to nuclear radiation. There are some items in category (1), such as IR sensors, which are definite exceptions, however. Thus those functional sub-systems in categories (2), (4), and some of (1), are worthy of consideration. Only the functional sub-systems which fall under category (2) have been examined to date.

Weapon System Study Results

The logic sub-systems under category (2) were expected to contain certain fundamental units, necessary to the operation of nearly all of these subsystems. The object in studying these sub-systems was to obtain those units most necessary to all the sub-systems and also most susceptible to nuclear radiations. These units were found to be fundamental only at the "basic circuit type" level. These basic circuit types were assigned priorities determined by their frequency of use and by their susceptibility to nuclear radiation.

TESTING AND ANALYSIS PROGRAM DEFINITION

Sample circuits for each of the high priority basic circuit types were obtained. These circuits were taken from weapon system vehicles now being designed. The original intent was to analyze these typical examples to determine their behavior in a nuclear radiation environment. The results of these analyses would then be compared with the experimentally determined behavior so that the analysis methods could be checked.

It was realized that, for each piece part used in these sample circuits, an intensive part testing procedure must be done. Also, once the testing was accomplished, analog devices would have to be devised to permit simulation of each of these piece parts. This would be the first time such an intensive testing and analog devising procedure would have been attempted. The difficulties which would be encountered are obvious.

WADD TN 61-8, Pt I   199

The sample circuits obtained were complicated by many special requirements peculiar to the application of the sample. Furthermore, the number of different types of piece parts used, when manufacturer, temperature compensation characteristic, accuracy requirements, frequency response requirements, power ratings, special mountings, etc., were taken into account, was hopelessly large. It was apparent that the typical examples could not be used directly, if more than one circuit was to be analyzed in a limited program. A different definition of basic circuit type was necessary. The samples examined were broken down into simpler "basic building block" circuits. At this level of breakdown, it was decided that the basic building block circuits could all be implemented by a standardized set of component parts so that families of piece parts could be tested together. This decision permitted the development of a feasible testing and analysis program.

The basic building block circuits to be tested have been defined, and the standard inventory of piece parts to be used in them has been decided upon. Since the testing of these piece parts will be directed toward furnishing data for circuit representation, the piece part testing procedure also must be defined. Some of this work has been completed.

FUTURE PROGRAM DEFINITION

REPRESENTATIVE HIGH PRIORITY BASIC CIRCUITS

After completion of the requirements study, a few actual circuit designs representative of the highest priority basic circuit types were selected from among the Minuteman Airborne Digital-Computer Circuits. A Flip-Flop, a Read Amplifier, and a Write Amplifier were examined in order to determine if these circuits were actually "basic" in themselves or if they were, in fact, a complex of even more basic "building-blocks" which could be combined to form these and the other configurations selected for analysis.

Of the three circuits under consideration, the Flip-Flop shown in Figure 70 is the least complex. Even so, it is observed that of the four transistors used in the circuit only two (Q2 and Q3) are essential to the "Flip-Flop" action. The other two transistors (Q1 and Q4) merely amplify the resulting signal. Furthermore, much of the complex input circuitry, while serving important functions such as timing, "fail-safing," speed-up, set and reset, etc., is not required in the basic Flip-Flop circuit.

BASIC BUILDING BLOCK CONCEPT

Building Blocks versus Basic Circuits

The samples obtained of the more important basic circuit types could be tested in their entirety for resistance to radiation. However, it was immediately apparent that these circuit types in themselves are too complex to permit ready analysis on any reasonably short schedule program. For example, the basic Flip-Flop circuit type sample shown in Figure 70 contains twenty-four components and 10 independent nodes, not counting the filter and voltage setting networks. There is, therefore, a set of ten simultaneous differential equations, containing at least 36 independent parameters which must be solved to analyze this circuit. To determine the response of the circuit to a transient radiation burst, many of the above parameters are functions of time.

The basic circuit types found to be most important may be broken down still further into building block circuits which can be added together to form the whole basic circuit type. The flip-flop of Figure 70 for example, can be broken down into a basic flip-flop circuit plus two grounded emitter amplifiers and two diode networks. Each of these can be analyzed separately for their transient radiation response. It is expected that these analyses will, in general, involve the use of an analog computer. The results will therefore be most useful in supplying an analysis method, rather than the specific analysis of the particular basic circuit. Once the method has been checked by actual testing of sample building block circuits, it will be available to analyze the more complex basic circuit types obtained from the system analysis.

Building Block Circuits to be Studied

Figures 70 through 83 are simplified representations of the basic building block circuits which resulted from the requirements study. These are:

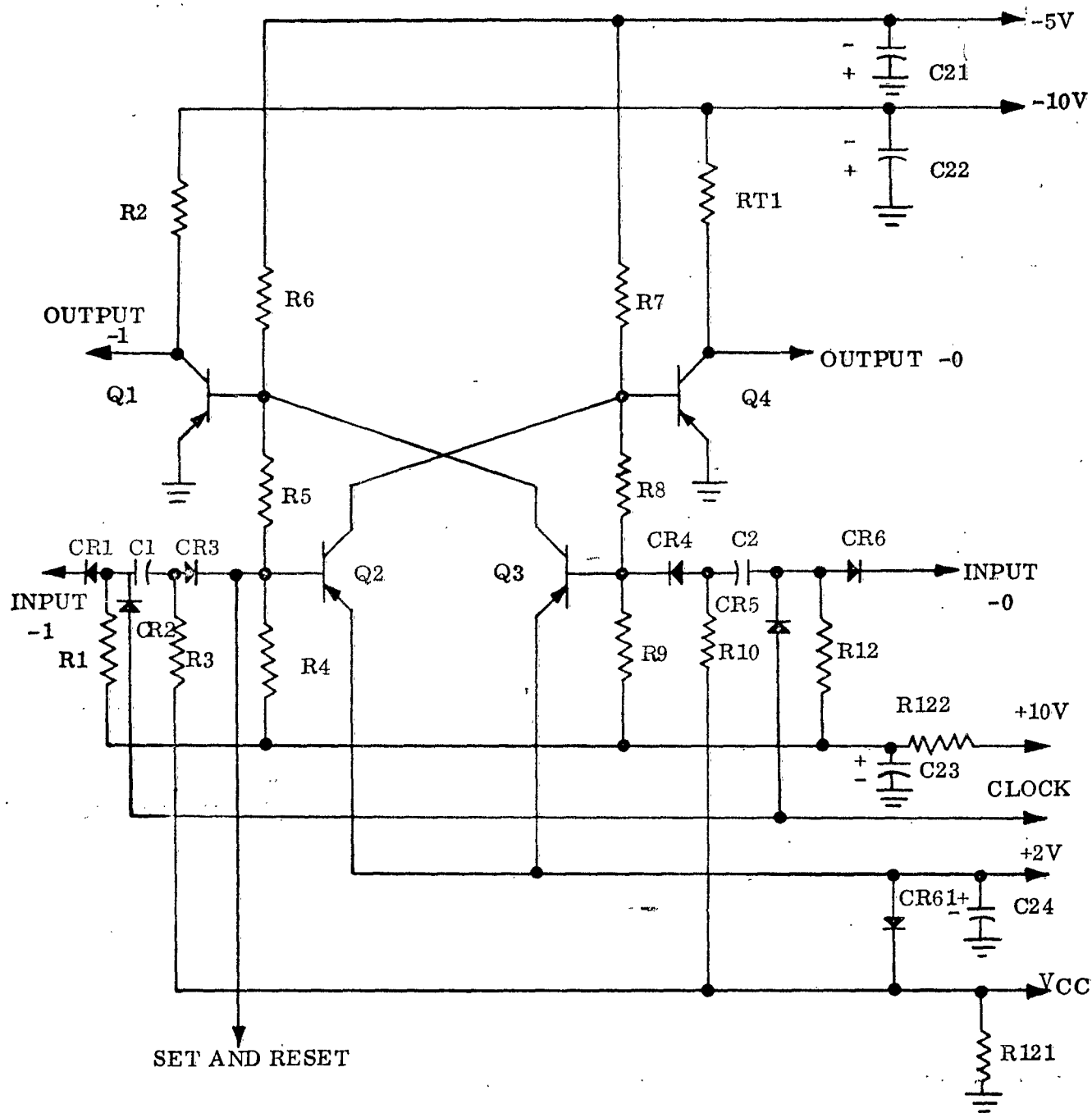Figure 70 – Basic Flip-Flop Amplifier.

1. Balanced amplifier   (Figure 71)

2. Super emitter follower   (Figure 72)

3. Phase inverter   (Figure 73)

4. Multivibrators

    a. Free running   (Figure 74)

    b. One-shot   (Figure 75)

    c. Controlled   (Figure 76)

5. D-C coupled multivibrator (Flip-Flop)   (Figure 77)

6. Clipper - limiters   (Figure 78) and
                                               (Figure 79)

7. Blocking oscillator   (Figure 80)

8. Single-stage amplifiers

    a. Common base   (Figure 81)

    b. Common emitter   (Figure 82)

    c. Common collector   (Figure 83)

9. Certain types of feedback circuits such as cross-coupled amplifier stages, mixer and converter, and discrimination stages and gates. (No example shown)

Three of the basic building block circuit types, which will include five circuits in all, have been tentatively chosen for future analysis and test. These are:

1. All three configurations of single-stage amplifiers (8).

2. A balanced, differential amplifier circuit (1).

3. A bistable multivibrator (flip-flop) curcuit (5).

Not only are these circuits the most basic building blocks, but they are also closely related to one another in configuration. As a result, a maximum of information may be obtained with a minimum of analysis and piece part testing.
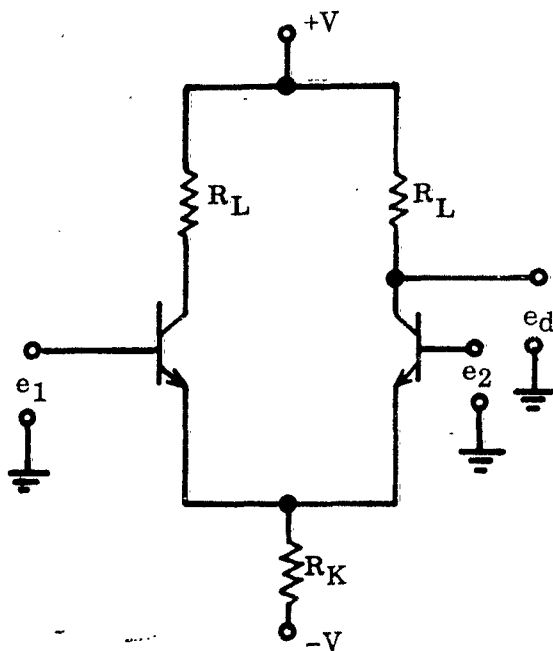
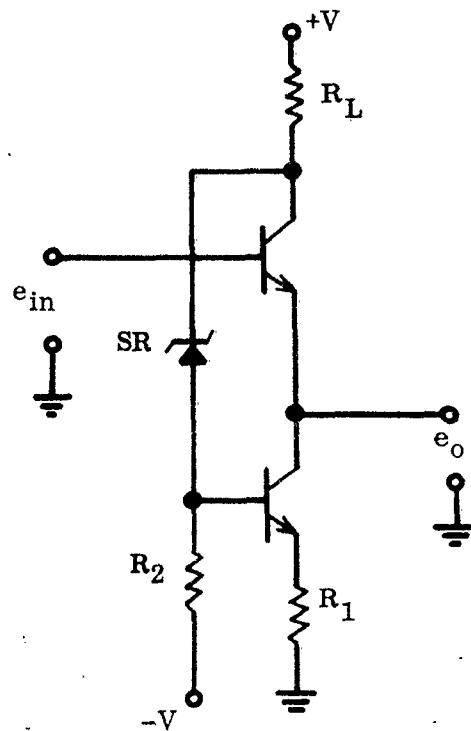Figure 71 - Balanced Amplifier.
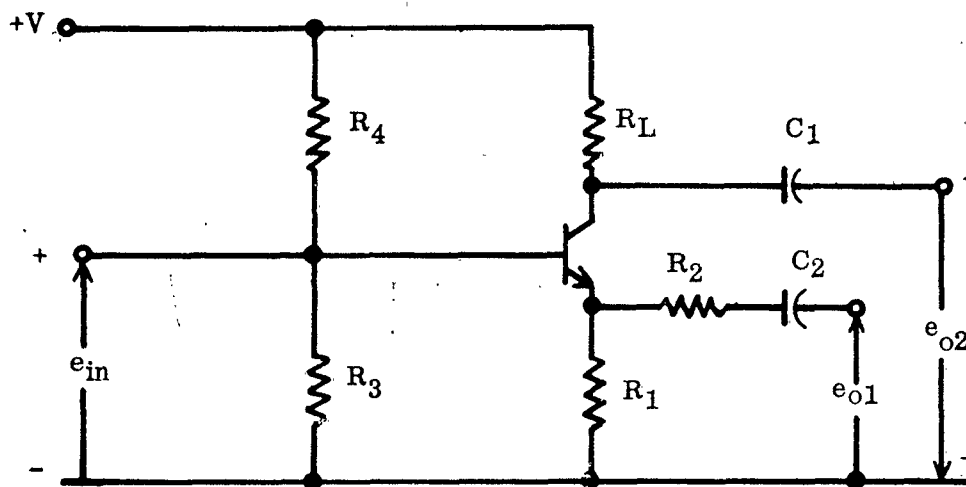

Figure 72 - Super Emitter Follower.
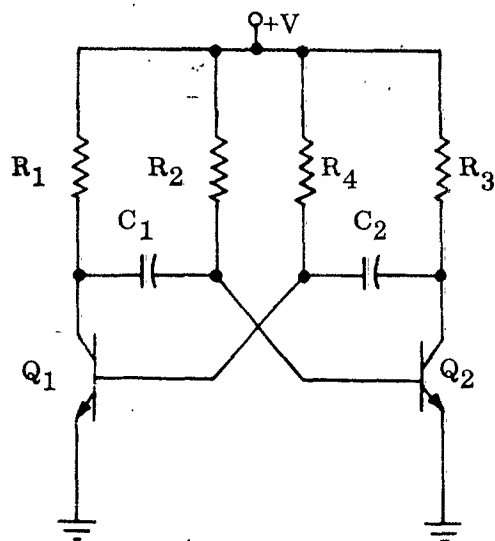

Figure 73 - Phase Inverter.
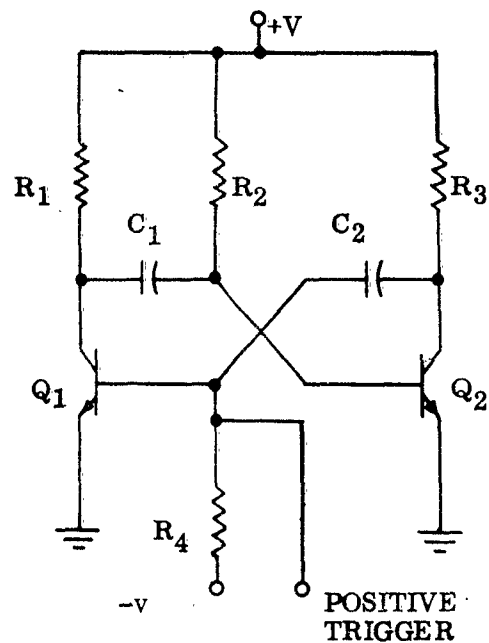
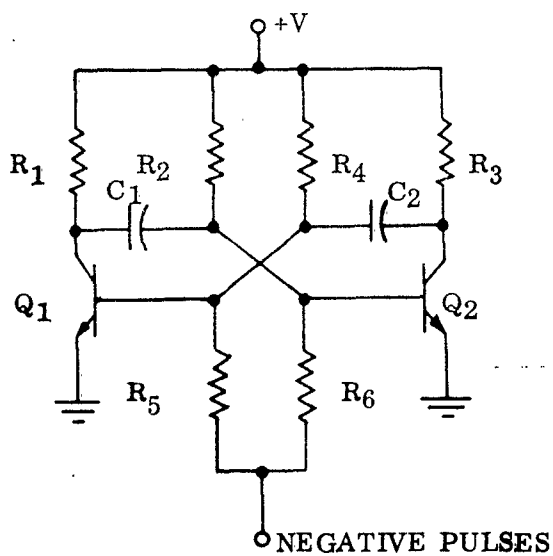Figure 74 – Free Running Multivibrator.

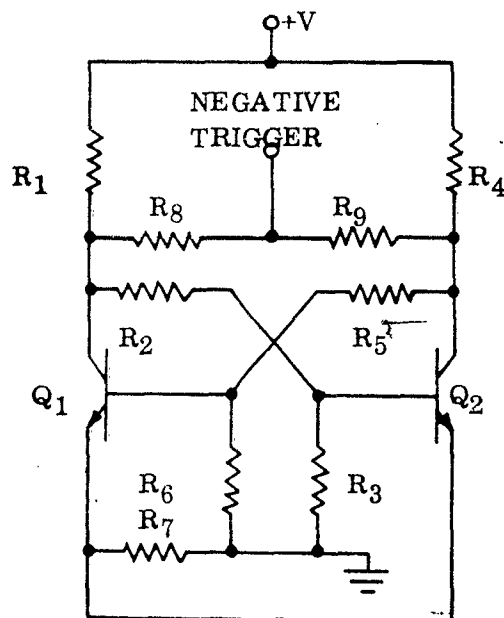Figure 75 – One Shot Multivibrator.

Figure 76 – Controlled Multivibrator.
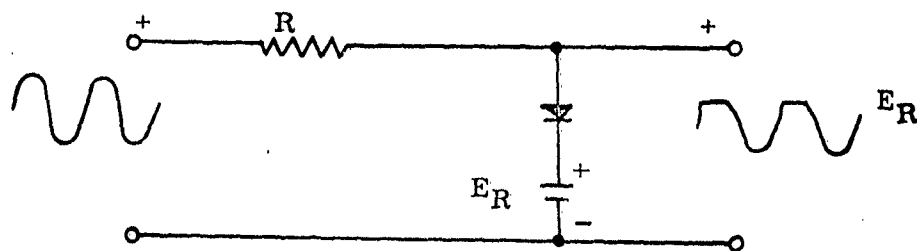
Figure 77 – D. C. Coupled Multivibrator.

Figure 78 - Diode Clipper.

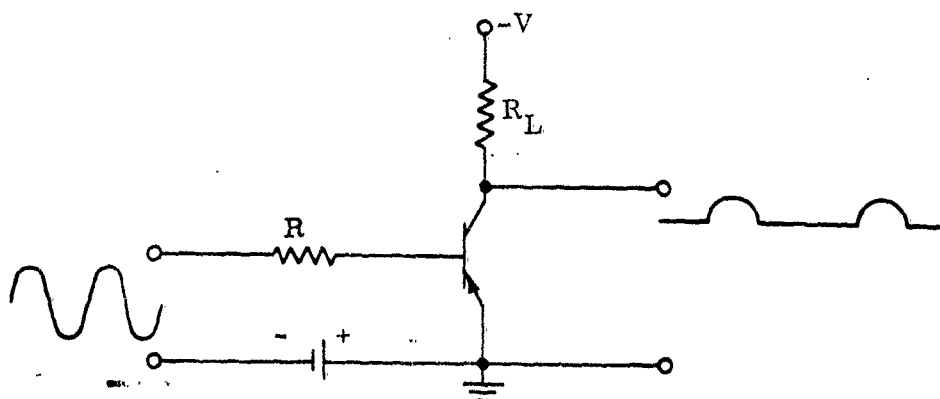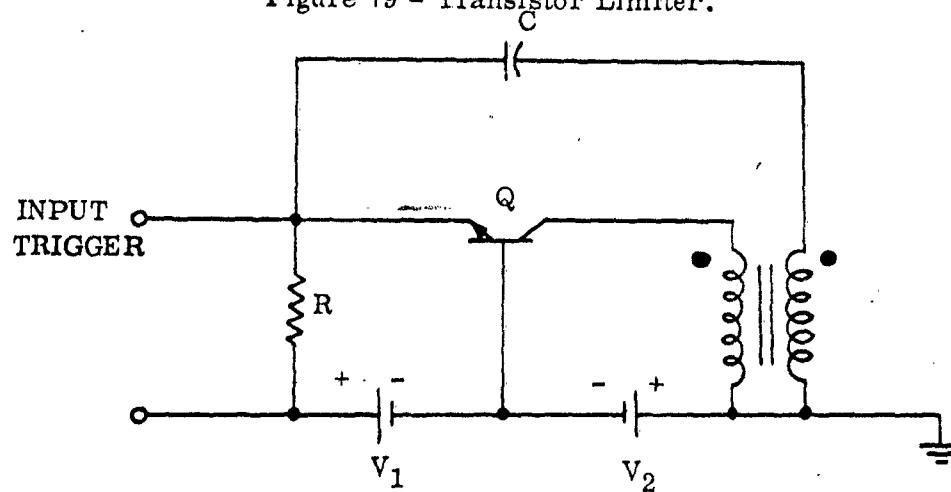Figure 79 - Transistor Limiter.
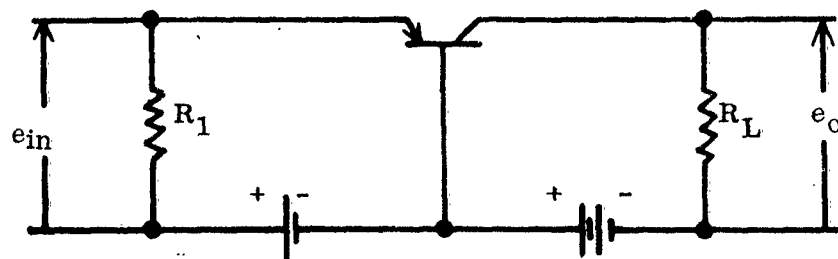

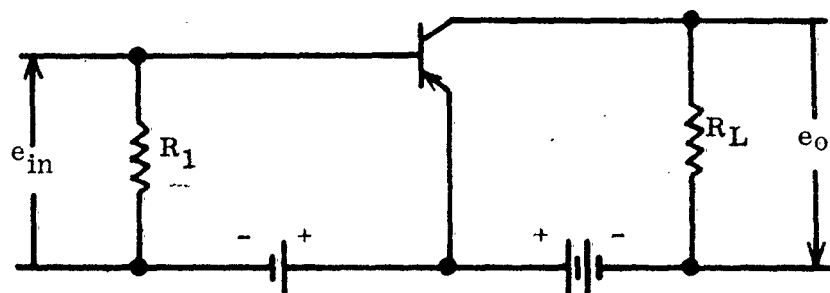Figure 80 - Blocking Oscillator.

Figure 81 - Common Base Amplifier Stage.
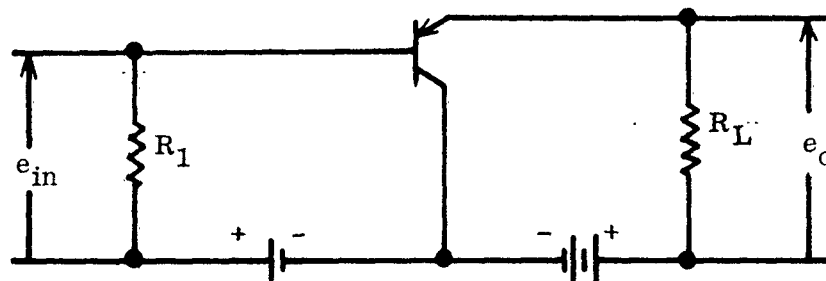

Figure 82 - Common Emitter Amplifier Stage.

Figure 83 - Common Collector Amplifier Stage.

SELECTION OF PIECE PARTS

General

Since the analysis program will be a program for developing analytical methods, it is not intended to furnish complete data on all possible piece parts which could be used in the basic building block circuits. Therefore, the testing portion of the program will be intentionally limited to obtaining data on only a small number of selected representative piece parts. These piece parts to be used in the program have already been selected. The following points were used in making the selections.

1. Select only piece parts which have general usefulness in the basic building block circuits. This eliminates such specialty items as switches, panel meters, neon bulbs, rectifiers, and temperature compensating elements. In addition, since chokes and vacuum tubes are not common elements in the basic circuits considered, they were also eliminated.

2. Select only those piece parts for which some radiation data is available, where possible.

3. Select only those ratings of piece parts which are most useful in the basic building block designs.

4. Where many different rating and values of the same type of component must be used, select complete families of piece parts so that interpolation of data is possible.

The piece parts selected for testing and design included only transistors, resistors, capacitors, and diodes (both normal semiconductor and zener types).

Transistors Selected

The transistors considered for selection are shown in Table 16. Each of these transistor types has been irradiated and a fair amount of data are available on them, mostly data concerned with permanent damage. From these transistors, two were selected for their applicability to the basic building block circuits. These are:

1. Texas Instrument 2N336, a silicon NPN transistor with a medium power rating (150 mw) and an alpha cutoff of 15 megacycles.

2. Philco 2N393, a germanium PNP transistor with a low power rating (50 mw), a high β (150) and an alpha cutoff of 40 megacycles.

Diodes Selected

The semiconductor diodes considered for selection were narrowed down to the 1N914 and 1N277. The 1N277 is a 0.2 microsecond recovery germanium diode with a maximum inverse voltage rating of 125 volts and a forward current rating of 100 milliamperes. Preliminary

TABLE 16

TRANSISTORS CONSIDERED FOR SELECTION

Type	Manu- facturer	Material	$f c\alpha$	Price	β typical	Available Data on Radiation Damage Transient	Permanent Reference	Power	Maximum I_{co}
2 N 393	Philco	G_e PNP	40 Mc	$ 4.00	150		58, 59	50 mw	5
2 N 495	Philco	S_i PNP	20	13.20	20	*β		120 mw	
2 N 338	GE/TI	S_i NPN	45		99	*β	59, 61	125 mw	
2 N 389	TI	S_i NPN	1		12-60	*β	58	85 W	
2 N 353	Philco	G_e PNP	7 Kc		40 min.		58	30 W	
2 N 174	Delco	G_e PNP	.2 Mc	$13.00	40		58	40 W	
2 N 139	RCA	G_e PNP	7 Kc		48 min.		58	80 mw	
2 N 336	TI/GE	S_i NPN	15 Mc	$20.00	76		62	150 mw	

*Transient β response has been measured on these transistors by IBM (ref. 60).

information was obtained on the transient radiation damage to this diode and is reported in Appendix F. The 1N914 is a fast recovery (1 nanosecond) silicon diode with a maximum inverse voltage rating of 75 volts and a 75 milliampere forward current. No radiation damage information is available on this diode but the requirements for a fast recovery diode which would be compatible with the 40 megacycle transistor dictated its selection.

Three zener diodes were also selected. These diodes are all of the same manufacturing type, differing only in the zener voltage. These are Hughes types 1N704, 1N708, and 1N714, with zener voltages of 3.7 to 4.5, 5.6, and 10 respectively. None of these diodes have been tested in a radiation environment but no others in these voltage ranges were available which had been tested.

Resistors Selected

The resistors selected are Allen Bradley composition resistors in all values from 10 ohms to 1 megohm. IBM has measured these in a pulsed radiation environment. The wattage ratings selected are 1/2 watt, 1 watt, and 2 watts. The tolerance selected is five percent.

Capacitors Selected

A very wide range of capacitor values is used in building block circuit design. These range from the 50 to 100 picofarad capacitors, used for spurious time constant elimination and "speed up" service, up to the electrolytic styles used for bypass. For this reason, three types of capacitors were selected.

First, for the low values from 100 picofarads to 1000 picofarads, silver mica capacitors manufactured by El Menco will be used. The voltage rating is 500 volts. For the medium capacitance range, 0.01 to 1 microfarad, Sprague Vitamin Q capacitors will be used. Their voltage rating is 400 volts.

Two types of tantalytic capacitors will be used for the higher capacitance ranges. For one microfarad and 0.1 microfarad sizes, Sprague solid dielectric capacitors will be used. Their voltage rating is 35 volts. For a ten microfarad size, a Sprague sintered slug capacitor was chosen. Its voltage rating is 35 volts. A 120 microfarad capacitor will be tested for leakage only. It is also a sintered slug type, made by Sprague. Its voltage rating is 15 volts. Some radiation damage data are available on all of these capacitor types.

PIECE PART TESTING

General

The methods of test and analysis must be defined to the extent that a complete series of tests may be planned out before any of these tests are performed. Since the testing program should lead to a method of analysis for predicting circuit behavior, all piece part testing should be oriented toward efficiently defining those properties important to a circuit representation

of each specific piece part to be used. The program cannot afford spurious piece part tests which are not directed toward this goal. Fox example, there are 363 different standard resistors within the ratings selected in the preceding section. However, the type of construction is the same for all of these resistors. Furthermore, there is a fine gradation of resistance values available within the resistance range selected. Therefore, only representative sample resistance values will be selected for testing. The behavior of other resistance values under radiation will be inferred by interpolation. Only those values of resistance will be measured for which a significant change occurs. Thus, the high resistance units are expected to undergo considerable change and will be tested. The lower values will demonstrate correspondingly less change under irradiation until a value of resistance is found for which no change is measurable. Testing will stop at this value.

Pre-Test Measurements

Resistors will be measured to four significant figures before and after mounting and after potting.

Capacitors will be measured for leakage resistance and, except for the large tantalytics, for capacitance.

The forward and reverse characteristics for each diode will be obtained.

Transistors will be individually typed for β, f_{α}, α_{co}, I_{co} and the common based hybrid parameters. In addition, common emitter characteristics will be plotted for each transistor.

Test Measurements

The development of circuit representations which satisfy circuit analysis requirements will dictate the test measurements to be made. A method of simultaneously measuring radiation-induced leakage and capacitance changes in a capacitor has been devised by this laboratory and will serve as an example.

The capacitor under test will be attached through a cable to one of the grounded arms of a parallel-resistance bridge located outside of the radiation field. A sinusoidal voltage at a frequency of 50 to 200 Kc will be mixed with a variable d-c voltage and then applied to the input terminals of the bridge. This voltage, together with the bridge ougput voltage will be fed into the inputs of a balanced differential amplifier having high common-mode rejection. The bridge will then be unbalanced slightly so that the sign, as well as magnitude, of a capacitance change may be observed. Leakage resistance and capacitance changes will then be measured respectively as a function of d-c level and peak-to-peak variations in the difference voltage.

This test method and the parameters which will be measured are directly related to the expected circuit representation of the capacitor. It also has a further advantage; the number of parameters which may be measured in a given test is maximized. For capacitors and resistors where uniformity of product is easily obtained, this advantage is not so important. For tran-

sistors and diodes, however, the maximization of the number of parameters measured in a single test assumes paramount importance.

A simple representation of a diode operated in the reversed bias direction is that of a battery in series with a resistance element. Both the battery voltage and the resistance are expected to change under irradiation. Both the battery voltage and the effective resistance should be measured in a single test on a single diode in order to obtain a consistent answer. In order to do this, one possibility is to devise a test which biases the diode at the correct operating point and which superimposes on this operating point an oscillating signal (either current or voltage) whose fundamental frequency is high compared with the duration of the transient irradiation pulse. The analysis of the (voltage or current) signal developed by the diode will provide information sufficient to determine both the battery voltage and the series resistance as a function of the intensity of the burst. One attempt at measuring these parameters is reported in Appendix VI. Due to test difficulties, results are not entirely successful from a circuit representation standpoint.

Transistors present an even greater measurement problem because six parameters must be measured simultaneously. A method of test is being considered which applies two square waves to the transistor, superimposed about the bias point. The resultant conjugate wave forms will allow a complete determination of all six transistor parameters of interest in a single test. So far this method is being only tentatively considered.

In all cases, any effect which might introduce significant errors will either be eliminated or, where this is not possible, the effect will be measured separately and subtracted out of the results.

CIRCUIT REPRESENTATION OF PIECE PARTS

Effects to be Represented

As the basic data on the radiation effects on piece parts and material becomes available through testing and review of the current literature, the circuit representations can be developed. The type of circuit representation to be developed will depend on the nature and complexity of the effect. The types of effects that are expected are:

1. Conductivity changes

2. Induced current

3. Induced voltage

4. Changes in dielectric constants

5. Variation in breakdown potential.

These changes will generally be a function of the pulse intensity and width, the material's absorption coefficient, and carrier relaxation times.

Circuit Representation of Capacitors and Resistors

Two simple examples of possible circuit representation can be constructed from material presented in the literature. For example, the International Business Machines Corporation measured the resistance change for two watt Allen Bradley resistors due to air ionization produced by a Godiva II burst. Resistors of between 10^2 to 10^7 ohms were studied. One film type resistor was also measured. The shunt resistance was computed by Boeing from IBM data and is shown on Figure 84. Since air ionization is directly proportional to the radiation rate, a best fit curve was drawn through the points. Voltage gradient information was not in the report; thus the variation of conductivity with voltage gradient was not considered but could explain the scatter of some of the points. From this data, it is seen that this resistor in air can be represented by:
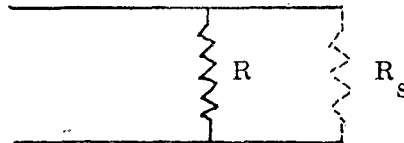
where the dashed resistor is the air shunt path R_s. From Figure 84 it is seen that

$$R_s = \frac{R_{so}}{I(t)}$$

where $R_{so} = 4 \times 10^{12}$ ohms r/sec.

$I(t)$ is the radiation rate in r/sec.

The mathematical representation for the shunt resistance is:

$$R_s = \frac{4 \times 10^{12}}{I(t)}$$

and for the resistor:

$$R'(t) = \frac{R(4 \times 10^{12})}{RI(t) + 4 \times 10^{12}}$$

where $R'(t)$ is the effective resistance of the resistor when exposed to radiation.

The same technique can be applied to the shunting resistance of a capacitor. During this test series at Kukla (see Appendix III), sufficient information was obtained to determine the
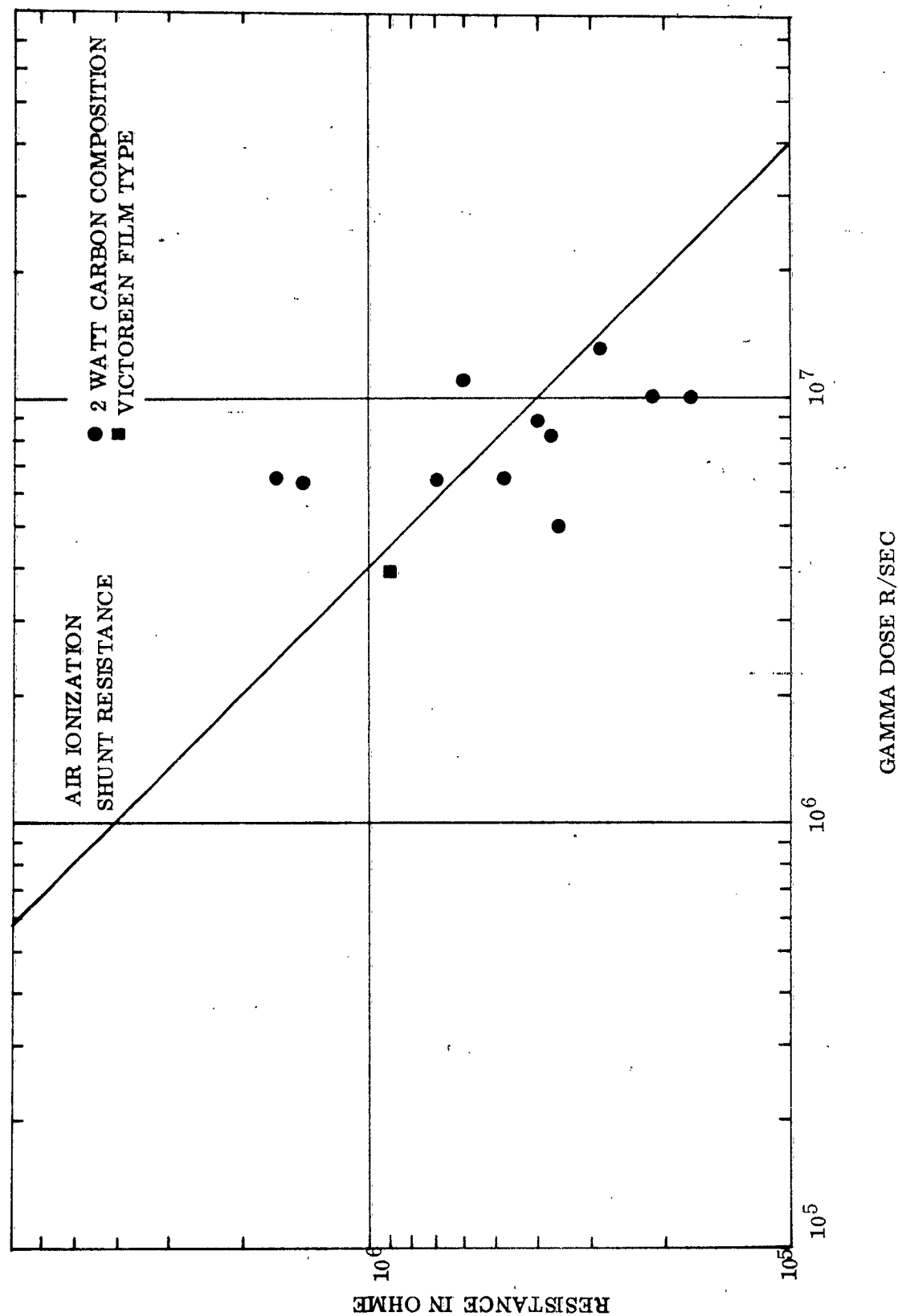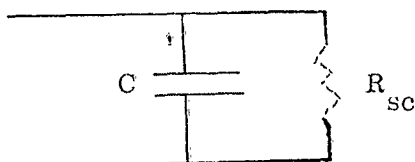
Figure 84 – Air Ionization Resistance Shunt.

leakage of specific capacitor grade dielectrics as a function of radiation rate. This work, shown in graph form in Figure 38 (in Appendix III) will allow the dielectric shunt leakage to be determined for a capacitor.

If it is assumed that the dielectric constant does not change, the equivalent circuit is represented by:

For Vitamin Q capacitors it is possible to relate the shunt resistance change to a whole series of capacitors having equal dielectric thickness but different capacitance values for:

$$\sigma = \sigma_o I^{\triangle}(t)$$

$$R_{sc} = \frac{K}{4\pi C \sigma_o I^{\triangle}(t)}$$

where σ is conductivity

C is capacitance

K is dielectric constant

$I(t)$ is radiation rate

$\triangle$ is a power factor generally between 0.5 and 1.0

For Vitamin Q capacitors:

$$R_{sc} = \frac{1.68 \times 10^8}{C I^{0.7}(t)}$$

Circuit Representation of Semiconductor Devices

As was mentioned in the previous section, the semiconductor diode is a more complicated device to represent than either the capacitor or the resistor. Three terminal active elements pose an even greater problem. If a transistor is operated in a region where it is approximately a linear device; and if, moreover, only its changes in currents and voltages are of importance, then it may be represented by a second order square matrix relating input and output currents and voltages. Thus, only four parameters are of interest. This number of parameters becomes inadequate if the D.C. or bias point behavior is of interest as well. For example, if the characteristic emitter family of curves and the corresponding collector family of curves are considered,

one sees that when the transistor is operated in a linear region, the linearized equations for a grounded base transistor configuration take the form:

$$i_c = i'_c + i_e + \frac{e_c}{R_{cb}}$$

$$i_e = \frac{e_e}{R_{eb}} + k\, i_c$$

where these equations fit the voltage current convention shown:
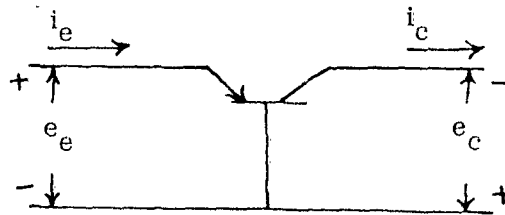
and where:

$$\alpha = \frac{\partial i_c}{\partial i_e} \quad \Big| \quad e_c = \text{constant}$$

$$(R_{cb})^{-1} = \frac{\partial i_c}{\partial e_c} \quad \Big| \quad i_e = \text{constant} .$$

i'_c = current discrepancy when extrapolated linear curve family is brought to the point where $e_c = i_e = 0$. It may be identified with I_{co} for an ideally linear transistor.

$$(R_{eb})^{-1} = \frac{\partial i_e}{\partial e_e} \quad \Big| \quad i_c = \text{constant}$$

$$k = \frac{\partial i_e}{\partial i_c} \quad \Big| \quad e_e = \text{constant}$$

A third term should appear in the equation for i_e, for symmetry reasons, although it is a vanishingly small term for a normal junction transistor.

The above treatment has indicated that there are six independent parameters relating input and output voltages and currents in a D.C. sense. Each of these parameters is expected to change in radiation environment. In addition, each of these parameters is not a constant independent of transistor bias, but is a non-linear quantity which changes as a function of the transistor currents and voltages. To treat a transistor fully and accurately as a circuit element, **the behavior of these six parameters as a function of radiation must be known.**

CIRCUIT ANALYSIS

General

Where possible, direct analytical solution of the system equations as affected by radiation will be used. For the majority of circuits, however, such a solution is likely to prove much too tedious. In this event, an analog solution of these equations will be obtained. In some cases, the direct analytical approach will lead to closed form solutions and are to be preferred over a completely analog solution because of the insight an analytical solution yields. Even here though, the closed form solution is likely to be only an indicated solution. Numerical solutions would still have to be obtained on an analog computer.

Results of Analyses

The analysis methods to be developed must be capable of reliably predicting the behavior of a given circuit under transient nuclear radiation conditions. It would be desirable, but it is not required, that the methods allow the synthesis of optimum hardness circuits by direct mathematical methods. It is sufficient that the methods be capable only of computing the transient voltage and current waveforms which exist within the circuit under irradiation.

The development of the analysis methods is in itself the prime goal of the program. This is not sufficient, however; one must have confidence in an analysis method before he is willing to use it. Therefore, the methods must be used on several circuits and the predictions obtained must be checked by experiment. When this is done, not only the analysis method but also the measured effects of transient nuclear radiation on several circuits will be obtained. These two items will thus be the direct results of the analysis program.

Example of Analysis Method

One simple example of the analysis of a circuit undergoing a transient radiation burst has been computed. This example was simple enough to permit an indicated closed form solution. The analysis has not yet been checked by direct experiment, and moreover, has not yet been extended to include the limits of accuracy of the solutions.

Consider a series connection of a capacitor C, a resistor R, and a constant battery voltage E. The equivalent circuits for both the capacitor and the resistor were shown in the last section. The battery voltage is assumed not to change under irradiation. Thus, assuming a resistor in air, Godiva type pulses (with half widths of about 100 μsec and radiation rates I(t) up to

10^7 roentgen/second), and a Vitamin Q type capacitor, one can take as a first approximation the following equivalent circuit:
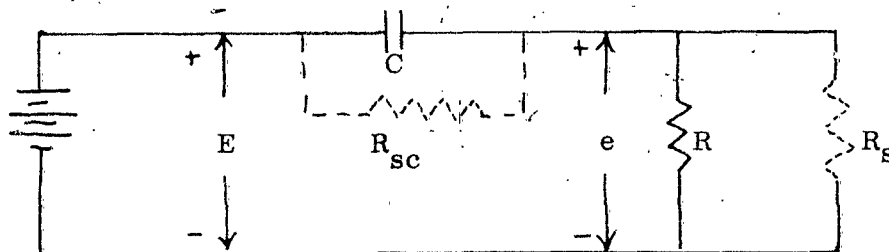
where
$$R_s = \frac{R_{so}}{I(t)} ; \qquad R_{sc} = \frac{K'}{C\, I^\Delta(t)}$$

$$R_{so} = 4 \times 10^{12} \;\Omega\, r/sec$$

$$K' = 1.68 \times 10^8 \;\Omega\,\mu f \left(\frac{r}{sec}\right)^\Delta \qquad \Delta = 0.7$$

From this equivalent circuit one obtains

$$10^{-6}\, C\, \frac{de}{dt} = (E - e)\, \frac{C\, I^\Delta(t)}{K'} - e\, \frac{R\, I(t) + R_{so}}{R\, R_{so}}$$

This may be written in the form

$$\frac{de}{dt} = f(t) - eg(t)$$

where $f(t)$ and $g(t)$ are known functions of time, the solution $e(t)$ can be given in closed form as:

$$e(t) = \exp\left[-\int^t g(s)ds\right] \cdot \int^t f(r)\exp\left[\int^r g(s)ds\right] dr$$

But even for this simple circuit, the analog solution of the differential equation gives the quickest results.

The circuit and the radiation pulse generating functions were set up on the PACE analog computer. The actual analog simulation use is shown in Figure 85. The transient response of the circuit for a gaussian radiation pulse using various combinations of R and C were determined.

Figure 86 shows that the maximum value of $e(t)$ increases with increasing size of R and also with increasing value of C (since the curve for $C = 0.01\mu f$, $R = 0.1$ MΩ was nearly identical with that for $C = 0.1\mu f$, $R = 0.01$ MΩ). Another fact can be read from Figure 86 the maximum in the output voltage for $C = 0.1\mu f$, $R = 0.01$ MΩ occurs earlier than that for $C = 0.01\mu f$, $R = 0.1$ MΩ, but later than that of the radiation rate, as is to be expected.
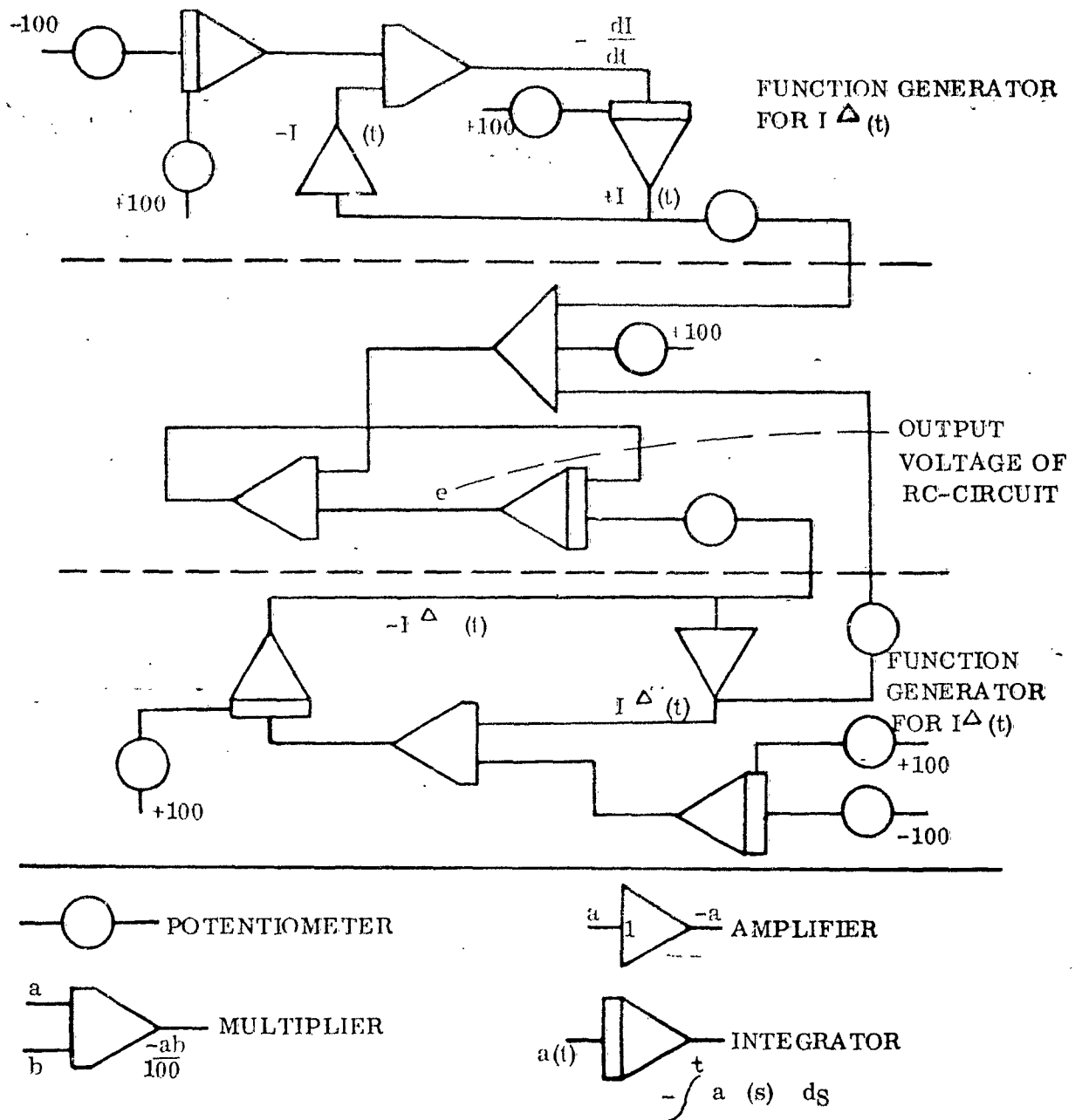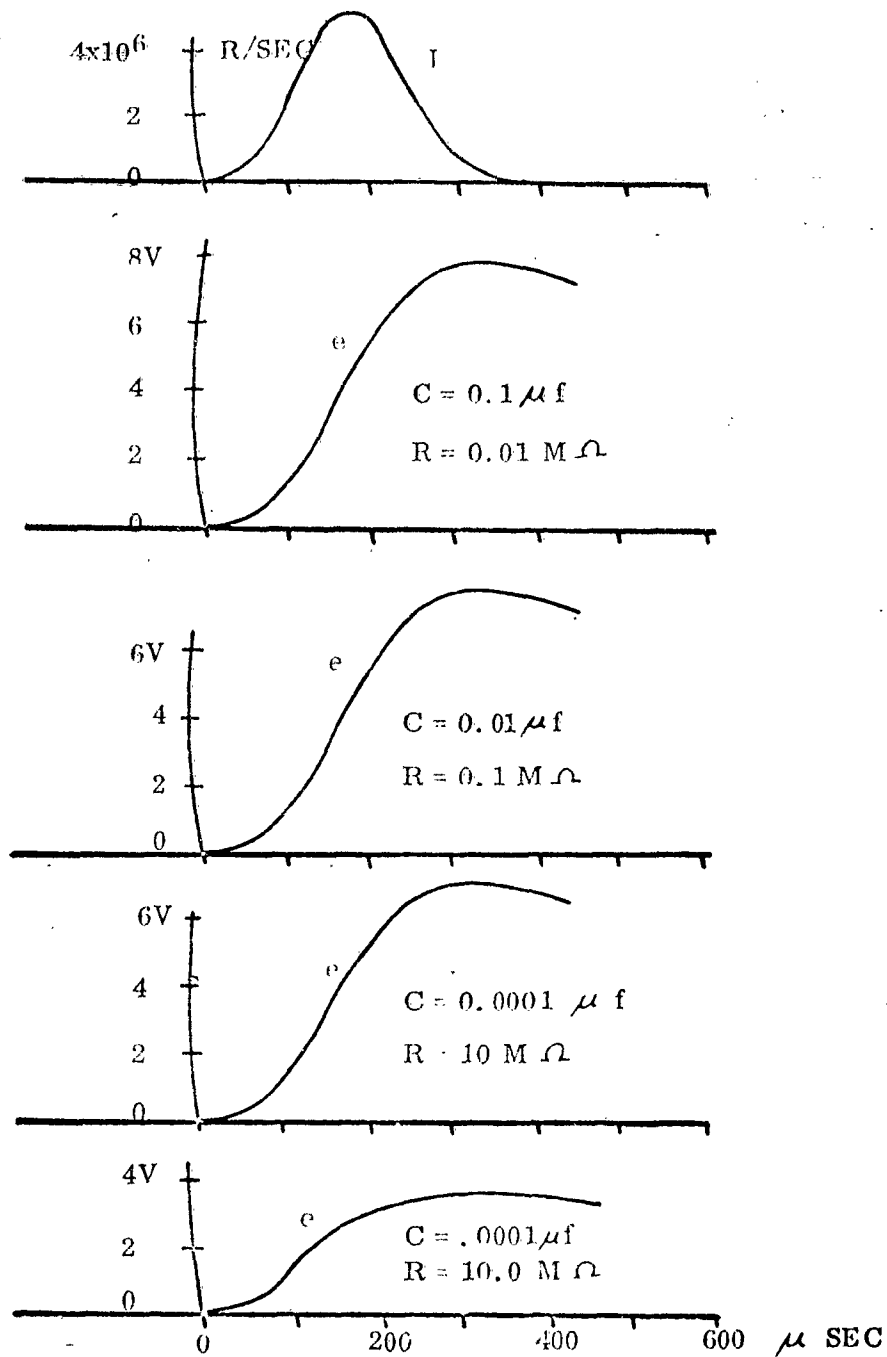
Figure 85 - Analog Simulation of RC Circuit.

Figure 86 – Output Voltage e(t) of RC Circuit For E = 100V and
Variabl RC I Denotes Radiation Pulse.

The curves e(t) are stopped at t = 480μ sec but the missing tails are only the normal exponential decays with the time constants RC valid without any radiation.

Figure 87 shows the output voltage e(t) of four different RC - circuits with equal time constants RC = 1 m sec. As is seen from the figure the maximum voltage increases with capacitance size up to a limit of eight volts.

The next phase of this program will be to measure the parameters of these circuits in a radiation environment, to determine the validity of the theoretical analysis.

CIRCUIT TESTING

The analysis methods to be developed will be applied to at least three circuits. These circuits will be built and tested, either in a critical assembly facility, or with the flash X-ray facility, or both. The parameters of each piece part within each circuit will be measured both before and after irradiation. During the burst, all circuit nodes will be instrumented and the transient waveforms obtained. The same precautions mentioned under piece part testing will also be taken here.

The experimentally obtained voltage waveforms for each irradiated circuit will be compared with the waveforms computed for that circuit. The pre-test measured parameters will be used in performing the circuit computation so that the error expectation will be zero. Any significant deviation of the measured waveforms from the calculated waveforms will be studied for the source of error. This error may have occurred in:

1. Obtaining original piece part data.

2. Piece part representation.

3. Analysis method.

4. Pre-test measurements.

5. Circuit test.

Wherever possible, the error will be traced to one of these causes. If it lies in the original piece part data, the parts will again be tested. In any case, an attempt will be made to eliminate the error and the circuit will be retested.
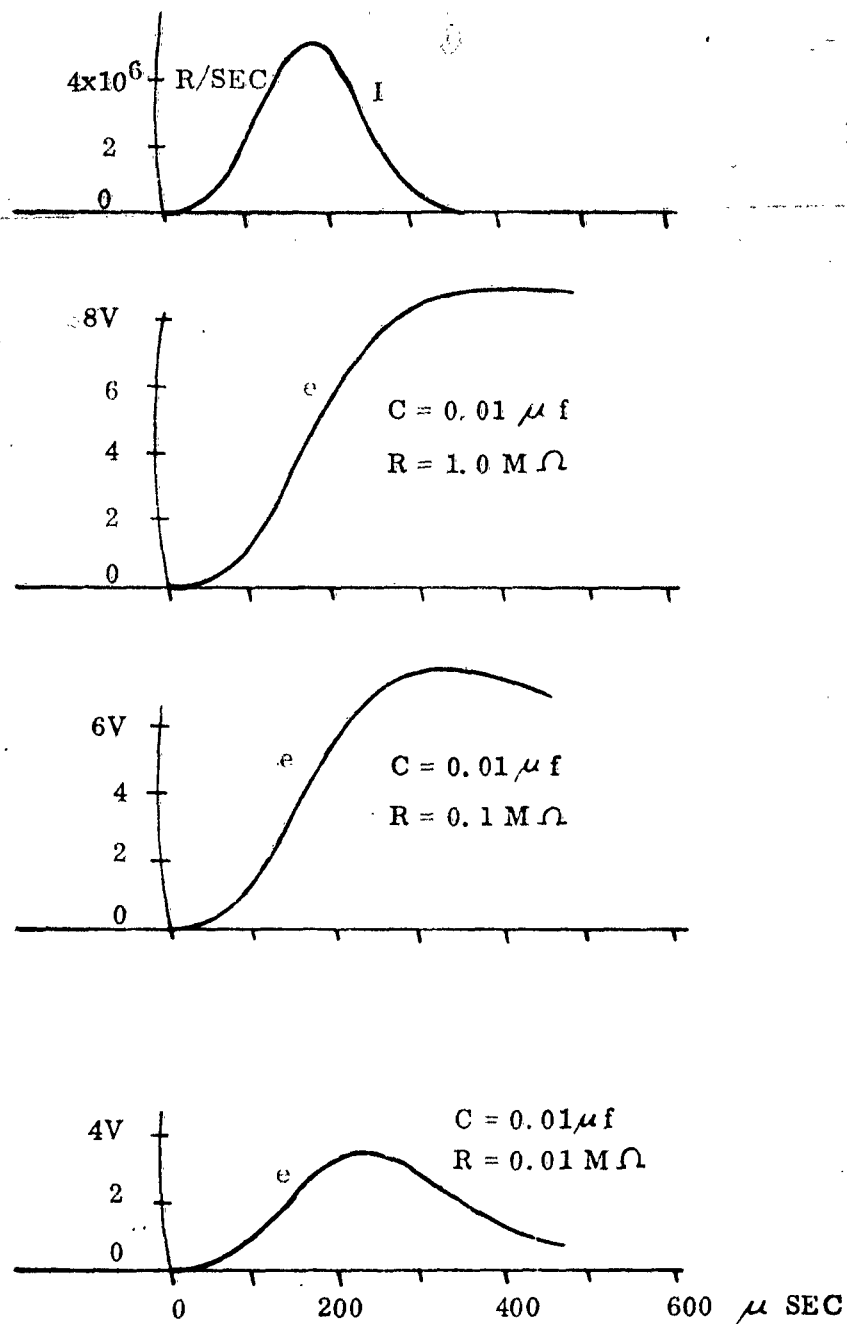
Figure 87 – Output Voltage e(t) of RC Circuit For E = 100V and Constant RC I Denotes Radiation Pulse.